DOCTOR OF SCIENCES

Structural characterization of cyclodextrins: from inclusion complexes to metal organic frameworks (MOFs)

Elasaad, Kossay

Award date:
2013

Awarding institution:
University of Namur

University of Namur
Faculty of Sciences
Department of Chemistry

Structural characterization of cyclodextrins: from inclusion complexes to Metal-Organic Frameworks (MOFs)

Essay by
Elasaad Kossay
In order to obtain the
PhD degree in Chemistry

Members of the jury:
Prof. Benoît Champagne (Jury President, University of Namur, Namur)
Prof. Johan Wouters (Promoter, University of Namur, Namur)
Prof. Ivan Jabin (ULB, Brussels)
Prof. Bernard Tinant (UCL, Louvain-la-Neuve)
Prof. Laurence Leherte (University of Namur, Namur)

2013

Rempart de la Vierge, 13
B - 5000 Namur (Belgique)

Imprimé en Belgique
ISBN : 978-2-87037 - 828-1
Dépôt légal: D/2013/1881/37

University of Namur
Faculty of Sciences
Rue de Bruxelles 61, B-5000 Namur, Belgique

Structural characterization of cyclodextrins: from inclusion complexes to Metal-Organic Frameworks (MOFs)

By Kossay Elasaad

Summary

Cyclodextrins (CD) are cyclic oligosaccharides composed of six to more than sixty glucose units. α-CD, β-CD and γ-CD are well known CD consisting of 6, 7 and 8 glycopyranose units, respectively, that are torus-like rings built up from glycopyranose units. The secondary hydroxyl groups are situated on one of the two edges of the ring, whereas all the primary ones are placed on the other edge. The ring is a conical cylinder, which is frequently characterized as a doughnut or wreath shaped truncated cone. The cavity is lined with hydrogen atoms and glycosidic oxygen bridges, respectively. The primary and secondary hydroxyls on the outside of the cyclodextrins make cyclodextrins water-soluble. The cavity of the cyclodextrin consists of a ring of C-H groups, a ring of glycosidic oxygen atoms and again a ring of C-H groups. This renders the interior of the cyclodextrin rings less polar. As a consequence, the hydrophilic sites which are outside of the torus enable CD to be soluble in water, whereas the apolar cavity site which provides a hydrophobic matrix, enables CD to form inclusion complex with a variety of hydrophobic guest molecules. In addition, CD contains repeating units of –OCCO– binding motif on both their primary and secondary faces. This makes CD able to form extended structures with metal cations of Group IA and IIA (MOFs).
The main goal of this thesis was to design, prepare and characterize new crystal systems based on cyclodextrins properties in combination with:

1. Para aminobenzoic acid (pABA) as a drug model to study the effect of complexation phenomena on the solubility of drugs. Their structure and mode of interaction were characterized by combination a theoretical and experimental approaches.
2. Potassium hydroxide to prepare cyclodextrin Metal-Organic Frameworks (CD-MOFs) formed by coordinating the cyclodextrins to potassium cation. Consequently, taking the advantages of this interaction between cyclodextrin and alkali metal cation, formation of inclusion complexes as CD-MOFs drug carrier was favored.
3. Aegelinol, a natural product, for analytical purposes to determine the absolute configuration of this compound by formation of an inclusion complex with a host of known chirality (cyclodextrins consists of several optically active D-glucose units). This should allow direct determination of the absolute configuration of the guest (aegelinol).

PhD thesis in Chemistry
18 December 2013
Research Unit in Physico Chemistry, Laboratory of Structural Biological Chemistry
Promoter: Prof. Johan Wouters

Université de Namur
Faculté des sciences
Rue de Bruxelles 61, B-5000 Namur, Belgique

Caractérisation structurale de cyclodextrines: de complexes d'inclusion aux architectures métallo-organiques (MOFs)

Par Kossay Elasaad

Résumé

Les cyclodextrines (CD) sont des oligosaccharides cycliques composés de six à plus de soixante unités de glucose. Les α-CD, β-CD et γ-CD sont des CD bien connues composées de 6, 7 et 8 unités glycopyranose, respectivement, qui sont en forme d'anneaux construits à partir d'unités glycopyranose. Les groupes hydroxyles secondaires sont situés sur l'un des deux bords de l'anneau, alors que tous les groupes hydroxyles primaires sont placés sur l'autre bord. L'anneau est un cylindre conique, qui est souvent décrit comme un beignet ou une couronne en forme de cône tronqué. La cavité est bordée par des atomes d'hydrogène et des oxygènes de ponts glycosidiques, respectivement. Les groupes hydroxyle primaires et secondaires à l'extérieur des cyclodextrines les rendent solubles dans l'eau. La cavité de la cyclodextrine se compose d'un anneau de groupes CH, un cycle d'atomes d'oxygène glycosidiques et encore une bague de groupes CH. Ceci rend l'intérieur des anneaux de cyclodextrine moins polaire. En conséquence, les sites hydrophiles qui sont à l'extérieur du tore rendent les CD solubles dans l'eau, tandis que le site de la cavité apolaire fournit une matrice hydrophobe qui permet aux CD de former un complexe d'inclusion avec une variété de molécules hôtes hydrophobes. En outre, les CD contiennent des motifs répétitifs –OCCO– de liaison sur leurs deux faces primaires et secondaires. Cela rend les CD capables de former des structures étendues avec des cations métalliques de groupe IA et IIA (MOF).
L'objectif principal de cette thèse était de concevoir, préparer et caractériser de nouveaux systèmes cristallins basés sur les propriétés des cyclodextrines en combinaison avec:
1. para-Aminobenzoïque (pABA) comme un modèle de drogue pour étudier l'effet des phénomènes de complexation sur la solubilité des médicaments et de caractériser leur structure et leur mode d'interaction par la combinaison d'une approche théorique et expérimentale.
2. L'hydroxyde de potassium pour préparer des cyclodextrines à architecture métallo-organiques (CD-MOF) formée par la coordination des cyclodextrines au cation potassium. Les avantages de cette interaction entre la cyclodextrine et le cation de métal alcalin ont été exploités pour favoriser la formation de complexes d'inclusion comme vecteur potentiel de médicament.
3. L'aegelinol, un produit naturel, à des fins d'analyse afin de déterminer la configuration absolue de ce composé par la formation d'un complexe d'inclusion avec un hôte de chiralité connue (une cyclodextrine se compose de plusieurs unités de D-glucose optiquement actifs). Cela devrait permettre de déterminer directement la configuration absolue de l'invité (aegelinol).

Thèse de doctorat en Sciences Chimiques
18 Decembre 2013
Unité de Recherche en Chimie Physique, Laboratoire de Chimie Biologique Structurale
Promoteur: Prof. Johan Wouters

Thanks…

At the end of the six years in the laboratory CBS, I would like to thank all those who have accompanied me throughout these years and who, in some way, have contributed to the preparation and success of this thesis.

First, I extend my gratitude to ***Professor Johan Wouters*** *for having me in his laboratory, for trusting me and giving me the opportunity to achieve a PhD. I also want to thank him for his advice and attention he has given me which allowed me to gain experience and enhance my knowledge throughout these years. (Thank you for everything…)*

Prof. Ivan Jabin, ***Prof. Bernard Tinant***, ***Prof. Benoît Champagne*** *and* ***Prof. Laurence Leherte****. Thank you very much for agreeing to serve part of my jury and throwing a critical and constructive look at my work.*

I would also like to thank all members of the laboratory ***CBS*** *for their help, support and for their good humor throughout the realization of this thesis. Thank you* ***Bernadette*** *for your great helps in solving crystal structures and for gives me a lot of tips in this field. And thanks to my current colleagues:* ***Jean***, ***Jerome***, ***Laurence***, ***Anaëlle***, ***Celine***, ***Grégoire***, ***Jenny***, *and* ***Guillaume****. Also thanks to my old colleagues:* ***Caroline.C***, ***Caroline.D***, ***Catherine***, ***Julie***, ***Pierre***, ***Christine***, ***Maureen***, ***Raphael***, *and* ***Jérémy****.*

Thank you IT professionals: ***Laurent*** *and* ***Frederic*** *for their help and advice.*

I also thank the member of service technique especially ***Mr. Charles Debois*** *and* ***Mme. Florence Collot****, for their permanent cooperation, help and sincere during my stay in the university residence.*

I also thank the ***Ministry of Higher Education in Syria*** *for its financial support.*

*A big thanks to the Supreme stature in my life, to the big professor, to my father (****Mohamed Elasaad)*** *and to the big heart, to my mother (****Zozohan Abd-Alrazak****), I wished to see you at*

this moments to kiss your hands, to thank you for all my life and asking you the blessing. My parents, I hope that I have brought you the pride…

A big thanks to my step-father, uncle ***Talal Shakake****, to my step-mother, aunt* ***Hazar Abd-Alrazak****, for all the support and encouragement, you are in the status of my family, to you all respect and appreciation…*

Thanks to my brothers: ***Oussama****,* ***Malek****,* ***Loay*** *and* ***Wael****, and to my sisters* ***Wafaa*** *and* ***Fatima****, to all my uncles and aunts, in particular, to the spirit of my* ***uncle Ahmed****, to my* ***uncle Jamal*** *with the hopes and prayers for his release from the injustice arrest…*

Thanks to all my friends: ***Abdo Beirekdar****,* ***Bahjat Aibach****,* ***Mohamed Al-Chihab****,* ***Raki Al-Mohamed****,* ***Tarad Jwaid*** *and* ***Mohamed Hamshou****.*

Last thank to ***the great people in Syria****, who suffers the murder, the hunger, the destruction, the displacement and the detention without any guilt in the absence of the global conscience for this human tragedy, with the hope of the return of the peace, the love and the security to this territory, amen...*

All those I have forgotten, thank you...

*Deep thanks to my beloved wife (****Hayat Shakake****), for support and sacrifices. For standing beside me in all moments and providing the comfort, the warmth, and the taking care of me, all my love and thanks to you, my dear...*

All the love for my small angels, my children: ***Hajar****,* ***Sham****, and* ***Muawyah****. They gave me the courage and motivation to continue my study...*

Symbols 11

Chapter 1. Introduction 14

1.1 Cyclodextrins 14

1.1.1 History 14

1.1.2 Preparation 15

1.1.3 Structure 16

1.1.4 Properties 20

1.2 Functionalization 23

1.3 Cyclodextrin-containing inclusion compounds 25

1.3.1 Formation 25

1.3.2 Application of inclusion compounds 27

1.3.3 Detection of inclusion compounds 28

1.4 Crystallographic Study of Cyclodextrins 29

1.5 Aim and outline of this thesis 38

1.6 References 40

Chapter 2. Crystallographic, UV spectroscopic and computational studies of the inclusion complex of α-cyclodextrin with *p*-aminobenzoic acid. 48

2.1 Introduction 49

2.2 Experimental 56

2.2.1 Materials 56

2.2.2 X-ray diffraction analysis 56

2.2.2.1 Crystallization 56

2.2.2.2 X-ray diffraction experiment 56

2.2.2.3 Structure solution and refinement 57

2.2.2.4 Statistical search in the Cambridge Structure Database 57

2.2.3 UV-visible absorption spectroscopy 59

2.2.4 Phase Solubility diagram 59

2.2.5 Computational methods 60

2.2.5.1 Ab initio geometry optimization 60

2.2.5.2 Semi-empirical simulation of complexes 60

2.2.5.3 Effects of solvation on simulation of complexes 61

2.3 Results and discussion 62

2.3.1 Crystal structure 62

2.3.1.1 Geometry of the host molecule 62

2.3.1.2 Geometry of the guest molecule 65

2.3.1.3 Host-Guest Interaction 71

2.3.1.4 Crystal packing 74

2.3.2 UV-Spectroscopy 75

2.3.3 Phase Solubility diagrams 85

2.3.4 Semi-empirical simulation of complexes 88

2.4 Conclusions 90

2.5 Supplementary data 91

2.6 References 92

Chapter 3. Using Cyclodextrin as linker in Metal-Organic Frameworks (MOFs) for drugs carriers and molecular absorption 96

3.1 General introduction 96

3.2 Results and discussion 100

3.2.1 α-CD-KOH MOF 100

3.2.2 New polymorph of α-CD 104

3.2.3 Crystal structures of α-CD.KOH-ABA complexes 107

3.3 Conclusion 117

3.4 Experimental 119

3.4.1 Crystallization 119

3.4.2 X-ray diffraction experiment 119

3.5 References 122

Chapter 4. Determination of the structure and the absolute configuration of Aegelinol and 1,10-(propane-1,3-diyl)-bis-(6,7-dimethoxy-2-methyl-1,2,3,4-tetrahydroisoquinoline) hydrochloride by using X-ray diffraction technique 126

4.1 Introduction 126

4.1.1 Absolute configuration 126

4.1.2 1,10-(propane-1,3-diyl)-bis-(6,7-dimethoxy-2-methyl -1,2,3,4-tetrahydroisoquinoline) 132

4.1.3 Aegelinol 134

4.2 Aim of this chapter 137

4.3 Results and Discussion 137

4.3.1 Crystal structure of 1,1'-(propane-1,3-diyl)-bis-(6,7-dimethoxy-2-methyl-1,2,3,4-tetrahydroisoquinolinum) 137

4.3.2 Crystal structure of Aegelinol 144

4.4 Experimental Section 155

4.4.1 Chemistry 155

4.4.2 X-ray studies 156
4.5 Conclusions 159
4.6 References 160
Chapter 5. Conclusion and perspectives 165
5.1 pABA-α-CD inclusion complex 165
5.2 CD-MOFs 166
5.3 Experimental absolute configuration determination 168
5.4 Perspectives 169
5.5 References 174

Symbols

1.	***Å***	*Angström*
2.	***A***	*Absorbance*
3.	***A.U.***	*Atomic Unit*
4.	***e***	*Electron*
5.	***J***	*Joule (energy unit)*
6.	***kcal***	*Kilo calorie (energy unit)*
7.	***M***	*Mol/Litre*
8.	***m***	*Meter*
9.	***cm***	*Centimeter*
10.	***mm***	*Millimeter*
11.	***ml***	*Milliliter*
12.	***g***	*Gram*
13.	***kg***	*Kilogram*
14.	K_a	*Acid dissociation constant*
15.	K_c	*Complex association constant*
16.	***K***	*Kelvin (unit of measurement of temperature)*
17.	K^+	*Potassium cation*
18.	Ca^{2+}	*Calcium cation*
19.	M^+	*Metal cation*
20.	***L***	*Ligand*
21.	***T***	*Temperature*
22.	***[α]***	*Specific rotation*
23.	***kV***	*Kilo volte*

24.	***mA***	*Milli Amber*
25.	$\boldsymbol{\lambda}$	*Wavelength*
26.	$\boldsymbol{\lambda_{max}}$	*The wavelength of maximum absorption*
27.	$\boldsymbol{\varepsilon}$	*Molar absorptivity*
28.	***CD***	*Cyclodextrin*
29.	***α-CD***	*Alpha-Cyclodextrin*
30.	***β-CD***	*Beta-Cyclodextrin*
31.	***γ-CD***	*Gamma-Cyclodextrin*
32.	***δ-CD***	*Delta-Cyclodextrin*
33.	***ABA***	*Aminobenzoic Acid*
34.	***pABA***	*Para-Aminobenzoic Acid*
35.	***oABA***	*Ortho-Aminobenzoic Acid*
36.	***mABA***	*Meta-Aminobenzoic Acid*
37.	***HPLC***	*High performance liquid chromatography*
38.	***NMR***	*Nuclear magnetic resonance*
39.	***MOFs***	*Metal-Organic Frameworks*
40.	***UV***	*Ultra Violet*
41.	***U(eq)***	*The equivalent isotropic displacement factor*
42.	$\boldsymbol{\Delta G}$	*Gibbs Energy Change*
43.	$\boldsymbol{\Delta S}$	*Entropy Change*
44.	$\boldsymbol{\Delta H}$	*Enthalpy Change*
45.	$\boldsymbol{S_0}$	*Equilibrium solubility*
46.	***CSD***	*Cambridge Structural Database*
47.	***CCDC***	*Cambridge Crystallographic Data Centre*
48.	$\boldsymbol{C_{\alpha\text{-}CD}}$	*Concentration of α-CD*

49.	$\boldsymbol{C_{pABA}}$	*Concentration of pABA*
50.	***nm***	*Nano Meter*
51.	***UVB***	*Ultra violet with wave length rang 315-280 (medium wave)*
52.	***Z***	*Number of formula in unit cell*
53.	***F***	*Structure factor*
54.	***I***	*Intensity*
55.	***h, k, l***	*Reciprocal space coordination's (Miller index)*
56.	***SD***	*Standard deviation*

Chapter 1

Introduction

Abstract

This chapter starts with a general historical overview of the discovery of cyclodextrins. Then the structure and some physical properties of cyclodextrins (CDs) are reviewed.

Due to their structure and physical properties cyclodextrins are known to form inclusion complexes with a variety of low molecular weight compounds. These complexes are applied in a number of fields.

1.1 Cyclodextrins

1.1.1 History

The compounds nowadays called cyclodextrins were first isolated in 1891 by Villiers. He discovered the formation of an oligosaccharide, when starch was enzymatically cleaved [1]. Schardinger confirmed his result in 1904. He further identified the cyclic structure of the glucose oligomers and the enzyme responsible for the synthesis of cyclodextrins [2]. Because of his pioneering work the name Schardinger dextrins is often used for cyclodextrins in early literature. In the early literature cyclodextrins are also sometimes called cycloamyloses or cyclomalto-oligosaccharides. The correct chemical structure of the cyclodextrins was not published until 1938. It was Freudenberg who characterized them as cyclic structures composed of α-1,4-linked glucose units (§ 1.1.2) [3]. After this publication it still took some years before the molecular weights of the three most important cyclodextrins were determined.

At that time the structures of these compounds were still uncertain, but in 1942 the structures of α and β-cyclodextrin were determined by X-ray crystallography [4]. In 1948, the X-ray structure of γ-cyclodextrin followed and it was recognized that CDs can form inclusion complexes.

The foundations of cyclodextrin chemistry were laid down in the first part of the 20th century. Only in 1953 the first patent on cyclodextrins and their inclusion complexes was registered [5]. Cramer and French were the first, who recognized and studied possible applications by forming complexes with these compounds. Because of their research the way was paved for the use of cyclodextrins as enzyme models [6-10]. However, until 1970 only small amounts of cyclodextrins could be produced and high production costs prevented their wide spread usage. Today the cost of cyclodextrins is reduced dramatically and as a result the group of scientists interested in cyclodextrins is continually growing.

1.1.2 Preparation

Plant photosynthesis produces two main products: starch and cellulose. Cellulose is an insoluble, resilient structure-forming component of cells. In contrast, starch is essentially an energy store. It is readily solubilized and converted into biochemically usable forms, and it is from these that cyclodextrins are prepared. Starch comprises two glucose polymers, both consisting of hundreds, or even thousands, of D-glucopyranoside residues: amylose and ramified amylopectin. Amylose contains only 1,4-glycosidic linkages, while the ramified amylopectin also contains 1,6-bonds. Degradation of starch with a variety of enzymes in the presence of water gives rise to the dextrins, which result from the hydrolysis of glycosidic linkages. Dextrins are used in the food, textile and paper industries, and are consumed in the production of bread, beer *etc*. If dextrins are

degraded by the glucosyltransferase enzyme, the primary product of the chain splitting (a linear oligosaccharide) undergoes intramolecular cyclisation, without the involvement of water, to give the cyclodextrins. Individual cyclodextrins are isolated from the mixture by complexation with non-polar guests such as toluene [Figure 1.1.1], which results in dramatic decreases in solubility. Industrially produced cyclodextrins are generally over 99 per cent pure [11].

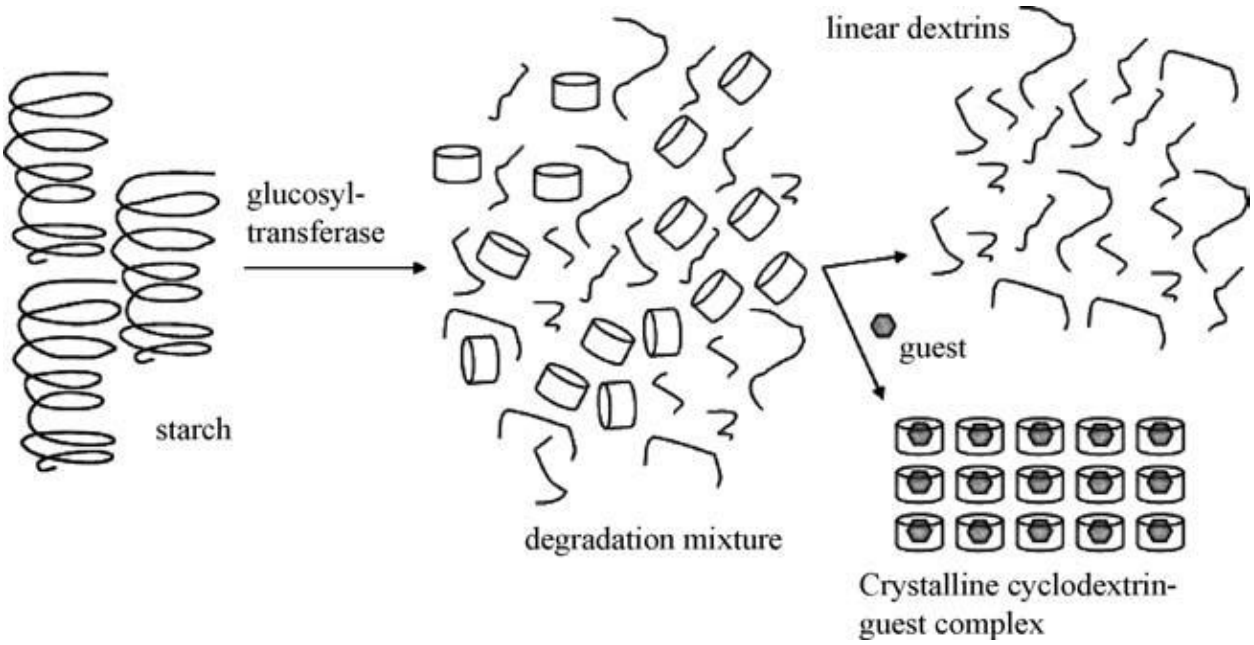

Figure 1.1.1 Isolation of the cyclodextrins by glucosyltransferase degradation of starch [11].

1.1.3 Structure

Cyclodextrins are obtained biotechnologically in large scale by the enzymatic degradation of starch, by making use of a glycosyl transferase from *Bacillus macerans* (later identified as *Clostridium butyricum*) [12]. In this process cleavage of a turn from the starch helix, is followed by intramolecular cyclization [13].
Mainly three cyclic oligosaccharides are obtained. They are called α-, β-, γ-cyclodextrin. The cyclodextrin portion of the name comes from dextrose, an early

synonym for glucose. These cyclodextrins consist of six, seven and eight D-glucose units, respectively, attached by α-1,4-linkages (Fig 1.1.2). Several other (minor) cyclodextrins are known, including *δ*-cyclodextrin and ε-cyclodextrin (nine and ten units, respectively), and the five-membered pre-*α*-cyclodextrin. Cyclodextrins consisting of less and more D-glucose units also exist [5], but they are too expensive for the development of practical applications. Other cyclic oligosaccharides derived from mannose and galactose are also known, but are much less studied.

(A)

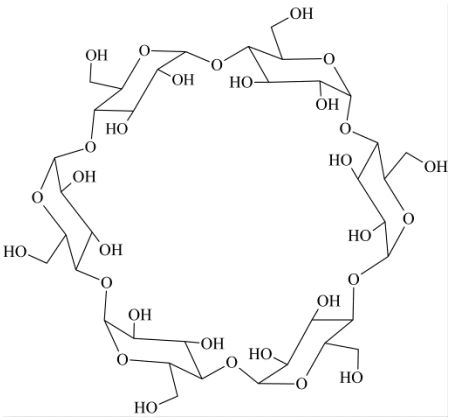

α-cyclodextrin

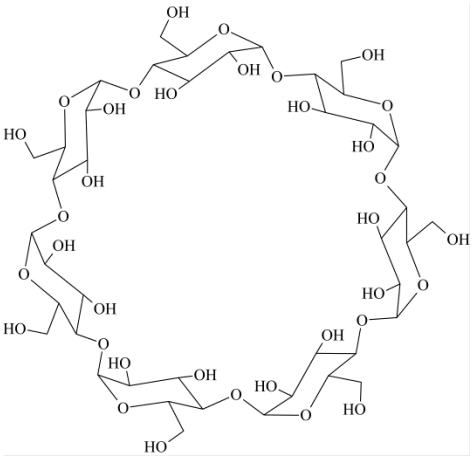

β-cyclodextrin

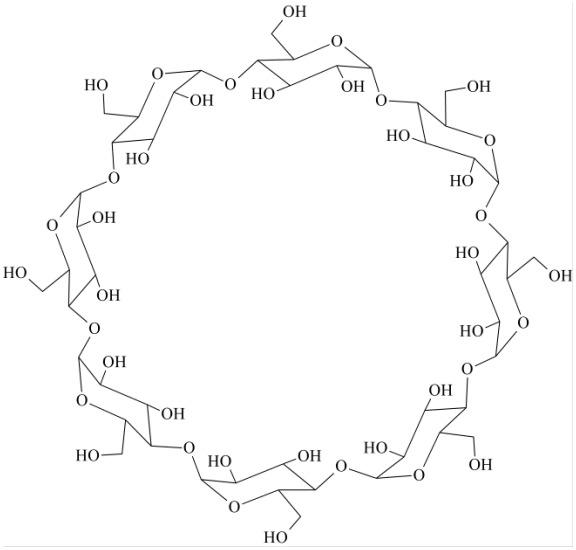

γ-cyclodextrin

(B)

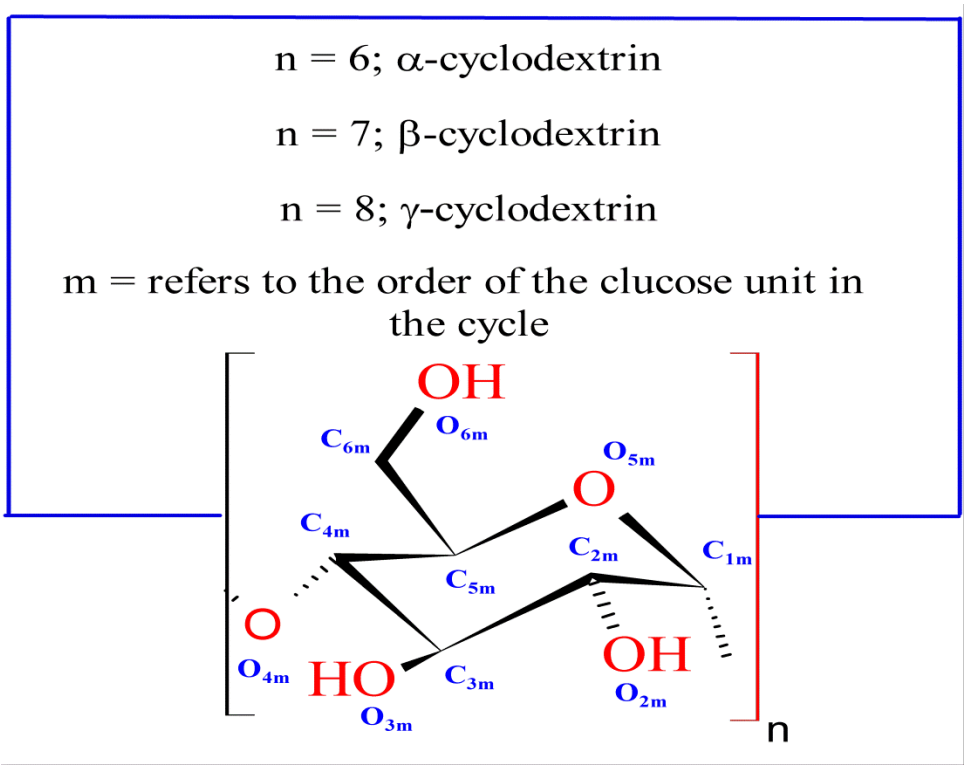

Fig 1.1.2 (A) A structure of α-, β- and γ-cyclodextrin and (B) General structure of cyclodextrins with its traditional numbering.

Each of the chiral glucose units is in the rigid $^{4}C_{1}$-chair conformation, giving the macro cycle the shape of a hollow conical cylinder. The conical cylinder, which is frequently characterized as a doughnut or wreath-shaped truncated cone, is formed by the carbon skeletons of the glucose units and the glycosidic oxygen atoms in between those. The primary hydroxyls of the glucose units are located at the narrow face of the cone (***primary face***) and the secondary hydroxyls at the wide face (***secondary face***). A schematic side view is shown in Fig 1.1.3. Primary hydroxyl groups have rotational flexibility around the C^5–C^6 bond to partially block the cavity. However, their conformation is confined to two types, ***gauche–gauche*** and ***gauche–trans***. In the former type, the C^6–O^6 bond is gauche to both

the C^5–O^5 and C^4–C^5 bonds while in the other type the C^6–O^6 bond is gauche to the C^5–O^5 bond and trans to the C^4–C^5 bond. In contrast the secondary hydroxyls are attached by relatively rigid chains and as a consequence they cannot rotate and are circularly aligned like the rim of a torus and hydrogen bonds are formed between an O^2–H hydroxyl group and the O^3–H hydroxyl group of an adjacent glucose unit.

The apolar C^3 and C^5 hydrogens and ether-like oxygens are at the inside of the torus-like molecules. The nonbonding electron pairs of the glycosidic oxygen bridges are directed towards the cavity center, producing a high electron density and lending to it a Lewis-base character [14]. This result in a molecule with a hydrophilic outside, which can dissolve in water, and an apolar cavity, which provides a hydrophobic matrix, described as a 'micro heterogeneous environment' [15].

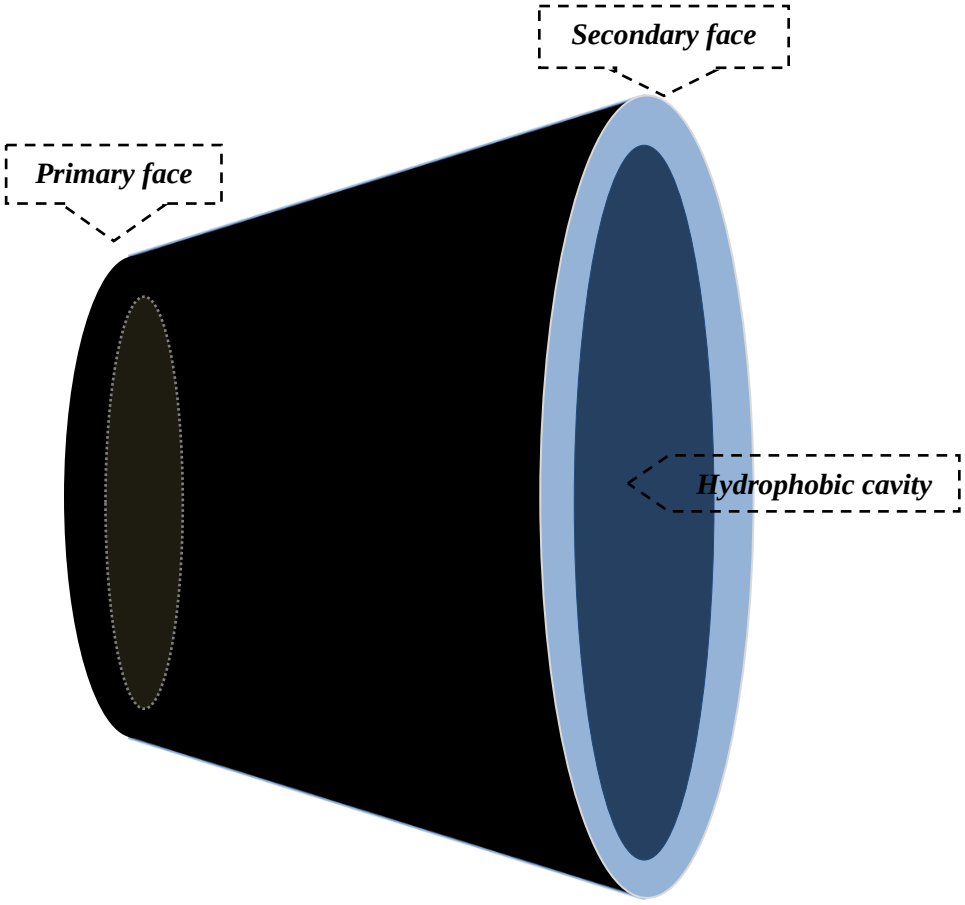

Fig 1.1.3 Schematic side view of cyclodextrin.

1.1.4 Properties

In general, the cyclodextrins form a relatively smooth series from *α*- to *γ*-cyclodextrin in terms of their physical and chemical properties, although very large cyclodextrins such as *δ*-cyclodextrin begin to deviate because they are less rigid than the smaller hosts and, as a consequence, exhibit much poorer guest complexation ability. Table 1.1.1 lists some important properties and the molecular dimensions of the three most common cyclodextrins [13,16].

The primary and secondary hydroxyls on the outside of the cyclodextrins make cyclodextrins water-soluble. One important exception to a smooth change in properties, however, is the cyclodextrins' water solubility, which is significantly less for the odd-numbered *β*-cyclodextrin than for *α*- and *γ*- cyclodextrin (as determined by refractometry; the measurement of the solution refractive index). The solubility of the odd-numbered δ-cyclodextrin is also less than for *α*- and *γ*-cyclodextrin, although the deviation is less marked. This relative insolubility of *β*-cyclodextrin has important consequences on its applications as a solution host. Number of explanations has been put forward for this anomalous behavior. Examination of the enthalpy and entropy of hydration show that both are less favorable for *β*-cyclodextrin than for the smaller and larger analogues. This has been attributed to the interruption of the hydrogen-bonded structure of water by aggregated *β*-cyclodextrin. The reasoning is that the six- and eight-fold symmetries of the other cyclodextrins are more compatible with the solvent cage, which has an even number of hydrogen-bond donors and acceptors. It has also been suggested that the intramolecular hydrogen bonds on the secondary face of *β*-cyclodextrin are responsible for its low solubility, limiting the interactions with solvent water. The analogous hydrogen-bonded network is incomplete in *α*-CD because of strain, whereas *γ*-CD is more flexible. Indeed, methylation of the secondary hydroxyl

groups increases β-CD solubility in water. Cyclodextrins are insoluble in most organic solvents. The cavity of the cyclodextrin rings consists of a ring of C-H groups, a ring of glycosidic oxygen atoms and again a ring of C-H groups. This renders the interior of the cyclodextrin rings less polar.

Table 1.1.1 Physical properties and molecular dimension of cyclodextrins.

Property	α-cyclodextrin	β-cyclodextrin	γ-cyclodextrin
Number of glucose units	6	7	8
Molecular weight($g.mol^{-1}$)	972	1135	1297
Water solubility ($g.100ml^{-1}$) 25°C	14.5	1.85	23.2
$\Delta H°$ solution ($kJ.mol^{-1}$)	32.1	34.7	32.3
$\Delta S°$ solution ($J.K^{-1}.mol^{-1}$)	57.7	48.9	61.4
Specific rotation $[\alpha]_D^{25}$	150.5±0.5	162.5±0.5	177.4±0.5
Surface tension (mN/m^2)	71	71	71
Melting temperature range (°C)	255-260	255-265	240-245
Internal diameter (Å)	5.0	6.2	8.0
External diameter (Å)	14.6	15.4	17.5
Height cone (Å)	7.9	7.9	7.9
Cavity volume ($Å^3$)	174	262	427
Cavity volume in 1 g cyclodextrin (cm^3)	0.10	0.14	0.20
Crystalline water (wt. %)	10.2	13-15	8-18
pKa (25ºC, by potentiometry)	12.33	12.20	12.08
Common guests	Benzene, phenol	Napthalene, 1-anilino-8-napthalenesulfonate	Anthracene, crown ethers,1-anilino-8-napthalenesulfonate

All of the cyclodextrins crystallize from water as hydrates containing varying amounts of water, depending on crystallization conditions. In each case, the semi-polar cyclodextrin cavity is filled with water molecules, which are of relatively high energy as a consequence of their limited interactions with the walls of the cyclodextrin cage. In solution, it has been suggested that a large contribution to the complexation of guest species is the expulsion of these high-energy water molecules from the cavity as part of an overall hydrophobic effect.

Cyclodextrins are stable under alkaline conditions. They can, however, be cleaved by acid hydrolysis. When acid hydrolysis of cyclodextrins takes place glucose is produced.

Cyclodextrins are almost nontoxic. One of the little toxicity of cyclodextrins is Hemolysis [17,18]. The hemolysis is a secondary event, resulting from the interactions of cyclodextrins with membrane components. It is reported that cyclodextrins at lower concentration protect the human erythrocytes against osmotic and heat-induced hemolysis. At higher concentrations, 37 °C, pH 7.4, in 10 $mmol.dm^{-3}$ isotonic phosphate buffers, however, they cause the release of cholesterol and phospholipids from the cell membrane resulting in cell disruption [17,19,20]. The activity of the cyclodextrins follows the order β-, γ- and α-cyclodextrin, where β-cyclodextrin is the most toxic.

Cyclodextrin complexation can give beneficial modification of guest molecules such as solubility enhancement, stabilization of labile guests, physical isolation of incompatible compounds and control of volatility and sublimation. Furthermore, the chemical reactivity of the guest is changed by the incorporation into the cavity.

1.2 Functionalization

A hydrophilic exterior, formed by two rims of hydroxyl groups surrounds the hydrophobic molecular cavity. Various functional groups can be covalently attached to the hydroxyl groups [21,22]. When the hydroxyl groups are modified, the complexation behavior of cyclodextrins can be altered and the relatively low water-solubility of β-cyclodextrin can be enhanced. Selective modification of cyclodextrins with catalytic groups can create an enzyme like activity. For these purposes, several functional groups were placed on the periphery of cyclodextrins. Based on their availability and cavity size most of the studies have utilized α- and β-cyclodextrin. The binding properties of functionalized cyclodextrins are in many cases identical to the binding properties of the parent cyclodextrins [42,23]. Complexation with functionalized cyclodextrins can, however, also take place in organic solvents since many of the functionalized cyclodextrins are soluble in organic solvents. Functionalization of cyclodextrins can concern complete sets of hydroxyls or partial functionalization.

As can be seen in Figure 1.1.2 (§ 1.1.3) the glucose repeating unit of a cyclodextrin contains three different hydroxyls. The glucose repeating unit contains one primary hydroxyl group at position 6. These primary hydroxyls are located at the narrow side of the cyclodextrin molecule. Each glucose unit also contains two secondary hydroxyl groups connected to C^2 and C^3. The primary and secondary hydroxyl groups have different reactivities. Also the two secondary hydroxyl groups have slightly different reactivities. This last difference is due to the fact that the hydroxyl groups attached to C^2 are closer to the hemi-acetal then the hydroxyl groups attached to C^3. This makes the hydroxyl groups attached to C^2 slightly more acidic and so they are slightly more reactive than the hydroxyl groups attached to C^3.

There are several reasons for the functionalization of a complete set of hydroxyls. The reason is often the enhancement of the solubility in water or in organic solvents, the protection of hydroxyl groups so other hydroxyl groups can react, or the activation of a set of hydroxyl groups by the introduction of good leaving groups for further fictionalization of that set. Acylation, alkylation, or silylation of complete sets of hydroxyls can enhance the solubility of cyclodextrins in common organic solvents.

Besides the functionalization of complete sets of hydroxyl groups it is also possible, to selectively functionalize one hydroxyl group of a cyclodextrin molecule. The selective monofunctionalization of cyclodextrins has been extensively studied for the primary hydroxyl face and less well for the secondary hydroxyl face. The reason is that selective functionalization of the more nucleophilic primary hydroxyls over the more acidic secondary hydroxyls is easier than the reverse [24-28].

Among the first cyclodextrin derivatives that appeared in the literature, were acylated cyclodextrins. Since then, many acylated cyclodextrins with different functionalization have been reported [29-34]. In many case these compounds were prepared for purification purposes and the acyl groups were removed after purification of the compound. Alkylation of the hydroxyls of cyclodextrins first takes place at the more nucleophilic C^6 and the more acidic C^2 hydroxyl groups [35]. Because the C^3 hydroxyl groups point to the center of the cavity when the C^2 hydroxyl groups are functionalized, they tend to react very slowly in the alkylation reaction. One of the most common alkylation is methylation. Methylation can be used to enhance the solubility of cyclodextrins in water. Methylation of free cyclodextrins can be performed for example with methyl iodide [36,37].

Protection of the nucleophilic primary hydroxyls by silylation leads to cyclodextrin derivatives, which are soluble in organic solvents and relatively easy to obtain as pure compounds. Because the formed silyl ethers are stable under most reaction conditions, the silylated cyclodextrins can be used as intermediates for further functionalization.

1.3 Cyclodextrin-containing inclusion compounds

1.3.1 Formation

Because of the relatively apolar cavity in comparison to the polar exterior, cyclodextrins can form inclusion compounds with hydrophobic guest molecules in aqueous solutions predominantly due to hydrophobic effect [38-40]. However, the possibility to form hydrophobic effect represents only one of the requirements.

When a complex is formed the surface of the hydrophobic interior of the cyclodextrin and the hydrophobic exterior of the guest molecule exposed to hydrophilic solvent is decreased. It must be emphasized that the phenomenon of cyclodextrin inclusion compound formation is a complicated process and in reality there are many factors that play a role [41]. This is illustrated by the fact that not only apolar compounds can be included but also acids, amides, small ions and even rare gases [42,43].

The driving force for guest inclusion involves a number of contributions, the importance of which is still a matter of some debate. Chiefly the factors of importance are:

- Steric fit;
- Release of high-energy water;
- Hydrophobic effects;

- Van der Waals interactions;
- Dipole–dipole interactions;
- Charge-transfer interactions;
- Electrostatic interactions;
- Hydrogen bonding.

Release of high-energy water and the hydrophobic effect, comprise two energetic components: enthalpic gain as high-energy solvent molecules rejoin the bulk and, entropic gain as two holes in the solvent (host and guest) are reduced to one (complex). The classical hydrophobic effect involves a clearly negative $\Delta S°$, but this is not always the case for cyclodextrin complexes because the cavity is not really non-polar. It has a variety of functionalities and is better described as 'semi-polar'. Another requirement is that the guest molecule must be able to fit inside the cavity of the cyclodextrin.

In addition to size fit and solvation effects, solid and solution complexes are often stabilized by additional enthalpically favorable interactions, such as hydrogen bonds between the guest and the primary or secondary cyclodextrin hydroxyl groups and dipolar interactions.

Table 1.1.1 (§ 1.1.4) shows that, in general, the size of guest that may be accommodated increases as the size of the cyclodextrin becomes larger, although there is some flexibility in the host structures and size fit is not a rigid criterion. Small molecules normally form 1:1 inclusion compounds. In such an inclusion compound, one cyclodextrin ring includes one guest. It is also possible, that the guest is only partly included by one cyclodextrin. This is the case when molecules larger than the cavity have to be included. When the molecule is even larger also 2:1 and other types of inclusion compounds can be formed. The geometric shape of

guest molecule also plays an important role in the type of complexation. Flat molecules, for example, sometimes lead to 3:2 complex type. As for the relatively long chain molecules, this leads to complex with higher orders.

Complexes can be formed either in solution or in the crystalline state and water is typically the solvent of choice. Inclusion complexation can be accomplished in a co-solvent system and in the presence of any non-aqueous solvent. The inclusion complex compound formation by cyclodextrins is historically carried out in water. However, also inclusion compound formation in dimethylformamide is described [44]. It is also possible to form inclusion compounds in the crystalline state [45]. Thus, the stability and the stoichiometry of formed inclusion complexes depend on the structure of the guest compound, on the kind of CD, and the solvent and additives applied.

1.3.2 Application of inclusion compounds

As discussed in § 1.1.1, until 1970 cyclodextrins were produced at small scale. Recent biotechnological advancements have resulted in dramatic improvements in cyclodextrin production, which has lowered their production costs. Industrial production of the most important member of the cyclodextrin family, *β*-cyclodextrin, is about 1500 tons per year, and its price is just a few US dollars per kilogram. This has led to a wider commercial availability of purified cyclodextrins and cyclodextrin derivatives. The beneficial modification of guest molecular properties after the formation of an inclusion compound leads to a large number of applications related to cosmetics and pharmaceutical sectors, generally as slow-release and compound-delivery agents, food technology, textiles, stationary phase in HPLC column, chemical sensors, nanoparticles, analytical chemistry, chemical synthesis and catalysis [13,18,46-63] As already mentioned, cyclodextrins are

practically nontoxic and as a result they are allowed in pharmaceuticals and foods. Stabilization of labile compounds and long-term protection of color, odor and flavor represent some of the possible applications in these areas [13,17,18].

1.3.3 Detection of inclusion compounds

Inclusion compounds can be detected by a variety of spectrometric methods. The most direct evidence for the inclusion of a guest into the cyclodextrin cavity in solution can be obtained by proton nuclear magnetic resonance spectroscopy (^{1}H-NMR). The chemical shifts for the protons attached to C^3 and C^5 move significantly upfield in the ^{1}H-NMR spectrum in the presence of a guest. The magnitude of the shifts increases slightly on going from α-cyclodextrin to β-cyclodextrin and dramatically on going to γ-cyclodextrin. Additionally the shift for the C^5 protons is larger than for the C^3 protons due to the rigid conical shape of the cyclodextrins. On the other hand the C^1, C^2 and C^4 protons located at the exterior of the cavity show only a marginal upfield shift [6].

Usually, the ^{1}H-NMR signals of the included guest molecules shift downfield compared to the free molecules [64,65]. In the ^{1}H-NMR spectra of inclusion compounds the signals of the guests are significantly broadened.

In addition to the magnetic properties of the protons, other physicochemical properties of the guest molecules are also varied upon inclusion complexation. Among others the electronic absorption, fluorescence, phosphorescence and optical rotation properties for the guests are more or less varied as a result of incorporation into a cyclodextrin cavity [66-82].

The structure of the inclusion compound can be detected with X-ray diffraction [83-88]. Especially X-ray analysis of cyclodextrin inclusion compounds

containing organometallics as guests has been used to investigate the structural and to some extent the dynamic host−guest interactions [83]. When the temperature is decreased, the disorder attributed to the absence of strong host−guest interactions, is reduced. This allows a more precise determination of the molecular parameters of the included species, and analysis of the influence of the geometry on the molecular conformation and electron density.

Thermal analysis has also been used in the study of inclusion compounds [89,90]. In some cases no melting peaks of the guests are observed after the formation of complexes. The thermal decomposition of inclusion compounds was studied only scarcely [91,92]. It was observed that the decomposition of the complexed guest occurs above the decomposition temperature of the uncomplexed molecule. Although scarcely studied this thermal decomposition behavior of guests included inside cyclodextrins and the increase of the stability of the guest when included, is used in a variety of applications.

1.4 Crystallographic Study of Cyclodextrins

From the discovery of cyclodextrins at the end of 19th century, it was more than 70 years before X-ray analysis explored the three-dimensional structure of cyclodextrins. In the early stage of cyclodextrin study, the cyclic structure of cyclodextrins was expected from various chemical analyses; however, without knowledge of the three-dimensional structure, it was difficult to fully understand the unique characteristics of cyclodextrins capable of forming inclusion complexes with a variety of guest compounds. X-ray structures provided the direct evidence of the inclusion of the guest molecule in the cyclodextrin cavity.

The development of the structural study of cyclodextrins in the last century has been summarized in several reviews [12,13,93-97]. In 1942, the

crystallographic method was first applied to cyclodextrins to determine molecular weight [4]. James et al. proposed a packing structure for several crystalline complexes of α-cyclodextrin with small guest molecules in 1959 [98]. Preliminary crystallographic data of β-cyclodextrin complexes with benzene derivatives were reported in 1968 [99]. The crystal structure first solved by X-ray analysis in 1965 was that of the α-cyclodextrin complex with potassium acetate [100]. Structures of two other well-known cyclodextrins, β-cyclodextrin and γ-cyclodextrin were determined in 1976 and 1980, respectively [101-103]. An up-to-date list of crystal structures determined by x-ray and/or neutron diffraction is collected in the Cambridge Crystallographic Database (*http://www.ccdc.cam.ac.uk/*).

Cyclodextrins consisting of 6 to 31 glucose units have been separated from a reaction product of cyclodextrin glycosyltransferase. Three dimensional structures of cyclodextrins have been determined for α-, β-, γ-, δ-, ε-, and ι-cyclodextrins which consist of 6, 7, 8, 9, 10, and 14 glucose units, respectively, by X-ray and neutron diffraction analyses [104-113]. The enzymatic degradation of starch by potato D-enzyme, a kind of α-amylase, produces cyclodextrins having more than 17 glucose units. Among these large cyclodextrins, the crystal structure of cyclomalatohexaicosaose consisting of 26 glucose units has been determined [114].

Cyclodextrins consisting of 6–9 glucose units exhibit a doughnut-shaped structure [104-110]. These cyclodextrins are approximately in the shape of a truncated polygonal cone. The macrocycle of cyclodextrins is distorted from its ideal structure with n-fold symmetry to relieve the steric hindrance between glucose units and distortion of the glycosidic linkage. Upon complex formation, cyclodextrins change their macrocyclic structure and adjust the structure of the cavity to accommodate the guest molecule. The shape of the cyclodextrin ring is

well characterized by using a polygon consisting of glycosidic O^{4n} atoms which are nearly coplanar Table 1.4.1 The radius of the polygon, that is the average of the distance from the center of the polygon to each O^{4n} atom, is a good measure to estimate the size of the macrocycle. The radius varies in the range from 4.2Å in α-cyclodextrin to 6.4Å in δ-cyclodextrin. The α-1,4 linkage is responsible for the conformational flexibility of the macrocycle. The pyranose ring is almost perpendicular to the O^{4n} plane but the average over all the glucose units indicates that the pyranose ring is generally tilted with its primary hydroxyl side towards the inside of the macrocyclic ring. The rotational movement of glucose units around the glycosidic linkage distorts the macrocyclic ring by increasing the degree of inclination of each glucose unit against the plane through the glycosidic O^{4n} atoms.

Table 1.4.1 Geometrical data of cyclodextrin [115].

	α (6)	**β (7)**	**γ (8)**	**δ (9)**	**ε (10)**	**ι (14)**
Radius of the O^4 polygon (Å)	4.2(1)	5.0(2)	5.9(1)	6.4(7)	6.9(4)	8.4(10)
$O^{4n}…O^{4(n+1)}$ distance (Å)	4.2(1)	4.3(1)	4.5(1)	4.5(1)	4.5(1)	4.5(1)
$O^{2n}…O^{3(n+1)}$ distance(Å)	3.0(1)	2.9(1)	2.8(1)	2.9(2)	3.2(2)	2.9(2)
Planarity of the O^{4n} polygon (Å)[(a)]	0.10	0.16	0.11	0.80	-	-
Glycosidic O^4 angle: $O^{4(n-1)}…O^{4n}…O^{4(n+1)}$	119(1)	118(1)	117(1)	116(2)	117(1)	118(1)
Tilt angle (°)[(b)]	13.0(10)	14.0(10)	19.0(9)	25.0(20)	-	-

[(a)] Root-mean-square deviation of O^{4n} atoms from their least-squares plane.
[(b)] Average angle between the O^{4n} plane and the plane through C^{1n}, C^{4n}, O^{4n}, $O^{4(n+1)}$and of each glucose unit.

The tilt of each glucose unit is evaluated by the ‘‘*tilt-angle*’’, which is defined as the angle measured between the plane of the O^{4n} polygon and the plane through

C^{1n}, C^{4n}, O^{4n}, and $O^{4(n+1)}$ of each glucose unit. The tilt angle is largely in the range from 10° to 20°. Such flexibility of glucose units is still restrained by intramolecular hydrogen bonds of secondary hydroxyl groups formed between adjacent glucose units. When these hydrogen bonds are disrupted, glucose units gain high flexibility around the glycosidic linkage as is seen in the structures of permethylated cyclodextrins and peracetylated cyclodextrins [116].

The water distribution in various forms of the crystalline hydrates is summarized in Table 1.4.2 Note that the solid-state cavity volume is limited for larger cyclodextrins by inclusion of glucose residues from adjacent hosts. Each cyclodextrin crystallizes in a variety of forms (denoted by Roman numerals for well-characterized cases). In general, the structures of the cyclodextrin hosts themselves do not vary greatly from one form to another, and the differences lie in the distribution of the water molecules. α-Cyclodextrin crystallizes from water in three forms, hexahydrate (Form I and Form II) and 7.57 hydrate (Form III) (CSD-code: BANXUJ) [117]. The flexible macrocyclic ring is demonstrated by the distinct conformational changes of α-cyclodextrin observed among these crystals. *α*-Cyclodextrin adopts an elliptically distorted, irregular shape in forms I and III, with two glucose units rotated about their glycosidic linkage to present the primary hydroxyl side inwards towards the cavity, making the cavity volume smaller. The form II hydrate is more regular. The structure of *α*-cyclodextrin hydrate form I (CSD-code: CHXAMH) is shown in Figure 1.4.1 [111].

β-cyclodextrin crystallizes in two forms, dodecahydrate (I) [112] (CSD-code: BCDEXD10) and undecahydrate (II) [113] (CSD-Code: BUVSEQ). Both forms of the *β*-cyclodextrin have similar host geometries, which are much more regular than *α*- cyclodextrin, but the change occurs in the arrangement of water molecules in the cavity with the occupancies of some of the disordered water sites being higher in

Table 1.4.2 Solid-state cyclodextrin hydrates.

	α	β	γ	δ
Number of water molecules (form)	6 (I) 6 (II) 7.57 (III)	12 (I) 11 (II)	19 14.1 15.7	13.75
Number of water molecules in cavity (form)	2 (I) 1 (II) 2.57 (III)	7.3 (I) 6.3 (II)	7.1 to 14.1 Two glucose units occupy cavity	Two glucose units occupy cavity; water distributed in open space on primary face

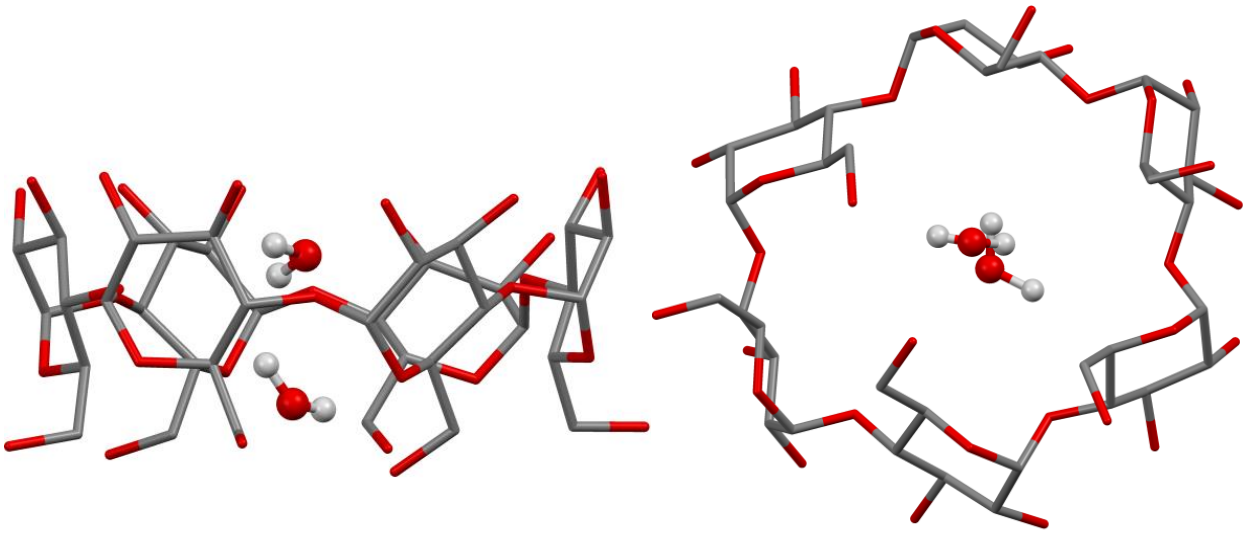

Figure 1.4.1 Two views of the X-ray crystal structure of form I of α-CD hydrate.

form I. γ-Cyclodextrin has the most symmetrical structure among the four cyclodextrins. The structure of γ-cyclodextrin closely resembles that of β-cyclodextrin, and again there is complex disorder of the water molecules [114] (CSD-code: CIWMIE10). Both hosts exhibit a regular array of intramolecular

hydrogen bonds on the primary face with O … O contacts in the range 2.70–3.00 Å. In contrast, *δ*-cyclodextrin is elliptically distorted and the ring deviates considerably from the planar structure, the structure is distorted into a boat-like shape, giving it a shallower cavity [115] (CSD-code: SIYKOA). In cyclodextrins consisting of more than nine glucose units, the macrocyclic ring is no longer doughnut shaped [Figure 1.4.2]. Because of the strain imposed on the glycosidic linkage, the molecule cannot retain the round structure; instead, the elliptical ring is bent into a shape like a saddle [116-118] in cyclodextrins composed of 10 and 14 glucose units, ε- and ι-cyclodextrin, respectively (CSD-Code: NOBBUB and NOBBUB).

The structure of a cyclodextrin consisting of 26 glucose units, the largest one whose structure has been determined by X-ray analysis, is not circular but consists of two left-handed amylose-like helixes [119] [Figure 1.4.3]. The molecule has two- fold symmetry and the two asymmetric parts are connected by glucose units with the trans arrangement. Inclusion of the guest molecule induces a structural change in the cyclodextrin. As shown in the structure of *δ*-cyclodextrin and its complex [121], complex formation changes the elliptically distorted macrocyclic ring to a round structure with pseudo nine-fold symmetry [110,121].

In crystals of cyclodextrin complexes, the crystal packing is generally governed by the arrangement of cyclodextrin molecules because they dominate the intermolecular contact to form the crystal lattice. However, the packing mode is not unique for a particular cyclodextrin but varies according to the guest molecule.

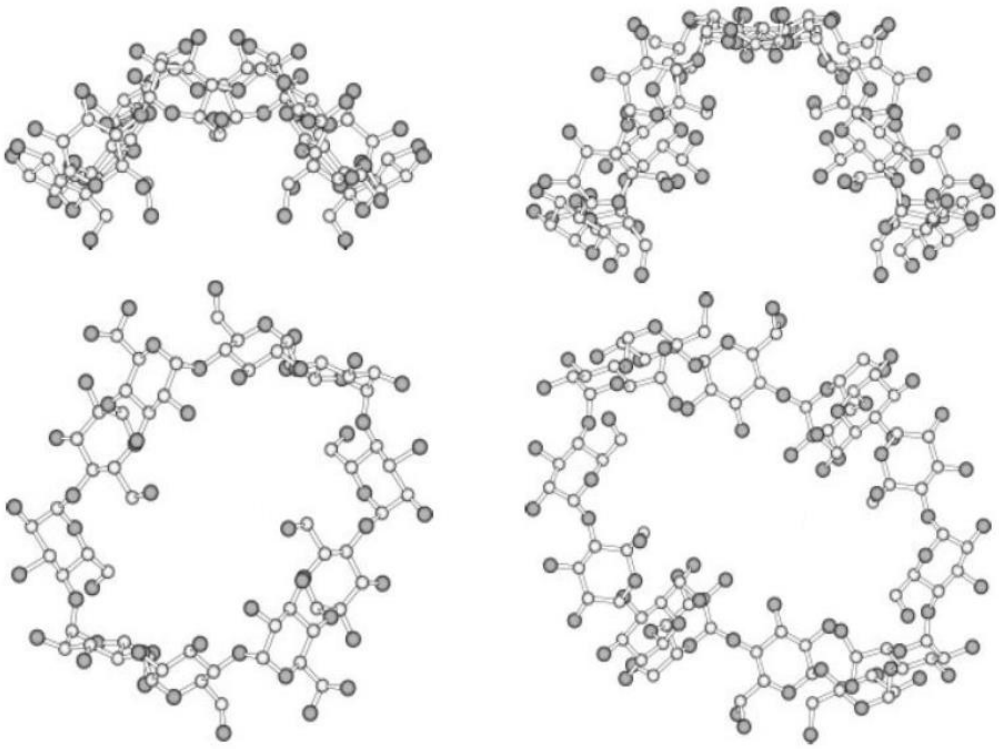

ε-cyclodextrin ι-cyclodextrin

Figure 1.4.2 Side and top views of the structures of ε- and ι-cyclodextrin consisting of 10 and 14 glucose units, respectively [120].

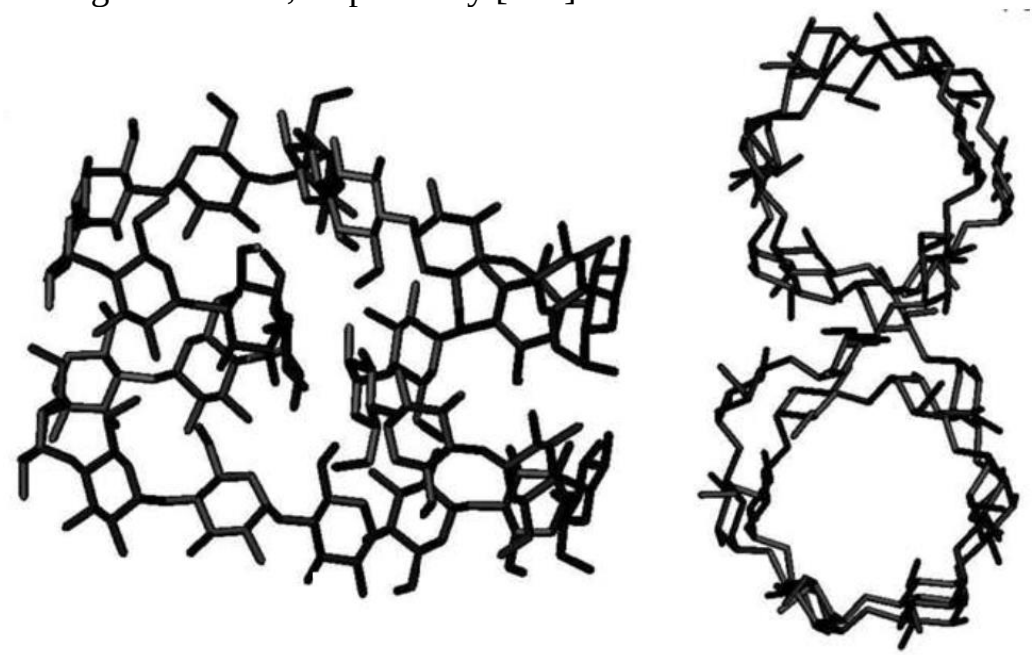

Figure 1.4.3 Side and top views of the structures of cyclomalatohexaicosaose consisting of 26 glucose units, the molecules consist of two left-handed helical structures related by a two-fold symmetry [119].

There are three packing types: cage type, channel type, and layer type, which are widely observed. The possible packing modes are illustrated in Figure 1.4.4. Guest molecules determine the selection of one of these packing modes, which provides a suitable cavity into which they can be stably accommodated.

The cage-type packing structure is frequently observed for relatively small guest molecules which can be enclosed in the host cavity. Cyclodextrin molecules are arranged in a herring-bone fashion and both ends of the host cavity are closed by adjacent molecules to create an isolated ‘‘*cage*’’ [Figure 1.4.4-A]. The channel-type structure is formed by linear stacking of cyclodextrin rings. This column-like structure has an infinite cylindrical channel that can accommodate a long molecule such as an alkyl chain or a linear polymer. There are two types of cyclodextrin arrangement, called ‘‘*head-to-head*’’ and ‘‘*head-to-tail*’’. The first structure is formed by the linear arrangement of head-to-head cyclodextrin dimers. In the dimer unit, the secondary hydroxyl side of two molecules is facing each other and connected by hydrogen bonds to create a barrel-like cavity [Figure 1.4.4-B]. In the head-to-tail packing structure, cyclodextrin rings are linearly stacked and the primary hydroxyl side faces the secondary hydroxyl side of the next molecule by hydrogen bonds [Figure 1.4.4-C]. The layer-type packing structure has been sometimes observed when the guest molecule is so large that a part of the molecule cannot be accommodated within the cyclodextrin cavity. Cyclodextrin rings are arranged in a plane to make a molecular layer and two adjacent layers are shifted with respect to each other by half a molecule, showing a brick-work pattern [Figure 1.4.4-D]. Both ends of the cavity are open to an intermolecular space of the adjacent layers. A part of the guest molecule not included in the host cavity protrudes into the intermolecular space and is in contact with host molecules of the adjacent layer.

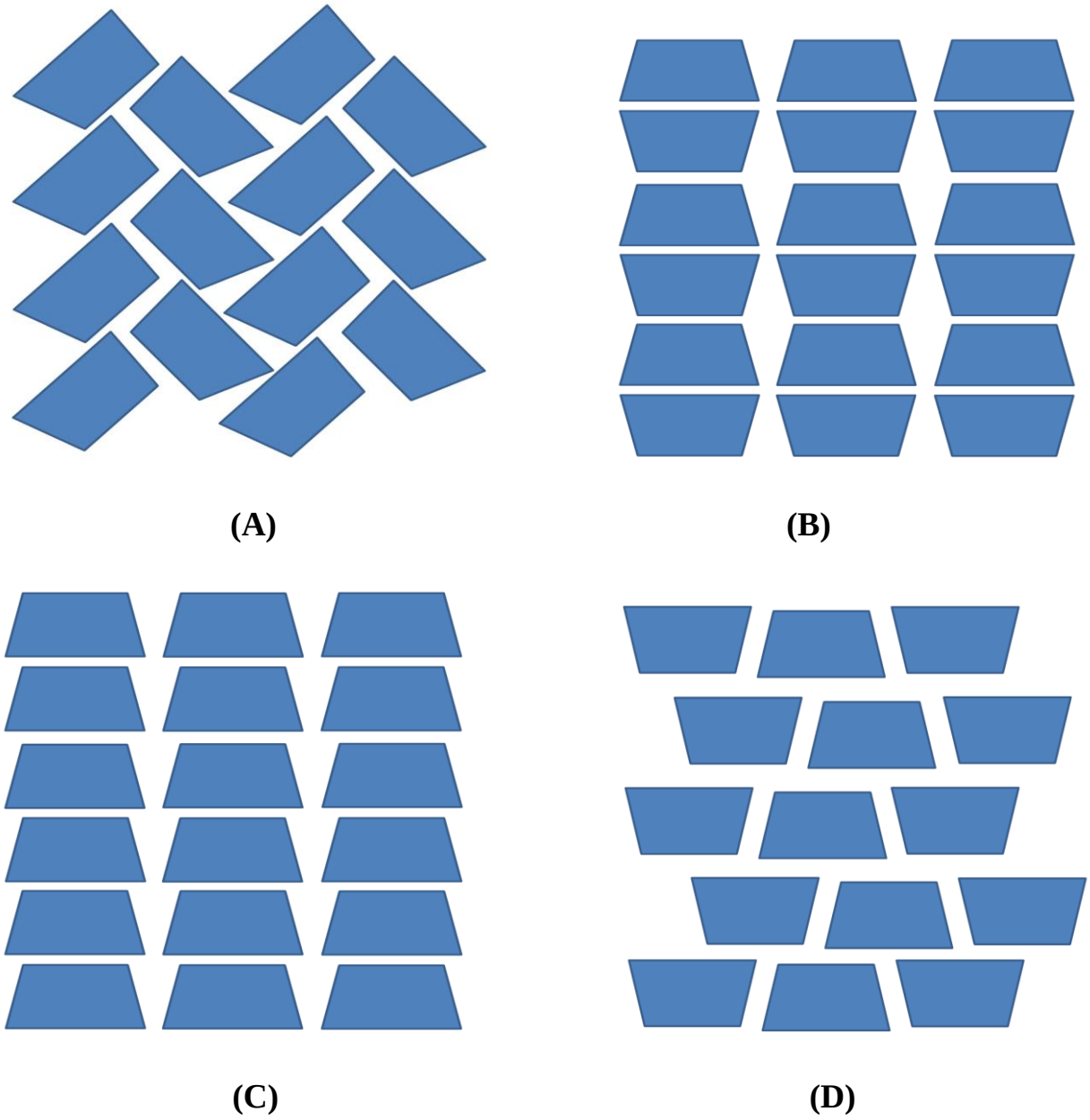

Figure 1.4.4 Schematic drawing of crystal packing: cage-type observed in the β-cyclodextrin complex with hexamethylenetetramine **(A)**, head-to-head channel-type observed in the α-cyclodextrin complex with iodine-iodide **(B)**, head-to-tail channel-type observed in sodium diclofenac **(C)** and layer-type observed in the α-cyclodextrin complex with p-nitrophenol **(D)**.

1.5 Aim and outline of this thesis

The main objective of this thesis was to design new crystal systems containing cyclodextrins in combination with:

1. Para aminobenzoic acid as a drug model to study the effect of complexation phenomena on the solubility of drugs and characterize their structure and mode of interaction by combination a theoretical and experimental approach. Despite of the existence of previous studies on the interaction between pABA and α-CD, but, to our knowledge, there are no crystal structure nor data about the effect of α-CD on the solubility of pABA. We provide here a comprehensive study from the solution to the crystalline state.

2. Potassium hydroxide to prepare cyclodextrin Metal-Organic Frameworks (CD-MOFs) formed by coordinating the cyclodextrins to potassium cation. Consequently taking the advantages of this interaction between cyclodextrin and alkali metal cation to favor formation of inclusion complexes as CD-MOFs drug carrier. In fact there are some crystal structures show metal cations coordinated by CDs, we present here an original strategy for using MOFs, based on interaction of potassium cation with CD, as a drug carrier.

3. Aegelinol, a natural product, for analytical purposes to determine the absolute configuration of this compound by formation of an inclusion complex with a host of known chirality (cyclodextrins consists of several optically active D-glucose units). This should allow direct determination of the absolute configuration of the guest (aegelinol). Many crystal structures of inclusion complexes of cyclodextrins with chiral molecules are already known, but, to our knowledge, no one used cyclodextrins as a reference to determine the absolute configuration by X-ray diffraction technique.

Single crystal X-ray diffraction technique was mainly used in this work to determine the crystal structures of the different treated systems. With regard that the preparation of suitable crystals has been performed by two different methods: crystallization by slow evaporation and crystallization by slow vapor diffusion.

The UV spectral technique was used to obtain estimates of K_c for the α-CD-pABA system. The method involves the measurement of absorbance changes of pABA in the absence and presence of α-CD. The UV spectral technique has been also used to estimate the solubility of pABA in absence and presence of α-CD by relying on the Beer-Lambert equation.

A theoretical investigation, by using Ab-initio energy minimization and semiempirical PM6 calculation has been also carried out on different pABA, α-CD and α-CD-pABA systems in order to evaluate relative stability of other stable complexes involving different forms of pABA.

1.6 References:

1. Villiers, Rend Acad. Sci. 1891, 112, 536-538.
2. F. Schardinger, Wien Klin. Wochenschr. 1904, 17, 207-209.
3. K. Freudenberg and M. Meyer-Delius, Ber. Dtsch. Chem. Ges. 1938, 71, 1596-1600.
4. French, D. and Rundle, R.E. J. Am. Chem. Soc. 1942, 64, 1651-1653.
5. K. Freudenberg, F. Cramer and H. Plieninger, German patent No. 1953, 895, 769,
6. M.L. Bender and M. Komiyama in Cyclodextrin chemistry, Springer Verlag, Berlin (D), 1978
7. J.A. Thoma and L. Steward in Starch: chemistry and technology, eds. R.L. Whistler and E.F. Paschall, Academic Press, New York (US), 1965, 1, 209.
8. F.R. Senti and S.R. Erlander in Non-stoichiometric compounds, ed. L. Mandelcorn, Academic Press, New York (US), 1964, 588-601.
9. F. Cramer and H. Hettler, Naturwissenschaften, 1967, 54, 625-632.
10. M.L. Bender and M. Komiyama in Bioorganic chemistry, ed. E.E. van Tamelen, Academic Press, New York (US), 1977, 1, 2, 19-57.
11. J. W. Steed and J. L. Atwood in Supramolecular Chemistry, 2nd edition © 2009 John Wiley & Sons, Ltd ISBN: 978-0-470-51233-3
12. D. French, Adv. Carbohydrate Chem. 1957, 12, 189-260.
13. W. Saenger, Angew. Chem. Int. Ed. Engl. 1980, 19, 344-362.
14. Szejtli, J. Past, present, and future of cyclodextrin research. Pure Appl. Chem. 2004, 76, 1825-1845,
15. Szetjli J. Downstream processing using cyclodextrins. TIBTRCH, 1989, 7, 171-174.

16. E. van Dienst in Water-soluble cyclodextrin-based host molecules, Ph.D. thesis, University of Twente (NL), 1994.
17. X. Shen, M. Belletête and G. Durocher, J. Phys. Chem. B, 1998, 102, 2502-2510.
18. J. Szetli in Cyclodextrin technology, Kluwer Academic Publishers, Dordrecht (NL), 1988.
19. K. Uekama, T. Irie, M. Sunada, M. Otagiri, K. Iwasaki, Y. Okano, T. Miyata and Y. Kasa, J. Pharm. Pharmacol. 1981, 33, 707-710.
20. K. Miyajima, M. Sawada and M. Nakagaki, Chem. Pharm. Bull. 1985, 33, 2587-2590.
21. R. Breslow, Acc. Chem. Res. 1995, 28, 146-153.
22. R. Breslow, M.F. Czarniecki, J. Emert and H. Hamaguchi, J. Am. Chem. Soc.1980, 102, 762-770.
23. G. Wenz, Angew. Chem. Int. Ed. Engl. 1994, 33, 803-822.
24. C.T. Rao and J. Pitha, Carbohydr. Res. 1991, 220, 209-213.
25. T. Lecourt, A. Herault, A. J. Pearce, M. Sollogoub, P. Sinay. Chem. Eur. J. 2004, 10, 2960-2971.
26. O. Bistri, P. Sina, J. J. Barbero, M. Sollogoub. Chem. Eur. J. 2007, 13, 9757-9774.
27. S. Guieu and M. Sollogoub. Angew. Chem. Int. Ed. 2008, 47, 7060 -7063.
28. Olivia Bistri, Pierre Sina, Jesùs Jim-nez Barbero, and Matthieu Sollogoub. Chem. Eur. J. 2007, 13, 9757- 9774.
29. Uekama, K.; Horikawa, T.; Yamanaka, M.; Hirayama, F. J. Pharm. Pharmacol. 1994, 46, 714-717
30. Hirayama, F.; Yamanaka, M.; Horikawa, T.; Uekama, K. Chem. Pharm. Bull. 1995, 43, 130-136

31. Hirayama, F.; Horikawa, T.; Yamanaka, M.; Uekama, K. Pharm. Sci. 1995, 1, 517-520
32. K.Harata, Chem.Lett. 1998, 162, 589-590
33. M.Anibarro, K.Gessler, I.Uson, G.M.Sheldrick, K.Harata, K.Uekama, F.Hirayama, Y.Abe, W.Saenger, J.Am.Chem.Soc. 2001, 123, 11854-11862.
34. M.R.Caira, G.Bettinetti, M.Sorrenti, L.Catenacci, D.Cruickshank, K.Davies, Chem.Commun, 2007, 162, 1221-1223.
35. J. Boger, R.J. Corcoran and J.-M. Lehn, Helv. Chim. Acta, 1978, 61, 2190-2218.
36. M. Born and H. Ritter, Adv. Mater. 1996, 8, 149-151.
37. J. Szetli, A. Liptak, I. Jodal, P. Fügedi, P. Nanasi and A. Neszmelyi, Stärke 1980,5, 165-169.
38. G. Wenz and B. Keller, Angew. Chem. Int. Ed. Engl. 1992, 31, 197-199.
39. I. Tabushi, Acc. Chem. Res. 1982, 15, 66-72.
40. S. Anderson, T.D.W. Claridge and H.L. Anderson, Angew. Chem. Int. Ed. Engl.1997, 36, 1310-1313.
41. K.A. Connors, Chem. Rev. 1997, 97, 1325-1358.
42. J.F. Wojcik and R.P. Rohrbach, J. Phys. Chem. 1975, 79, 2251-2253.
43. F. Cramer and F.M. Henglein, Angew. Chem. 1956, 68, 649-653.
44. M. Maciejewski, A. Gwizdowski, P. Peçzak and A. Pietrzak, J. Macromol. Sci. -Chem. 1979, A13, 87-109.
45. S. Makedonopoulou, I.M. Mavridis, K. Yannakopoulou and J. Papaioannou, Chem. Commun. 1998, 19, 2133-2134.
46. L.D. Wilsom and R.E. Verall, J. Chem. Phys. B 1998, 102, 480-488.
47. Hans-Jorgebnu Schmann and Eckhard Schollmeyer. J. Cosmet. Sci., 2002, 53, 185-191.
48. Tomoki Ogoshi and Akira Harada. Sensors, 2008, 8, 4961-4982.

49. Sanjoy Kumar Das, Rajan Rajabalaya, Sheba David, Nasimul Gani, Jasmina Khanam, Arunabha Nanda. RJPBCS, 2013, 4, 2, 1694-1720.
50. Arun Rasheed, Ashok Kumar C. K., Sravanthi V. V. N. S. S. Sci Pharm. 2008, 76, 567-598.
51. Jun Li, Xian Jun Loh. Advanced Drug Delivery Reviews, 2008, 60, 1000-1017.
52. Sergey V. Kurkov, Thorsteinn Loftsson. International Journal of Pharmaceutics, 2013, 453,167-180.
53. Eva Schneiderman, Apryll M. Stalcup. Journal of Chromatography B, 2000, 745, 83-102.
54. Dominique Duchênea, Gilles Ponchel, Denis Wouessidjewe. Advanced Drug Delivery Reviews, 1999, 36, 29-40.
55. Krzysztof Cal, Katarzyna Centkowska. European Journal of Pharmaceutics and Biopharmaceutics, 2008, 68, 467-478.
56. Lajos Szente and Jozsef Szejtli. Trends in Food Science & Technology, 2004, 15, 137-142.
57. Marcus E. Brewster, Thorsteinn Loftsson. Advanced Drug Delivery Reviews, 2007, 59, 645-666.
58. Rebecca L. Carrier, Lee A. Miller, Imran Ahmed. Journal of Controlled Release, 2007, 123, 78-99.
59. Thorsteinn Loftsson and Dominique Duchêne. International Journal of Pharmaceutics, 2007, 329, 1-11.
60. Mamata Singh, Rohit Sharma, U.C. Banerjee. Biotechnology Advances, 2002, 20, 341-359.
61. G. Astray, C. Gonzalez-Barreiro, J.C. Mejuto, R. Rial-Otero, J. Simal-Gándara. Food Hydrocolloids, 2009, 23, 1631-1640.
62. E.M. Martin Del Valle. Process Biochemistry, 2004, 39, 1033-1046.

63. Usha Rashmi Bhaskara-Amrit, Pramod B. Agrawal and Marijn M.C.G. Warmoeskerken. AUTEX Research Journal, 2011, 11, 4, 94-101.
64. G. Wenz and B. Keller, Angew. Chem. Int. Ed. Engl. 1992, 31, 197-199.
65. H. Saito, H. Yonemura, H. Nakamura and T. Matsuo, Chem. Lett. 1990, 19, 535-538.
66. S. Hamai and N. Satoh, Carbohydr. Res. 1997, 304, 229-237.
67. R.L. Schiller, S.F. Lincoln and J.H. Coates, J. Chem. Soc., Faraday Trans. 1, 1987, 83, 3237-3248.
68. W.G. Herkstroeter, P.A. Martic, T.R. Evans and S. Farid, J. Am. Chem. Soc. 1986, 108, 3275-3280.
69. S. Hamai, J. Phys. Chem. 1990, 94, 2595-2600.
70. S. Scypinski and L.J. Cline Love, Anal. Chem. 1984, 56, 322-330.
71. S. Hamai, J. Am. Chem. Soc. 1989, 111, 3954-3957.
72. S. Hamai, J. Phys. Chem. B 1997, 101, 1705-1712.
73. R.I. Gelb, L.M. Schwarz and D.A. Laufer, J. Chem. Soc., Perkin Trans. 2 1984, 15-21.
74. Ramnik Singh, Nitin Bharti, Jyotsana Madan, S. N. Hiremath. Journal of Pharmaceutical Science and Technology, 2010, 2, 171-183.
75. Martín L, León A, Martín MA, del Castillo B, Menéndez JC. J Pharm Biomed Anal, 2003, 32, 991-1001.
76. Camelia NicolecuI, Corina Aramă, Crina-Maria Monciu. FARMACIA, 2010, 58, 77-88.
77. Abd-Elgawad Radi and Shimaa Eissa. The Open Chemical and Biomedical Methods Journal, 2010, 3, 74-85.
78. Qing Lu, Jinsheng Zhao, Min Wang, Zhong Wang. Int. J. Electrochem. Sci. 2011, 6, 3868-3877.

79. Dhananjay S Ghodke, Premchand D Nakhat, Pramod G Yeole, Nilofer S Naikwade, Chandrkant S Magdum and Rohit R Shah. Iranian Journal of Pharmaceutical Research, 2009, 8, 145-151.
80. Rosa Iacovino, Jolanda Valentina Caso, Filomena Rapuano, Agostino Russo, Marina Isidori, Margherita Lavorgna, Gaetano Malgieri and Carla Isernia. Molecules 2012, 17, 6056-6070.
81. Sanghoo Lee, Soonho Kwon, Hye-Jin Shin, Eunae Cho, Kyoung-Ryul Lee, and Seunho Jung. Bull. Korean Chem. Soc. 2009, 30, 1864-1866.
82. Octavian Popescu and Aurelia Grigoriu. Cellulose Chem. Technol., 2012, 46, 295-300.
83. D.R. Alston, A.M.Z. Slawin, J.F. Stoddart and D.J. Williams, Angew. Chem. Int.Ed. Engl. 1985, 24, 786-787.
84. Y. Odagaki, K. Hirotsu, T. Higuchi, A. Harada and S. Takahashi, J. Chem. Soc. Perkin Trans. 1, 1990, 4, 1230-1231.
85. K. Gessler, T. Steiner, G. Koellner and W. Saenger, Carbohydr. Res. 1993, 249,327-344.
86. T. Steiner, G. Koellner and W. Saenger, Carbohydr. Res. 1992, 228, 321-332.
87. T.J. Brett, S. Liu, P. Coppens and J.J. Stezowski, Chem. Commun. 1999, 6, 551-552.
88. W. Saenger and T. Steiner, Acta Cryst. 1998, A54, 798-805.
89. M.M. Meier, M.T.B. Luiz, B. Szpoganicz and V. Soldi, Thermochim. Acta 2001, 375, 153-160.
90. H. Jiao, S.H. Goh and S. Valiyaveettil, Macromolecules 2002, 35, 1399-1402.
91. Carmen Rodríguez-Tenreiro, Carmen Alvarez-Lorenzo, A. Concheiro and J. J. Torres-Labandeira, Journal of Thermal Analysis and Calorimetry, 2004, 77, 403-411.

92. V.T. Yilmaz, A. Karadag and H. Içbudak, Thermochim. Acta 1995, 261, 107-118.
93. Saenger, W. (1984). Inclusion compounds. Vol. 2, Atwood, J.L.,Davies, J.E.D.D., and MacNicol, D.D.Eds., Academic Press (London), pp. 231-259.
94. Harata, K. (1991). Inclusion Compounds,Vol. 5, Atwood, J.L., Davies, J.E.D.D., and MacNicol, D.D. Eds., Oxford University Press (New York), pp. 311-344.
95. Harata, K. (1996). Comprehensive Supramolecular Chemistry, Vol. 3, Cyclodextrins. Azejtli, J. and Osa, T. Eds., Pergamon Press (UK), pp. 279-304.
96. Saenger, W., Jacob, J., Gessler, K., Steiner, T., Hoffman, D., Sanbe, H., Koizumi, K., Smith, M., and Takaha, T. Chem. Rev. 1998, 98, 1787-1802.
97. Harata, K. Chem. Rev. 1998, 98, 1803-1827.
98. James, W.J., French, D., and Rundle, R.E. Acta Crystallogr. 1959, 12, 385-389.
99. Hamilton, J.A., Steinrauf, L.K., and VanEtten, R.L., Acta Crystallogr. Sect. B, 1968, 24, 1560-1562.
100. Hybl, A., Rundle, R.E., and Williams, D.E. J. Am. Chem. Soc. 1965, 87, 2779-2788.
101. Hamilton, J.A., Sabesan, M.N., Steinrauf, L.K., and Gebbs, A., Biochem. Biophys. Res. Commun, 1976, 73, 659-664.
102. Maclennan, J.M. and Stezowski, J.J. Biochem. Biophys. Res. Commun. 1980, 92, 926-932.
103. Lindner, K. and Saenger, W. Biochem. Biophys. Res. Commun. 1980, 92, 933-938.
104. Manor, P.C. and Saenger, W. J. Am. Chem. Soc. 1974, 96, 3630-3639.
105. Chacko, K.K. and Saenger, W. J. Am. Chem. Soc. 1981, 103, 1708-1715.
106. Lindner, K. and Saenger, W. Acta Crystallogr. Sect. B, 1982 , 38, 203-210.
107. Lindner, K. and Saenger, W. Carbohydr. Res. 1982, 99, 103-115.

108. Maclennan, J.M. and Stezowski, J.J. Biochem. Biophys. Res. Commun. 1980, 92, 926-932.

109. Harata, K. Bull. Chem. Soc. Jpn. 1987, 60, 2763-2767.

110. Fujiwara, T., Tanaka, N., and Kobayashi, S. Chem. Lett. 1990, 739-742.

111. P.C.Manor, W.Saenger. J. Am. Chem. Soc. 1974, 96, 3630-3639.

112. K.Lindner, W.Saenger. Carbohydr. Res. 1982, 99, 103-115.

113. T.Fujiwara, M.Yamazaki, Y.Tomizu, R.Tokuoka, K.-I.Tomita, T.Matsuo, H.Suga, W.Saenger, Nippon Kagaku Kaishi. J. Chem. Soc. Jpn. 1983, 181-187.

114. K.Harata, Bull.Chem.Soc.Jpn. 1987, 60, 2763-2767.

115. T.Fujiwara, N.Tanaka, S.Kobayashi. Chem.Lett. 1990, 19, 738-742.

116. Endo, T., Nagase, H., Ueda, H., Kobayashi, S., and Shiro, M. Anal. Sci. 1999, 15, 613-614.

117. Jacob, J., Gebler, K., Hoffmann, D., Sanbe, H., Koizumi, K., Smith, S.M., Takaha, T., and Saenger, W. Carbohydr. Res. 1999, 322, 228-246.

118. Harata, K., Endo, T., Ueda, H., and Nagai, T. Supramol. Chem. 1998, 9, 143-150.

119. Gessler, K., Uson, I., Takaha, T., Krauss, N., Smith, S.M., Okada, S., Sheldrick, G.M., and Saenger, W. Proc. Natl. Acad. Sci. USA, 1999, 96, 4246-4251.

120. Helena Dodziuk in Cyclodextrins and Their Complexes. Copyright © 2006 WILEY-VCH Verlag GmbH & Co. KGaA, Weinheim ISBN: 3-527-31280-3.

121. Kazuaki Harata, Hiroaki Akasaka, Tomohiro Endo, Hiromasa Nagase and Haruhisa Ueda. Chem. Commun., 2002, 16, 1968-1969.

Chapter 2

Crystallographic, UV spectroscopic and computational studies of the inclusion complex of α-cyclodextrin with *p*-aminobenzoic acid.

This work has been published in part in: Supramolecular Chemistry, Vol. 24, No. 5, May 2012, 312–324
(A reprint of this work is available at the end of this thesis)

Abstract

Crystal structure of the cyclomaltohexaose (α-Cyclodextrin, α-CD) inclusion complex with ***p***-Aminobenzoic acid (pABA) has been determined by X-ray diffraction. The host:guest stoichiometry is 1:1. The pABA molecule is included in the cavity with its axis coincident with the axis of α-Cyclodextrin; the benzoic group is inserted in the cavity, while the amino group sticks out from the cavity. Four water molecules are located near the cavity rims and in interstices between molecules of α-CD participating to a dense network of intermolecular hydrogen bonds. UV-visible spectroscopy was applied to estimate the stability constant (K_c) at different temperatures on the basis of the Benesi-Hildebrand equation. This allowed calculation of complexation ΔH_c and ΔS_c on basis of the Van't Hoff equation. The results are in good agreement with the values obtained by other methods in literature. Phase solubility profiles indicate that the solubility of pABA is significantly increased in the presence of α-CD, at different pH values, and it was classified as A_L- type, indicating a 1:1 stoichiometric inclusion complex in solution. A theoretical investigation has also been carried out on the α-CD-pABA systems in order to search for other stable complexes. PM6 semiempirical calculations were performed to investigate equilibrium geometries of inclusion complexes formed between α-CD and neutral, anionic, cationic and zwitterionic

forms of pABA. Two possible orientations were considered (A, with the carboxylic end inside the cavity and B, with the amino group inside the cavity). Preference between A or B orientations of each α-CD-pABA form results from different H-bond interaction patterns.

2.1 Introduction

In pharmaceutical practice poor water solubility of drugs is a well-known problem. At present about 40% of the drugs in the development pipelines and up to 60% of the compounds coming directly from synthesis are poorly soluble [1]. To act on target receptors, drugs must generally be dissolved in the physiological fluid and thereafter absorbed through entrance ports. Various methods have been used to increase the dissolution rate including micronization, modification of the physicochemical properties of the drug, addition of water-soluble polymers or complex formation with Cyclodextrins (CDs).

4-Aminobenzoic acid (**pABA**) is an organic compound with the formula $H_2NC_6H_4CO_2H$. pABA is a white grey crystalline substance that is only slightly soluble in water. It consists of a benzene ring substituted with an amino group and a carboxyl group.

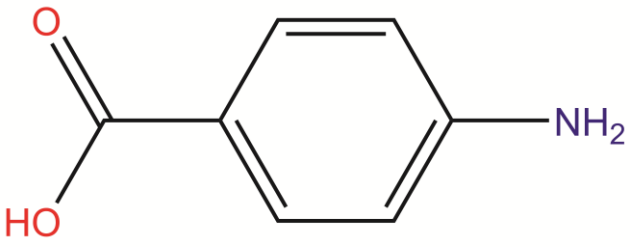

4-aminobenzoic acid (**pABA**)

In industry, pABA is prepared mainly by two routes:

1) Reduction of 4-nitrobenzoic acid and the Hoffman degradation of the monoamide derived from terephthalic acid.[2]
2) Food sources of pABA include liver, brewer's yeast (and unfiltered beer), kidney, molasses, mushrooms, and whole grains.[3]

pABA is an intermediate in the bacterial synthesis of folate. pABA has been referred to as Vitamin B_{10}.[4] Some bacteria in the human intestinal tract such as *E. coli* generate pABA from chorismate.[5-6] Humans lack the enzymes to convert pABA to folate, and therefore require folate from dietary sources such as green leafy vegetables. Although some intestinal bacteria can synthesize folate from pABA[7] and some *E. coli* can synthesize folate,[8] this requires six enzymatic activities in folate synthesis which are not all done in the same bacteria Fig 2.1.1. In humans pABA is considered nonessential and is not recognized as a vitamin [9].

Sulfonamide drugs are structurally similar to pABA, and their antibacterial activity is due to their ability to interfere with the conversion of pABA to folate by the enzyme dihydropteroate synthetase. Thus, bacterial growth is limited through folate deficiency without effect on human cells Fig 2.1.1 [10].

The potassium salt of pABA is used as a drug against fibrotic skin disorders, such as Peyronie's disease, under the trade name Potaba [11]. pABA is also occasionally used in pill form by sufferers of irritable bowel syndrome to treat its associated gastrointestinal symptoms, and in nutritional epidemiological studies to assess the completeness of 24-hour urine collection for the determination of urinary sodium, potassium, or nitrogen levels. Despite the lack of any recognized syndromes of pABA deficiency in humans, many claims of benefit are made by

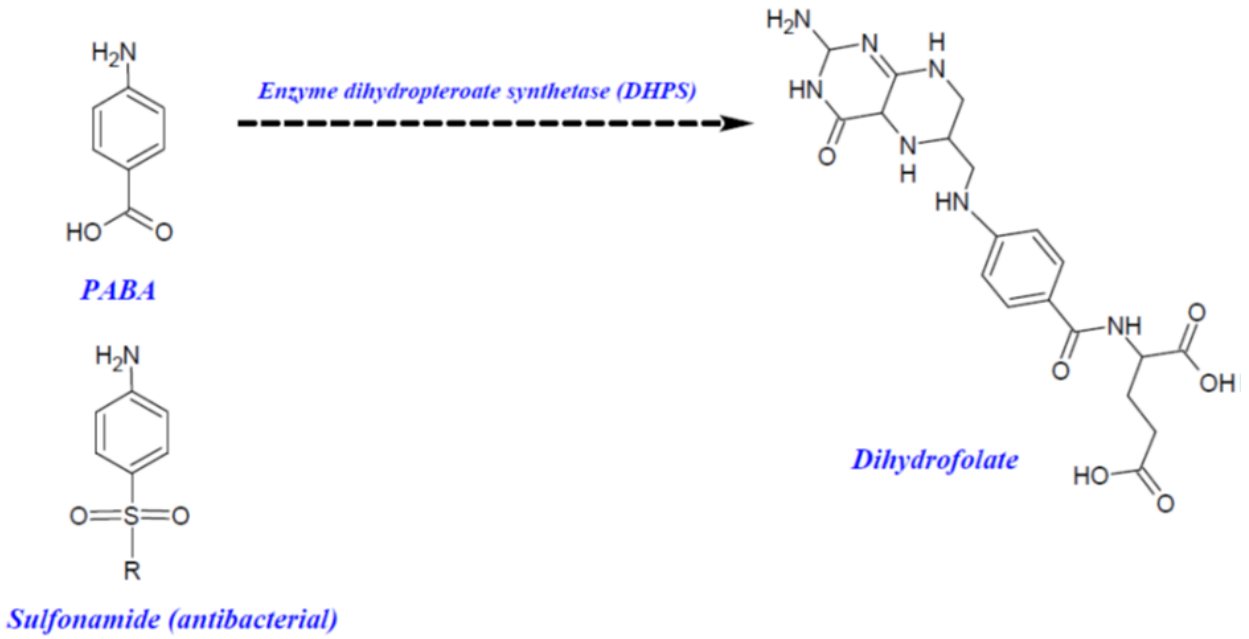

Fig 2.1.1 Synthesize folate from pABA by bacteria.

commercial suppliers of pABA as a nutritional supplement. Benefit is claimed for fatigue, irritability, depression, weeping eczema (moist eczema), scleroderma (premature hardening of skin), patchy pigment loss in skin (vitiligo), and premature grey hair.[12] It is also sometimes claimed that oral supplements of pABA can make the skin less sensitive to sun damage.

pABA mainly finds use in the biomedical sector. Other uses include its conversion to specialty azo dyes and crosslinking agents. In the past, pABA was widely used in sunscreens as a UV filter. It is a UVB absorber, meaning that it can absorb wavelengths between 290-320 nm.[13] Patented in 1943, pABA was one of the first active ingredients to be used in sunscreen.[14] The first *in vivo* studies on mice showed that pABA reduced UV damage. In addition, pABA was shown to protect against skin tumors in rodents. [15] Animal and *in vitro* studies in the early 1980s suggested pABA might increase the risk of cellular UV damage.[16] On the basis of these studies as well as problems with allergies and clothing discoloration,

pABA fell out of favor as a sunscreen. However, water-insoluble pABA derivatives such as padimate O are currently used in some products.

pABA is largely nontoxic; the median lethal dose of pABA in dogs (oral) is 2 g/kg [2]. Allergic reactions to pABA can occur. pABA is formed in the metabolism of certain ester local anesthetics, and many allergic reactions to local anesthetics are the result of reactions to pABA [17].

p-Aminobenzoic acid (pABA) crystallizes in two different polymorphic forms: the α-polymorph (The unit-cell dimensions are: a = 18.551, b = 3.860, c = 18.642 Å, β = 93.56°; Z = 8 and space group is P21/n [CSD-Code: AMBNAC01], which is the commercially available form and appears as long, fibrous needles, and the β-polymorph (The unit-cell dimensions are: a = 6.275, b = 8.550, c = 12.800 Å, and β = 108.30°; Z =4 and space group P21/c[CSD-Code: AMBNAC04] [18-22], which appears in the form of prisms [Fig 2.1.2 and Fig 2.1.3].

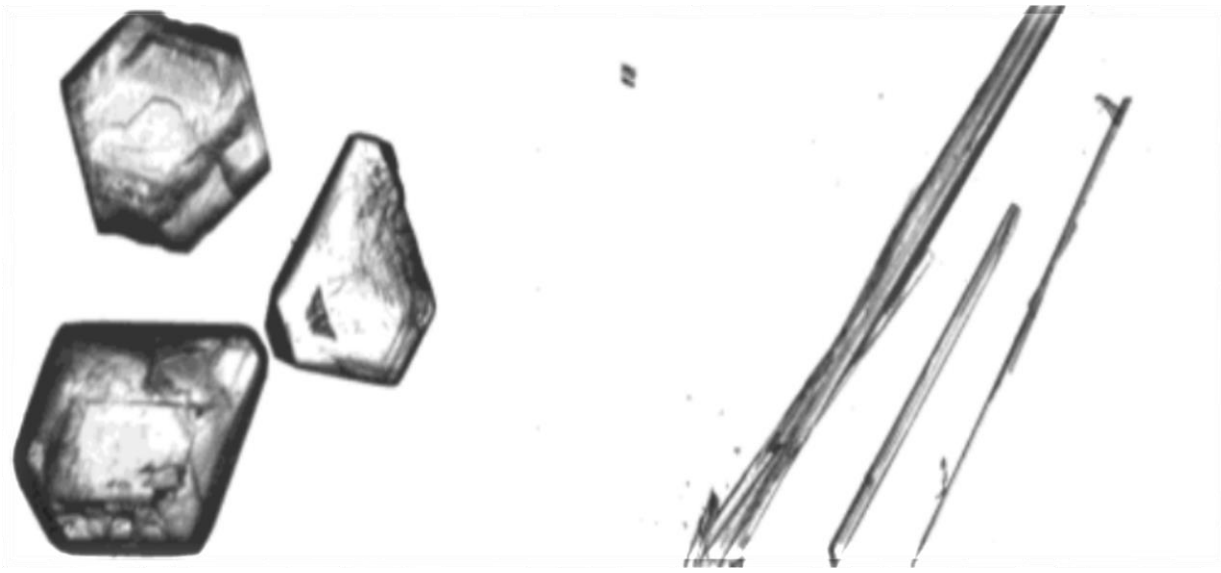

Fig 2.1.2 The prismatic crystals are the β-modification, and needles are the α-modification of pABA. [21]

The system is enantiotropic* with a transition temperature of 25 °C, below which the β-form is the stable polymorph. At the transition temperature, the enthalpy of the β-form is about 5.5 kJ/mol lower than that of the α-form, and the entropy is

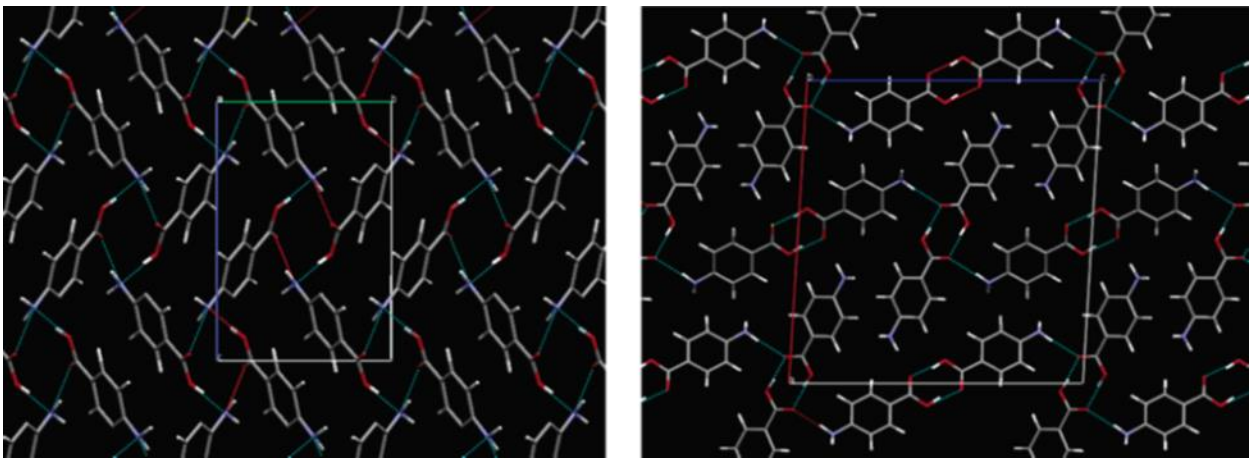

β-modificaton α-modificaton

Fig 2.1.3 Crystal structure of different polymorphic forms of pABA [21].

about 19 J/mol lower. The β-form crystals usually need hours or days to grow at the very slow cooling method, while needles usually appear easily in seconds by slow evaporation or slow cooling methods. By careful control of supersaturation and temperature, cooling crystallization can be performed to produce the pure β-form in water and in ethyl acetate. The α-form structure is governed by carboxylic acid dimers [Fig 2.1.3] and is kinetically favored since it is believed that the corresponding dimers easily form in the solution, especially in less polar solvents. The solubilities of the two forms are quite close [Table 2.1.1].[21]

*In terms of thermodynamics, there are two types of polymorphism. For a monotropic system, a plot of the free energy of the various polymorphs against temperature do not cross before all polymorphs melt, in other words, any transition from one polymorph to another will be irreversible. For an enantiotropic system, a plot of the free energy against temperature shows a crossing point before the various melting points, and it may be possible to convert reversibly between the two polymorphs on heating and cooling.

Table 2.1.1 Solubility of p-Aminobenzoic Acid, g/kg Solvent.[21]

	solubility [g/kg]							
	water				ethyl acetate			
t [°C]	β-form	SD	α-form	SD	β-form	SD	α-form	SD
−11					63.5	0.4		
−5					63.5	0.1	72.7	0.5
0					63.5	0.2	72.7	0.1
5	2.3	0.1	2.5	0.0	68.1	0.1	74.8	0.2
10	2.7	0.0	3	0.1	73.1	0.3	78.1	0.1
15	3.4	0.0	3.7	0.1	80.5	0.3	83.4	0.0
20	4.2	12.0	4.5	0.1	87.1	0.3	89.1	0.0
24	5.0	0.0	5.1	0.0	94.5	0.2	93.9	0.1
28	6.0	0.0	5.9	0.0			97.5	0.1
32	7.1	0.0	6.7	0.1			102.4	0.1
36							106.4	0.2
40	10.1	0.1	9.1	0.1				
42							120.4	0.2
45	12.6	0.2	10.9	0.2				
50			12.8	0.1			128.9	0.5

SD: standard deviation

Crystal structures of α-CD complexes with various guests have been reported [23], suggesting that a para-substituted phenol is a suitable guest for α-CD. Crystal structures of α-CD complexes with *p*-Hydroxybenzoic acid (*p*-$COOHC_6H_4OH$), *p*-Nitrophenol (*p*-$NO_2C_6H_4$-OH), *p*-Iodophenol, and *p*-Fluorophenol have been successfully determined [24-26]. A number of studies were performed on the inclusion complex of pABA with α-CD in solution using calorimetry, circular dichroism, florescence, ^{1}H NMR, fluorimetry and theoretical methods [27-35]. Complex formation of α- and β-cyclodextrins with pABA in water at 298.15 K was studied by ^{1}H NMR by Irina et al [33]. The formation of 1:1 inclusion complexes in the two systems was observed. The complex formation was shown by the changes in the chemical shifts of both host and guest. The changes were clearly observed in the chemical shifts of signals related to H(3) and H(5) protons that are located inside the macrocyclic cavity at the wider and narrow rims of

Cyclodextrins, respectively, and they are most sensitive to the inclusion process [Fig 2.1.4].

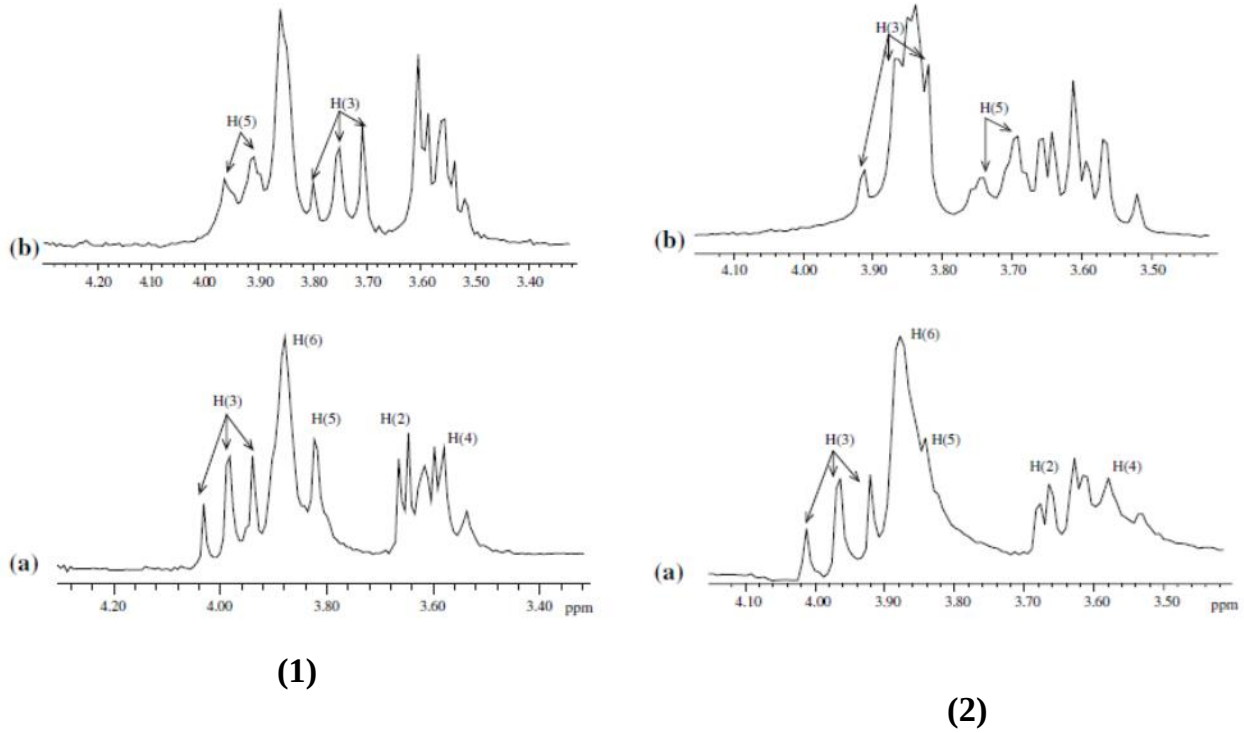

(1) **(2)**

Fig 2.1.4

1) Partial 1H NMR spectra (200 MHz, 298.15 K) of 5 mM α-CD alone (a) and in the presence of 5 mM pABA (b). [33]
2) Partial 1H NMR spectra (200 MHz, 298.15 K) of 5 mM β-CD alone (a) and in the presence of 5 mM pABA (b). [33]

Crystal structure of β-cyclodextrin complex with pABA was determined by single-crystal X-ray diffraction. The space group of the β-cyclodextrin–pABA complex is $P2_1$ with cell parameters $\boldsymbol{a}$ = 15.2196(10), $\boldsymbol{b}$ = 10.2279(7), $\boldsymbol{c}$ = 20.9321(14) Å, $\boldsymbol{\beta}$ = 110.9270(10)° and Z = 2 [CSD-Code: VOJLIQ] [35]. With a host:guest stoichiometry of 1:1.

To the best of our knowledge, no crystal structure of inclusion complex of pABA and α-CD has been reported so far. In the present study the crystal structure of the α-CD and pABA inclusion complex has been determined, UV-visible spectroscopic has been applied to determine the stability constant (K_c) and

thermodynamic parameters (ΔH_c and ΔS_c) of pABA complexation with α-CD, and a theoretical investigation has been carried out on different α-CD-pABA systems in order to evaluate relative stability of other stable complexes involving different forms of pABA.

2.2 Experimental

2.2.1 Materials

pABA (analytical reagent grade) and α-CD were purchased from Sigma-Aldrich, GmbH P.O. 1120, 89552 Steinheim, Germany. Other reagents were of analytical reagent grade and doubly distilled water was used throughout. Buffer solutions at pH=1.5, 3.5, and 6.0 were prepared by using phosphoric acid (85%) and its mono and disodium salts.

2.2.2 X-ray diffraction analysis

2.2.2.1 Crystallization

Crystals of α-CD in complex with pABA were prepared by dissolving α-CD (0.1mmol) in water (2.5 mL) at 65°C and pABA (0.1mmol) in ethanol (2.5 mL) at 65°C. Both solutions were mixed and stirred at 65°C for 6 hours. Then the mixture was stored at room temperature. Colorless crystals suitable for X-ray data collection were obtained by slow evaporation after one week.

2.2.2.2 X-ray diffraction experiment

X-ray diffraction experiment was carried out on an Oxford Gemini R Ultra using Mo K_α radiation (λ=0.71073Å) operating at 50 kV, 30 mA. A single crystal of the complex of α-CD-pABA was mounted on the head of the 4-circle kappa

goniometer. A total of 17075 unique reflections were measured in the θ-range 3.28-32.57°. Data reduction was carried out with the CrysAlisPro program [36]. Crystal data collection and refinement details are listed in Table 2.2.1. The structure belongs to the orthorhombic $P2_12_12_1$ space group with unit cell dimensions ***a*** =13.4823(3), ***b*** =15.5091(2), ***c*** =24.8256(4) Å.

2.2.2.3 Structure solution and refinement.

The structure of the complex was determined by direct methods and refined using full-matrix least-squares based on F^2 with the program SHELX [37], based on 775 parameters and 2 restraints. The refinement converged to R1 = 0.0554 for 9586 Fo > 4sig(Fo) and 0.1022 for all 17075 data. Four water molecules (two ordered and two disordered over two positions) were located in difference Fourier maps. All non-hydrogen atoms were anisotropically refined. Secondary hydroxyl groups were refined with two alternate conformations. Hydrogen atoms were calculated at ideal positions and refined using a riding model except those attached to some hydroxyl groups and on the two ordered water molecules that were located in difference Fourier maps.

2.2.2.4 Statistical search in the Cambridge Structure Database.

A statistical survey of the Cambridge Structural Database was performed searching for aromatic rings substituted by a carboxylic (-COOH), or carboxylate ($-COO^-$) group, and in its para position an amino ($-NH_2$), or ammonium ($-NH_3^+$) group. The statistical procedures used the VISTA software associated with CSD/2011 package [23]. In this study we focused on the C–O and C_{ar}–C bound lengths in carboxylic or carboxylate groups and on the C_{ar}–N bond length in amino or ammonium groups. The results were compared with the values in the crystal structure to establish the protonation state of pABA in the complex.

Table 2.2.1 Crystallographic data.

Chemical formula	$C_{36}H_{60}O_{36}.C_7H_7NO_2.4H_2O$
Formula weight ($g.mol^{-1}$)	1120.00
Temperature (K)	293(2)
Wavelength (Å)	0.71073
Crystal system	orthorhombic
Space group	$P2_12_12_1$
a (Å)	13.4823(3)
b (Å)	15.5091(2)
c (Å)	24.8256(4)
α (°)	90.000
β (°)	90.000
γ (°)	90.000
Volume ($Å^3$)	5190.99(16)
Z	4
Crystal size (mm)	0.50×0.30×0.18
Calculated density ($g.cm^{-3}$)	1.498
F(0 0 0)	2468
Theta range for data collection (°)	3.28 - 32.57
Limiting indices	$-20 \leq h \leq 17$, $-13 \leq k \leq 23$, $-37 \leq l \leq 33$
Reflections collected/unique	37378 / 17075
R (int)	0.0293
Data / restraints / parameters	17075 / 2 / 778
Goodness-of-fit (S) on F^2	0.9
Refinement method	Full-matrix least-squares on F^2
Final R indice (for 9586 with $F_0^2 > 4\sigma(F_0^2)$)	0.0553
Final R indices (all 17075data)	0.1021
Largest difference peak and hole ($e/Å^3$)	0.37 And -0.50

2.2.3 UV-visible absorption spectroscopy

UV-visible absorption spectra were recorded with a ***UVIKON XS*** spectrophotometer (Bio-TEK, Milano, Italy) at 1, 5, 10, 15, 20, 25°C using 1 cm quartz cuvettes. Temperature was controlled by a cooling jacket ***Julabo*** bath circulation thermostat (model F30-HC/8 Julabo Labortechnik, Seelback, Germany) connected to the spectrophotometer. All solutions were prepared in distilled water. The concentration of pABA was held constant at 5×10^{-5} M. The concentration of α-CD varied from 0 to 5×10^{-3} M. The pH was controlled by 0.5 M phosphate buffers. Samples were incubated inside the spectrophotometer for 30 minutes at the working temperature before recording the spectra.

2.2.4 Phase Solubility diagram

Phase-solubility diagrams allow evaluation of the affinity between α-CD and pABA in water. Phase solubility studies were performed according to the method reported by Higuchi and Connors [38]. pABA, in an amount that exceeded its solubility, was taken into a tube in which 10 ml of buffer (pH 6.0, 3.5, and 1.5) containing various concentrations of α-Cyclodextrin (0-25 mmol) were added. These tubes were sealed and shaken at 25°C for 72 hours. This amount of time is considered sufficient to reach equilibrium. Subsequently, aliquots were filtered immediately through Whattman filter paper and diluted. A portion of the sample was analyzed by UV spectrophotometer to determine the solubility of pABA by means of pABA calibration curves.

2.2.5 Computational methods

2.2.5.1 Ab initio geometry optimization

Ab-initio energy minimization was performed on pABA in different ionization forms (neutral/zwitterionic, protonated, deprotonated) to better approach geometry of the different protonation states. Calculation was done with the Gaussian09 [39] program in the ground state using the 6-311G (5d, 7f) standard basis set and the B3LYP functional density method. Resulting geometries were compared with the crystal structure data retrieved from the Cambridge Structure Database (CSD).

2.2.5.2 Semi-empirical simulation of complexes

Starting geometry for the α-CD-pABA inclusion complex was based on the crystal structure obtained in this work. In a first step, all water molecules were removed. Two possible orientations for pABA inside the α-CD cavity were simulated: in orientation A, the carboxylic group (COOH) of pABA is located inside the α-CD cavity while orientation B corresponds to the amino group (NH_2) inside the cavity [Fig 2.2.1]. Orientation B was generated by exchanging the carboxylic and amino groups from the starting X-ray crystal structure by means of the builder module (***Vega ZZ*** [40]). The final structures were saved as PDB file in order to prepare a suitable format file (***OpenBabelGUI*** [41]) to start semi-empirical **PM6*** calculation (***MOPAC2009*** [42]). The input structures were edited

*PM6 is a semi-empirical method for the quantum calculation of molecular electronic structure in computational chemistry. It is based on the Modified Neglect of Diatomic Overlap (**MNDO**), which in turn is based on the Neglect of Differential Diatomic Overlap integral approximation (**NDDO**).

$$H_f = E_{tot} + k_B T$$
$$E_{tot} = E_t + E_r + E_v + E_e$$

to adjust the protonation state of pABA: cationic form (extra H on the amino group and charge = +1), anionic form (no H on the carboxylic group and charge = -1), neutral form (protonated carboxylic group and unprotonated amine, charge = 0) and zwitterionic form (unprotonated carboxylic group and protonated amine, charge = 0)). The systems were energy optimized using the PM6 method to locate low energy structures of complexes.

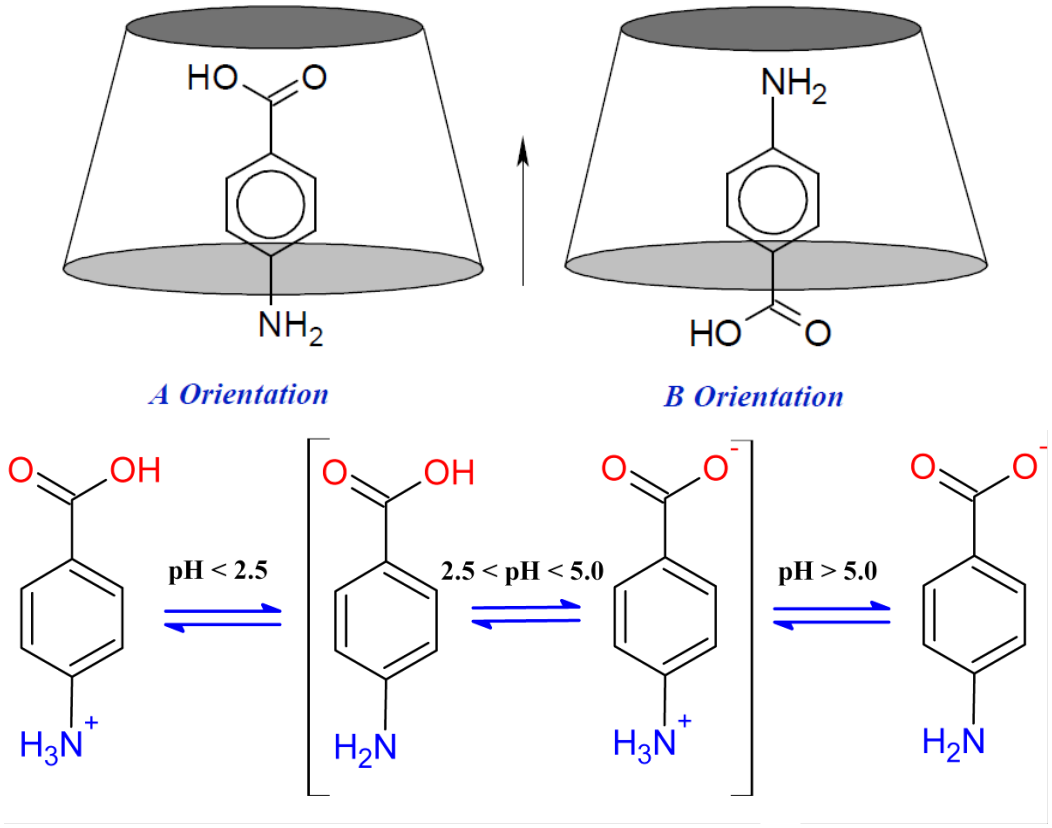

Fig 2.2.1 Two possible orientations of pABA (A and B) in α-CD (top), and pABA forms at different pH values (bottom).

2.2.5.3 Effects of solvation on simulation of complexes.

In order to study the influence of solvation on the overall stability of the complexes, all the previous starting structures (orientations A or B with the

different protonation states for pABA) were placed in a 10 Å sphere containing 66 water molecules and the same procedure of energy minimization (PM6 level) was applied on those solvated systems. [Fig 2.2.2]

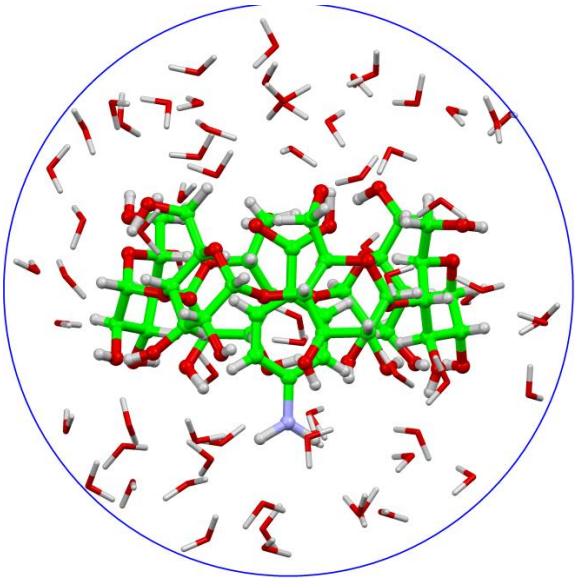

Fig 2.2.2 α-CD inclusion complex with pABA is placed in a 10 Å sphere containing 66 water molecules

2.3 Results and discussion

2.3.1 Crystal structure

The structures of the host and guest molecules are given in Fig 2.3.1. Gn denotes the n^{th} glucosidic residue of the α-CD. In our crystal structure, α-CD forms a 1:1 inclusion complex with pABA [Fig 2.3.2].

2.3.1.1 Geometry of the host molecule

All glucose residues are in the normal $^{4}C_{1}$ chair conformation, and the overall α-CD molecules show distorted hexagon geometry. The diagonal distance measured between the glycosidic oxygen atoms (O_{4n}) are $O_{41}\cdots O_{44}$ = 8.289(2), $O_{42}\cdots O_{45}$ = 8.221(2), and $O_{43}\cdots O_{46}$ = 8.931(2) Å. A similar distorted structure was

observed for other α-CD complexes with phenyl derivatives [43]. Selected geometric parameters for the α-CD host molecule are listed in Table 2.3.1.

The glycosidic O_{4n} atoms lie in a plane within 0.0752 Å, the $O_{4n}\cdots O_{4(n+1)}$ distances varying between 4.103(2) and 4.468(2) Å, and the values of the angles between $O_{4(n-1)}\cdots O_{4n}\cdots O_{4(n+1)}$ differing significantly from 120°, the ideal value for an angle in a regular hexagon. Indeed, these values range from 113.71(4)° to123.95(5)°, denoting that the cavity is distorted due to inclusion. The annular shape of α-CD is stabilized by inter-glucose hydrogen bonds connecting the secondary hydroxyl groups O_{3n} and $O_{2(n+1)}$ of the neighboring glucosidic units [Table 2.3.1] (average $O_{3n}\cdots O_{2(n+1)}$ distance 2.849(2) Å, ranging from 2.708(2) to2.984(2) Å). The orientation of the C_{6n}-O_{6n} bond is described by torsion angles

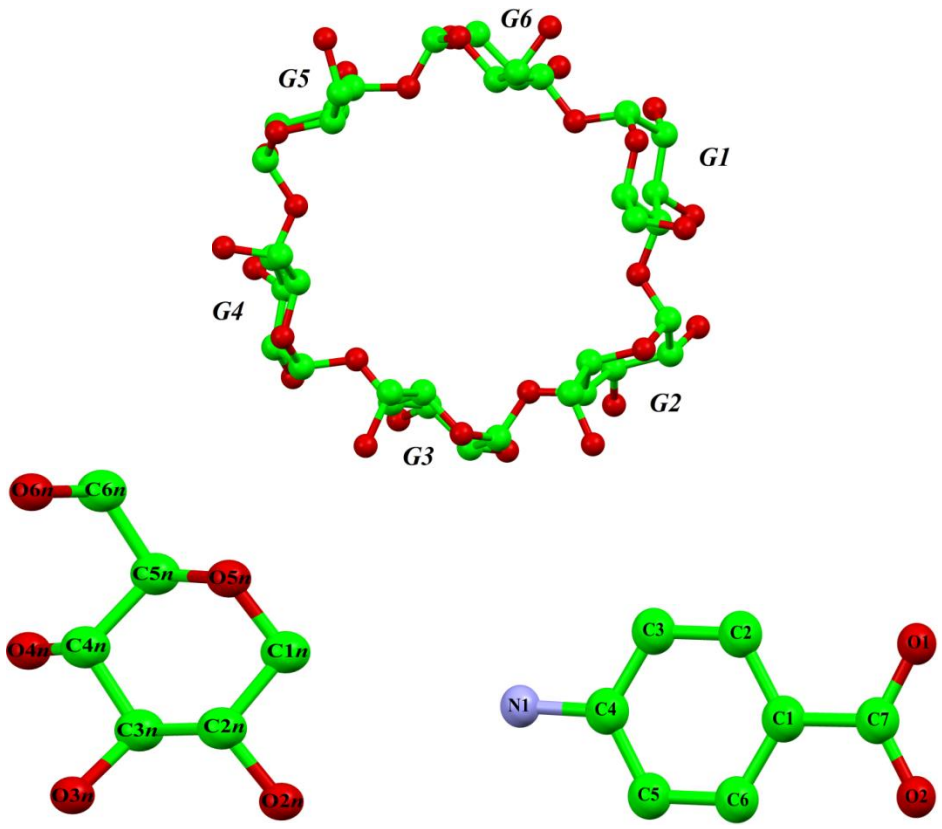

Fig 2.3.1 Structure and numbering scheme of α-Cyclodextrin and p-Aminobenzoic acid. Only numbering of one glycosidic residue (Gn) of the α-CD is presented.

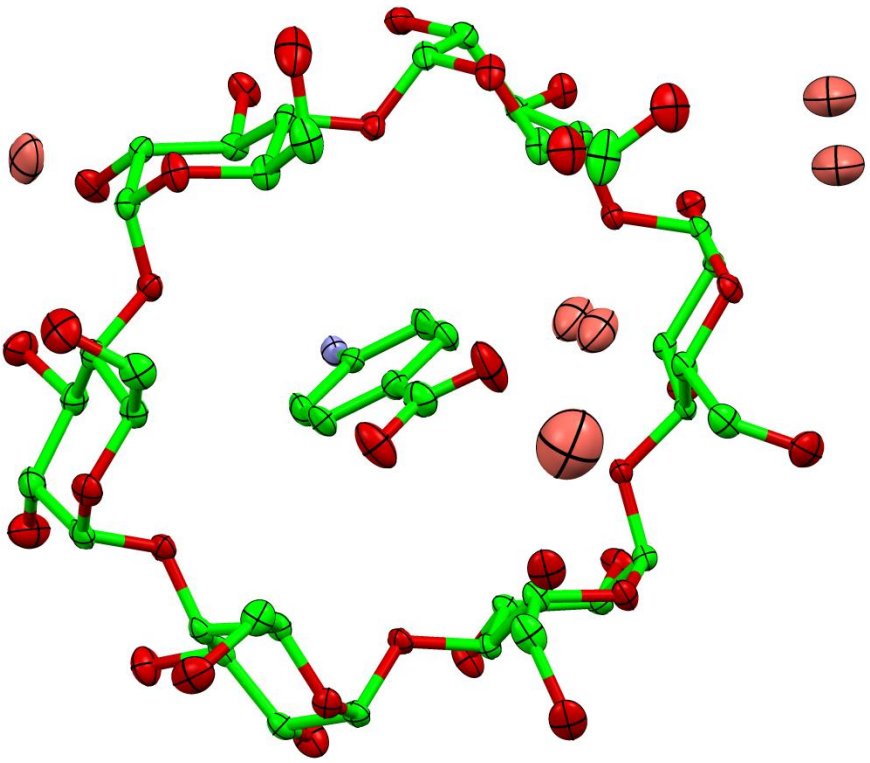

Fig 2.3.2 Axial view of the X-ray structure of the 1:1 host-guest inclusion complex of α-Cyclodextrin (α-CD) and p-Aminobenzoic acid (pABA). Water molecules are shown with light red color. Hydrogen atoms were omitted for clarify.

C_{4n}-C_{5n}-C_{6n}-O_{6n} and O_{5n}-C_{5n}-C_{6n}-O_{6n}, listed in Table 2.3.1. Most of the primary hydroxyl groups (major disordered site) adopt the gauche-gauche conformation (mean torsion angles C_{4n}-C_{5n}-C_{6n}-O_{6n} and O_{5n}-C_{5n}-C_{6n}-O_{6n} 49.9(3)° and -71.4(3)°, respectively) and point out the cavity. In G3 and G5, O_{6n} are disordered in two sites with occupancy 60:40 % in G3 and 75:25 % in G5. A gauche-trans orientation is adopted for the second site and O_{6n} points inside the cavity. Four ordered water molecules are situated outside the cavity at borders of the toroid rims and in interstices between α-CD molecules. Two water molecules, W2 and W4, are disordered in two sites with occupancy 50:50 % and 60:40 %, respectively. Table 2.3.2 lists the hydrogen bonds in this complex. No direct hydrogen bonds were found between the host and its guest.

Table 2.3.1 α-CD macrocyclic characteristics.

Residue	D [a] (Å)	φ [b] (Å)	d [c] (Å)	D [d] (Å)	Torsion angle (°) C_{4n}-C_{5n}-C_{6n}-O_{6n}	Torsion angle (°) O_{5n}-C_{5n}-C_{6n}-O_{6n}
G1	4.374 (2)	122.2 (1)	-0.098(1)	2.821(3)	42.9(3)	-78.6(3)
G2	4.194 (2)	123.9 (1)	0.050(1)	2.708(2)	49.7(3)	70.5(3)
G3	4.105 (2)	113.7 (1)	0.056(1)	2.804(2)	51.5(12) 175.9(15)	-73.0(13) 59.7(23)
G4	4.468 (2)	122.8 (1)	-0.113(1)	2.985(2)	52.4 (2)	-69.9(3)
G5	4.171 (2)	122.3(1)	0.064(1)	2.883(3)	66.2(5) -153.3(17)	-55.0(4) 84.6(28)
G6	4.149 (2)	114.6 (1)	0.040(1)	2.883(3)	46.3(3)	-75.6(3)

[a] Distance between atoms O_{4n}...$O_{4(n+1)}$.
[b] Angles between atoms $O_{4(n-1)}$…O_{4n}...$O_{4(n+1)}$.
[c] Deviations (Å) from the least-squares optimum plan of the six O_{4n} atoms.
[d] Intramolecular hydrogen-bond distance between O_{3n}…$O_{2(n+1)}$.

2.3.1.2 Geometry of the guest molecule

In the crystal structure, the anionic form of pABA is observed in the inclusion complex with α-CD. Indeed, no extra electron density peak is observed in difference Fourier maps neither close to the COO^- nor the NH_2 groups that could account for an extra H atom. Deprotonation of the carboxylic function is further established by similar values for the two C-O bond lengths (1.255(3) and 1.275(3) Å). The carboxylate and the benzene ring are coplanar with torsion angles: O_1 - C_7 - C_1 - C_2 = -0.1(5)°, O_1 - C_7 - C_1 - C_6 = -178.4 (3)°, O_2 - C_7 - C_1 - C_2 = 177.2(3)°, and O_2 - C_7 - C_1 - C_6 = -1.2(5)°. Non-hydrogen atoms in pABA lie in a plane within 0.0343 Å, favoring electronic delocalization and leading to a short C_{Ar}- C_7 distance equal to 1.473(4) Å. Delocalization is prolonged to the nitrogen atom with a short C_{Ar}-N distance equal to 1.398(3) Å, and a marked sp^2 hybridization character of the nitrogen atom with valence angles: C_4 - N_1 - H_{1N1}=104.2(3.2) °,

Table 2.3.2 Hydrogen bonds in α-CD–pABA complex with H...A < r(A) + 2.0 Å and DHA > 110°.

D-H	A	d(D-H) Å	d(H..A) Å	<DHA °	d(D..A) Å
O21-H21O	O36	0.820	2.12	155.6	2.883(3)
O21-H21O	O46	0.820	2.30	113.8	2.740(3)
O22-H22O	O24$_{i}$	0.820	1.97	163.8	2.769(2)
O23-H23O	N1$_{i}$	0.820	1.95	167.8	2.755(3)
O24-H24O	O33	0.820	2.03	156.4	2.804(2)
O25-H25O	O34	0.820	2.19	164.8	2.985(2)
O25-H25O	O44	0.820	2.33	113.7	2.762(2)
O26-H26O	O4WA$_{ii}$	0.820	2.02	158.6	2.801(6)
O26-H26O	O4WB$_{ii}$	0.820	2.34	119.8	2.839(9)
O31-H31O	O22	0.820	2.00	174.6	2.821(3)
O32-H32O	O23	0.820	1.91	166.8	2.708(2)
O33-H33O	O35$_{i}$	0.820	2.03	133.6	2.666(2)
O34-H34O	O32$_{iii}$	0.820	1.89	170.7	2.698(2)
O35-H35O	O26	0.820	2.11	157.0	2.885(3)
O36-H36O	O64$_{iv}$	0.82	2.05	176.1	2.872(3)
O61-H61O	O33$_{v}$	0.820	2.14	125.4	2.701(3)
O62-H62O	O65A$_{vi}$	0.820	2.04	172.3	2.857(4)
O62-H62O	O4WB$_{vii}$	0.820	2.63	126.0	3.179(9)
O63A-H63A	O65Av$_{iii}$	0.820	2.19	155.0	2.956(4)
O63B-H63B	O2WB	0.820	2.33	127.3	2.90(1)
O64-H64O	O36i$_{x}$	0.820	2.30	127.7	2.872(3)
O65A-H65A	O1W$_{ii}$	0.820	2.07	166.5	2.872(4)
O65B-H65B	O21$_{x}$	0.820	2.52	144.2	3.220(9)
O66-H66O	O34$_{iv}$	0.820	2.23	133.1	2.853(3)
N1-H1N1	O66$_{xi}$	0.81(5)	2.21(5)	137(5)	2.861(3)
N1-H2N1	O25$_{i}$	0.95(5)	2.09(5)	171(5)	3.032(3)
O1W-H1W1	O52	0.86(2)	2.26(3)	157(5)	3.063(3)
O1W-H1W1	O65A$_{vi}$	0.86(2)	2.48(5)	109(4)	2.875(4)
O1W-H2W1	O4WB$_{vii}$	0.82(2)	2.28(5)	125(4)	2.84(1)
O3W-H1W3	O2$_{xi}$	1.04(2)	1.73(4)	138(5)	2.601(6)
O3W-H1W3	O1$_{xi}$	1.04(2)	2.50(3)	152(4)	3.462(6)
O3W-H2W3	O2WB$_{xi}$	1.02(2)	1.49(5)	126(4)	2.248(9)
O3W-H2W3	O2WA$_{xi}$	1.02(2)	1.70(3)	158(5)	2.675(8)

Symmetry***: i*** [x-1/2, -y+1/2, -z], ***ii*** [x+1, y, z], ***iii*** [x+1/2, -y+1/2, -z], ***iv*** [-x+3/2, -y+1, z+1/2], ***v*** [-x+1/2, -y+1, z+1/2], ***vi*** [x-1, y, z], ***vii*** [-x, y+1/2, -z+1/2], ***viii*** [x-1/2, -y+3/2, -z], ***ix*** [-x+3/2, -y+1, z-1/2], ***x*** [-x+1, y+1/2, -z+1/2], ***xi*** [-x+1, y-1/2, -z+1/2].

A refers to the first occupied site of disordered ***O$_{6n}$***.

B refers to the second occupied site of disordered ***O$_{6n}$***.

C_4- N_1 - H_{2N1}= 108.7(3.7)°, and H_{1N1} - N_1 - H_{2N1}= 129.4(4.6)°.

A general search in the CSD [23] of aromatic compounds containing a carboxylic or amino group, [Fig 2.3.3], confirms that the mean C−O bond lengths in Ar-COO^- fragments (1035 fragments retrieved) are 1.255(±0.022) and 1.253(±0.028) Å, and the mean of C_{Ar} -C_{carb} bond lengths is 1.509(±0.021)Å in case of the anionic forms (deprotonated). For Ar-COOH neutral forms (1259 fragments retrieved) the bonds differ significantly with C=O and C−OH mean bond lengths of 1.227(±0.025) and 1.302(±0.025) Å, respectively, and the mean of C_{Ar} -C_{carb} bond lengths is 1.485(±0.018) Å. The mean of C_{Ar} -N bond lengths in Ar-NH2 fragments (1696 fragments retrieved) is 1.396(±0.037) Å, and the mean of valence angles around N are: CAr-N-H1=115.1(±6.5)°, CAr-N-H2=115.1(±6.2)°, and H1-N-H2=115.3(±8.4)°. In Ar-NH3+ fragments (509 fragments retrieved) the mean of CAr -N bond length is 1.465(±0.014) Å, and the mean valence angles around of N are: CAr -N-H1= 110.157(±2.596)°, CAr -N-H2= 109.906(±3.195)°, CAr -N-H3= 110.0(±2.6)°, H1-N-H2=108.8(±4.4)°, H1-N-H3=108.8(±4.4)°, and H2-N-H3=108.6(±5.8)°. The bond lengths in our crystal pABA molecule are: 1.255(3) and 1.275(3) Å for C−O in carboxylic group, 1.395(3) Å for CAr-N, and 1.472(4) Å for CAr-C, in good agreement with the values associated with an anionic form of pABA. This is further confirmed by geometries optimized ab initio (B3LYP-6-311G (5d, 7f)) and with the semiempirical PM6 method for the different protonation states of pABA: neutral, cationic, anionic, and zwitterionic form [Table 2.3.3].

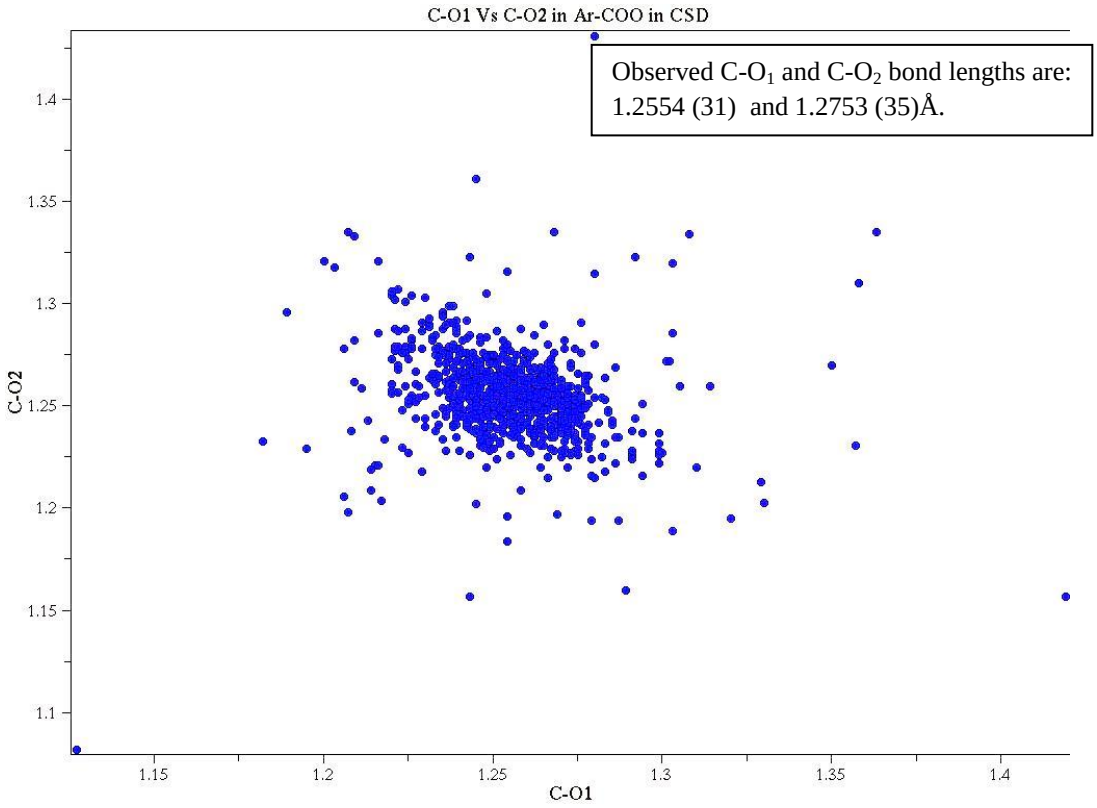
C-O1 Vs C-O2 in Ar-COO in CSD
Observed C-O1 and C-O2 bond lengths are: 1.2554 (31) and 1.2753 (35)Å.
C-O2
C-O1
1.1
1.15
1.2
1.25
1.3
1.35
1.4

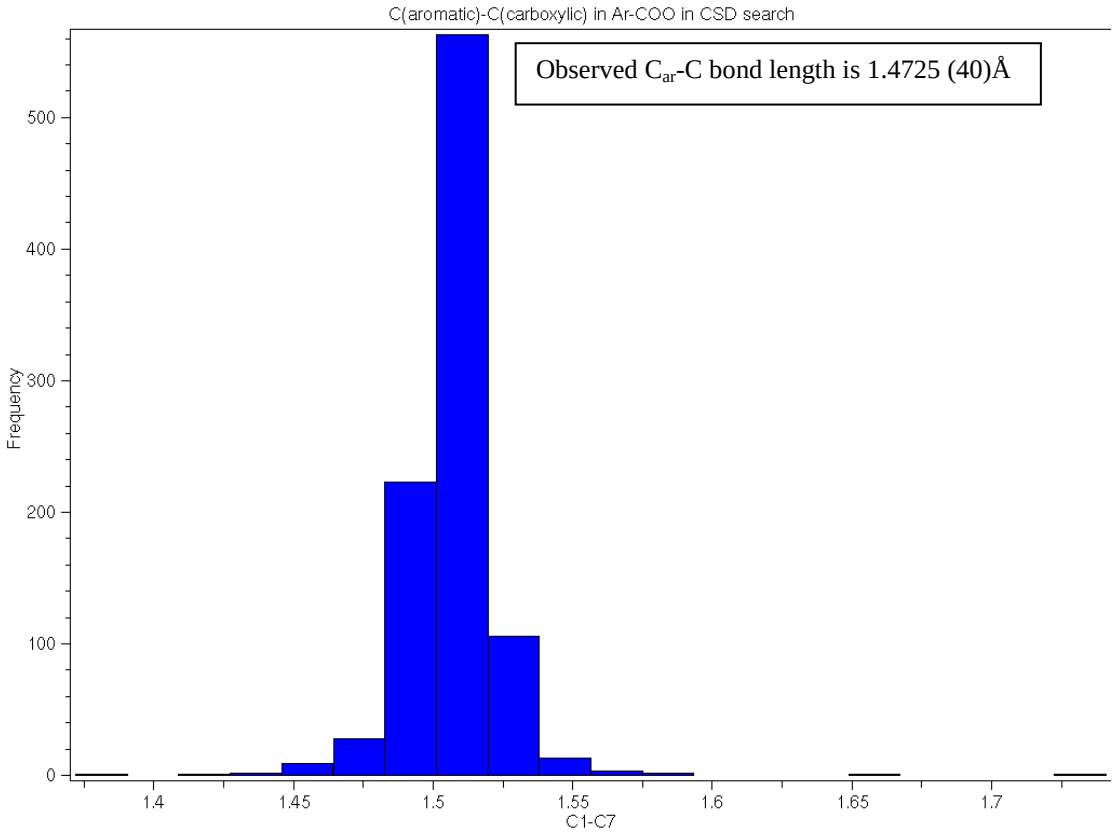
C(aromatic)-C(carboxylic) in Ar-COO in CSD search
Observed Car-C bond length is 1.4725 (40)Å
Frequency
C1-C7
0
100
200
300
400
500
1.4
1.45
1.5
1.55
1.6
1.65
1.7

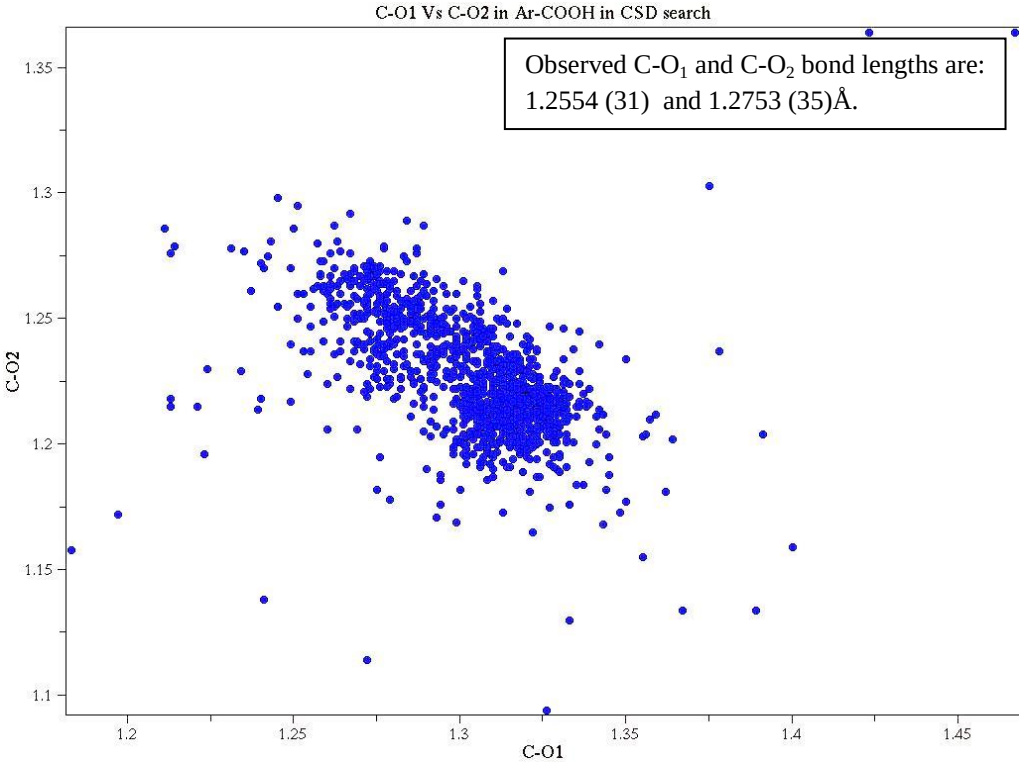
C-O1 Vs C-O2 in Ar-COOH in CSD search
Observed C-O1 and C-O2 bond lengths are: 1.2554 (31) and 1.2753 (35)Å.
C-O2
C-O1
1.35
1.3
1.25
1.2
1.15
1.1
1.2
1.25
1.3
1.35
1.4
1.45

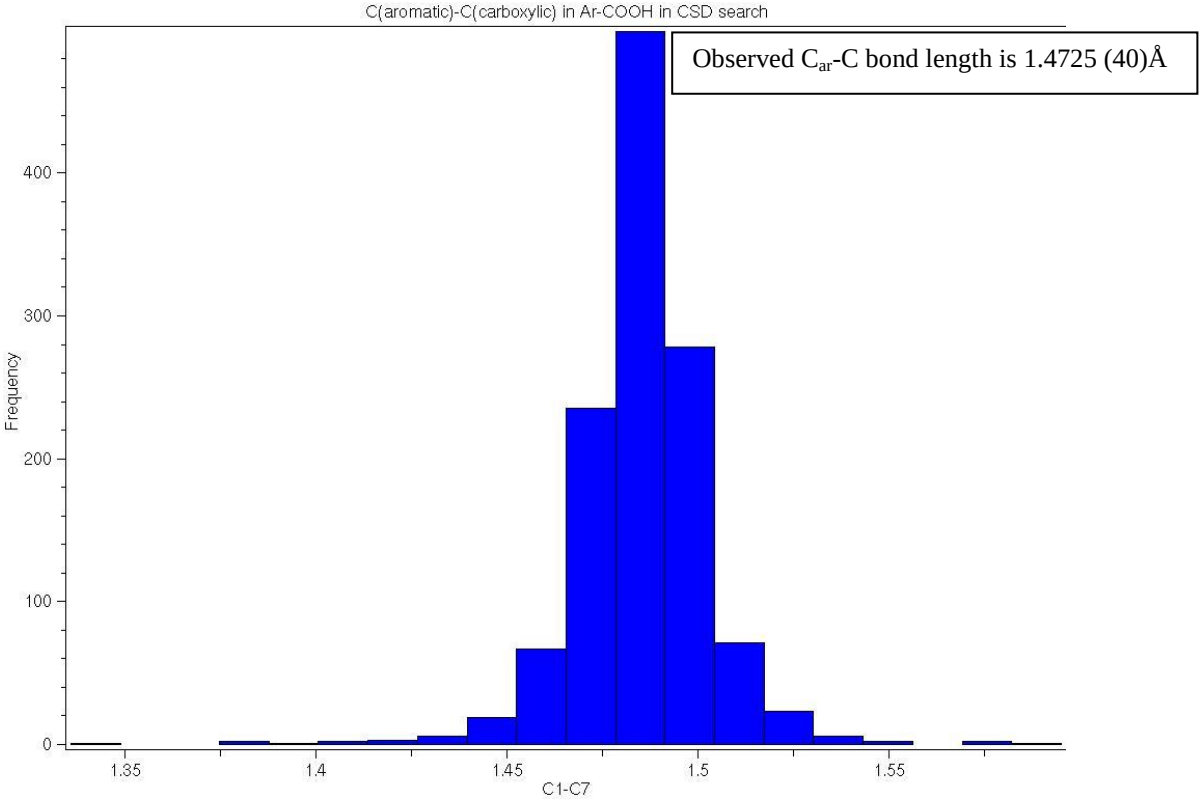
C(aromatic)-C(carboxylic) in Ar-COOH in CSD search
Observed Car-C bond length is 1.4725 (40)Å
Frequency
C1-C7
400
300
200
100
0
1.35
1.4
1.45
1.5
1.55

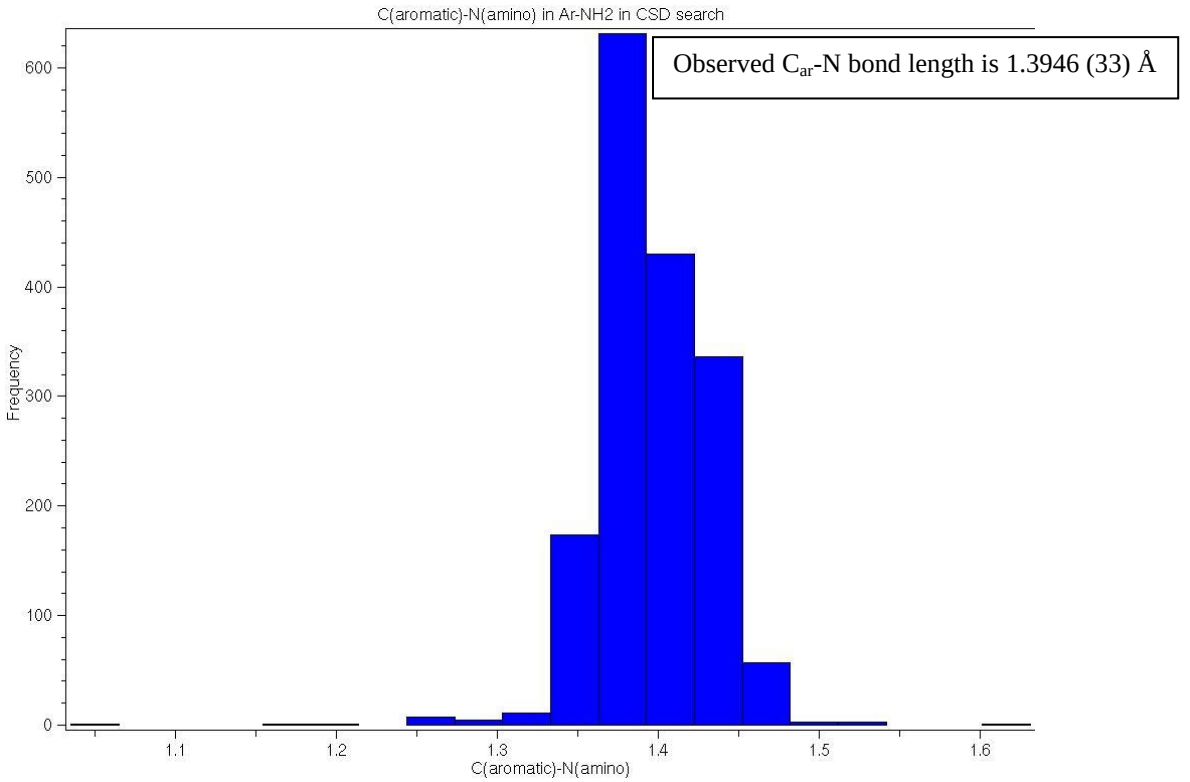

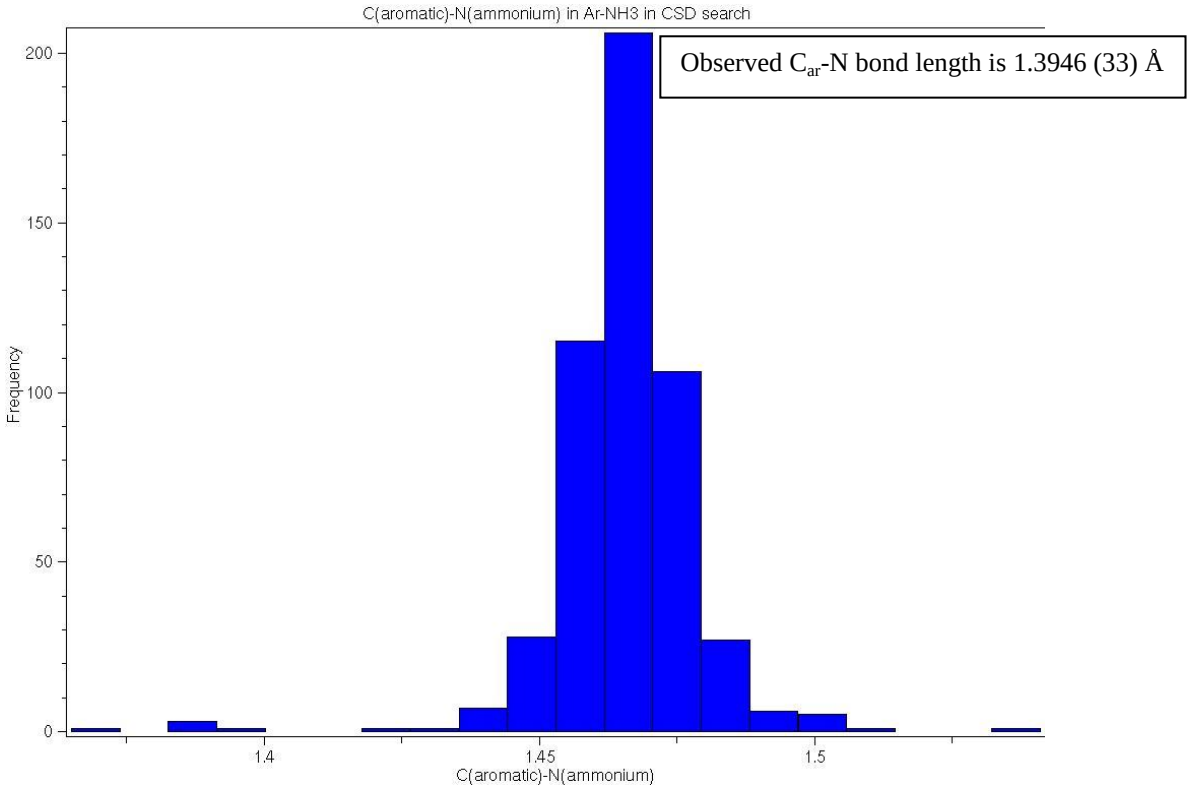

Fig 2.3.3 Results of CSD search for Ar-COO^-, Ar-COOH, Ar-NH_2, and Ar-NH_3^+.

According to the values coming from the theoretical studies and taking into account the experimental values [Table 2.3.3]; it is clear that the anionic form of pABA must be adopted in our crystal structure. This conclusion opens the question of the type and position of the counter cation. No extra electronic density was observed in difference Fourier maps that could correspond to a cation. So we suggest that one of the water molecules could be protonated to serve as a counter cation of anionic pABA.

Table 2.3.3 The bond lengths in carboxylic (or carboxylate) and amino (or ammonium) groups in different pABA form resulting from Ab-initio and PM6 minimization.

		C_7-O_1 (Å)	C_7-O_2 (Å)	C_4-N_1 (Å)	C_1-C_7 (Å)
pABA (Crystal structure)		1.2554 (31)	1.2753 (35)	1.3946 (33)	1.4725 (40)
Anionic-pABA	*Ab-initio*	1.28	1.28	1.41	1.53
	PM6	1.24	1.25	1.44	1.55
Neutral-pABA	*Ab-initio*	1.24	1.39	1.38	1.46
	PM6	1.21	1.39	1.39	1.46
Zwitterionic-pABA	*Ab-initio*	1.28	1.28	1.51	1.54
	PM6	1.23	1.23	1.50	1.56
Protonated-pABA	*Ab-initio*	1.23	1.37	1.51	1.49
	PM6	1.20	1.37	1.50	1.50

2.3.1.3 Host-Guest Interaction

In the crystal structure, pABA is deeply inserted into the cavity of α-CD, with the amino group protruding from the wide site of the cavity and the carboxyl at the narrow side as shown in Fig 2.3.2. The molecular plane of pABA forms an angle of 87.20(3)° with the plane made by the six O_{4n} atoms of the α-CD. The mass center of the aromatic ring is 1.23 Å below the mass center of the O_{4n} glycosidic atoms [Fig 2.3.4]. The corresponding values obtained from the β-CD-pABA inclusion complex are 72.3° and 1.64 Å [35]. As a consequence, the pABA

molecule better fits the α-CD cavity than the β-CD one, in agreement with results of studies in solution [28]. It is noteworthy that the location of the aromatic ring is similar in other α-CDs complexes with aromatic guests [24-26, 46-49]. This is probably due to the fact that this position is sterically favorable for the aromatic ring.

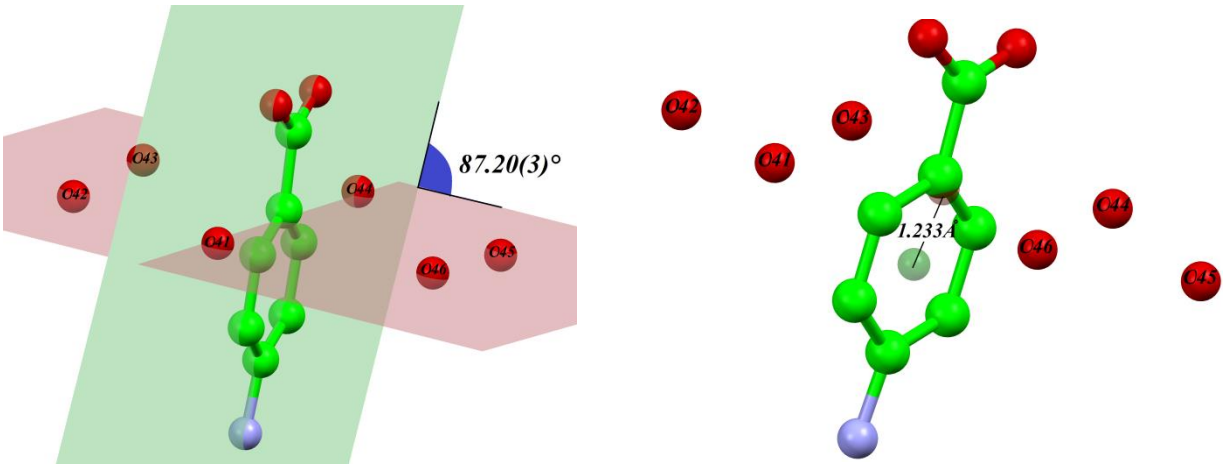

Fig 2.3.4. Definition of the angle between molecular plane of pABA (in green) and the plane made by six glycosidic oxygen atoms O_{4n} (in pink).

Host-guest interactions play a crucial role in determining the orientation of guest molecules in the cavity of α-CD [44]. In the case of the pABA-α-CD complex, the guest is held in the host cavity mainly by van der Waals contacts (with α-CD) and hydrogen bonds (mediated through water molecules). Selected observed hydrogen bonds in the complex are listed in Table 2.3.2. The bonds listed in the table are those for which the distance between the acceptor and the hydrogen atom are smaller than the radius of the acceptor atom plus 2.0 Å, and the angle between the donor atom, the hydrogen and the acceptor atom is larger than 110°.

No direct hydrogen bond is observed between α-CD and its included guest molecule. Indirect hydrogen bonds further stabilize pABA inside α-CD *via* water molecules. Additional hydrogen bonds involve the amino and carboxylic groups of

pABA and the hydroxyl groups of adjacent α-CD molecules, [Fig 2.3.5 and Table 2.3.2].

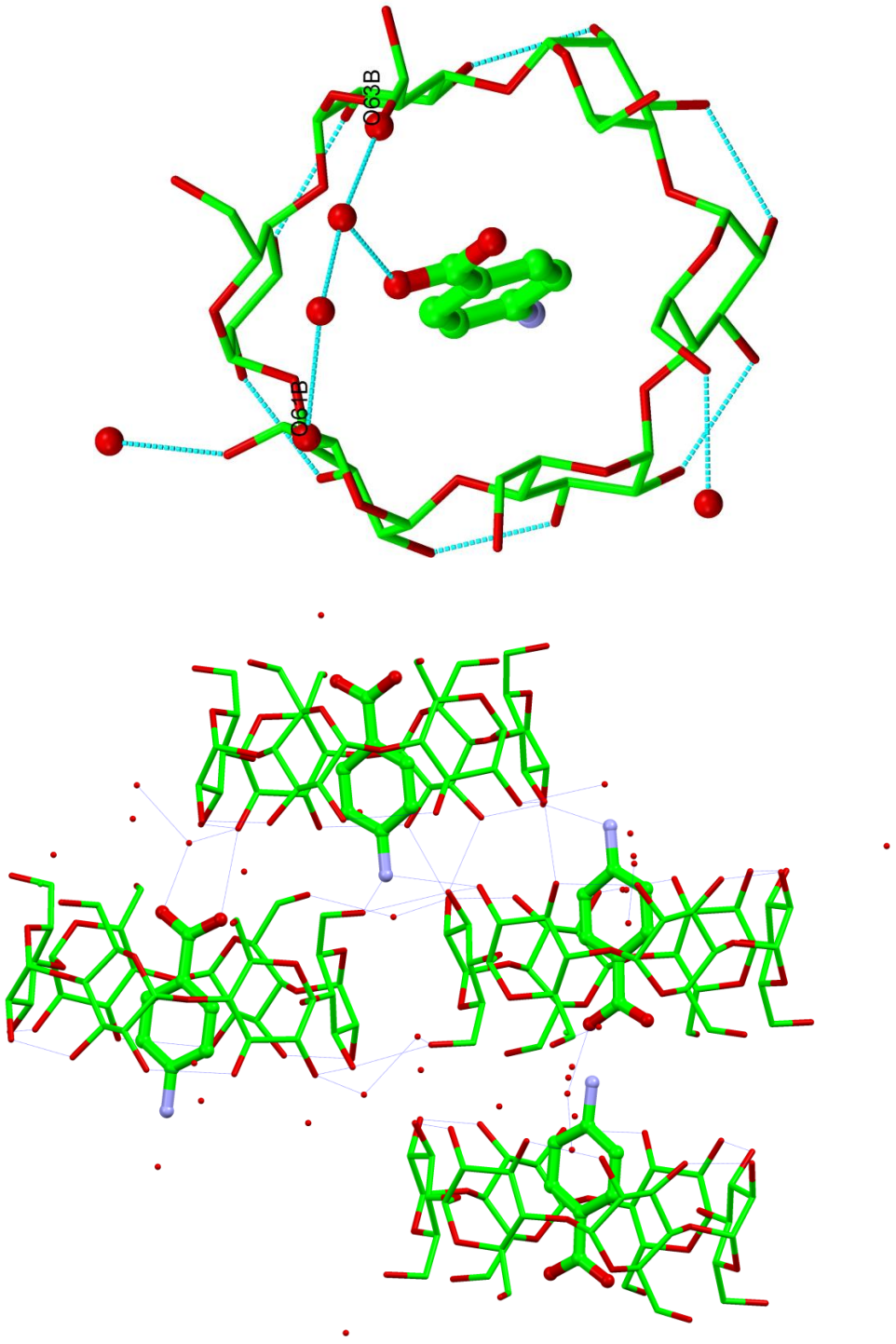

Fig 2.3.5 Hydrogen bonds network in a-CD –pABA inclusion complex.

2.3.1.4 Crystal packing

α-CDs molecules are arranged in the crystal cell nearly parallel to its ***ac*** plane, forming a molecular layer [Fig 2.3.6]. The least-squares plane through the six O_{4n} atoms forms an angle of 5.7° with respect to the *ac* plane. This crystal arrangement is different from the cage-type structure [49-53] since both ends of the cavity are open to the space between the layers. The α-CDs molecules, which lie in the next layer, are slipped so that the overlap of the annular apertures is quite small. Therefore, in this arrangement, α-CDs molecules do not form a continuous channel such as the one found in other channel type structures [45,46,55]. The guest molecules are situated nearly parallel to the ***bc*** plane. The empty space between the α-CDs molecules is filled with four water molecules. Crystal packing is further stabilized by intra-layers hydrogen bonds formed between hydroxyl groups, by the hydrogen bonds formed between the guests and hosts from different layers, and by those formed between α-CDs molecules [Fig 2.3.5].

a)

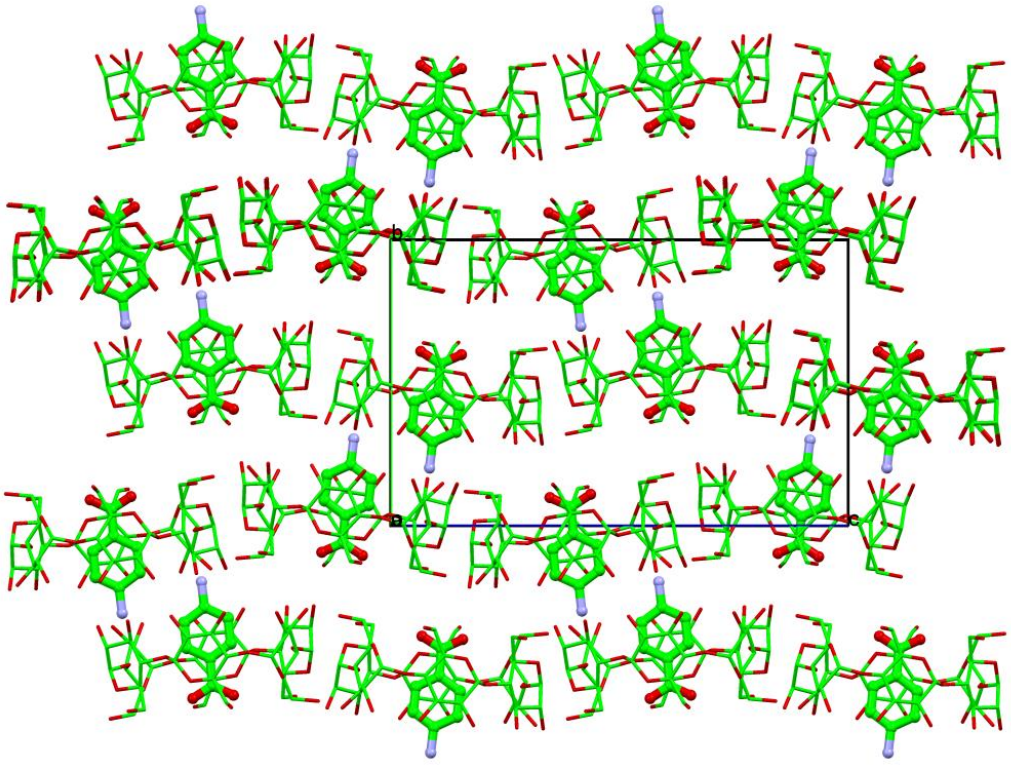

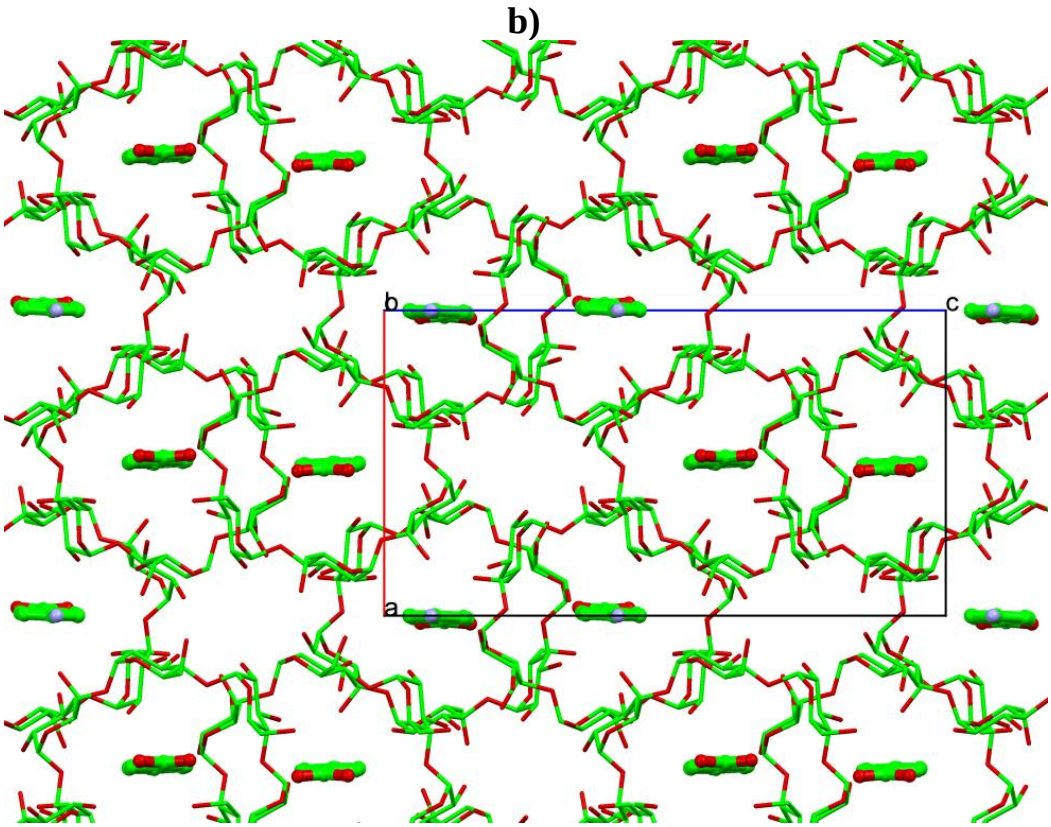

Fig 2.3.6 Drawing of the packing of the complex, viewed along the ***a*** axis (**a**) and ***b*** axis (**b**).

2.3.2 UV-Spectroscopy

Absorption spectra (between 200 and 350 nm) of pABA in presence of increasing concentrations of α-CD are shown in Fig 2.3.7. In this wavelength range, pABA exhibits two maxima (284 and 222 nm) at pH=3.5. Addition of increasing amounts of α-CD to the aqueous pABA solution resulted in a small bathochromic shift and a significant increase in the pABA absorption. These results confirm that pABA forms an inclusion complex with α-CD in solution. Inclusion of the pABA molecule into the macrocyclic cavity is accompanied by changes in its environment, causing changes in the absorption and a bathochromic shift.

In order to determine the stoichiometry and stability constant of the inclusion complex, the dependence of the pABA absorbance with respect to the α-CD

concentration was analyzed using the Benesi-Hildebrand equation [55]. Distinct equations are expected for a 1:1 (Eq. 1) or a 1:2 complex (Eq. 2) between pABA and α-CD.

$$A = A_0 + \frac{\Delta\varepsilon . K_{(1:1)} . C_{pABA} . [C_{\alpha - CD}]}{1 + K_{(1:1)} . C_{pABA}} \quad ....(1)$$

$$A = A_0 + \frac{\Delta\varepsilon . K_{(2:1)} . C_{pABA} . [C_{\alpha - CD}]^2}{1 + K_{(2:1)} . C_{pABA}} \quad ....(2)$$

Where

- A and A_0 are the absorption of pABA in presence and absence of α-CD, respectively;
- $\Delta\varepsilon = \varepsilon_{CD.pABA} - \varepsilon_{pABA}$ is the difference in the molar absorptivities between free and complexed pABA;
- C_{pABA} and $C_{\alpha\text{-CD}}$ are the initial concentrations of pABA and α-CD, respectively;
- $K_{(1:1)}$ is the stability constant of the 1:1complex.
- $K_{(2:1)}$ is the stability constant of the 2:1complex.

These equations can be rewritten in more useful forms (Eq. 3 and 4) which show a linear relationship between $\frac{1}{\Delta A}$ and $\frac{1}{C_{\alpha - CD}}$ in the case of a 1:1 complex.

$$\frac{1}{\Delta A} = \frac{1}{\Delta\varepsilon \times K_{(1:1)} \times C_{pABA}} \cdot \frac{1}{[C_{\alpha - CD}]} + \frac{1}{\Delta\varepsilon \times C_{pABA}} \quad ....(3)$$

$$\frac{1}{\Delta A} = \frac{1}{\Delta\varepsilon \times K_{(2:1)} \times C_{pABA}} \cdot \frac{1}{[C_{\alpha - CD}]^2} + \frac{1}{\Delta\varepsilon \times C_{pABA}} \quad ....(4)$$

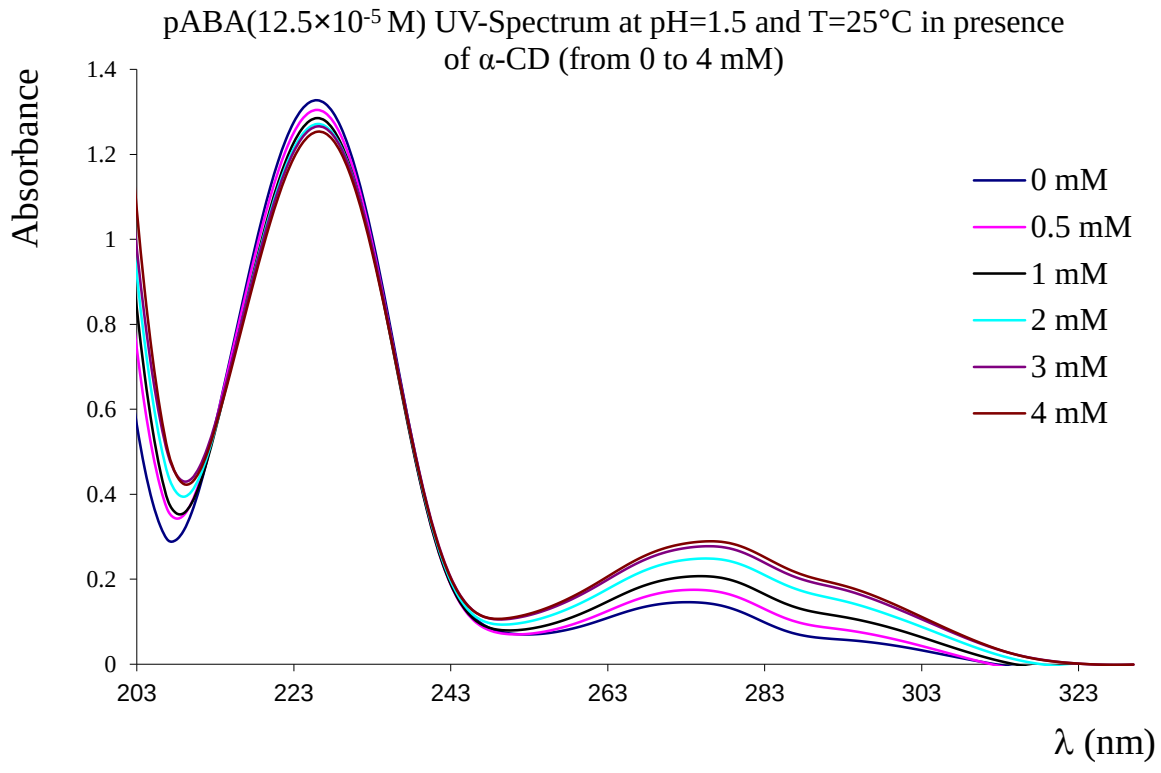
pABA(12.5×10-5 M) UV-Spectrum at pH=1.5 and T=25°C in presence of α-CD (from 0 to 4 mM)
Absorbance
1.4
1.2
1
0.8
0.6
0.4
0.2
0
203
223
243
263
283
303
323
λ (nm)
0 mM
0.5 mM
1 mM
2 mM
3 mM
4 mM

a)

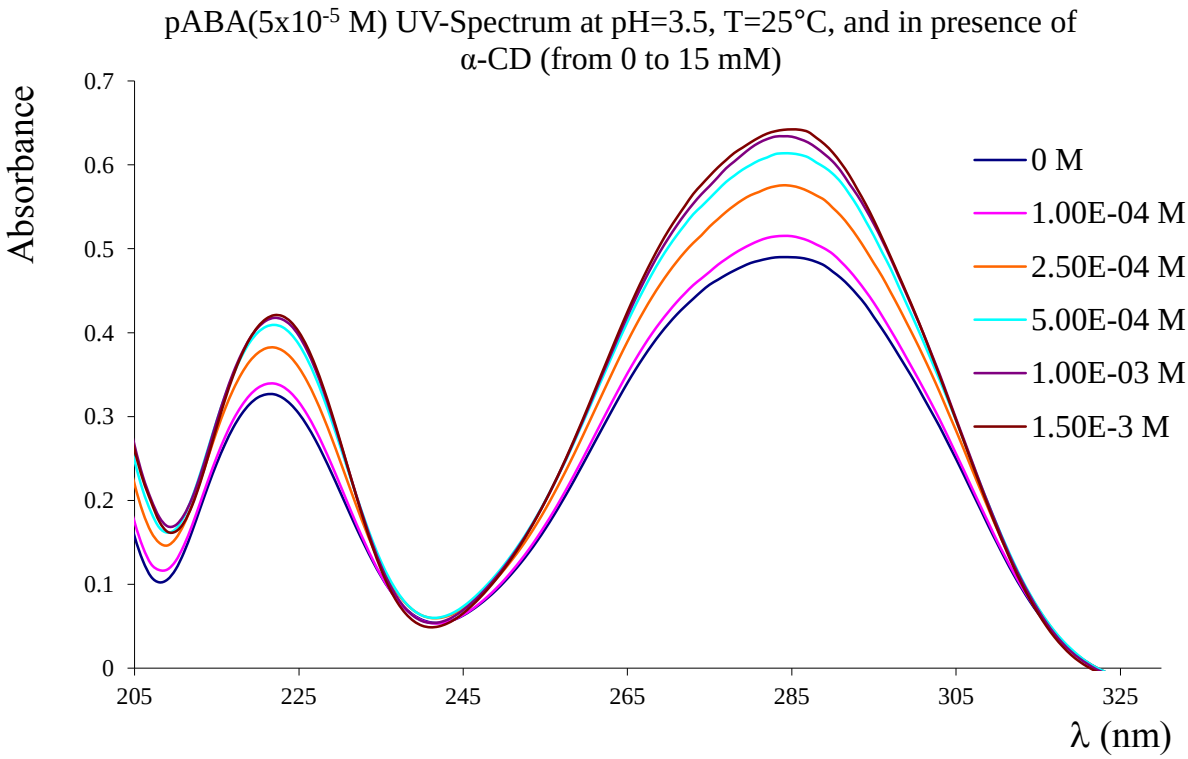
pABA(5x10-5 M) UV-Spectrum at pH=3.5, T=25°C, and in presence of α-CD (from 0 to 15 mM)
Absorbance
0.7
0.6
0.5
0.4
0.3
0.2
0.1
0
205
225
245
265
285
305
325
λ (nm)
0 M
1.00E-04 M
2.50E-04 M
5.00E-04 M
1.00E-03 M
1.50E-3 M

b)

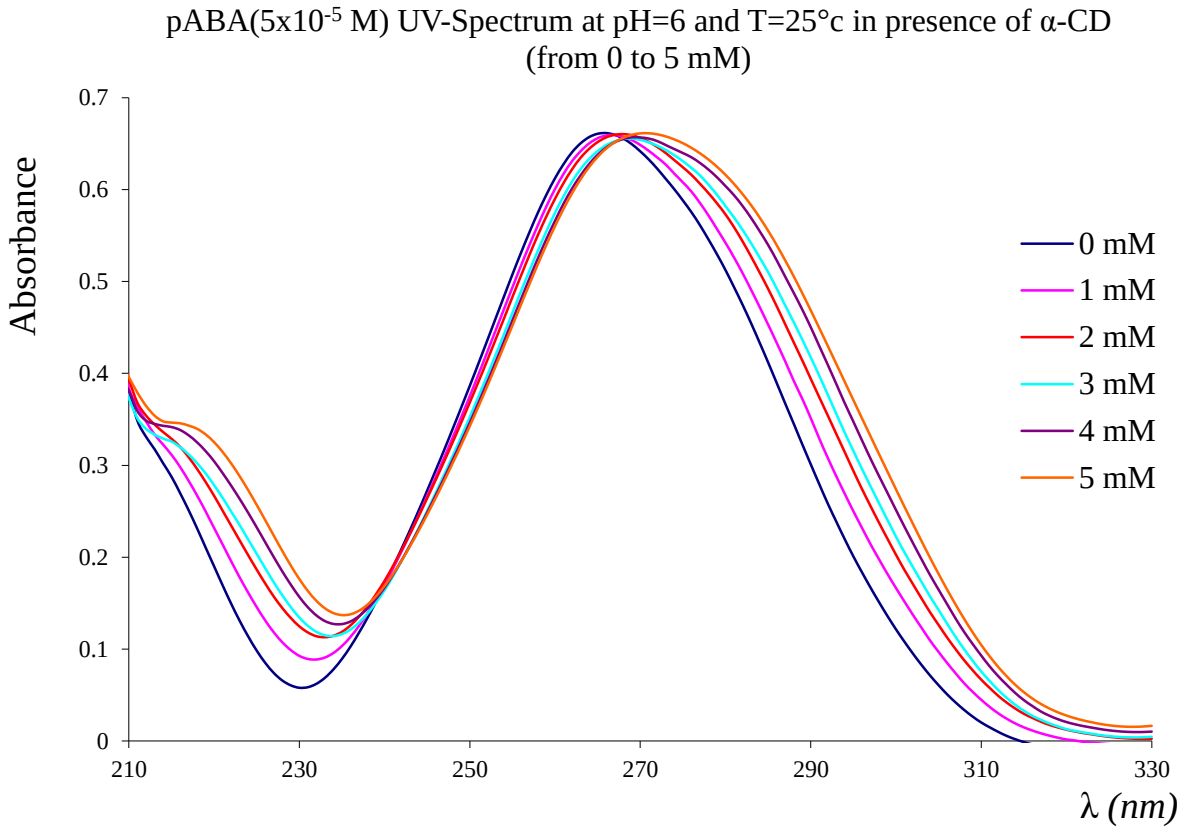

c)

Fig 2.3.7 Absorption spectra of pABA: **a)** 12.5 $\times 10^{-5}$ at pH=1.5, **b)** 5×10^{-5} M at pH=3.5, **c)** 5×10^{-5} M at pH=6.0, in absence and presence of different concentrations of α-CD.

In the case of pABA, stability constants of the complex were determined by measuring the change in maximum absorption of pABA (at ~280 and ~220 nm), ΔA, in the presence of increasing concentrations of α-CD. The dependency of ΔA on the α-CD concentration is shown in Fig 2.3.8. The data could be fitted to equation 3 corresponding to a 1:1 stoichiometry. From these data, complexation constant, K_c, of pABA by α-CD is estimated to 2319.4±241.0 and 596.0±80.5 M^{-1} at pH=3.5 and 1.5 respectively at T= 25°C. Values of 1400±35 and 1000±148 M^{-1} were obtained at pH=3.5 and 2.0 (T=20°C), respectively, by fluorescence method [56].

Repeating the same procedure at different temperatures (4, 10, 15, 20, and 25°C) showed that the stability constant increases with decreasing temperature Table 2.3.4.

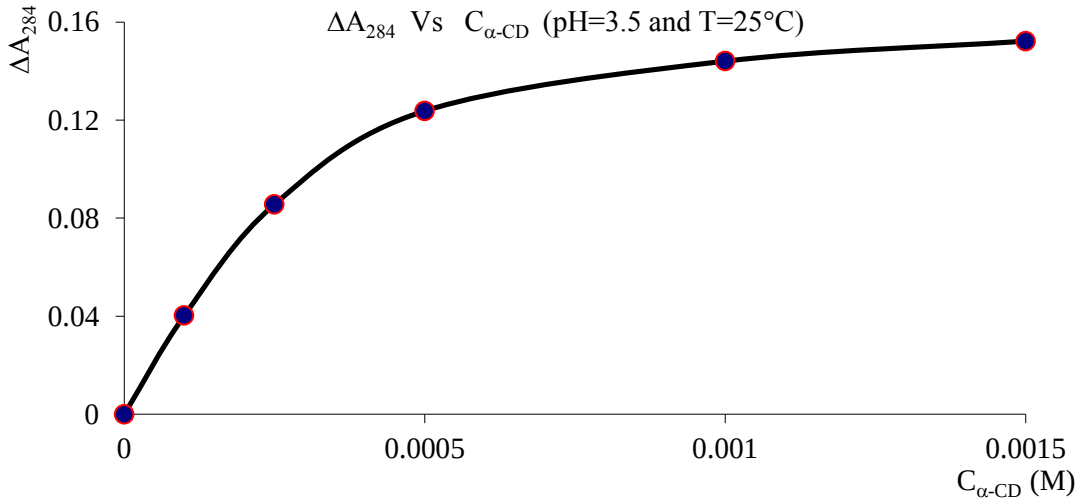

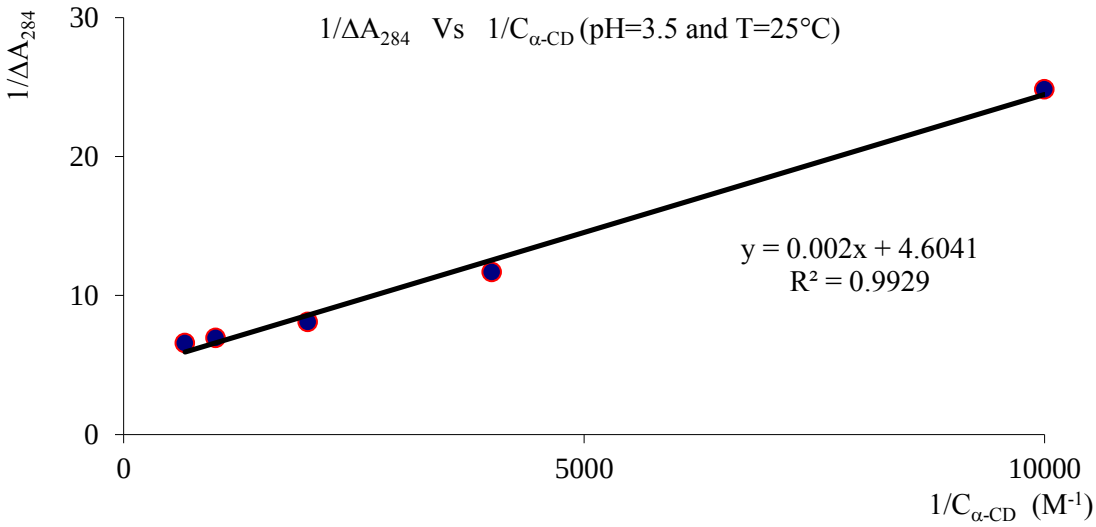

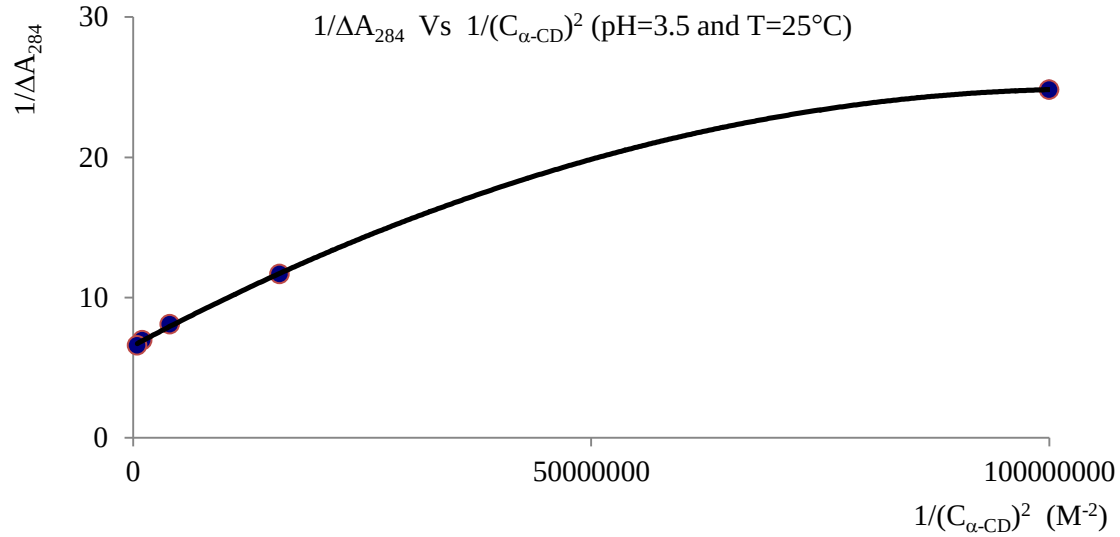
1/ΔA284 Vs 1/(Cα-CD)2 (pH=3.5 and T=25°C)
1/ΔA284
30
20
10
0
0
50000000
100000000
1/(Cα-CD)2 (M-2)

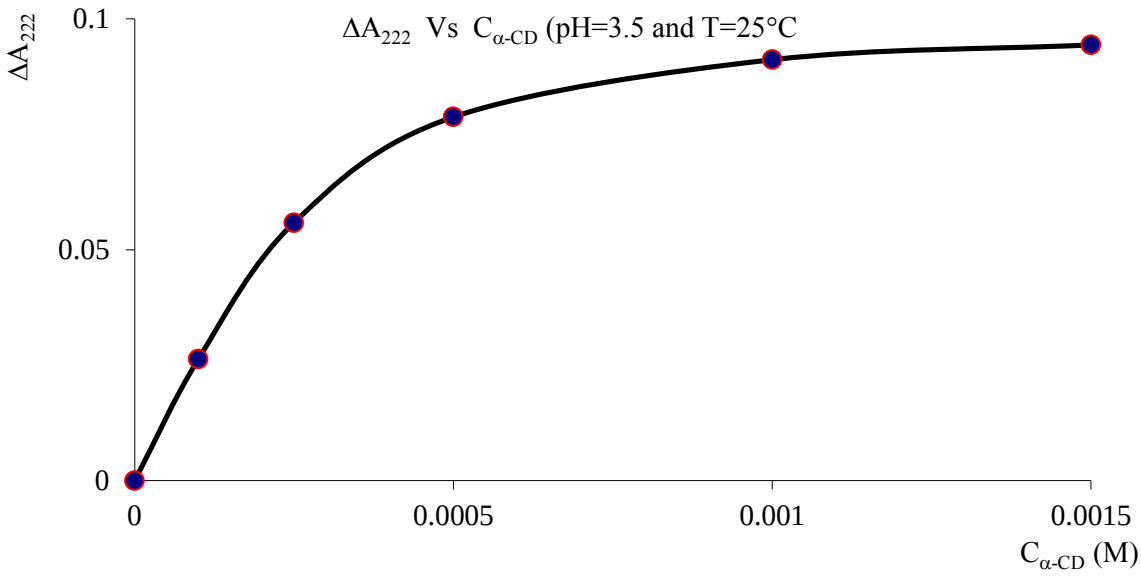
ΔA222 Vs Cα-CD (pH=3.5 and T=25°C
ΔA222
0.1
0.05
0
0
0.0005
0.001
0.0015
Cα-CD (M)

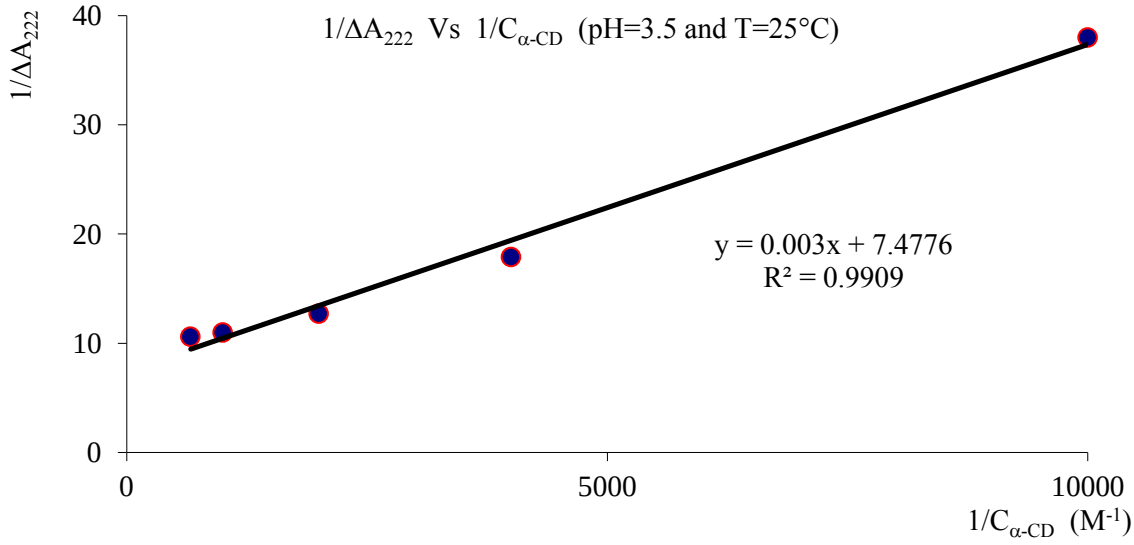
1/ΔA222 Vs 1/Cα-CD (pH=3.5 and T=25°C)
1/ΔA222
40
30
20
10
0
y = 0.003x + 7.4776
R² = 0.9909
0
5000
10000
1/Cα-CD (M-1)

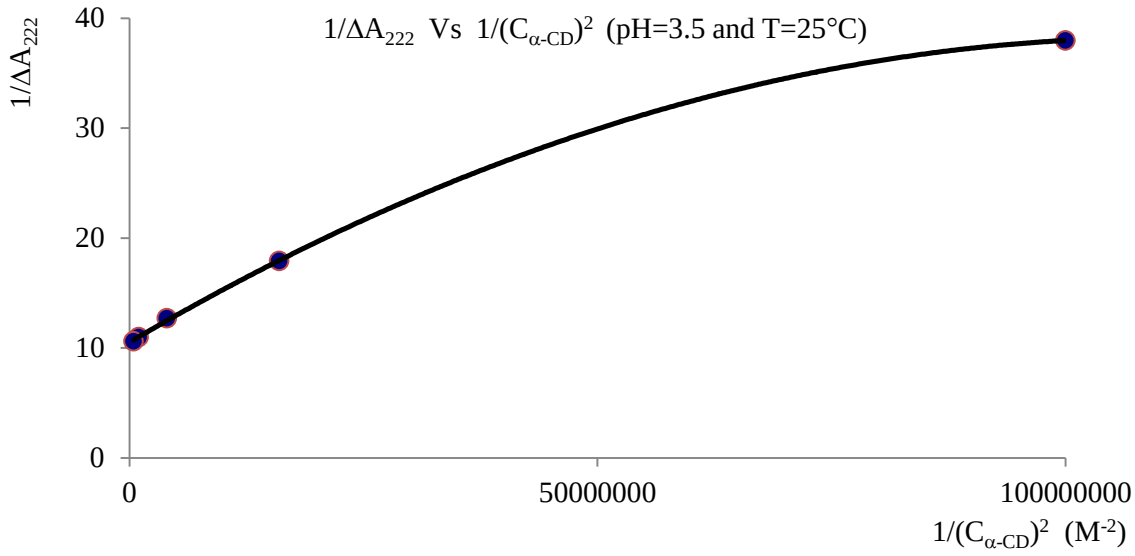
1/ΔA222 Vs 1/(Cα-CD)2 (pH=3.5 and T=25°C)
1/ΔA222
40
30
20
10
0
0
50000000
100000000
1/(Cα-CD)2 (M-2)

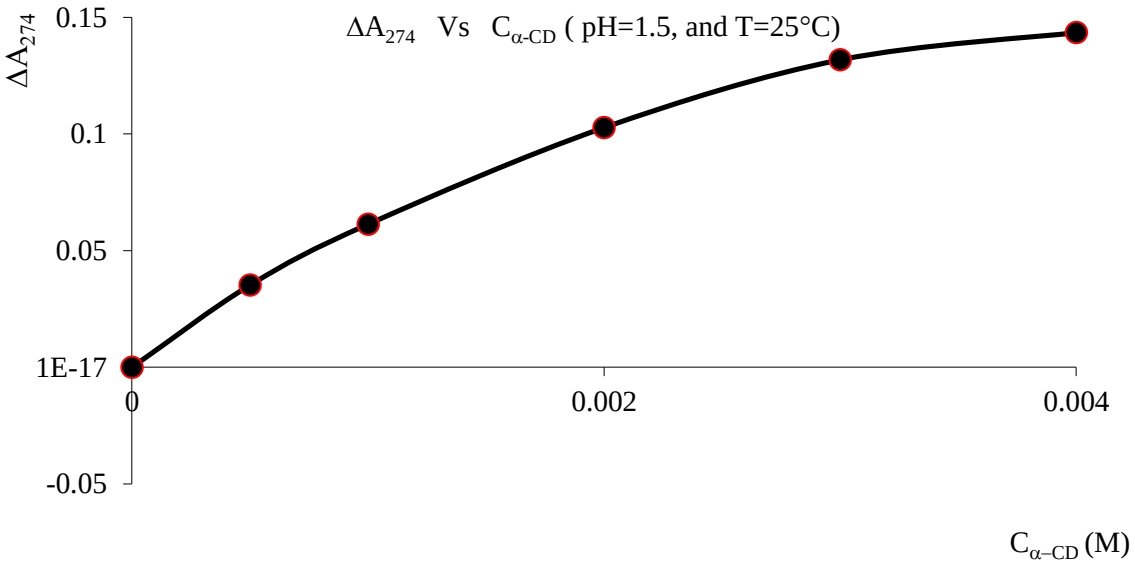
ΔA274 Vs Cα-CD (pH=1.5, and T=25°C)
ΔA274
0.15
0.1
0.05
1E-17
-0.05
0
0.002
0.004
Cα–CD (M)

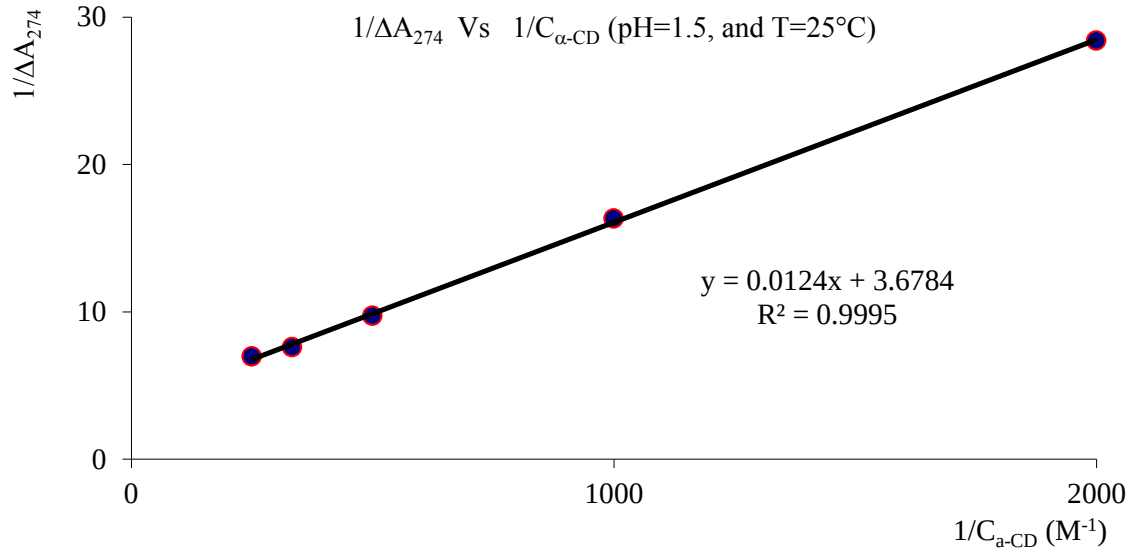
1/ΔA274 Vs 1/Cα-CD (pH=1.5, and T=25°C)
1/ΔA274
30
20
10
0
y = 0.0124x + 3.6784
R² = 0.9995
0
1000
2000
1/Ca-CD (M-1)

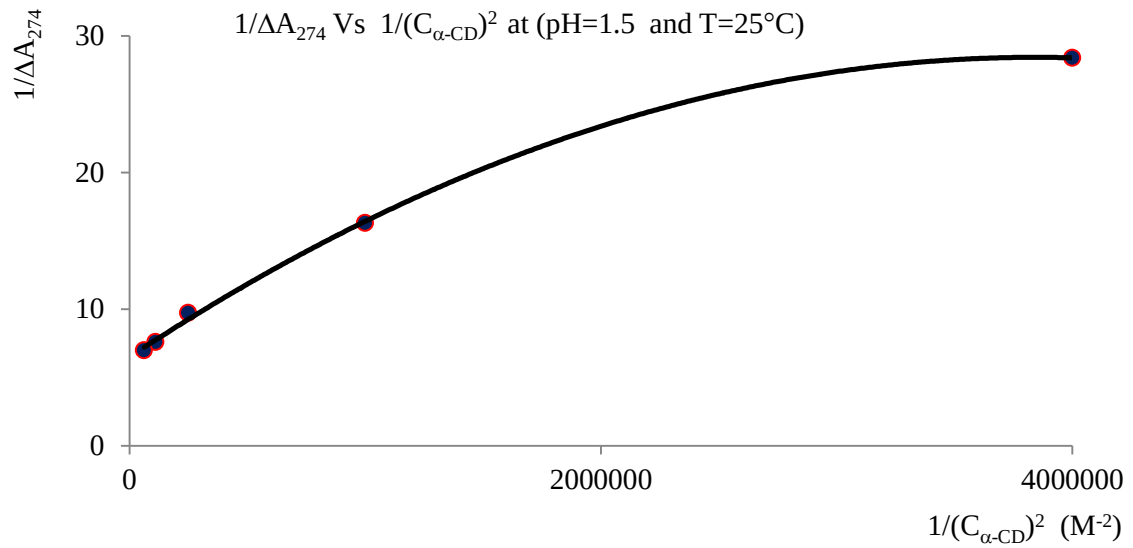
1/ΔA274 Vs 1/(Cα-CD)2 at (pH=1.5 and T=25°C)
1/ΔA274
30
20
10
0
0
2000000
4000000
1/(Cα-CD)2 (M-2)

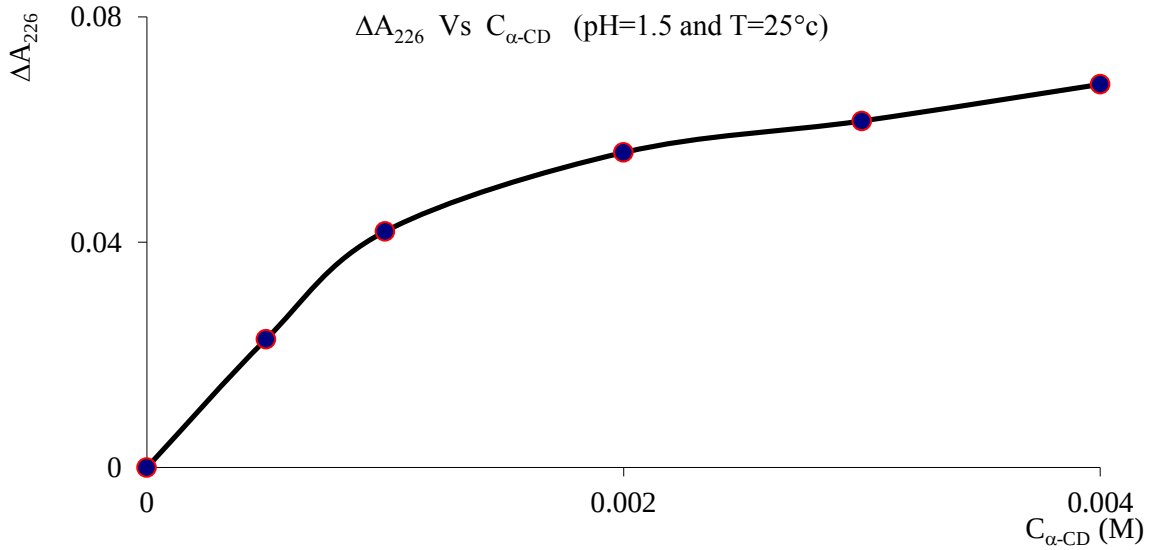
ΔA226 Vs Cα-CD (pH=1.5 and T=25°c)
ΔA226
0.08
0.04
0
0
0.002
0.004
Cα-CD (M)

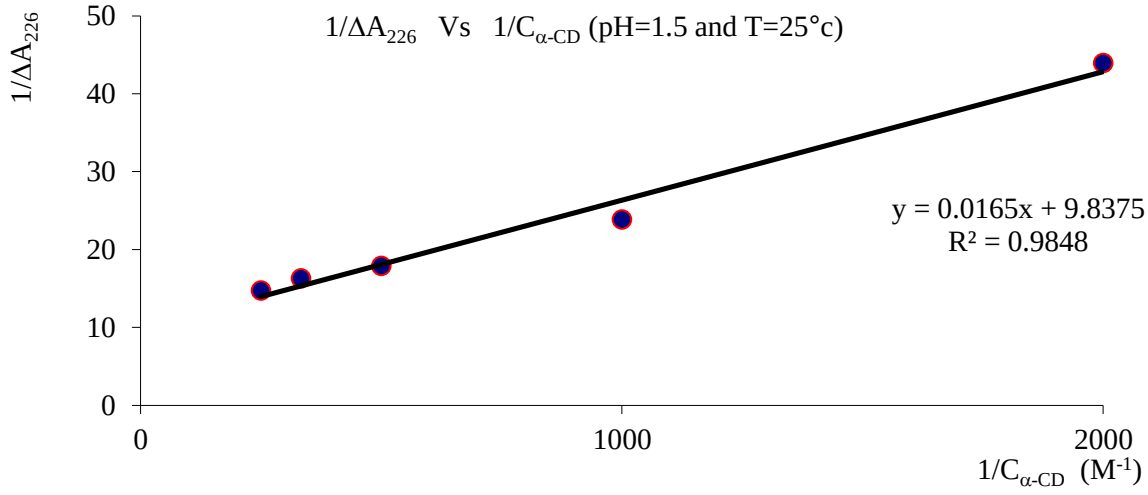
1/ΔA226 Vs 1/Cα-CD (pH=1.5 and T=25°c)
1/ΔA226
50
40
30
20
10
0
y = 0.0165x + 9.8375
R² = 0.9848
0
1000
2000
1/Cα-CD (M-1)

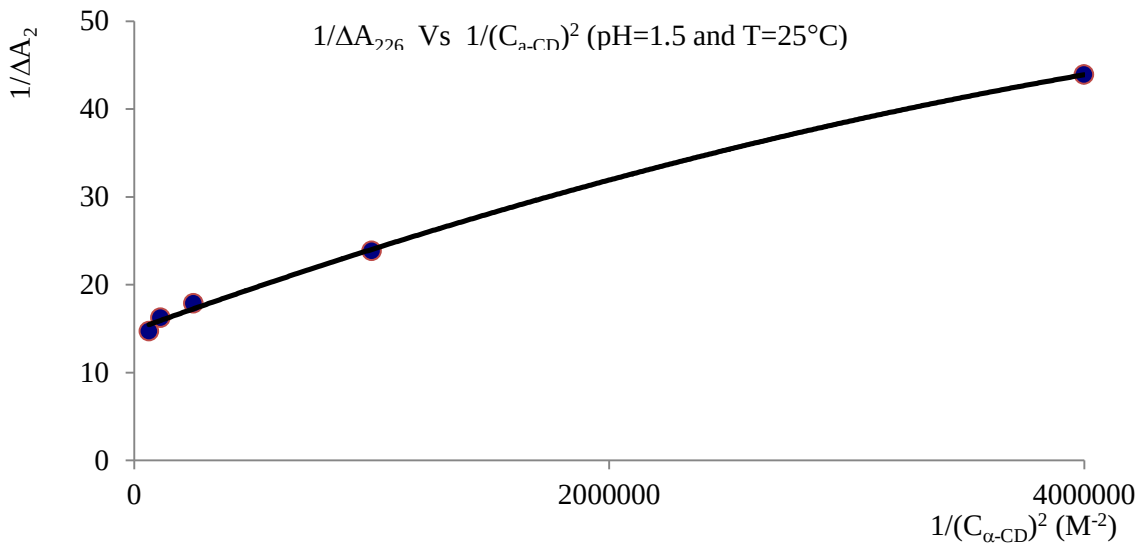

Fig 2.3.8 Dependence of ΔA_{max} of pABA solutions (5×10^{-5} M at pH=3.5 and 12.5×10^{-5} at pH= 1.5) on the α-CD concentration. Benesi-Hildebrand plots (linear relationship between *1/ΔA* and $1/C_{\alpha\text{-CD}}$ and non linear relationship between *1/Δa and* $1/(C_{\alpha\text{-CD}})^2$) assuming formation of a 1:1 complex between pABA and α-CD give access to stability constants of the complex.

Table 2.3.4 Stability constants K_c (M^{-1}) for pABA-α-CD complex at pH=3.5 and different temperatures.

	4 °C	10 °C	15 °C	20 °C	25 °C
K_c (λ_{max}=222 nm) M^{-1}	3155.4±298.3	2972.7±317.3	2854.9±317.5	2698.3±314.6	2503.2±272.2
K_c (λ_{max}=284 nm) M^{-1}	2880.2±188.3	2686.1±121.4	2505.2±155.6	2414.7±232.0	2319.4±241.0

Use of the Van't Hoff equation gives direct access to ΔH° and ΔS° of complex formation, [Fig 2.3.9 and Table 2.3.5]. The data presented in Table 2.3.4 and Table 2.3.5 indicates that the complex formation of pABA with α-CD is exothermic.

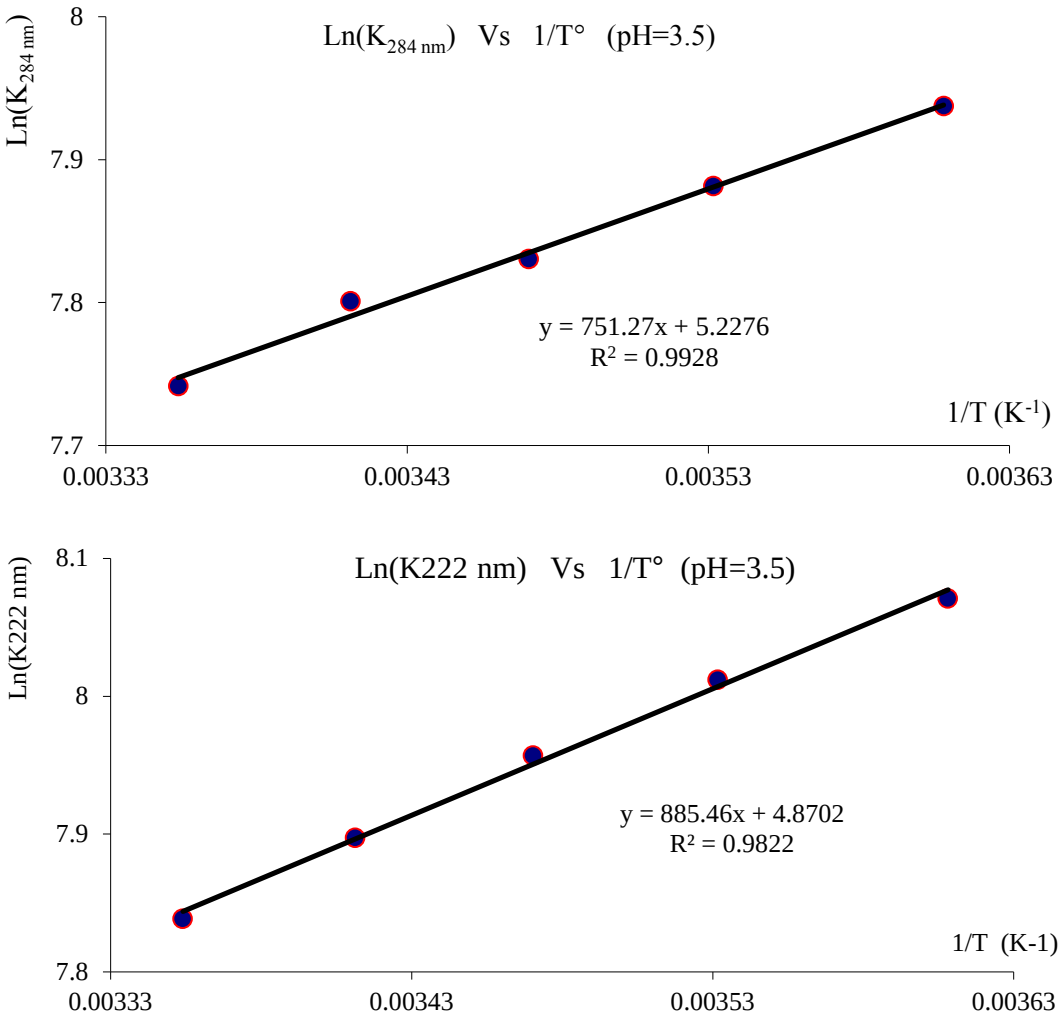

Fig 2.3.9 Van't Hoff analysis (dependence of Ln(K) of pABA-α-CD complex formation on the temperature (1/T) at pH=3.5 (K values determined from data at λ_{max}= 284 and 222 nm) give access to thermodynamic parameters ΔH° and ΔS° for the 1:1 complex formation of pABA with α-CD .

Table 2.3.5 ΔH° and ΔS° of complex formation, calculated from UV-spectroscopy data at pH=3.5.

	λ_{max} = 222 nm	λ_{max} = 284 nm
ΔH° (kJ.mol^{-1})	-8.69±0.88	-6.25±0.31
ΔS° (J.K^{-1}.mol^{-1})	35.9±3.1	43.5±1.1

Thus, the complex of pABA with α-CD is enthalpy-entropy stabilized. Enthalpy and entropy values include the contributions from the following main processes:

1) Partial breaking of the hydration shells of the solutes.
2) Exclusion of cavity-bound water molecules that are considered as "enthalpy-rich" [57].
3) Conformational changes (*e.g.* deviation from symmetry and restriction of conformational flexibility).
4) Direct binding due to non-covalent interactions (van der Waals interactions, H-bonding, hydrophobic effects, electrostatic interactions) [57].
5) Hydration of complex.

The observed small ΔH° value [Table 2.3.5] may be a result of the important role of hydrophobic effect and dehydration of the solutes occurring upon penetration of the pABA molecule into the hydrophobic cavity of α-CD. This happens when the guest molecule is deeply inserted into the Cyclodextrin cavity, as can be seen from the crystal structure of the complex. Positive entropy changes [Table 2.3.5], underline the extensive dehydration accompanied by the release of water molecules from the solvation shells of reagents into the bulk aqueous solution. Furthermore, van der Waals contacts of pABA with the apolar cavity of cyclodextrin can play a significant role in the complexation process, resulting in a positive ΔS° [57].

2.3.3 Phase Solubility diagrams

An apparent stability constant (K_c) can be calculated from the phase solubility diagrams using the equation 5, according to the hypothesis of a 1:1 stoichiometric of the complex [38].

$$K_c = \frac{Slope}{S_0(1-Slope)} \quad \text{.... (5)}$$

The slope was obtained from the initial straight line portion of the plot of the pABA solubility against the α-CD concentration, and S_0 is the equilibrium solubility of pABA in water. Phase-solubility diagrams for the complex formation between pABA and α-CD are presented in Fig 2.3.10. Our data indicate that the solubility of pABA in water depends on the pH of the solution: it is higher for the charged (protonated (pH = 1.5) and unprotonated (pH = 6)) forms: S_0 = 0.145, 0.030, and 0.170 M at pH = 1.5, 3.5, and 6.0, respectively. The phase-solubility diagrams show that the aqueous solubility of pABA increases linearly as a function of the α-CD concentration.

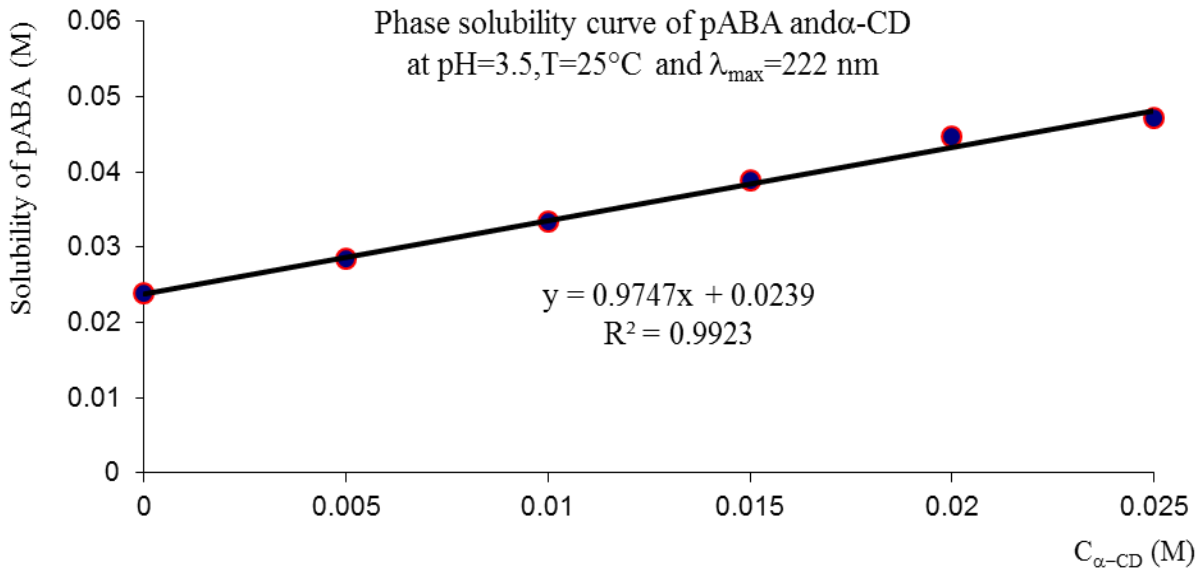

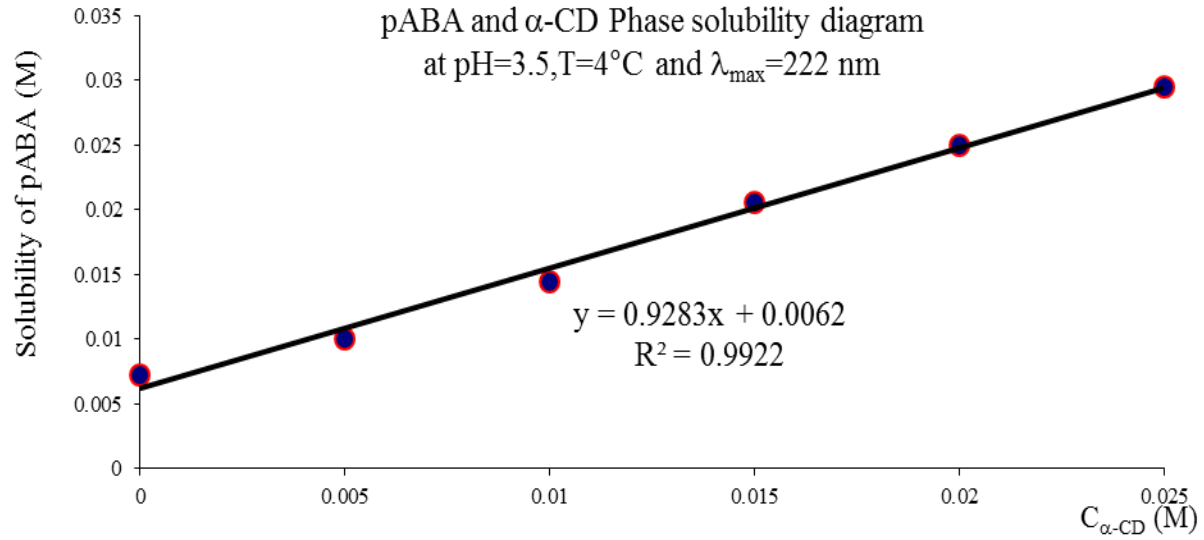
pABA and α-CD Phase solubility diagram
at pH=3.5,T=4°C and λmax=222 nm
Solubility of pABA (M)
0.035
0.03
0.025
0.02
0.015
0.01
0.005
0
0
0.005
0.01
0.015
0.02
0.025
Cα-CD (M)
y = 0.9283x + 0.0062
R² = 0.9922

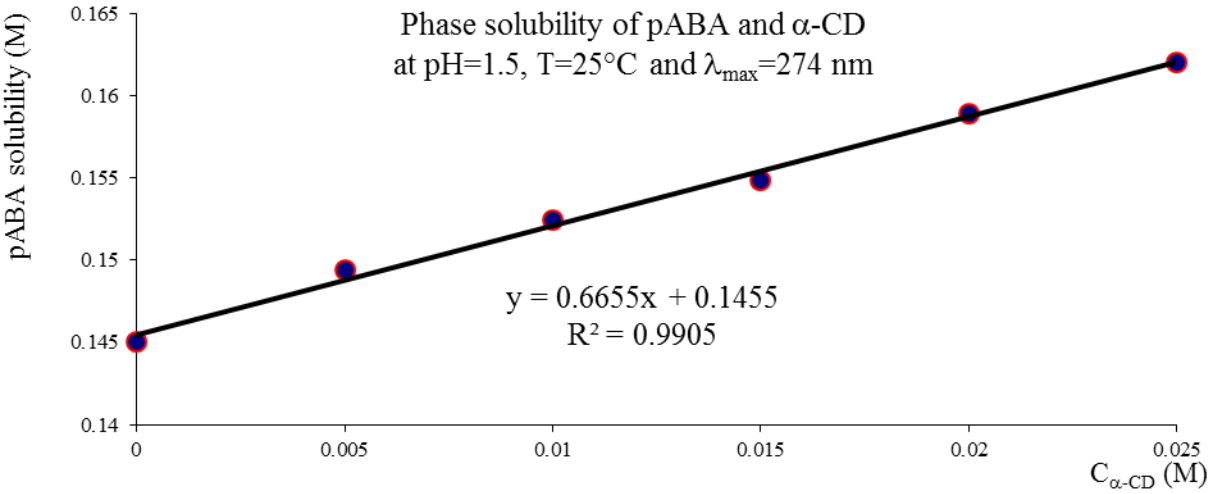
Phase solubility of pABA and α-CD
at pH=1.5, T=25°C and λmax=274 nm
pABA solubility (M)
0.165
0.16
0.155
0.15
0.145
0.14
0
0.005
0.01
0.015
0.02
0.025
Cα-CD (M)
y = 0.6655x + 0.1455
R² = 0.9905

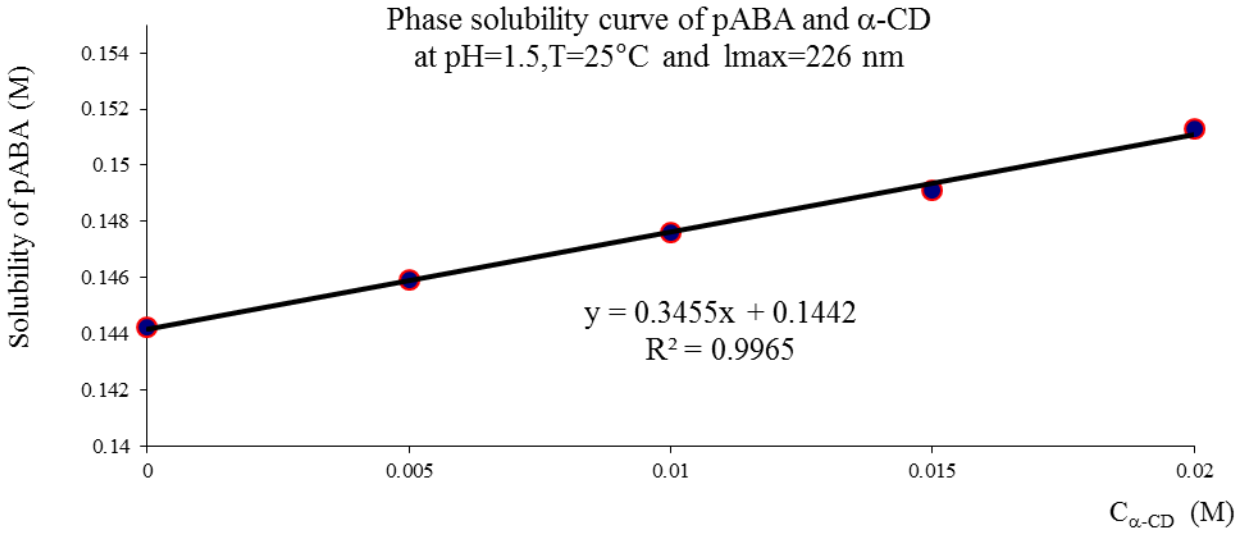
Phase solubility curve of pABA and α-CD
at pH=1.5,T=25°C and lmax=226 nm
Solubility of pABA (M)
0.154
0.152
0.15
0.148
0.146
0.144
0.142
0.14
0
0.005
0.01
0.015
0.02
Cα-CD (M)
y = 0.3455x + 0.1442
R² = 0.9965

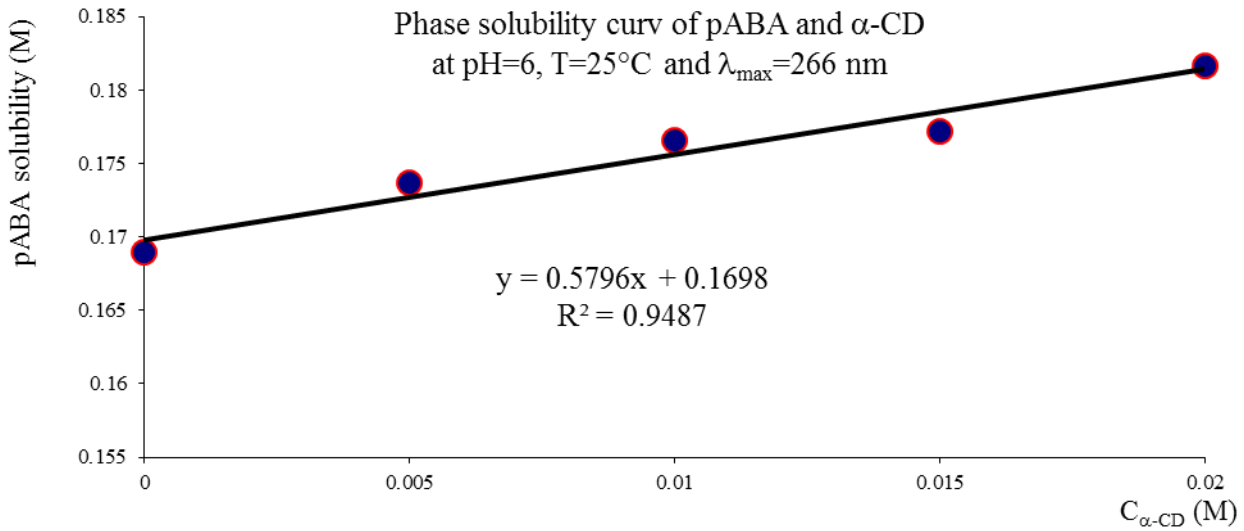

Fig 2.3.10 Phase solubility diagrams of pABA-α-CD system at pH=3.5, 1.5, and 6.0.

The linear host-guest correlation with a slope of less than 1 confirms the formation of a 1:1 complex in solution with respect to α-CD concentration. The increase in solubility of pABA resulting from inclusion in α-CD is more important at pH 3.5 (compare slopes). This study shows that the complex between pABA and α-CD is more stable at pH=3.5, with an apparent stability constant, $K_{(1:1)}$, obtained from the slope of the solubility diagrams, of 736.9±132.4 and 1710.7±219.6 M^{-1} at 25 and 4°C respectively.

2.3.4 Semi-empirical simulation of complexes

pABA can exist in three forms (neutral, anion and cation) according to the pH of the environment [Fig 2.2.1]. *Ab initio* (B3LYP-6-311G (5d,7f)) calculations have been applied to optimize the geometry of the different protonation forms of pABA alone. The results were used as a complement to crystal structures retrieved from the CSD to analyze the crystal structure of this guest in α-CD (see point 2.1.2). Similar results have been obtained using the PM6 semi-empirical method. Based on those calculations, the most stable form is the protonated state (E_{B3LYP} =

-476.394 A.U. *(-12963.16 eV)*; E_{PM6} = -1721.625 eV) followed by the neutral and zwitterionic states (E_{B3LYP} = -476.170 *(-12957.06 eV)* and -476.064 A.U. *(12954.18 eV)*; E_{PM6} = -1715.149 and -1712.645 eV, respectively). The anionic form is the less stable (E_{B3LYP} = -475.604 A.U. *(12941.66 eV)*; E_{PM6} = -1703.001 eV). Interestingly, it is this last form that is observed in the crystal structure of the inclusion complex with α-CD, illustrating the fact that stabilization effects resulting from complexation by the Cyclodextrin do affect differently the distinct protonation forms of pABA.

Therefore, different structures of α-CD-pABA inclusion complexes have been simulated. Two possible orientations of pABA inside the α-CD cavity have been retained, one (orientation A) with the carboxylic group of pABA located inside the α-CD cavity and the other (orientation B) corresponding to the amino group inside the cavity. For both orientations, the different protonation states of pABA (protonated, anionic, neutral, or zwitterionic) were considered. Effect of solvation on the overall stability of the complexes was also approached. Energy minimization of the different complexes was performed (PM6 level).

The optimized geometries were reasonable when water molecules where included in the calculation. In the absence of explicit water molecules, the *in vacuum* optimized complexes with neutral pABA (orientation A) or zwitterionic pABA (orientation B) converged to distorted geometries. This is in agreement with a similar study performed on inclusion complexes of pABA and β-CD [58]. All the other systems converged to chemically reasonable complexes, suggesting that the PM6 method is well adapted to study the pABA-CD systems. In particular, the PM6 method reproduced the crystal structure rather well. Indeed, the enthalpy of formation of pABA included in α-CD was the most negative with the anionic form of pABA, in orientation A ($\Delta H_{f(PM6)}$ = -158.77 kcal) compared to the anionic form

of the guest in orientation B ($\Delta H_{f(PM6)}$ = -142.78 kcal). This result is in excellent agreement with the crystal structure reported in this study. The PM6 method suggests that complexation of the anionic form is favored compared to the other protonation states of pABA ($\Delta H_{f(PM6)}$ = -158.77, -129.90, -111.95, and +81.25 kcal) for complexes with anionic $pABA^-$, zwitterionic $pABA^{+/-}$, neutral pABA, and cationic $pABA^+$ forms, in orientation A. Similar calculations performed on complexes including pABA and β-CD [58] led to different results. In that work, orientation B was more stable but, in agreement with our results, the complex with anionic pABA was favored. The geometries of the studied complexes found with the PM6 method confirm that pABA is deeply included in α-CD, with the aromatic ring for each species of pABA totally embedded in the α-CD cavity especially for the A orientation.

2.4 Conclusions

Our crystallography study shows that pABA forms a 1:1 complex with α-CD and is deeply included into the cavity of the cyclodextrin, with the amino group protruding from the wide site of the cavity and the (unprotonated) carboxylate at the narrow side. The crystal structure corresponds to the anionic form of pABA. The pABA guest is held in the host cavity mainly by van der Waals contacts and hydrogen bonds. Spectroscopic studies of the interactions of pABA with α-CD demonstrate the insertion of pABA into the Cyclodextrin cavity in solution, with formation of a 1:1 inclusion complex with stability constant 2319.4±241.0 M^{-1} at 25°C and pH=3.5. The phase solubility studies confirm the formation of a 1:1 pABA-α-CD inclusion complex. The solubility of pABA in water is markedly enhanced by complexation with α-CD. The calculations carried out with the PM6 method show that inclusion complexes of different pABA protonation states with α-CD lead to stable structures and this confirms experimental observations. During

this theoretical study, orientation A (carboxylic group inside) was more favorable than orientation B (amino group inside), in agreement with our crystal structure.

2.5 Supplementary data

Tables of atomic coordinates, bond lengths, and bond angles have been deposited with the Cambridge Crystallographic Data Center, CCDC Nos. 845857 for the α-CD–pABA complex. These data may be obtained free of charge, on request, from The Director, Cambridge Crystallographic Data Center, 12 Union Road, Cambridge, CB2lEZ, UK (fax: + 44-1223-336033; e-mail: *deposit@ccdc.cam.ac.uk* or *www: http://www.ccdc.cam.ac.uk*). A copy of electronic files is also supplied on the CD available as annex to this thesis.

2.6 References

1. Merisko-Liversidge, E. Nanocrystals: Resolving pharmaceutical formulation issues associated with poorly water-soluble compounds. In Abstract of Papers, Particles Conference, Orlando, Florida, United States, 2002.
2. Maki, T.; Takeda, K. "Benzoic Acid and Derivatives". Ullmann's Encyclopedia of Industrial Chemistry. Wiley-VCH. doi:10.1002/14356007.a03_555. 2000.
3. http://www.healthsupplementsnutritionalguide.com/pABA.html#FOODS.
4. Para-aminobenzoic acid poisoning. National Institute of Health: National Library of Medicine. 2007. Archived from the original on 14 June 2007. Retrieved 2007-06-19.
5. Christopher T. Walsh, M ark D. Erion, Alan E. Walts, John J. Delany III, and Glenn A. Berchtold, Biochemistry, 1987, 26, 4134-4145.
6. Gilles J. C. Basset, Eoin P. Quinlivan, Stéphane Ravanel, Fabrice Rébeillé, Brian P. Nichols, Kazuo Shinozaki, Motoaki Seki, Lori C. Adams-Phillips, James J. Giovannoni, Jesse F. Gregory, and Andrew D. Hanson, Proc Natl Acad Sci U S A. 2004, 101, 1496-1501.
7. Wegkamp A, Oorschot W, de Vos WM, and Smid EJ, Appl Environ Microbiology, 2007, 73, 2673-2681.
8. http://2008.igem.org/Team:Caltech/Project/Vitamins.
9. http://www.nlm.nih.gov/medlineplus/ency/article/002518.htm.
10. Michael Kent, Advanced Biology, Oxford University Press, 2000, p. 46 ISBN 978-0-19-914195-1.
11. http://pubchem.ncbi.nlm.nih.gov/summary/summary.cgi?cid=978.
12. http://healthlibrary.epnet.com/GetContent.aspx?token=5b000b40-3809-4cb2-88a4-68bfd31b5c51&chunkiid=21831.
13. Science News, 1998, 153, 360-361.

14. F. P.; Mitchnick, M.; Nash, J. F. Photochem. Photobiol. 1998, 68, 243-256.
15. H.; Thune, P.; Eeg Larsen, T. Arch. Dermatol. Res. 1990, 282, 38-41.
16. Osgood, Pauline J.; Moss, Stephen H.; Davies, David J. G. Journal of Investigative Dermatology, 1982, 79, 354-357.
17. http://emedicine.medscape.com/article/1844551-overview.
18. T.F.Lai, R.E.Marsh, Acta Crystallogr., 1967, 22, 885-893.
19. S.Gracin, A.Fischer, Acta Crystallogr., Sect.E: Struct. Rep. Online 2005, 61, o1242-o1244.
20. Alleaume, M.; Salas-Ciminago, G.; Decap, J. Compt. Rend., Ser. C 1966, 262, 416-417.
21. Sandra Gracin and Åke C. Rasmuson, Crystal Growth & Design, 2004, 4, 1013-1023
22. Vasilieva, S.: Para-aminobenzoic acid inhibits a set of SOS functions in Escherichia coliK12. Mutat. Res. 2001, 496, 89-95.
23. Cambridge Structural Database System, Cambridge Crystallographic Data Centre 12 Union Road, Cambridge CB2 1EZ, UK. See http://www.ccdc.cam.ac.uk/products/csd/
24. Harata, K. Bull. Chem. Soc. Jpn. 1977, 50, 1416-1424.
25. Harata, K. Carbohydr. Res. 1976, 48, 265-270.
26. Harata, K. Bioorg. Chem. 1981, 10, 255-265.
27. Lewis, E. A.; Hansen, L. D. J. Chem. Soc. Perkin Trans. 1973, 2, 2081-2085.
28. Shuang, S. M.; Yang, Y.; Pan, J. H. Anal. Chim. Acta. 2002, 458, 305-310.
29. Stalin, T.; Rajendiran, N. Chem. Phys. 2005, 322, 311-322.
30. Stalin, T.; Shanthi, B.; Vasantha Rani, P.; Rajendiran, N. J. Chem. 2006, 55, 21-29.
31. Stalin, T.; Rajendiran, N. J. Photochem. Photobiol. A. 2006, 182, 137-150.
32. Terekhova, I. V.; Obukhova, N. A. J. Solution. Chem. 2007, 36, 1167-1176.
33. Terekhova, I. V.; Kumeev, R. S.; Alper, G. A. J. Incl. Phenom. Macrocycl. Chem. 2007, 59, 301-306.

34. Kartsova, L. A.; Komarova, N. V. J. Analytical Chem. 2003, 58, 972-978.
35. Yimin Zhang ; Shanbao Yu; Feng Bao. Carbohydr. Res. 2008, 343, 2504-2508.
36. CrysAlisPro, Oxford Diffraction Ltd.,Version 1.171.33.55. (Released on 05-01-2010 CrysAlis171 .NET). See http://www.oxford-diffraction.com
37. G. M. Sheldrich, Acta Cryst. 2008, A64, 112-122.
38. Higuchi T, Connors KA. Phase solubility diagram. Adv Anal chem. Instrum. 1965, 4, 117-212.
39. Gaussian 09, Revision A.02, M. J. Frisch, G. W. Trucks, H. B. Schlegel, G. E. Scuseria, M. A. Robb, J. R. Cheeseman, G. Scalmani, V. Barone, B. Mennucci, G. A. Petersson, H. Nakatsuji, M. Caricato, X. Li, H. P. Hratchian, A. F. Izmaylov, J. Bloino, G. Zheng, J. L. Sonnenberg, M. Hada, M. Ehara, K. Toyota, R. Fukuda, J. Hasegawa, M. Ishida, T. Nakajima, Y. Honda, O. Kitao, H. Nakai, T. Vreven, J. A. Montgomery, Jr., J. E. Peralta, F. Ogliaro, M. Bearpark, J. J. Heyd, E. Brothers, K. N. Kudin, V. N. Staroverov, R. Kobayashi, J. Normand, K. Raghavachari, A. Rendell, J. C. Burant, S. S. Iyengar, J. Tomasi, M. Cossi, N. Rega, J. M. Millam, M. Klene, J. E. Knox, J. B. Cross, V. Bakken, C. Adamo, J. Jaramillo, R. Gomperts, R. E. Stratmann, O. Yazyev, A. J. Austin, R. Cammi, C. Pomelli, J. W. Ochterski, R. L. Martin, K. Morokuma, V. G. Zakrzewski, G. A. Voth, P. Salvador, J. J. Dannenberg, S. Dapprich, A. D. Daniels, O. Farkas, J. B. Foresman, J. V. Ortiz, J. Cioslowski, and D. J. Fox, Gaussian, Inc., Wallingford CT, 2009. See http://www.gaussian.com
40. Vega ZZ release 2.3.2.38, Windows version. Copyright 1996-2009, Alessandro Pedretti & Giulio Vistoli. See http://www.vegazz.net
41. OpenBabelGUI © 2006 by Chris Morley, version 2.2.3 (released on 31-07-2009). See http://openbabel.org/wiki/Main_Page

42. MOPAC2009, James J. P. Stewart, Stewart Computational Chemistry, Version 9.310L. See http://OpenMOPAC.net
43. Harata, K. Bull. Chem. Soc. Jpn. 1977, 50, 1416-1424.
44. Harata, K. Chem. Rev. 1998, 98, 1787-1802.
45. Harata, K. Bull. Chem. Soc. Jpn. 1976, 49, 1493-1501.
46. Harata, K. Bull. Chem. Soc. Jpn. 1976, 49, 2066-2072.
47. Harata, K. Bull. Chem. Soc. Jpn. 1975, 48, 2409-2413.
48. Saenger, W. Beyer, K; and Manor, P.C. Acta crystallogr.,Sect. B. 1976, 32, 120-128.
49. McMullan, R. K., Saenger, W., Fayos, J. and Mootz, D. Carbohydr. Res. 1973, 31, 211-227.
50. Manor P. C. and Saenger, W. J. Am. Chem. Soc. 1974, 96, 3630-3639.
51. Saenger, W., McMullan, R. K., Fayos, J. and Mootz, D. Acta Crystallogr. Sect. B, 1974, 30, 2019-2028.
52. Saenger W. and Noltemeyer, M. Chem. Ber. 1976, 109, 503-517.
53. Hingerty B. and Saenger, W. J. Am. Chem. Soc. 1976, 98, 3357-3365.
54. Hybl, A., Rundle, R. E. and Williams, D. E. J. Am. Chem. Soc. 1965, 87, 2779-2788.
55. Benesi, H.A., Hildebrand, J.H.: A spectrophotometric investigation of the interaction of iodine with aromatic hydrocarbons. J. Am. Chem. Soc. 1949, 71, 2703-2707.
56. Shuang Shaomin, Yang Yu, Pan Jinghao. Analytica Chimica Acta. 2002, 458, 305-310.
57. Liu, L., Guo, Q.-X.: The driving forces in the inclusion complexation of cyclodextrins. J. Inclus. Phenom.Macrocycl. Chem. 2002, 42, 1-14.
58. Madi Fatiha, Khatmi Djameleddine, largate Leila, Orbital, 2009, 1, 26-37.

Chapter 3

Using Cyclodextrin as linker in Metal-Organic Frameworks (MOFs) for drugs carriers and molecular absorption

3.1 General introduction

Metal-Organic Frameworks (MOFs) are crystalline compounds built from metal ions or clusters coordinated to predominately rigid organic molecules. They form one-, two-, or three-dimensional structures (Fig 3.1.1) that are often porous.

The synthesis and characterization of MOFs is one of the most rapidly developing areas of chemical science now. These materials have unquestionably enormous potential for many practical applications. MOFs attract attention as materials for adsorptive hydrogen (energy storage) because of their exceptionally high specific surface areas and chemically tunable structures [1]. Hydrogen molecules are stored in a MOF by adsorbing to its surface. Compared to an empty gas cylinder, a MOF-filled gas cylinder can store more gas because of adsorption that takes place on the surfaces. Furthermore, MOFs have a fully reversible uptake-and-release behavior: since the storage mechanism is based primarily on *physisorption*, there are no large activation barriers to be overcome when liberating the adsorbed hydrogen [2]. In addition to the above, several possible applications of MOFs are also found as drug-delivery, sensors, luminescence materials, magnetic materials, catalysis, gas separations, etc. [3]

MOF, generally, is composed of two major components: a metal ion (or cluster of metal ions) and an organic molecule called a linker. The choice of metal and linker has significant effects on the structure and properties of the MOF. For

example, the metals coordination preference influences the size and shape of pores by dictating how many ligands can bind to the metal and in which orientation. The organic linkers are typically mono-, di-, tri-, or tetravalent ligands [2]. Many linkers or ligands are known in synthesis of MOFs. In the early years of MOFs research, mostly simple and readily available organic linkers were utilized in MOF synthesis; we enumerate, for example but not limited to, oxalic acid, malonic acid, succinic acid, glutaric acid, phthalic acid, isophthalic acid, citric acid, and squaric acid. In recent years the targeted synthesis of specifically functionalized linkers has become a major object of research [4-12]. The utilization of such functionalized linkers can significantly change the properties of synthesized MOFs.

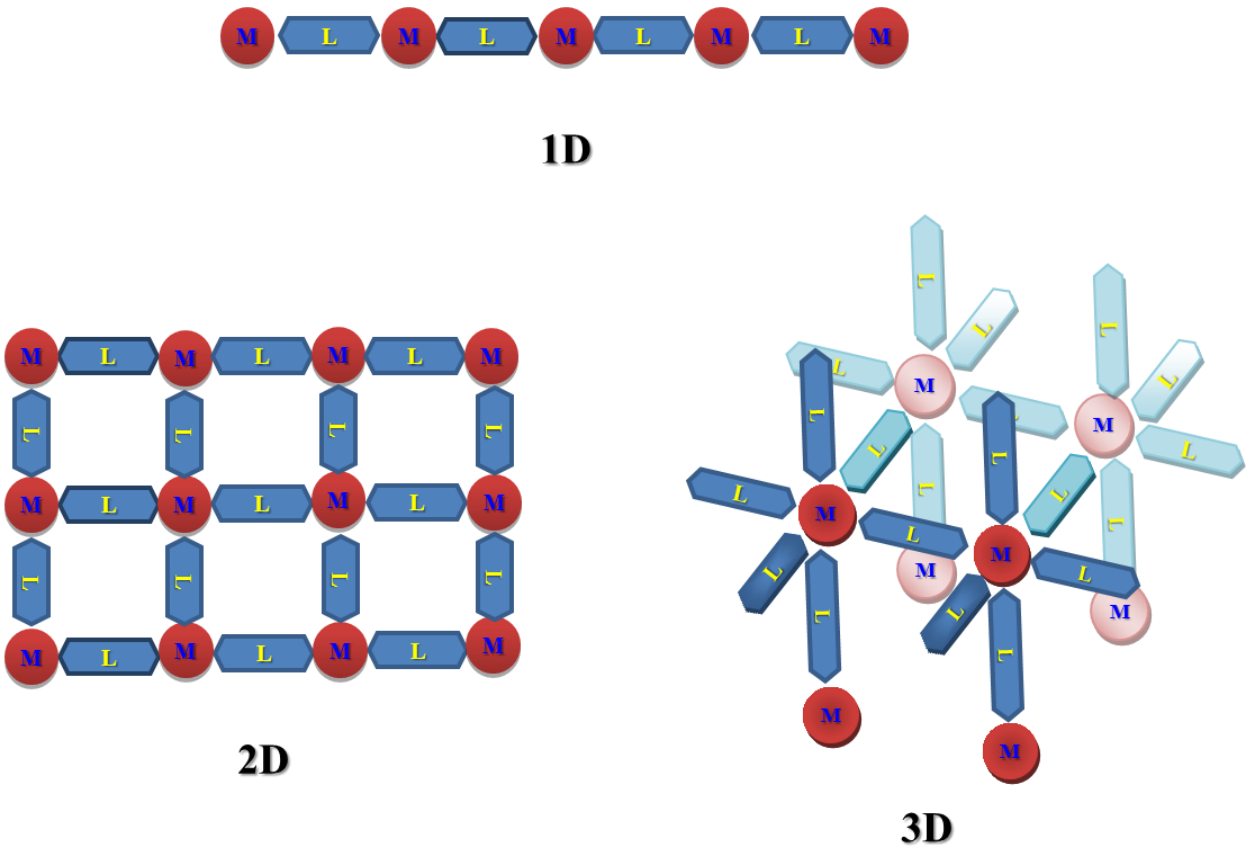

Figure 3.1.1: Simple scheme showing three possible forms (1D, 2D and 3D) of MOFs. **M** = Metal cation, **L** = Linker.

Until recently, only a handful of MOFs have been derived from natural products. Recently, several works have been reported on this topic [13-15]. Stoddart et al. show in their pioneering works the fact that a common feature of all the polyoxygenated ligands which bind alkali and alkaline earth metal cations are –OCCO– repeating units with gauche conformations defining their C–C bond [Fig 3.1.2]. This geometry orients the hard oxygen donors in a manner which allows them to interact seamlessly with hard Group IA and IIA metal cations and is undoubtedly responsible for the strong monopole–dipole interactions that lead cooperatively to large association constants for complexes incorporating a number of them. For example, [18]crown-6 was found to bind K^+ ions in methanol with a stability constant (K_a) in excess of 10^6 M^{-1}, diazamacrobicyclic polyethers like [2.2.2]cryptand were shown by Lehn and Sauvage to exhibit K_a values as high as 10^{15} M^{-1} for the binding of alkali metal cations in methanol.[16-23] Smaldone et al, also, expected that α1,4-linked D-glucopyranosyl residues which constitute the repeating units in cyclodextrin display the –OCCO– binding motif on both their primary and secondary faces, in addition to their hollow structure, augurs well for their being able to form extended structures with Group IA and IIA metal cations. In spite of there is little or no evidence that cyclodextrins bind alkali and alkaline earth metal cations strongly in aqueous solution, they have, actually, prepared a beautiful and brilliant structure of a MOF comprised of γ-cyclodextrin (γ-CD) rings coordinated to alkali metal, producing highly porous materials from completely nontoxic and naturally occurring materials [24-25]. The overall topology of the resultant MOF is cubic with extended linear pores along their crystallographic axes. The complexes were prepared simply by combining 1.0 molar equivalent of γ-CD with 8.0 molar equivalents of KOH in aqueous solution, followed by vapor diffusion of MeOH into the solution during 2–7 days. In this structure eight-coordinate M^+ ions assist in the assembly of (γ-CD)6 cubes. The six

γ-CD units occupy the faces of a cube and link these cubes to form a three dimensional MOF having open porous of 1.7 nm diameter in an extended fashion accessible one to the other. Six pore windows of 0.78 nm diameter are defined by the γ-CD tori which adopt the faces of the cube and the framework has an estimated total pore volume of 54% [Fig 3.1.2 (c)].

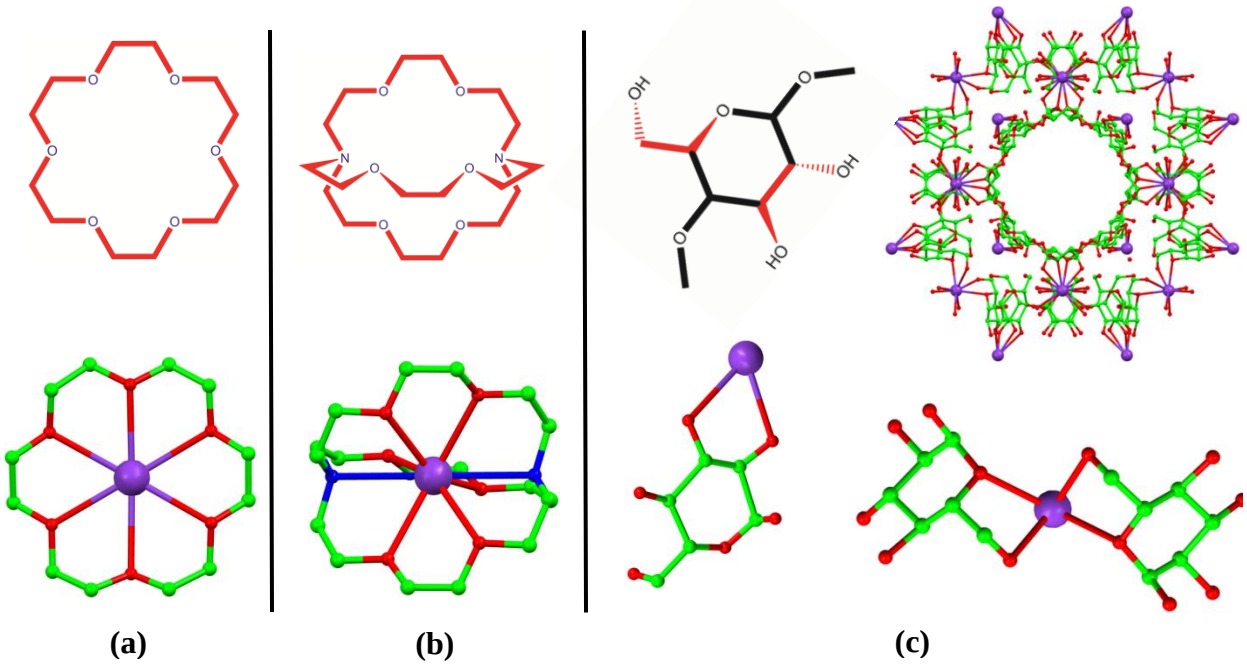

Figure 3.1.2: Examples of polyoxygenated compounds which can be used to coordinate alkali or alkaline earth metal cations. In all cases, the –OCCO– or –OCCN– bidentate moieties, capable of chelation to hard Group IA and IIA metal cations, are colored in red. **(a)** The structural formula of 18-crown[6] and the crystal structure of its 1:1 complex with a K^+ ion. **(b)** The structural formula of [2.2.2]cryptand, and the crystal structure of its 1:1 complex with a K^+ ion. **(c)** One of the eight α1,4-linked D-glucopyranosyl residues which comprise γ-CD, with the two possible –OCCO– coordination sites highlighted in red and the possible modes of coordination of K^+ ions to the primary and secondary faces of γ-CD in the crystal structure. The crystal structures were redrawn from CCDC depositions KOSRAL [26] and KCRYPT10 [27] and [24] respectively, with counterions and hydrogen atoms removed for clarity.

There are also a number of solid-state structures in literatures in which the coordination of these cations by cyclodextrins has been observed. Both Group IA and IIA metal cations have been shown to link molecules of α-CD, β-CD and γ-CD by coordinating (***i***) to their primary hydroxyl groups, [28], (***ii***) to their secondary hydroxyl groups, [29-32] or (***iii***) to a combination of both of these binding sites.

[24, 25, 33-39]. The wide range of coordination geometric shapes which have been observed, results presumably from the absence of preorganization of the numerous oxygen atoms that are capable of coordinating to the metal cations.

In this context, and as part of our study plans to prepare inclusion complexes systems between cyclodextrins and aminobenzoic acids as drugs models, we performed a study on the cyclodextrin MOFs (CD-MOFs) formed by coordinating the cyclodextrins to potassium cation. One original structure of MOFs is reported here. We have also decided to take the advantages of this interaction between cyclodextrin and alkali metal cation to favour formation of inclusion complexes as drug carrier, after failing to prepare these kinds of complexes in the conventional way. In this work, we report a strategy to overcome this problem using cyclodextrin MOFs and we are looking forward to show how the alkali metal cation can play a cofactor role for preparation of such inclusion complexes.

3.2 Results and discussion

3.2.1 α-CD-KOH MOF

α-CD forms, easily, a 1:2 complex with KOH [Figure 3.2.1(a)]. This complex crystallizes in orthorhombic $P2_12_12_1$ space group. The cyclodextrin adopts a cage structure and crystal packing is stabilized by oxygen atoms that coordinate potassium cation and intermolecular and intramolecular hydrogen bondings. This structure is of general interest in the context of polymorphism of cyclodextrins and the coordination of the metal cation by the cyclodextrin is of particular interest with respect to formation of original Metal-Organic Frameworks (MOFs).

The overall structure of α-CD is consistent with its other crystal structures. The torsion angles defining the orientation of C(6)–O(6) bonds show two different types of conformation: gauche-trans for G3 and G4 and gauche-gauche for the

other residues. The particular orientation of the C(6)–O(6) bonds of the G3 and G4 residues probably results from hydrogen bonding of the primary O(63) and O(64) with water molecules O1W and O2W which in their turn are hydrogen bonded to the included methanol guest [Figure 3.2.1(b)].

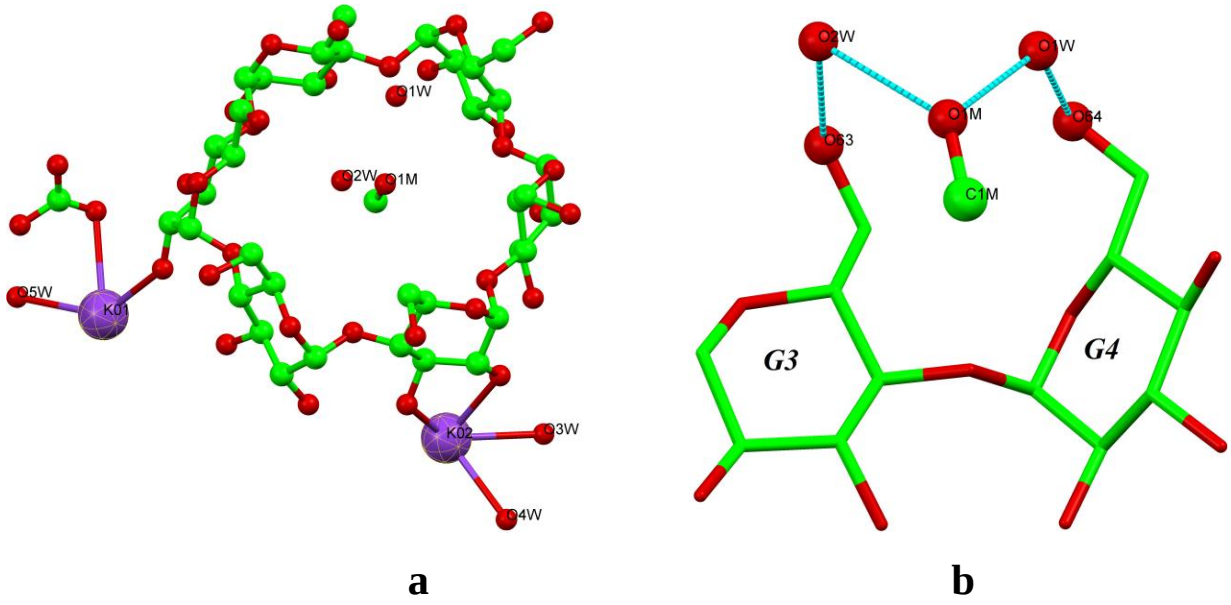

Figure 3.2.1. **(a)** 1:2 complex of α-CD with KOH. **(b)** The particular orientation of the C(6)–O(6) bonds of the G3 and G4 residues results from hydrogen bonding with water molecules O1W and O2W which in their turn are hydrogen bonded to the included methanol molecule. Hydrogen atoms and solvent molecules were omitted for clarity.

The α-cyclodextrin molecules form, through 2_1 axes, a closed herringbone-like pattern along ***ac*** plane as monomer units Figure 3.2.2. This arrangement is stabilized by coordination to potassium ions and by hydrogen bonds. Strong inter- and intra-molecular hydrogen bondings involve hydroxyl groups and water molecules [Table 3.2.1].

The environment of both potassium ions is comprised of eight O atoms coming mainly from hydroxyl groups. The majority of distances [Table 3.2.2] are longer than the sum of the ionic radii of K and O (2.66 Å). Methanol occupies the cavity of the α-cyclodextrin and is stabilized by H bonds with two water molecules

O1W and O2W which are in hydrogen bonding distance with the two hydroxyl group in G3 and G4.

Table 3.2.1. Hydrogen Bonds in α-CD-KOH complex.

D– H	***A***	***D–H (Å)***	***H…A (Å)***	***D…A (Å)***	***D–H…A (°)***
O1W-H1W1	O1M	0.94	1.810	2.57 (1)	136.5
O1W-H2W1	O64	0.79	2.090	2.50 (1)	112.2
O2W-H1W2	O1M	0.86	1.970	2.78 (1)	155.5
O2W-H2W2	O63	0.86	2.100	2.92 (1)	161.3
O3W-H1W3	O1W$_{i}$	0.87	2.120	2.65 (1)	118.5
O3W-H2W3	O61$_{ii}$	0.86	1.910	2.770 (4)	178.8
O4W-H1W4	O56$_{iii}$	0.87	2.200	2.915 (4)	138.7
O4W-H1W4	O66$_{iii}$	0.87	2.590	3.133 (4)	121.0
O4W-H2W4	O2W$_{i}$	0.87	1.840	2.708 (5)	179.1
O5W-H1W5	O62$_{iv}$	0.91	2.590	3.459 (3)	160.0
O5W-H2W5	O1C	0.87	1.777	2.597 (3)	155.5
O21-H21O	O36	0.82	1.988	2.800 (3)	170.4
O21-H21O	O46	0.82	2.458	2.855 (3)	110.8
O22-H22O	O1C$_{iv}$	0.82	1.840	2.642 (3)	165.2
O23-H23O	O32	0.82	2.073	2.881 (3)	168.2
O23-H23O	O42	0.82	2.344	2.771 (3)	113.2
O24-H24O	O33	0.82	2.023	2.831 (3)	168.2
O24-H24O	O43	0.82	2.369	2.766 (3)	110.6
O25-H25O	O1C$_{v}$	0.82	1.800	2.609 (3)	168.9
O26-H26O	O3C$_{vi}$	0.82	1.688	2.508 (3)	177.4
O31-H31O	O22	0.82	1.950	2.768 (3)	175.6
O31-H31O	O41	0.82	2.560	2.910 (3)	107.5
O32-H32O	O3C$_{iv}$	0.82	1.861	2.673 (3)	170.5
O33-H33O	O2C	0.82	1.970	2.740 (3)	156.1
O34-H34O	O25	0.82	2.049	2.868 (3)	176.7
O34-H34O	O44$_{vii}$	0.82	2.520	2.882 (3)	108.0
O35-H35O	O26	0.82	1.956	2.757 (3)	165.2
O35-H35O	O45	0.82	2.580	2.936 (3)	108.2
O36-H36O	O24$_{vi}$	0.82	2.351	2.924 (3)	127.5
O61-H61O	O2C$_{viii}$	0.82	2.025	2.810 (3)	160.2
O62-H62O	O4W$_{iii}$	0.82	1.868	2.661 (4)	162.5
O63-H63O	O5W$_{ix}$	0.82	2.050	2.854 (3)	166.2
O64-H64	O24$_{x}$	0.82	2.342	3.027 (6)	141.4
O65-H65O	O62$_{v}$	0.82	1.863	2.673 (3)	169.3
O66-H66O	O5W$_{viii}$	0.82	2.021	2.814 (3)	162.7

Symmetry : ***i****[x-1, y, z],* ***ii****[-x, y-1/2, -z+5/2],* ***iii****[-x, y+1/2, -z+5/2],* ***iv****[x-1/2, -y+3/2, -z+2],* ***v****[x, y-1, z],* ***vi****[x-1/2, -y+1/2, -z+2],* ***vii****[x,1+y,z],* ***viii****[-x+1/2, -y+1,z+1/2],* ***ix****[x+1/2, -y+3/2, -z+2],* ***x****[x+1/2, -y+1/2, -z+2]*

Table 3.2.2 Potassium coordination in α-CD-KOH complex.

K_1		K_2	
M–L	**Bond length (Å)**	**M–L**	**Bond length (Å)**
K01—-O23	2.649 (2)	K02—-O34$_{i}$	2.718 (3)
K01—-O65$_{i}$	2.741 (2)	K02—-O31	2.790 (2)
K01—-O35$_{i}$	2.850 (2)	K02—-O3W	2.884 (3)
K01—-O5W	2.951 (2)	K02—-O21	2.913 (2)
K01—-O2C	2.955 (2)	K02—-O4W	2.958 (4)
K01—-O53$_{ii}$	3.027 (2)	K02—-O24$_{i}$	3.160 (3)
K01—-O25$_{iii}$	3.331 (2)	K02—-O63$_{iv}$	3.225 (2)
K01—-O55$_{i}$	3.362 (2)	K02—-O66$_{v}$	3.253 (3)

Symmetry : ***i****[x-1/2, -y+1/2, -z+2],* ***ii****[x-1/2, -y+3/2, -z+2],* ***iii****[x, y+1, z],* ***iv****[x-1, y, z],* ***v****[-x, y+1/2, -z+5/2]*

Analysis of the title compound crystal structure shows the presence of carbonate. The geometry of the ion is compatible with a fully deprotonated carbonate ion (-2), as confirmed by a search performed in the CSD and comparison of the bond lengths in the reported crystal structure. The carbonate forms the counter-ion of two potassium cations. As for the source of carbonate in the structure, there are two possibilities: it might be coming from non-pure potassium hydroxide (85%); alternatively, it may be the result of the contact of atmospheric carbon dioxide with the alkali solution.

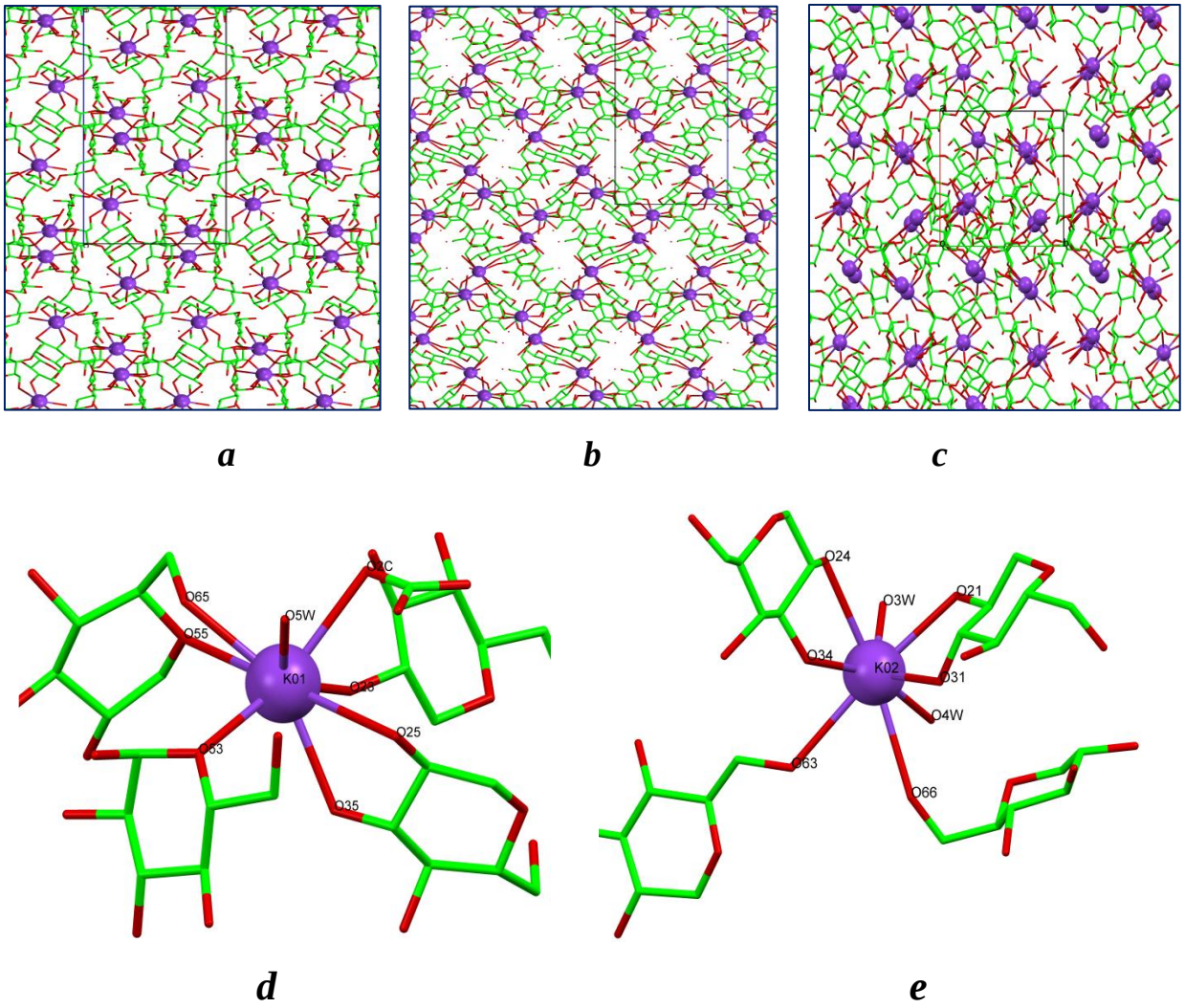

Figure 3.2.2 **(a, b, c)** Crystal packing, in α-CD-KOH complex, in a, b and c direction respectively. **(d, e)** Potassium coordination in α-CD-KOH complex.

3.2.2 New polymorph of α-CD

Irina *et al* showed in their ^{1}H NMR study on CDs complexes that α-CD and β-CD form 1:1 inclusion complexes with para and meta-aminobenzoic acid (pABA and mABA) and they discussed the influence of the cyclodextrin cavity size and position of the side amino group in the aromatic ring of aminobenzoic acid molecule on the binding mode and the complex stability [40]. In spite of this evidences on the formation of inclusion complexes between CDs and ABA family, all our tireless efforts to produce these complexes in crystalline state by

conventional ways ended in failure with the exception of para-aminobenzoic acid (pABA), which was easily prepared from water/ethanol solution by slow evaporation. This has been discussed in detail in chapter1, and compared with the two known structures of β-CD with pABA and oABA (the two structures are, already, known in literatures [41]). In fact all our effort to make complexes between α-CD and oABA and mABA result in a new form of α-CD with crystals having a hexagonal external shape [Figure 3.2.3(a)], and a hexagonal R3 internal crystal system [*cell parameters: a = b = 23.6696(4)Å, c = 109.0704(15)Å, α = β = 90° and γ = 120°, the structure converged at R1 = 0.0774 for 29042 [$F_o > 4\sigma(F_o)$] and 0.0873 for all 34303 data after applying squeeze refinement procedure to treat the problem with the disordered solvent inside the structure*].

In this structure, the asymmetric unit contains 12 × one third α-CD molecules and 43 water molecules, most of these waters positions are not fully occupied due to disorder. The rest of the molecules are generated by the 3-fold axis. The average bond-length and angles are in the correct range and similar to those in the other α-CD structures. All glucose residues are in the normal $^4C_1$ chair conformation, and the overall α-CD molecules show nearly regular hexagon geometry, the $O_{4n}\ldots O_{4(n+1)}$ distances varying between 4.179(5) and 4.296(6) Å, and the values of the angles between $O_{4(n-1)}\ldots O_{4n}\ldots O_{4(n+1)}$ being close to 120°, the ideal value for an angle in a regular hexagon. Indeed, these values range from 118.6(1)° to 121.5(1)°, denoting that the cavity is not distorted due to absence of inclusion with big molecules. The annular shape of α-CD is stabilized by inter-glucose hydrogen bonds connecting the secondary hydroxyl groups O_{3n} and $O_{2(n+1)}$ of the neighboring glucosidic units. The hexagonal diagonal distances, measured between the glycosidic oxygen atoms (O_{4n}), range from 8.408(4) to 8.483(5) Å. α-CD displays a porous structure consisting of long channels resulting from stacking of molecules

in head to head trimers extended along the ***c***-axis [Figure 3.2.3(b,c)]. All their glucosidic (O_{4n}) planes are parallel to ***ab*** plan.

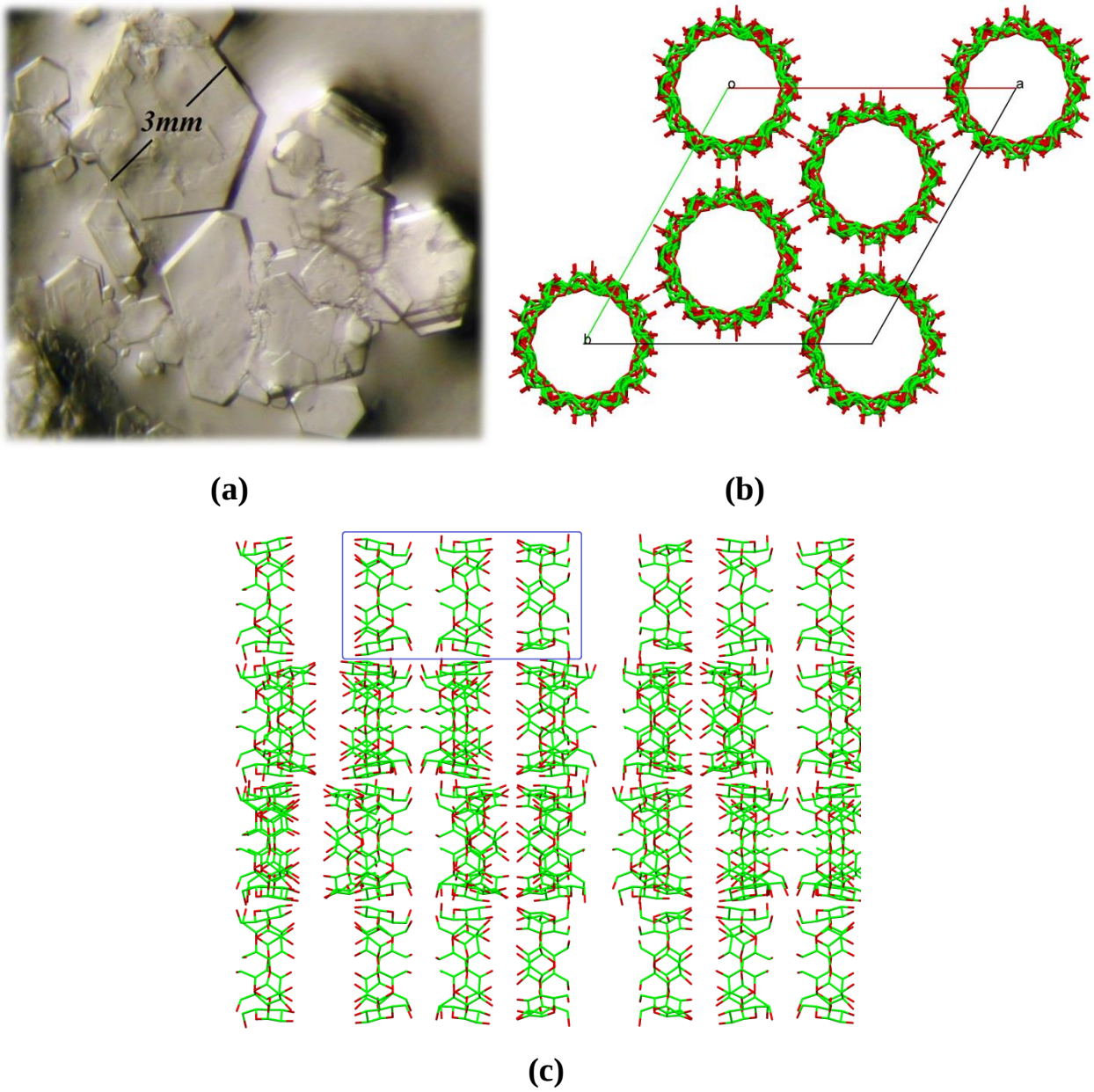

Figure 3.2.3 **(a)** hexagonal shaped crystals of a-CD-new polymorph, **(b,c)** long channels formed by stacking of α-CD molecules in head to head trimers extended along the *c*-axis. Hydrogen atoms and solvent molecules were omitted for clarity.

We were able to calculate an approximate value for the void volume inside the structure using the contact surface with a 1.2 Å probe radius in ***Mercury*** software.

This calculation resulted in a unit cell void volume of 16131.35Å^3 and equal to 30.5% of the structure. This might give potential application in the field of gas storage and molecular absorption.

3.2.3 Crystal structures of α-CD.KOH-ABA complexes

Going back to our subject, the establishment of an inclusion complex systems, we decided to use both properties of cyclodextrin, i.e., the ability of CDs to form inclusion complexes by mean of their hydrophobic cavity, and to form MOFs with alkali metal cations by mean of their multiple –OCCO– binding motifs, in order to develop a new strategy to capture ABA molecules inside the cyclodextrins cavities. This strategy is based on two main steps:

1) The first step is preparation of a salt from ABA and KOH.

2) The second step aims to construct MOFs by mixing this salt with CD. This has to stabilization of the ABA^- ions, which form the contortions for K^+ cations, inside the MOFs network.

This strategy has enabled us to prepare two α-CD inclusion complexes in MOFs with both mABA (**MOF-1**) and oABA (**MOF-2**) in presence of KOH. The structures belong to the monoclinic $P2_1$ space group with unit cell dimensions:
a *= 16.4499(5),* ***b****=14.1657(4),* ***c*** *= 23.5031(6) Å and* ***β*** *= 93.206(2) in* ***MOF-1***
a *= 14.1031(6),* ***b*** *= 23.3959(8),* ***c*** *=16.6293(7) Å and* ***β*** *= 95.139(4) in* ***MOF-2****.*
The basic building block, in these two crystal structures, is a box designed by two α-CD molecules forming a head-to-head dimer containing the ABA ions inside the cavity. K^+ cations, in this case, play role as a lock to this box and a link with the other boxes to construct a long 1D MOFs, as shown in Figure 3.2.4. We think that the formation mechanism of these systems is based on the electrostatic attraction

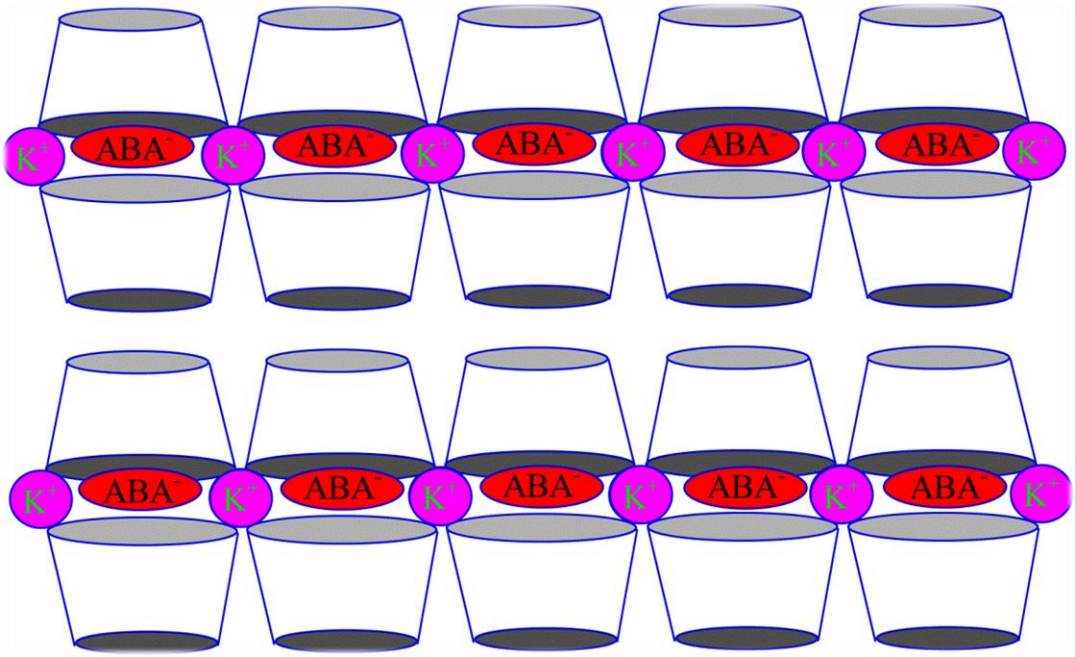

Figure 3.2.4 Simple scheme shows 1D MOFs constructed by linking boxes formed by two α-CD molecules in a head-to-head dimer by potassium cations and containing the ABA ions.

between opposite ions as the planar negative ions (ABA^-) help in alignment of both α-CD molecules to form a dimer and then attracting potassium cations to fix and lock this dimer. Or vice versa, where the potassium cations link α-CD molecules and then they attract ABA^- ions to take place within the cavity. Both assumptions are powered by the previous results: it was found that the α-CD easily reacts with potassium cations, while all our attempts to prepare the complex in the absence of potassium hydroxide lead to a hexagonal structure with channels built by stacking of α-CD molecules in the form of head to head trimers. This underlines the role played by the planar ABA molecules in guidance of α-CD stacking [Figure 3.2.3(c)].

Two α-CD molecules, **A** and **B**, form a head-to-head dimer in both ***MOF-1*** and ***MOF-2*** [Figure 3.2.5], in which the glycosidic (O_{4n}) atoms lie in a plane within 0.0373 and 0.1630Å in ***MOF-1*** and 0.0822 and 0.2203Å in ***MOF-2***, for molecule **A** and **B** respectively, [Figure 3.2.6 (a,b)]. These two glycosidic (O_{4n})

plans in **A** and **B** molecules make an angle 10.68(3) ° in ***MOF-1*** and 4.61(3) ° in ***MOF-2***. The corresponding distance from center to center of the two O_{4n} planes is 7.256 Å in ***MOF-1*** versus 7.336Å in ***MOF-2***. All glucose residues, in both MOFs, are in the normal $^4C_1$ chair conformation, and the overall α-CD molecules show distorted hexagon geometry. This appears more clearly in molecule **A** in both **MOF-*1*** and ***MOF-2***, where the diagonal distance measured between the glycosidic oxygen atoms (O_{4n}) range from 8.203(5)-8.786(5) Å and 8.432(5) - 8.494(5) Å in

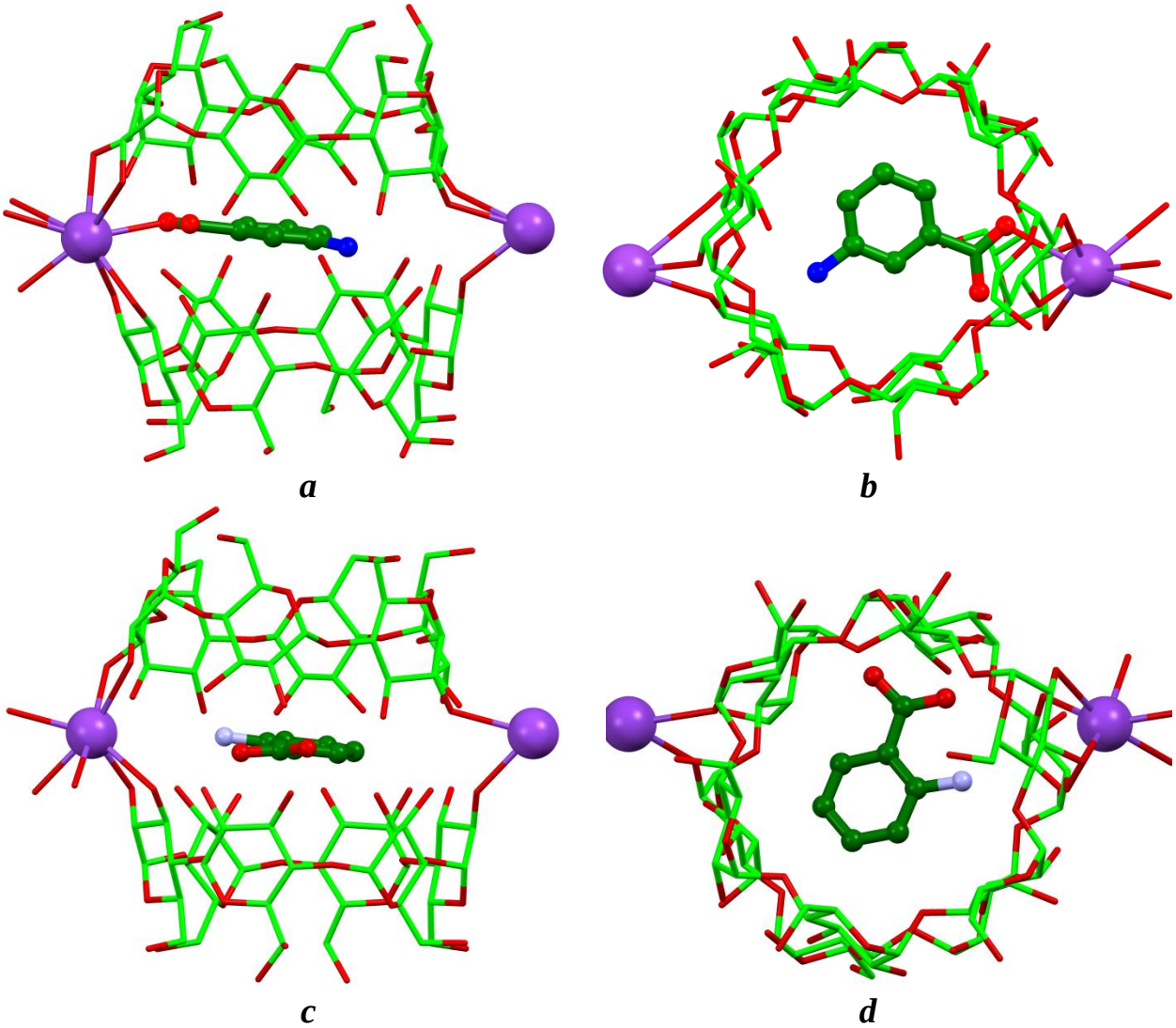

Figure 3.2.5 The structures of α-cyclodextrin MOFs with (***a,b***) *m*-aminobenzoate potassium and (***c,d***) *o*-aminobenzoate potassium. Hydrogen atoms and solvent molecules were omitted for clarify.

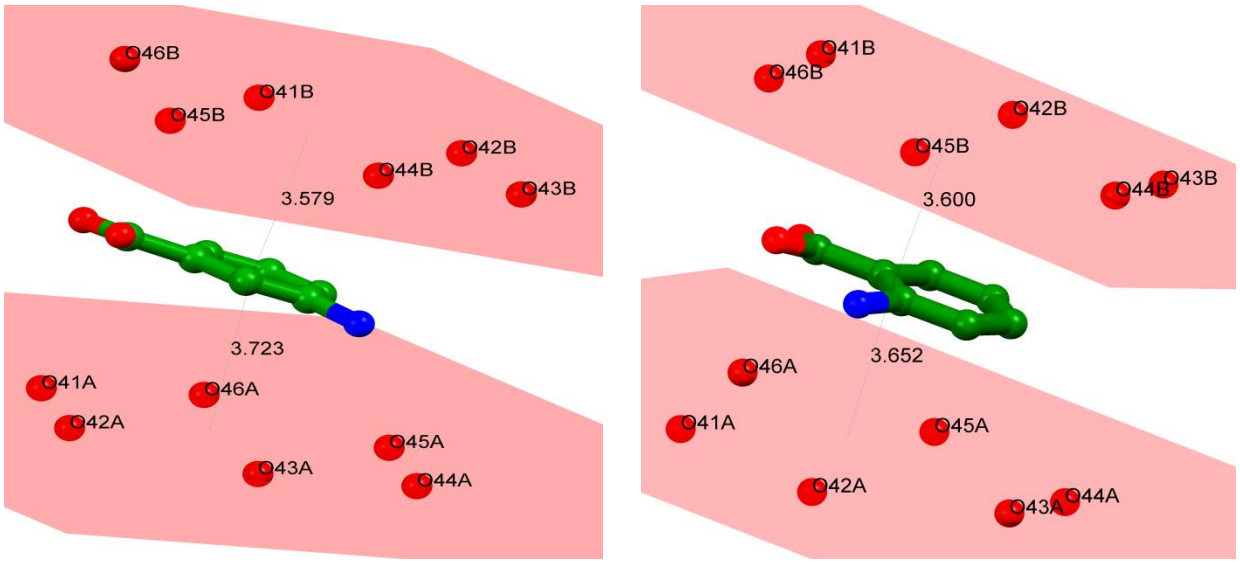

a ***b***

Figure 3.2.6 Definition of the planes made by six glycosidic oxygen atoms O4n (in red): **(*a*)** with mABA, **(*b*)** with oABA.

the molecules **A** and **B** respectively for the ***MOF-1***, and from 8.150(7)-8.641(7)Å and 8.121(7)-8.598(7) Å in the molecules **A** and **B** respectively for the ***MOF-2***. A similar distorted structure was, also, observed in other α-CD complexes [42]. The $O_{4n}\ldots O_{4(n+1)}$ distance varies between 4.094(5)- 4.401(5) Å and 4.180(5)- 4.331(6) Å, and the $O_{4(n-1)}\ldots O_{4n}\ldots O_{4(n+1)}$ angles range from 115.4(1)-122.9(1)° and 113.1(1)-121.6(1)° in the molecules **A** and **B** respectively for the ***MOF-1***. These distances range from 4.112(7)-4.272(7)Å and 4.024(7)-4.336(7) Å, and the angles range from 114.8(2)-124.2(2)° and 117.0(2)-125.1(2)° in the molecules **A** and **B** respectively for the ***MOF-2*** **[**Table 3.2.3].

The annular geometry of α-CD molecules is stabilized by interglucose $O_{3n}\ldots O_{2(n+1)}$ hydrogen bonds with O…O distances ranging from 2.723(2)-3.620(1) Å in ***MOF-1*** and from 2.735(4)-3.524**(1)**Å in ***MOF-2***. There are 5 water molecules located outside the α-CD cavities beside of 7 methanol molecules. Three of them occupy the centers of α-CD cavities and the rest are located at the edges of α-CD

Table 3.2.3 α-CD macrocycle characteristics.

MOF-1						
α-CD Molecule	***Residue***	***D[a](Å)***	***φ[b](°)***	***d[c](Å)***	***T_1[d](°)***	***T_2[e](°)***
A	***G1***	*4.262(7)*	*121.5(1)*	*0.018(3)*	*57.0(7)*	*-65.7(6)*
	G2	*4.112(7)*	*122.9(1)*	*0.031(3)*	*47.4(7)*	*-72.5(6)*
	G3	*4.248(7)*	*115.6(1)*	*-0.047(3)*	*57.6(6)*	*-65.1(6)*
	G4	*4.272(7)*	*121.7(1)*	*0.012(3)*	*54.5(6)*	*-69.1(5)*
	G5	*4.215(7)*	*122.8(1)*	*0.040(3)*	*-171.9(6)* *42.5(9)*	*70.6(7)* *-75.0(7)*
	G6	*4.255(7)*	*115.4(1)*	*-0.055(3)*	*58.7(6)*	*-63.2(6)*
B	***G1***	*4.254(7)*	*118.5(1)*	*-0.183(3)*	*60.5(7)*	*-62.3(6)*
	G2	*4.315(7)*	*121.6(1)*	*0.009(3)*	*57.9(6)*	*-64.1(6)*
	G3	*4.024(7)*	*118.9(1)*	*0.066(3)*	*-175.9(5)*	*62.4(6)*
	G4	*4.336(7)*	*120.7(1)*	*0.029(3)*	*65.1(6)*	*-57.3(6)*
	G5	*4.279(7)*	*118.1(1)*	*-0.202(3)*	*55.1(6)*	*-67.6(6)*
	G6	*4.157(7)*	*119.7(1)*	*0.282(3)*	*-161.8(5)*	*76.2(7)*
MOF-2						
Molecule	***Residue***	***D[a](Å)***	***φ[b](°)***	***d[c](Å)***	***T_1[d](°)***	***T_2[e](°)***
A	***G1***	*4.262(7)*	*124.2(2)*	*-0.221(4)*	*55.4(8)*	*-66.3(8)*
	G2	*4.112(7)*	*118.2(2)*	*-0.088(4)*	*-155.1(8)*	*84(1)*
	G3	*4.248(7)*	*118.1(2)*	*0.285(4)*	*61.1(8)*	*-61.0(7)*
	G4	*4.272(7)*	*122.1(2)*	*-0.166(3)*	*55.2(8)*	*-66.6(8)*
	G5	*4.215(7)*	*119.4(2)*	*-0.136(3)*	*52.1(9)*	*-72.5(8)*
	G6	*4.255(7)*	*114.8(2)*	*0.327(4)*	*57.9(8)*	*-65.4(7)*
B	***G1***	*4.254(7)*	*117.1(2)*	*0.104(4)*	*-179.1(6)* *53.7(6)*	*59.1(9)* *-68.2(6)*
	G2	*4.315(7)*	*125.1(2)*	*-0.079(4)*	*43.9(9)*	*-76.1(8)*
	G3	*4.024(7)*	*117.0(2)*	*-0.034(3)*	*47.4(8)*	*-73.3(7)*
	G4	*4.336(7)*	*119.5(1)*	*0.118(3)*	*-177.4(6)*	*62.7(8)*
	G5	*4.279(7)*	*122.6(2)*	*-0.090(3)*	*51.0(8)*	*-67.6(7)*
	G6	*4.157(7)*	*118.2(2)*	*-0.020(4)*	*49.7(9)*	*-71.4(7)*

a Distance between atoms $O_{4n}\ldots O_{4(n+1)}$.
b Angles between atoms $O_{4(n-1)}\ldots O_{4n}\ldots O_{4(n+1)}$.
c Deviations (Å) from the least-squares optimum plane of the seven O_{4n} atoms.
[d] Torsion angle (°) C_{4n}–C_{5n}–C_{6n}–O_{6n}.
[e] Torsion angle (°) O_{5n}–C_{5n}–C_{6n}–O_{6n}.

molecules in ***MOF-1***, while 9 water molecules and 4 methanol molecules are cocrystallized in ***MOF-2*** with two methanol molecules taking place at the centers of the two α-CD cavities. Hydrogen bonds between the two α-CDs molecules **A** and **B,** in addition to those among α-CDs, the guest and solvent molecules are listed in Table 3.2.4.

Table 3.2.4 Hydrogen Bonds in ***MOF-1*** and ***MOF-2***.

MOF-1					
D– H	***A***	***D–H (Å)***	***H…A (Å)***	***D…A (Å)***	***D–H…A (°)***
O21B–H21C	$O2_{i}$	0.82	1.87	2.655(7)	159
N1–H1B	$O34B_{ii}$	0.86	2.56	3.195(8)	131
O1M–H1M	$O62A_{viii}$	0.82	1.96	2.638(6)	139
O3M–H3M	$O61B_{ix}$	0.82	1.93	2.719(7)	162
O4M–H4M	O6M	0.82	1.95	2.701(11)	152
O5M–H5M	O3M	0.82	1.91	2.720(15)	170
O6M–H6M	O65A	0.82	1.94	2.658(11)	145
O7M–H7M	O5W	0.82	1.89	2.622(19)	148
O21A–H21C	$O36A_{ii}$	0.82	2.12	2.939(6)	174
O21A–H21C	O46A	0.82	2.45	2.844(5)	111
O22A–H22C	O31A	0.82	2.43	3.018(6)	129
O22B–H22D	O32B	0.82	2.49	2.850(6)	108
O22B–H22D	O36A	0.82	2.44	3.099(5)	138
O23A–H23C	O1	0.82	2.57	3.182(6)	132
O23A–H23C	O33A	0.82	2.59	2.897(6)	104
O23A–H23C	$O35B_{ii}$	0.82	2.43	3.063(5)	134
O23B–H23D	O3W	0.82	1.97	2.730(7)	155
O1W–H1W1	$O35A_{iv}$	1.13	2.55	3.050(7)	105
O24A–H24C	O33A	0.82	2.02	2.836(6)	170
O24A–H24C	O43A	0.82	2.46	2.853(5)	111
O1W–H2W1	$O31A_{iv}$	1.06	2.02	3.070(7)	170
O25B–H25C	$O2W_{vii}$	0.82	1.93	2.678(6)	152
O26A–H26C	$O21A_{v}$	0.82	1.97	2.781(5)	168
O26B–H26D	O1	0.82	2.23	2.833(7)	131
O26B–H26D	O45B	0.82	2.38	2.795(7)	112
$O2W_{viii}$–H2W2	O32A	0.84	2.00	2.827(7)	168
$O3W_{v}$–H1W3	O1W	0.87	2.23	2.936(7)	138
O3W–H1W3	$O36A_{iv}$	0.87	2.45	2.848(6)	109
O3W–H2W3	$O21B_{ii}$	0.86	2.18	2.814(7)	131
O4W–H1W4	O4M	0.87	2.15	2.790(10)	130
O4W–H2W4	O66B	0.86	1.89	2.754(9)	179
O31A–H31C	$O31B_{ii}$	0.82	2.22	3.035(6)	170
O31B–H31D	O22B	0.82	2.59	3.033(6)	116
O5W–H1W5	O4W	0.87	1.92	2.711(16)	152
O32A–H32C	O23A	0.82	1.96	2.734(6)	157
O32B–H32D	O23B	0.82	2.10	2.911(6)	171
O32B–H32D	O42B	0.82	2.45	2.844(5)	110
O5W–H2W5	$O63B_{ii}$	0.84	2.01	2.848(14)	173
O33A–H33C	$O25B_{ii}$	0.82	2.47	2.945(5)	118
O33A–H33C	$O35B_{ii}$	0.82	2.53	3.043(5)	122
O34A–H34C	$O24B_{ii}$	0.82	2.56	3.044(5)	119
O34A–H34C	$O25A_{ii}$	0.82	2.21	2.836(5)	133
O34B–H34D	O25B	0.82	1.91	2.723(6)	175
O34B–H34D	O44B	0.82	2.56	2.928(5)	109

O35A–H35C	O26A	0.82	2.00	2.799(5)	163
O35A–H35C	O45A	0.82	2.46	2.827(5)	108
O35B–H35D	O25B	0.82	2.46	2.810(6)	107
O35B–H35D	O33A$_{i}$	0.82	2.46	3.043(5)	129
O36A–H36C	O32B	0.82	1.95	2.767(5)	171
O36B–H36D	O21B$_{ii}$	0.82	2.03	2.831(6)	166
O61A–H61E	O5M$_{iii}$	0.82	1.68	2.445(14)	154
O61B–H61F	O62B$_{x}$	0.82	2.24	2.710(7)	117
O62A–H62E	O2M$_{iii}$	0.82	1.92	2.676(8)	153
O62B–H62F	O52B	0.82	2.43	2.787(7)	107
O62B–H62F	O61A$_{v}$	0.82	2.04	2.763(8)	146
O63A–H63E	O54B$_{vi}$	0.82	2.54	3.133(6)	130
O63A–H63E	O64B$_{vi}$	0.82	2.22	2.895(6)	140
O63B–H63F	O3M	0.82	1.96	2.749(7)	162
O64B–H64F	O1M$_{vii}$	0.82	1.88	2.700(6)	179
O66A–H66E	O61B$_{iv}$	0.82	2.47	3.237(8)	157
O66B–H66F	O7M	0.82	2.01	2.830(11)	177

Symmetry*: i [x,-1+y,z], ii [x,1+y,z] iii [-1+x,y,z], iv [-x,1/2+y,1-z], v [-x,-1/2+y,1-z], vi [-x,1/2+y,-z], vii [1-x,-1/2+y,-z], viii [1+x,y,z], ix [1-x,1/2+y,1-z], x [1-x,-1/2+y,1-z].*

MOF-2

D– H	*A*	*D–H (Å)*	*H…A (Å)*	*D…A (Å)*	*D–H…A (°)*
O1W– H1W1	O35B$_{i}$	0.84	2.05	2.805(8)	149
N1 – H1A	O2	0.86	2.06	2.690(9)	129
O1M– H1M	O4M	0.82	2.18	2.66(2)	117
O1W– H2W1	O2W	0.85	2.48	2.879(7)	109
O1W– H2W1	O33B	0.85	2.49	3.283(8)	156
O2M– H2M	O10A	0.84	2.21	2.88(4)	138
O2W– H1W2	O25A$_{ii}$	0.87	1.97	2.693(8)	140
O3M– H3M	O65B$_{i}$	0.82	1.87	2.678(8)	170
O2W– H2W2	O23A	0.82	2.24	2.657(7)	112
O4M– H4M	O62A$_{iii}$	0.82	2.25	2.863(17)	131
O3W– H1W3	O62B	0.84	1.94	2.723(9)	156
O3W– H2W3	O66B	0.84	1.93	2.729(7)	159
O4W– H1W4	O32B	0.87	1.96	2.831(7)	177
O4W– H2W4	O34B$_{iv}$	0.83	2.07	2.896(7)	173
O5W– H1W5	O9W$_{v}$	0.85	2.17	2.939(12)	150
O5W– H2W5	O61B$_{vi}$	0.85	2.13	2.844(10)	141
O5W– H2W5	O63A$_{vi}$	0.85	2.37	2.763(9)	108
O6W– H1W6	O53A	0.84	2.10	2.942(8)	176
O6W– H2W6	O7W	0.88	1.99	2.867(10)	177
O7W– H1W7	O52B$_{vii}$	0.89	2.22	2.952(8)	139
O7W– H2W7	O6W	0.85	2.44	2.867(10)	112
O8W– H1W8	O64A$_{ii}$	0.86	2.33	2.914(10)	126
O8W– H2W8	O9W$_{viii}$	0.84	2.21	2.853(13)	133
O9W– H1W9	O65A$_{ii}$	0.89	2.32	3.028(14)	137
O9W– H2W9	O56A	0.85	2.25	3.095(11)	172
O21A– H21C	O1$_{i}$	0.82	1.88	2.618(7)	149
O21A– H21C	O46A	0.82	2.57	2.863(7)	103
O21B– H21D	O2	0.82	2.30	3.117(7)	177
O22A– H22C	O31A	0.82	1.99	2.799(7)	167
O22A– H22C	O41A	0.82	2.39	2.808(8)	112
O22B– H22D	O32B	0.82	2.52	2.894(7)	109
O22B– H22D	O36A	0.82	2.38	3.194(7)	170
O23A– H23C	O2W	0.82	2.38	2.657(7)	101
O23A– H23C	O33A	0.82	2.54	2.885(7)	106
O23A– H23C	O35B$_{i}$	0.82	2.51	3.277(7)	155
O23B– H23D	O32B	0.82	2.19	2.852(6)	137
O23B– H23D	O42B	0.82	2.50	2.804(7)	103
O24A– H24C	O33A	0.82	2.14	2.949(7)	169

O24A– H24C	O43A	0.82	2.42	2.807(7)	110
O24B– H24D	$O22B_{vii}$	0.82	1.88	2.670(7)	162
O25A– H25C	O34A	0.82	2.05	2.866(7)	172
O25A– H25C	O44A	0.82	2.44	2.830(7)	110
O25B– H25D	$O33A_{ii}$	0.82	2.42	3.016(7)	130
O25B– H25D	$O21B_{ix}$	0.82	2.08	2.671(7)	129
O26A– H26C	$O35A_{ii}$	0.82	2.03	2.843(7)	170
O26A– H26C	O45A	0.82	2.41	2.818(7)	111
O31A– H31C	$O2_{i}$	0.82	2.07	2.662(7)	129
O31B– H31D	O1	0.82	2.56	3.028(7)	118
O31B– H31D	$O21A_{ii}$	0.82	2.11	2.875(7)	156
O32A– H32C	O23A	0.82	1.96	2.765(7)	166
O32B– H32D	O26A	0.82	2.52	2.955(7)	115
O32B– H32D	O36A	0.82	2.05	2.835(7)	161
O33A– H33C	O23A	0.82	2.60	2.885(7)	102
O33A– H33C	$O35B_{i}$	0.82	2.21	3.013(7)	166
O33B– H33D	O24B	0.82	2.09	2.777(7)	142
O34A– H34C	$O34B_{i}$	0.82	2.06	2.849(7)	160
O34B– H34D	O25B	0.82	1.94	2.735(6)	162
O34B– H34D	O44B	0.82	2.56	2.922(7)	108
O35A– H35C	$O33B_{i}$	0.82	2.11	2.873(7)	155
O35B– H35X	$O26B_{ii}$	0.82	2.21	2.985(7)	158
O35B– H35X	$O45B_{ii}$	0.82	2.48	2.829(7)	107
O36A– H36C	O1	0.82	1.92	2.693(7)	156
O36B– H36D	$O2_{i}$	0.82	2.29	3.031(7)	151
O36B– H36D	$O21B_{i}$	0.82	2.54	2.891(7)	107
O61A– H61E	$O63A_{x}$	0.82	1.97	2.754(7)	159
O62A– H62E	$O10A_{i}$	0.86	2.50	3.240(20)	145
O62B– H62F	$O8W_{iv}$	0.82	1.87	2.660(10)	160
O63A– H63E	$O5W_{xi}$	0.82	1.95	2.763(9)	172
O63B– H63F	O3M	0.82	1.97	2.740(8)	157
O64A– H64E	$O66A_{xii}$	0.82	1.90	2.712(7)	169
O64B– H64F	O54B	0.82	2.44	2.824(7)	110
O64B– H64F	$O66A_{vii}$	0.82	2.13	2.863(8)	150
O65A– H65E	$O3W_{xiii}$	0.82	1.98	2.759(7)	159
O65B– H65F	$O51A_{vii}$	0.82	2.59	3.145(7)	126
O65B– H65F	$O61A_{vii}$	0.82	2.02	2.760(7)	150
O66A– H66E	$O63B_{iv}$	0.82	1.95	2.727(7)	157
O66B– H66F	O5W	0.82	1.95	2.764(8)	176

Symmetry*: i [-1+x,y,z], ii [1+x,y,z], iii [1+x,y,1+z], iv[1-x,-1/2+y,1-z], v [x,y,1+z], $_{vi}$ [-x,-1/2+y,1-z], vii[1-x,1/2+y,1-z], viii [1-x,1/2+y,-z], ix [2-x,1/2+y,1-z], x [-x,-1/2+y,-z], xi [-x,1/2+y,1-z], $_{xii}$ [-x,1/2+y,-z], xiii [-1+x,y,-1+z].*

The crystal structures of ***MOF-1*** and ***MOF-2*** reveal that K^+ cations not only assist in the assembly of $(\alpha\text{-CD})_2$ boxes, but they also serve to link these boxes together in a one-dimensional array extended throughout crystal parallel to **b**-axis in **MOF-1** and to **a**-axis in **MOF-2**. Each K^+ cation is involved in the assembly of pairs of α-CD repeating motifs by coordination to the secondary faces of adjacent α-CD tori, through their secondary hydroxyl groups. At this level of structure, significant differences between the two MOFs appears in the nature of ligands that

coordinate the K^+ cation and in the coordination number of K^+ cation [Figure 3.2.7].

In ***MOF-1***, K^+ links four contiguous α-CD molecules by coordination to their secondary faces and one oxygen atom comes from the carboxylate group of mABA, K^+…O bond lengths range from 2.697(5) to 3.273(4) Å, resulting in an overall coordination number of eight around each K^+ ion. In ***MOF-2***, K^+ links, also, four contiguous α-CD molecules by coordination to their secondary faces and

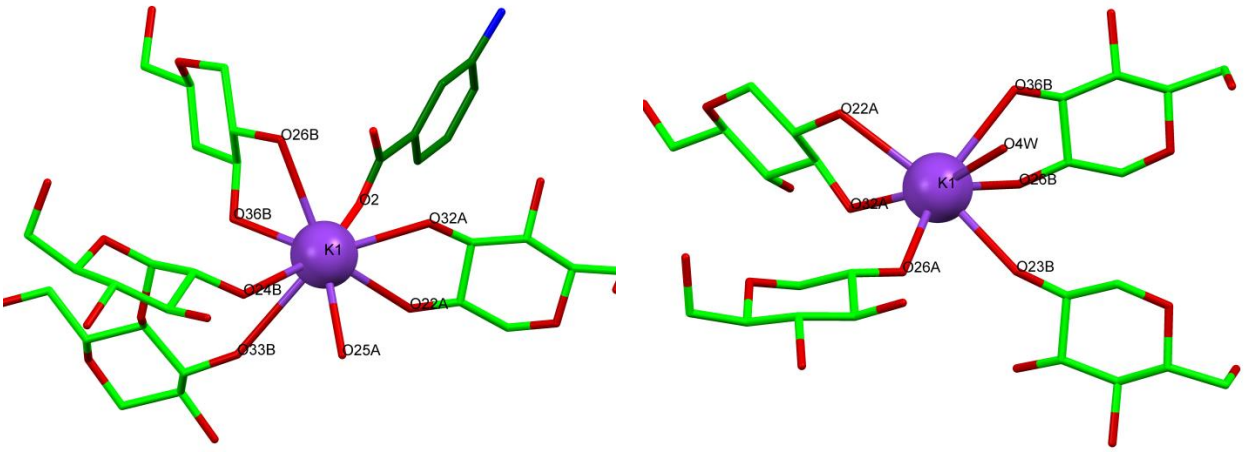

a ***b***

Figure 3.2.7 Potassium coordination **(a)** in ***MOF-1*** and **(b)** in ***MOF-2***.

one oxygen atom of water molecules, with K^+…O bond lengths ranging from 2.662(5)-2.918(5) Å, resulting in an overall coordination number of seven around each K^+ ion. The majority of K^+…O bonds lengths, in both MOFs, are longer than the sum of the ionic radii of K and O (2.66 Å) [Table 3.2.5].

The anionic form of mABA and oABA is observed in the complex with α-CD.KOH where it plays the role of counterion for the potassium cation. No extra electron density peaks are observed in difference Fourier maps neither close to the

Table 3.2.5 Potassium coordination in ***MOF-1*** and ***MOF-2***.

MOF-1		***MOF-2***	
M–L	**Bond length (Å)**	**M–L**	**Bond length (Å)**
K1–O2	2.893(6)	K1–O4W	2.897(7)
K1–O24B	2.822(4)	K1–O22A	2.861(5)
K1–O22A	2.840(5)	K1–O23B	2.732(5)
K1–O25A	2.745(4)	K1–O26A	2.721(6)
K1–O26B	3.028(5)	K1–O26B	2.719(5)
K1–O32A	2.697(5)	K1–O32A	2.662(5)
K1–O36B	2.703(5)	K1–O36B	2.918(5)
K1–O33B	3.273(4)		

COO^- nor the NH_2 groups that could account for an extra H atom. Deprotonation of the carboxylic function is further established by similar values for the two C-O bond lengths: 1.273(8) and 1.232(8) Å in mABA, 1.277(9) and 1.270(9) Å in oABA. Both mABA and oABA are planar entities with non-hydrogen atoms lie in a plane within 0.0469 and 0.0930 Å, respectively. The $mABA^-$ anion plays role as one of the eight ligands that bind the potassium cation through the $-COO^-$ group ($K^+ \ldots O^- = 2.893(5)$ Å). In contrast, this is not observed in the case of $oABA^-$ anion. The angles between the aromatic rings of the guest ions and the two O_{4n} plans are 10.68(3)° and 4.61(3)° in ***MOF-1,*** 4.70(9)° and 5.31(9)° in ***MOF-2*** [Figure 3.2.6].

The overall stacking arrangement of the MOFs in the crystal structure is in head-to-head monomers linked together by K^+ cations forming chains extended along the ***b***-direction in ***MOF-1***, and the ***a***-direction in ***MOF-2***, which are stacked in a zipper-like fashion in these directions. This leads to an extensive hydrogen bonding, not only between the secondary hydroxyls groups of both α-CD rings

forming the dimers, but also including the primary hydroxyls groups of the α-CD rings and the solvent molecules. This gives the cavities a slightly elliptical shape [Figure 3.2.8].

3.3 Conclusion

The interaction between potassium cations and α-CD have been established and well characterized in the crystalline state. The structure shows 3D MOFs and α-CD adopts a cage crystal structure packing stabilized, mainly, by coordinating the potassium cation through the –OCCO– motifs, in addition to intermolecular and intramolecular hydrogen bondings. A new morph of α-CD belonging to the tube crystal structure packing form has been accidentally established during the attempt to produce an inclusion complex with mABA and oABA. This new morph has a potential application in the field of gas storage and molecular absorption. Although present during crystallization, the "guest" mABA or oABA is not present in the crystal. Its presence is however essential to obtain this polymorphic form. A new technique was found to prepare a drug carrier based on the cyclodextrins by relying on their ability to form MOFs with alkali metals cations and possession of a hydrophobic cavity to receive the drug molecule inside. Two MOFs were prepared by this technique between α-CD and K^+mABA^- and K^+oABA^- showing a1D MOFs where K+ cations assist in the assembly of two α-CD molecules to form a box containing a guest inside the cavity.

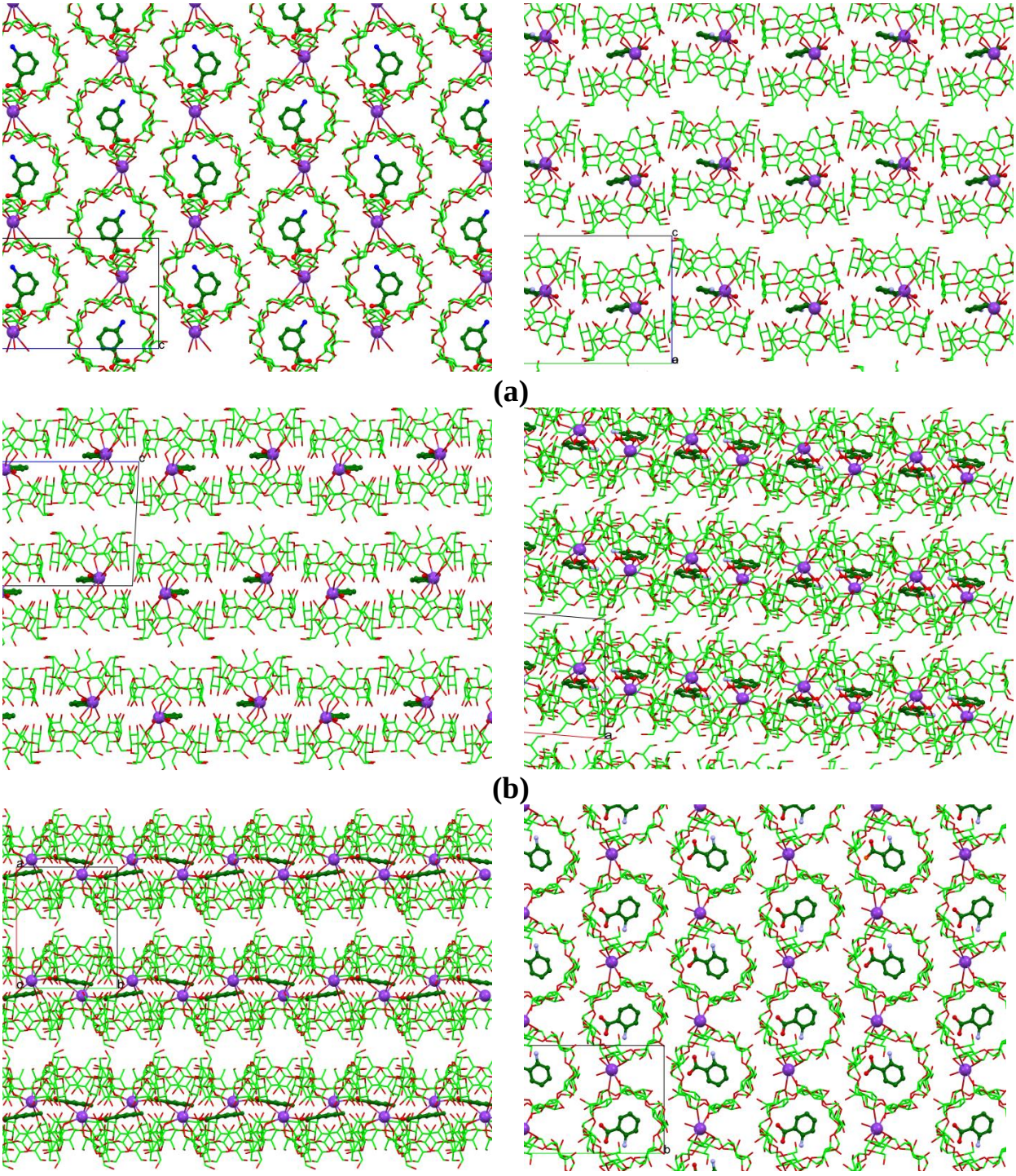

Figure 3.2.8 Drawing of the packing of the ***MOF-1*** (left) and ***MOF-2*** (right), viewed along ***a*** axis (**a**), ***b*** axis (**b**) and ***c*** axis (**c**).

3.4 Experimental

3.4.1 Crystallization

Crystals of α-CD-KOH MOF were prepared by dissolving α-CD and KOH in water in 1:8 stoichiometry. The solution was stirred and heated about 60°C. Then 1 ml of this solution was taken in a 3ml tube and this in turn was placed in a 100 ml flask containing methanol. The slow diffusion of methanol vapor in aqueous solution causes a decrease in the solubility of the substances in the mixture of water / methanol and thus formation of crystals. Colorless crystals, parallelepiped prism shaped, suitable for X-ray data collection were obtained after one week.

An attempt, also, has been performed to prepare inclusion complex between α-CD and oABA and mABA, by dissolving α-CD (0.1mmol) in water (2.5 mL) at 65°C and oABA or mABA (0.1mmol) in ethanol (2.5 mL) at 65°C. Both solutions were mixed and stirred at 65°C for 6 hours. Then the mixture was stored at room temperature. Colorless crystals, hexagonal prism shaped, suitable for X-ray data collection were obtained by slow evaporation after one week.

Crystals of complexes between α-CD and K^+oABA^- and K^+mABA^- salts were prepared by dissolving oABA or mABA and KOH in water and then adding α-CD to the solution. 1 ml of this solution was taken in a 3ml tube and this in turn was placed in a 100 ml flask containing methanol. Colorless crystals, parallelepiped prism shaped, suitable for X-ray data collection were obtained in a few days.

3.4.2 X-ray diffraction experiment.

X-ray diffraction experiments were carried out at low temperature (~150° K) on an Oxford Gemini R Ultra using Mo Kα radiation (λ= 0.7107 Å) operating at 50 kV, 40 mA in case of a-CD-KOH, ***MOF-1*** and ***MOF-2***, and using Cu Kα radiation

(λ= 1.5418 Å) in case of new polymorph of α-CD. Data reduction was carried out with the CrysAlisPro program [43].

The structures were determined by direct method using SIR2011 package [44] and refined using full-matrix least-squares based on F^2 with the program SHELX [45]. The refinement procedures converged to R1= 0.0395 for I > 2sigma(I) and 0.0499 for all data in α-CD-KOH, 0.0774 for I > 2sigma(I) and 0.0873 for all data in α-CD new polymorph, 0.0733 for I > 2sigma(I) and 0.0782 for all data in ***MOF-1*** and 0.0896 for I > 2sigma(I) and 0.1017 for all data in ***MOF-2***. Water and methanol molecules were located in difference Fourier maps. All non-hydrogen atoms were anisotropically refined. Secondary hydroxyl groups were refined with two alternate conformations. Hydrogen atoms were calculated at ideal positions and refined using a riding model except those attached to some hydroxyl groups and on the water molecules that were located in difference Fourier maps. Selected crystal data collection and refinement details are listed in Table 3.4.1.

Table 3.4.1 Crystallographic data.

Crystallographic data	**α-CD-KOH**	**α-CD new polymorph**	**MOF-1**	**MOF-2**
Chemical formula	$C_{36}H_{60}O_{30}$,K_2CO_3, CH_3OH, $5H_2O$	$4C_{36}H_{60}O_{30}$, nH_2O	$2C_{36}H_{60}O_{30}$,$KC_7H_6NO_2$, $7CH_3OH$, $5H_2O$	$2C_{36}H_{60}O_{30}$,$KC_7H_6NO_2$, $4CH_3OH$, $10H_2O$
Temperature (K)	150(2)	150(2)	150(2)	150(2)
Wavelength (Å)	Mo Kα λ= 0.7107	Cu Kα λ= 1.5418	Mo Kα λ= 0.7107	Mo Kα λ= 0.7107
Crystal system	Orthorhombic	Hexagonal	Monoclinic	Monoclinic
Space group	$P2_12_12_1$	R3	$P2_1$	$P2_1$
a (Å)	13.1136(3)	23.6696(4)	16.4499(5)	14.1031(6)
b (Å)	13.9866(4)	23.6696(4)	14.1657(4)	23.3959(8)
c (Å)	28.7054(8)	109.0704(15)	23.5031(6)	16.6293(7)
α (°)	90.00	90.00	90.0	90.0
β (°)	90.00	90.00	93.206(2)	95.139(4)
γ (°)	90.00	120.00	90.0	90.0
Volume ($Å^3$)	5265.0(2)	52920(2)	5468.2(3)	5464.8(4)
Z	4	36	2	2
Crystal description	Parallelepiped	Hexagonal prism	Prism	Prism
Theta range for data collection (°)	3.37 - 29.23	2.69 - 67.57	3.16 - 28.16	3.24 - 29.20
Limiting indices	$-15 \le h \le 15$ $-16 \le k \le 13$ $-30 \le l \le 34$	$-28 \le h \le 24$ $-24 \le k \le 25$ $-110 \le l \le 129$	$-15 \le h \le 15$ $-16 \le k \le 13$ $-30 \le l \le 34$	$-13 \le h \le 19$ $-31 \le k \le 29$ $-21 \le l \le 22$
Reflections collected/unique	9137 / 7440	34303/29042	16961/15713	17413/14917
R (int)	0.0264	0.0302	0.0401	0.0798
Data/restraints/parameters	9137/2/732	34303/1/3097	16961/48/1457	17413/65/1454
Goodness-of-fit (S) on F^2	0.971	1.047	1.076	1.090
Refinement method	Full-matrix least-squares on F2	Full-matrix least-squares on F2	Full-matrix least-squares on F2	Full-matrix least-squares on F2
Final R indices [I > 2sigma(I)]	0.0395	0.0774	0.0733	0.0896
Final R indices (all data)	0.0499	0.0873	0.0782	0.1017
Largest difference peak and hole ($e/Å^3$)	0.445, -0.373	1.178, -0.754	1.023, -0.922	1.181, -0.519

3.5 References

1. Leslie J. Murray , Mircea Dincă and Jeffrey R. Long Chem. Soc. Rev., 2009,38, 1294-1314.
2. Alexander U. Czaja , Natalia Trukhan and Ulrich Müller Chem. Soc. Rev., 2009,38, 1284-1293.
3. Ryan J. Kuppler, Daren J. Timmons, Qian-Rong Fang, Jian-Rong Li, Trevor A. Makal, Mark D. Young, Daqiang Yuan, Dan Zhao, Wenjuan Zhuang and Hong-Cai Zhou. Coordination Chemistry Reviews, 2009, 253, 3042–3066.
4. A. D. Burrows, C. G. Frost, M. F. Mahon, C. Richardson, Angew. Chem., Int. Ed. 2008, 47, 8482-8486.
5. Y. Zhao, L. Liu, W. Zhang, C. Sue, Chem. Eur. J. 2009, 13356-13380][Q. Li, W. Zhang, O. S. Miljanic, C. –H. Sue, Y. –L. Zhao, L. Liu, C. B. Knobler, J. F. Stoddart and O. M. Yaghi, Science, 2009, 325, 855-859.
6. A. D. Burrows, C. G. Frost, M. F. Mahon and C. Richardson. Chem. Commun. 2009, 28, 4218-4220.
7. K. K. Tanabe, C. A. Allen, S. M. Cohen, Angew. Chem., Int. Ed. 2010, 49, 9730-9733.
8. R. K. Deshpande, J. L. Minnaar, S. G. Telfer, Angew, Chem., Int. Ed. 2010, 49, 4598-4602.
9. K. Gedrich, I. Senkovska, I. A. Baburin, U. Mueller, O. Trapp, S. Kaskel, Inorg. Chem. 2010, 49, 4440-4446.
10. D. Zhao, D. J. Timmons, D. Yuan, H.-C. Zhou, Acc. Chem. Res. 2011, 44, 123-133.
11. J. M. Roberts, O. K. Farha, A. A. Sarjeant, J. T. Hupp, K. A. Scheidt, Cryst. Growth Des. 2011, 11, 4747-4750.
12. D. J. Lun, G. I. N. Waterhouse, S. G. Telfer, J. Am. Chem. Soc. 2011, 133, 5806-5809.

13. Imaz, I.; Rubio-Martinez, M.; An, J.; Sole-Font, I.; Rosi, N. L.; Maspoch, D. Chem. Commun. 2011, 47, 7287–7302.
14. Smaldone, R. A.; Forgan, R. S.; Furukawa, H.; Gassensmith, J. J.; Slawin, A. M. Z.; Yaghi, O. M.; Stoddart, J. F. Angew. Chem., Int. Ed. 2010, 49, 8630–8634.
15. Gassensmith, J. J.; Furukawa, H.; Smaldone, R. A.; Forgan, R. S.; Yaghi, O. M.; Stoddart, J. F. J. Am. Chem. Soc. 2011, 133, 15312–15315.
16. Dietrich, B.; Lehn, J.-M.; Sauvage, J.-P. Tetrahedron Lett. 1969, 10, 2885-2888.
17. Dietrich, B.; Lehn, J.-M.; Sauvage, J.-P. Tetrahedron Lett. 1969, 10, 2889-2892.
18. Truter, M. R.; Pedersen, C. J. Endeavour, 1971, 30, 142-145.
19. Moras, D.; Metz, B.; Weiss, R. Acta Crystallogr., Sect. B 1973, 29, 383-388.
20. Lehn, J.-M.; Sauvage, J. P.; Dietrich, B. J. Am. Chem. Soc. 1970, 92, 2916-2918.
21. Lehn, J.-M.; Sauvage, J.-P. J. Chem. Soc. D, Chem. Commun. 1971, 9, 440-441.
22. Lehn, J.-M.; Sauvage, J.-P. J. Am. Chem. Soc. 1975, 97, 6700-6707.
23. Kauffmann, E.; Lehn, J.-M.; Sauvage, J.-P. Helv. Chim. Acta 1976, 59, 1099-1111.
24. Forgan, R. S.; Smaldone, R. A.; Gassensmith, J. J.; Furukawa, H.; Cordes, D. B.; Li, Q.; Wilmer, C. E.; Botros, Y. Y.; Snurr, R. Q.; Slawin, A. M. Z.; Stoddart, J. F. J. Am. Chem. Soc. 2012, 134, 406-417.
25. Stoddart, J. F. Chem. Soc. Rev. 1979, 8, 85-142.
26. Han, S.; Wei, Y.; Valente, C.; Lagzi, I.; Gassensmith, J. J.; Coskun, A.; Stoddart, J. F.; Grzybowski, B. A. J. Am. Chem. Soc. 2010, 132, 16358-16361.
27. Moras, D.; Metz, B.; Weiss, R. Acta Crystallogr., Sect. B 1973, 29, 383-388.

28. Bogdan, M.; Caira, M. R.; Farcas, S. I. Supramol. Chem. 2002, 14, 427 -436.
29. Noltemeyer, M.; Saenger, W. J. Am. Chem. Soc. 1980, 102, 2710-2722.
30. Benner, K.; Klufers, P.; Schuhmacher, J. Angew. Chem., Int. Ed. Engl. 1997, 36, 743-745.
31. Benner, K.; Ihringer, J.; Klufers, P.; Marinov, D. Angew. Chem., Int. Ed. 2006, 45, 5818-5822.
32. Lippold, I.; Vlay, K.; Gorls, H.; Plass, W. J. Inorg. Biochem. 2009, 103, 480-486.
33. Charpin, P.; Nicolis, I.; Villain, F.; de Rango, C.; Coleman, A. W. Acta Crystallogr., Sect. C 1991, 47, 1829-1833.
34. Chetcuti, P. A.; Moser, P.; Rihs, G. Organometallics 1991, 10, 2895-2897.
35. Caira, M. R.; Griffith, V. J.; Nassimbeni, L. R.; Vanoudtshoorn, B. J. Chem. Soc., Chem. Commun. 1994, 1061-1062.
36. Nicolis, I.; Coleman, A. W.; Charpin, P.; de Rango, C. Acta Crystallogr., Sect. B 1996, 52, 122-130.
37. Caira, M. R.; Griffith, V. J.;Nassimbeni, L. R. J. Incl. Phenom. Macro. Chem. 1998, 32, 461-476.
38. Nicolis, I.; Coleman, A. W.; Selkti,M.;Villain, F.; Charpin, P.; de Rango,C. J. Phys. Org. Chem. 2001, 14, 35-37.
39. Lippold, I.; Gorls, H.; Plass, W. Eur. J. Inorg. Chem. 2007, 1487-1491.
40. Irina V. Terekhova; Roman S. Kumeev; Gennadiy A. Alper. J Incl Phenom Macrocycl Chem. 2007, 59, 301-306.
41. Yimin Zhang *, Shanbao Yu, Feng Bao. Carbohydrate Research. 2008, 343, 2504–2508.
42. Harata, K. Bull. Chem. Soc. Jpn. 1977, 50, 1416-1424.
43. CrysAlisPro, version 1.171.33.55; Oxford Diffraction Ltd.: Oxfordshire, UK, 2010.

44. M. C. Burla, R. Caliandro, M. Camalli, B. Carrozzini, G. L. Cascarano, C. Giacovazzo, M. Mallamo, A. Mazzone, G. Polidori and R. Spagna. *SIR2011*: a new package for crystal structure determination and refinement. *J. Appl. Cryst.* 2012, 45, 357-361.
45. G. M. Sheldrich, *Acta Crystallographica Section A.* 2008, *64*, 112-122.

Chapter 4

Determination of the structure and the absolute configuration of Aegelinol and 1,10-(propane-1,3-diyl)-bis-(6,7-dimethoxy-2-methyl-1,2,3,4-tetrahydroisoquinoline) hydrochloride by using X-ray diffraction technique

Abstract

The absolute configuration and crystal structure of three stereoisomers of 1,10-(propane-1,3-diyl)-bis-(6,7-dimethoxy-2-methyl-1,2,3,4-tetrahydroisoquinoline) hydrochloride, after resolution by semi-preparative chiral HPLC, and aegelinol, a pyranocoumarin isolated from *Ferulago asparagifolia* Boiss (Apiaceae), has been determined by crystallography. Absolute configuration of the first mentioned compounds were obtained directly by Flack parameter, while the crystal structure of the inclusion complex of aegelinol in β-cyclodextrin allowed unambiguous determination of the absolute configuration of the stereogenic center of aegelinol.

4.1 Introduction

4.1.1 Absolute configuration

An absolute configuration in stereochemistry is the spatial arrangement of the atoms of a chiral molecular entity or group and when the absolute configuration is obtained the assignment of R or S is based on the Cahn-Ingold-Prelog priority rules [1].

Absolute configuration of synthetic chiral molecules can often be deduced from knowledge of reaction mechanisms in organic chemistry applied to well-

characterized transformations from starting materials of known absolute configuration to the final products. Optical rotation and circular dichroism can also be used to predict absolute configuration, usually based on rules for the sign of the rotation angle or circular dichroism bands. Nuclear magnetic resonance (NMR) is blind to chirality, but ancillary methods for deducing absolute configuration using chiral shift reagents or chemical derivatives have been devised. However, whenever methods such as organic reaction mechanisms, optical rotation, circular dichroism or NMR are relied upon fully over time, exceptions necessarily arise that result in erroneous predictions. Conversely, X-ray crystallography, with its many technical improvements in recent years, has become the recognized standard for the a priori determination of the absolute configuration of chiral molecules.

All enantiomerically pure chiral molecules crystallize in one of the 65 Sohncke Groups (*Chiral Space Groups: these 65 space groups contain only rotation or screw axes. They are space group numbers: 1, 3-5, 16-24, 75-80, 89-98, 143-146, 149-155, 168-173, 177-182, 195-199 and 207-214*). Rigorous differentiation of enantiomers by the X-ray diffraction method is now possible through several ways. For example, a comparison of the intensities of Bijvoet pairs or of the R factors for the two possible structures can suggest the correct absolute structure. One of the more powerful and simple approaches is using the Flack parameter ***x(u)***, because this single parameter clearly indicates the absolute structure [2-3]. The processes used to decide the absolute structure by Flack parameter use the anomalous dispersion effect (anomalous scattering effect).

The scattering of X-rays from electrons is called Thomson scattering. It occurs because the electron oscillates in the electric field of the incoming X-ray beam and an oscillating electric charge radiates electromagnetic waves. Thus, X-rays are radiated from the electron at the same frequency as the primary beam. However, most electrons radiate π radians (180◦) out of phase with the incoming beam, as

shown by a mathematical model of the process. The motion of an electron is heavily damped when the X-ray frequency is close to the electron resonance frequency; this occurs near an absorption edge of the atom, this led to changing the relative phase of the radiated X-rays to $\pi/2$ (90°) and giving rise to the phenomenon of anomalous (resonant) scattering. If anomalous scattering takes place, the atomic scattering factor*(Fig 4.1.1) is altered to take this into account. Only some of the electrons in the atom are affected and they will scatter the X-rays roughly $\pi/2$ out of phase with the incident beam. Electrons scattering exactly $\pi/2$ out of phase are represented mathematically by an imaginary component of the scattering factor and they cease to contribute to the real part.[4]

However, atomic scattering factors have imaginary parts due to the anomalous dispersion effect, and Friedel's law is broken by this effect. As it has been mentioned above, the anomalous dispersion occurs when a wavelength λ is selected that is near the absorption edge of an atom creates a partial ionization process. Some new X-ray radiation is generated from the inner electron shells of the atoms. Thus the atomic scattering factor can therefore be best described as a complex number:

$$f_j = f_{j,o} + \Delta f_j' + i.\Delta f_j''$$

Where:

- f_j : is the atomic scattering factor.
- $f_{j,o}$: is a function of diffraction angle θ and equal to the number of electrons in the j^{th} atom at $\theta = 0$.
- $\Delta f_j'$ and $\Delta f_j''$: are an atom type and λ dependent.
- $i = \sqrt{-1}$, the imaginary unit.

* An atom that can be considered as a set of Z electrons (its atomic number) can be expected to scatter Z times that which an electron does. An atom scatters Z times only in the direction of the incident beam, decreasing with the increasing of the θ angle (the angle between the incident radiation and the direction where we measure the scattering). We give the name atomic scattering factor to the ratio between the amplitude scattered by an atom and a single electron.

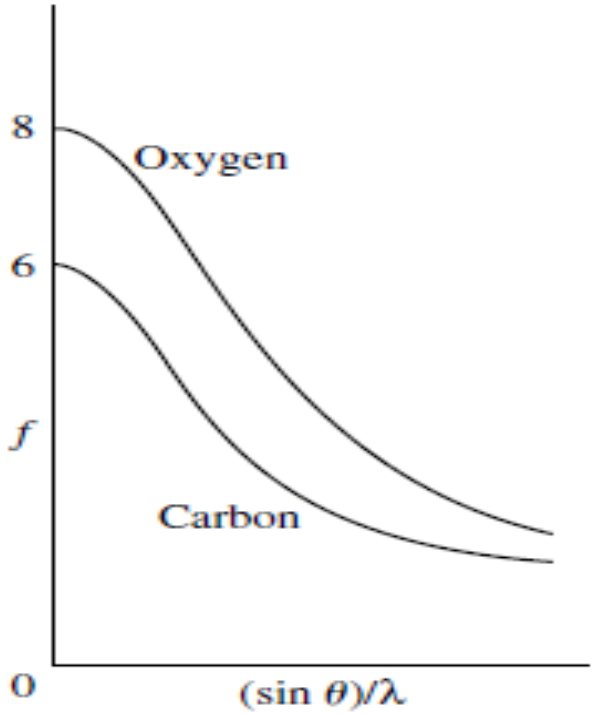

Fig. 4.1.1 Dependence of atomic scattering factors on diffraction angle θ.

We can conclude from the previous discussion that if atomic scattering factors did not have imaginary parts, the Friedel pairs would have exactly the same amplitudes (Friedel's law) i.e., the scattering intensity $|F(h\ k\ l)|^2$ from crystal plane (h k l) is equal to $|F(-h\ -k\ -l)|^2$ from the opposite crystal plane (-h -k -l). In this case the intensity is given:

$$I(hkl) = |F(h\ k\ l)|^2$$

In the case of the anomalous dispersion, the atomic scattering factors have imaginary parts; the Friedel pairs wouldn't have exactly the same amplitudes:

$$|F(h\ k\ l)|^2 \neq |F(-h\ -k\ -l)|^2$$

Then the Flack parameter can be calculated during the structural refinement using the equation given below:

$$I(hkl)=(1-x)\ |F(hkl)|^2 + x|F(-h-k-l)|^2$$

Where:

- x : is the Flack parameter usually found to be between 0 and 1.
- $I(hkl)$: is the scaled observed intensity at the position hkl.
- $F(hkl)$: calculated structure factor:

It can be expressed in terms of the contents of a single unit cell as:

$$F(hkl) = \sum_{j=1}^{N} f_j \, e^{2\pi i(hx_j + ky_j + lz_j)}$$

- N: is the number of atoms in the unit cell.
- f_j : is the atomic scattering factor of j^{th} atom.
- $i = \sqrt{-1}$, the imaginary unit.
- x_j, y_j and z_j are the fractional coordinates that give the position of the j^{th} atom.

If the ***x*** value is near **0**, with a small standard uncertainty ***(u)***, the absolute structure given by the structure refinement is likely correct, and if the value is near **1**, then the inverted structure is likely correct. If the value is near **0.5**, the crystal may be racemic or twinned. The technique is most effective when the crystal contains both lighter and heavier atoms. Light atoms usually show only a small anomalous dispersion effect.

There are conditions under which one may say that the absolute structure of the crystal has been determined satisfactorily:

- Firstly one wants to know whether the absolute configuration determination is sufficiently precise by looking to see whether the standard uncertainty ***u*** of the Flack parameter ***x(u)*** is sufficiently small: in general u should be less than 0.04 but this value may be relaxed to 0.10 for a compound proven by other means to be enantiomerically pure.
- Secondly the value of the Flack parameter itself should be close to zero within a region of three standard uncertainties i.e. $\boldsymbol{u} < 0.04$ (or $\boldsymbol{u} < 0.10$ for a chemically proven enantiomeric excess of 100%) and $|\boldsymbol{x}| < 3\boldsymbol{u}$ [5].

However, the absolute configuration could not be determined by anomalous dispersion effects in the diffraction measurement on the crystal due to the absence of atoms heavier than oxygen. This gives rise to standard uncertainties on the Flack parameter which is too large for reliable absolute configuration determination [5]. Options for the absolute structure determination of light atom compounds are still possible:

1) Recently Rob Hooft came up with a new statistical method based on Bayesian statistics (Statistical analysis of Bijvoet pair differences). This method gives access to a Hooft's parameter which is very similar to Flack parameter (Hooft, R.W.W.; Straver, L.H.; Spek, A.L. Determination of absolute structure using Bayesian statistics on Bijvoet differences. J. Appl. Cryst. 2008, 41, 96–103.)[10].

2) Preparing a salt from the compound (e.g. add HBr in case of tertiary N).

3) Co-crystallize with heavy atom compounds (e.g. CBr4).

4) Co-crystallize with compound with known absolute configuration (e.g. CDs).

In many cases, thus, it may be necessary to perform a derivatization of the compound to get a crystalline product. If a chiral reagent is used for this purpose, a second stereogenic center of known absolute configuration is introduced and the X-ray structure obtained is then unambiguous and gives the absolute configuration of the first compound. This approach is classical when salts can be formed, which is not the case for some molecules.

4.1.2 1,10-(propane-1,3-diyl)-bis-(6,7-dimethoxy-2-methyl -1,2,3,4-tetrahydroisoquinoline)*

Synthesis and purification of compounds were performed by the group of Prof. J.-F. Liégeois at ULg.

Small conductance Ca^{2+}-activated K^+ (SK) channels play a role in modulating the firing rate and the firing pattern of neurons [6]. A blockade of these targets could be useful for the treatment of cognitive dysfunction, neuronal hyperexcitability or dopamine related disorders [7]. Currently, available blockers are not suitable pharmacological tools being either peptides or quaternized small molecules [8]. Therefore, from N-methyl-laudanosine a medium potency blocking compound with a quick reversibility [9], it was developed bis-isoquinolinium derivatives with an increased affinity and activity [10].

The mixture of stereoisomers of 1,10-(propane-1,3-diyl)-bis-(6,7-dimethoxy-2-methyl-1,2,3,4-tetrahydroisoquinoline) (Fig 4.1.2) was obtained by reduction of the corresponding bis-isoquinolinium analogue [10] with sodium borohydride under nitrogen atmosphere in methanol. Then, each stereoisomer was isolated by resolution of the bis-tetrahydroisoquinoline mixture by semi-preparative chiral HPLC using a Chiralcel® OD-H column and a mixture of 2-propanol (80)/hexane (20) containing 0.05% diethylamine at a flow rate of 1 mL/min (Fig. 4.1.3). In these conditions, the retention time for the first eluted enantiomer (E1), the meso and the second enantiomer (E2) are ~ 7 min, 10 min and 23 min respectively. Finally, the three compounds are converted into their hydrochloride salt which crystallized in a mixture of methanol/diethyl ether. The hydrochloride forms of both enantiomers E1 and E2 were solubilized in MeOH for specific rotation measurements. The $[\alpha]_D^{20}$ of the first eluted enantiomer, E1, and the second eluted

* Part of this work has been published (European Journal of Medicinal Chemistry **2010**, 45, 3240-3244) A reprint of this paper is given as supplementary material.

enantiomer, E2, are +34.8° and -34.5° respectively.

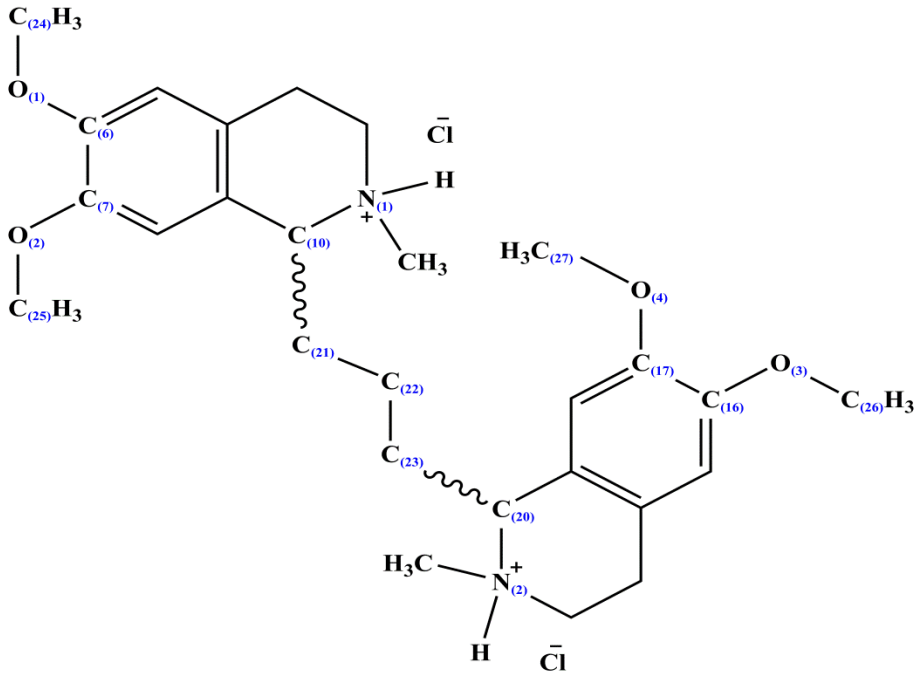

Fig.4.1.2 Chemical structure of 1,10-(propane-1,3-diyl)-bis-(6,7-dimethoxy-2-methyl-1,2,3,4-tetrahydroisoquinoline) dihydrochloride. Numbering of selected atoms is presented.

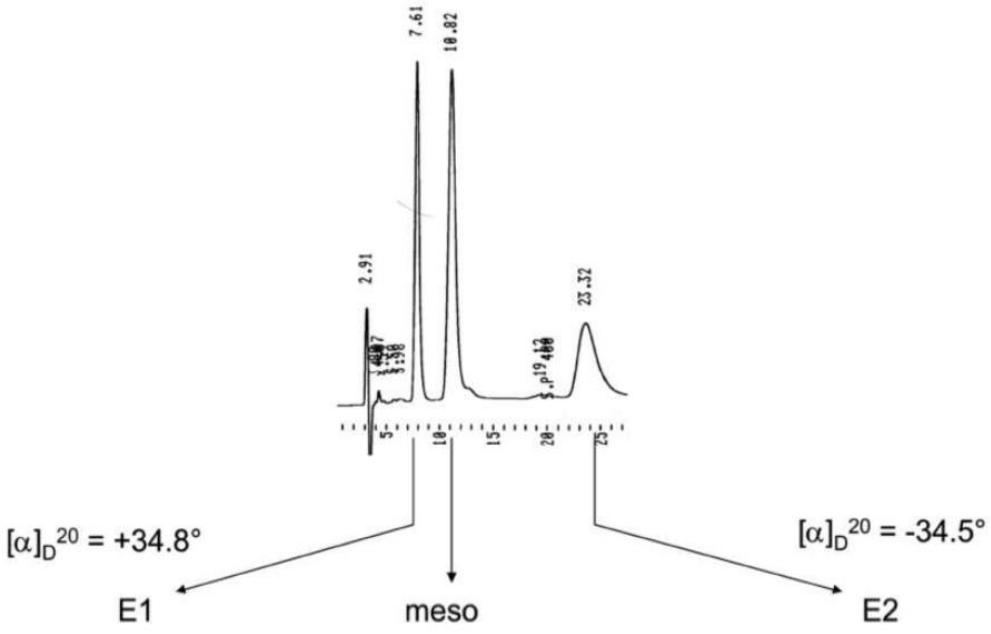

Fig.4.1.3 Resolution of a diastereoisomeric mixture of 1,10-(propane-1,3-diyl)-bis-(6,7 dimethoxy-2-methyl-1,2,3,4-tetrahydroisoquinoline) using a Chiralcel® OD-H column and a mixture of 2-propanol (80)/hexane(20) containing 0.05% diethylamine at a flow rate of 1 mL/min.

4.1.3 Aegelinol*

Aegelinol [11] is a pyranocoumarin that was isolated from Ferulago asparagifolia Boiss (Apiaceae), a species growing in Turkey [11]. Aegelinol has also been reported as a minor lactonic constituent of Aegle marmelos [12]. Three abundant pyranocoumarins (grandivittin (2), agasyllin (3) and aegelinol benzoate (4)) (Fig. 4.1.4) were also isolated from the roots of Ferulago campestris collected in Sicily and aegelinol (1), their hydrolysis product, and agasyllin (3) showed a significant antibacterial effect against Gram-negative and Gram-positive bacteria [13].

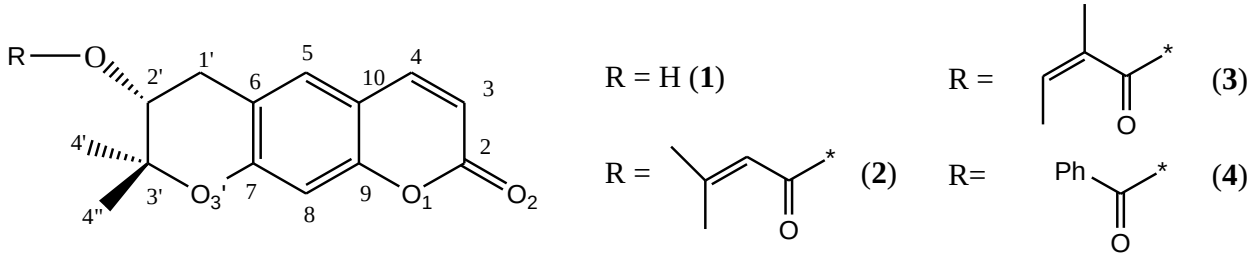

Fig. 4.1.4 The chemical structure and numbering scheme of pyranocoumarins.

The absolute configuration of (1) could not be determined because NMR spectral data of α and β epimers do not significantly differ. Optical rotation measurements however suggest an α configuration for the compound [11]. Compounds (2-4) are ester derivatives of aegelinol (1), whose absolute configuration at C-2' was also not clear. Abyshev et al. [14] reported an (S) C-2' absolute configuration, although they cited the degradative determination of the absolute configuration performed by Lemmich [15]. On the other hand, Erdelmeyer et al. [16] indicated an (R) C-2' configuration. In both cases, the reported optical rotation of the compound was negative. Hydrolysis of the three esters gives the same compound (1) with a negative optical rotation. Consequently,

* Part of this work has been published (Crystals **2012**, 2, 1441-1454). A reprint of this paper is given as supplementary material.

Basile et al [17] decided to determinate the absolute stereochemistry by means of Mosher's and Horeau's (indirect) methods [18-20] and assigned from their NMR data an R configuration for (1) and its esters (2-4).

To circumvent this limit, we decided to co-crystallize aegelinol (**1**) with β-cyclodextrin. In principle, formation of such an inclusion complex with a host of known chirality (β-cyclodextrin consists of seven optically active D-glucose units) should allow direct determination of the absolute configuration of the guest (aegelinol). Indeed, in principle, cyclodextrins form diastereoisomers by including optically active guests within their cavity and should be excellent reagents for the resolution of racemic compounds (and subsequent determination of their absolute configuration). In practice, possibly due to their round and symmetrical structure, only low optical resolution is achieved [21]. As a matter of fact, only a limited number of crystal structures of inclusion complexes of cyclodextrins with chiral guests are available in the Cambridge Structure DataBank (CSD), among which permethylated α-cyclodextrin binding S- and R-mandelic acid (CECMAY10 and CECMEC10- respectively) [22] or R- and S-isomers of flurbiprofen and S-ibuprofen (COYXAP10, COYXET20 [23] and RONWOG [24] respectively) included within the cavity of permethylated β-cyclodextrin. Selected examples of crystal structures of cyclodextrin's inclusion complexes with different chiral molecules are presented in Table 4.1.1, [25-43].

Table 4.1.1. Selected examples of crystal structures of cyclodextrin's inclusion complexes with different chiral molecules available in the Cambridge Structure DataBank (CSD).

CSD (refcode)	Structure name	reference
CECMAY10	Permethylated-α-cyclodextrin (S)-madelic acid	[22]
CECMEC10	Permethylated-α-cyclodextrin (R)-madelic acid	[22]
COYXAP10	Permethylated-α-cyclodextrin (R)-flurbiprofen	[23]
COYXET20	Permethylated-α-cyclodextrin (S)-flurbiprofen	[23]
RONWOG	Permethylated-α-cyclodextrin (S)-ibuprofen	[24]
QOYLEV	hexakis(2,3,6-Tri-O-methyl)-α-cyclodextrin (R)-1,7-dioxaspiro(5.5)undecane clathrate	[25]
QOYLIZ	heptakis(2,3,6-tri-O-methyl)-β-cyclodextrin (S)-1,7-dioxaspiro(5.5)undecane clathrate hydrate	[25]
RACVIA	hexakis(2,3,6-Tri-O-methyl)-α-cyclodextrin (S)-1,7-dioxaspiro(5.5)undecane clathrate hexahydrate	[26]
RACVIA01	hexakis(2,3,6-tri-O-methyl) α-cyclodextrin (R)-(-)-1,7-dioxaspiro[5.5]undecane clathrate hydrate	[27]
AGAZIR	β-Cyclodextrin N-acetyl-L-phenylalanine clathrate dodecahydrate	[28]
AGAZUD	β-Cyclodextrin N-acetyl-D-phenylalanine clathrate hydrate	[28]
BEGWEQ	bis(β-Cyclodextrin) ((3S-trans)-3-((1,3-benzodioxol-5-yloxy)methyl)-4-(4-fluorophenyl)piperidine) clathrate hydrate	[29]
BIJHOR	α-Cyclodextrin 1-phenylethanol tetrahydrate clathrate	[30]
CETKUI	heptakis(2,3,6-Tri-O-methyl)-β-cyclodextrin (-)-(R)-methyl-5-(p-tolyl)imidazolidine-2,4-dione clathrate	[31]
DOCVUM04	bis(β-Cyclodextrin) bis(N-acetyl-L-phenylalanine methyl ester) clathrate hydrate	[32]
VOQDOU	bis(β-Cyclodextrin) bis(N-acetyl-L-phenylalanine amide) clathrate hydrate	[32]
VOQDUA	bis(β-Cyclodextrin) bis(N-acetyl-p-methoxy-L-phenylalanine methyl ester) clathrate hydrate	[33]
DOCVUM06	bis(β-Cyclodextrin) bis(N-acetyl-L-phenylalanine methyl ester) clathrate hydrate	[34]
EKOGOA	Per-O-methyl-β-cyclodextrin (S)-1-(p-bromophenyl) ethanol clathrate	[35]
EKOGOA01	Per-O-methyl-β-cyclodextrin (S)-1-(p-bromophenyl) ethanol clathrate	[36]
YIRZOP	hexakis(2,3,6-Tri-O-methyl)-α-cyclodextrin (S)-1-phenylethanol clathrate	[37]
ZIFQOU	(S)-Naproxen heptakis(2,3,6-tri-O-methyl)-β-cyclodextrin	[38]
GETPAW	β-Cyclodextrin (R)-(-)-fenoprofen clathrate hydrate	[39]
JEJWOK	hexakis(2,3,6-Tri-O-methyl)-α-cyclodextrin (R)-1-phenylethanol monohydrate clathrate	[40]
JEJXAX	hexakis(2,3,6-Tri-O-methyl)-α-cyclodextrin (S)-1-phenylethanol monohydrate clathrate	[40]
PACJEJ	3,5-Dihydroxy-4-(3-hydroxy-4 methoxydihydrocinnamoyl) phenyl)-2-O-(a-L-rhamnopyranosyl)-b-D-glucopyranoside β-cyclodextrin clathrate hydrate	[41]
POVSIC	β-Cyclodextrin trans-cyclohexane-1,4-diol hydrate	[42]
TUSHEV	bis(α-cyclodextrin) (R)-camphor clathrate hydrate	[43]
TUSHIZ	bis(α-cyclodextrin) (S)-camphor clathrate tetradecahydrate	[43]

4.2 Aim of this chapter

In the present work, we report on our efforts to determine, by X-ray crystallography, the structure and the absolute configuration of 1,10-(propane-1,3-diyl)-bis-(6,7-dimethoxy-2-methyl-1,2,3,4-tetrahydroisoquinoline) and aegelinol. And we show that crystallization of an inclusion complex of aegelinol in β-cyclodextrin solved the problem of the inaccurate absolute configuration determination by X-ray anomalous dispersion effects in light atom compounds.

4.3 Results and Discussion

4.3.1 Crystal structure of 1,1'-(propane-1,3-diyl)-bis-(6,7-dimethoxy-2-methyl-1,2,3,4-tetrahydroisoquinolinum)

The crystal structures of the three stereoisomers, E1, E2, and meso of the 1,1'-(propane-1,3-diyl)-bis-(6,7-dimethoxy-2-methyl-1,2,3,4-tetrahydroisoquinolinum) hydrochloride salts (Fig.4.3.1), correspond to the hydrochloride salts of the isoquinoliniums.

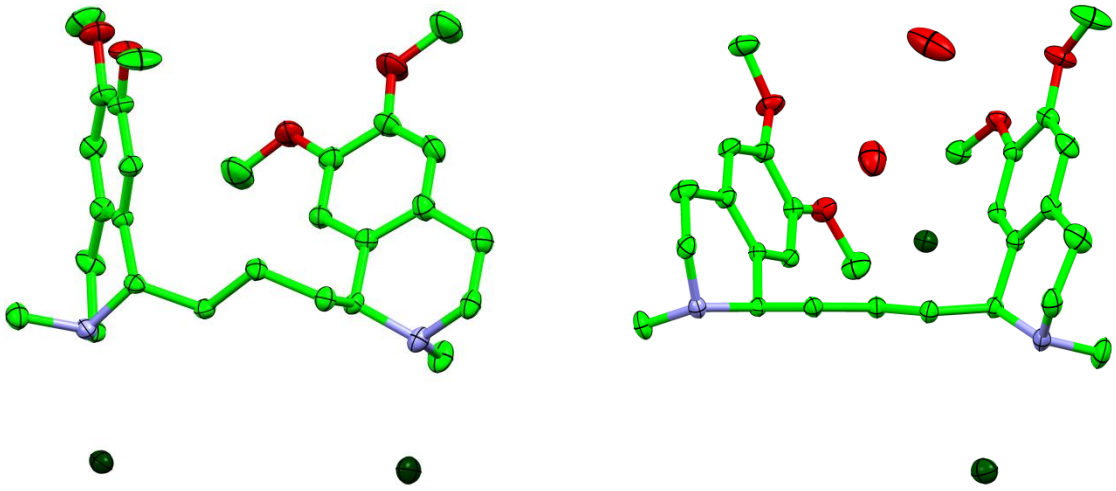

Fig. 4.3.1 Crystal structure conformation (ORTEP thermal motion diagram drawn at 50% probability) of E1 (left) and meso (right). Structure E2 (mirror image of E1) is not presented. H atoms have been omitted for clarity. Only two water molecules are present in the asymmetric unit of the meso structure.

Main crystal data are summarized in Table 4.3.1. Interestingly, the meso structure co-crystallized with 5 water molecules. Stereochemistry of C10 and C20 has been unambiguously established as underlined by the Flack parameters [2] reported in Table 4.3.1: C10 (S)/C20 (S) for E1, C10 (R)/C20 (R) for E2, C10 (R)/C20 (S) and C10 (S)/C20 (R) for meso.

Table 4.3.1. Main statistics on data quality and refinement for the crystal structures of 1,1'-(propane-1,3-diyl)-bis-(6,7-dimethoxy-2-methyl-1,2,3,4-tetrahydroisoquinolinum)

Crystallographic data	***E1***	***Meso***	***E2***
Formula	$C_{27}H_{38}N_2O_4.2\ HCl$	$C_{27}H_{38}N_2O_4.2\ HCl.5H_2O$	$C_{27}H_{38}N_2O_4.2\ HCl$
Mol. Wt.	527.51	617.59	527.51
Dimensions (mm^3)	0.43× 0.37 × 0.07	0.4 × 0.2 × 0.05	0.42× 0.12 × 0.04
Crystal system	monoclinic	monoclinic	monoclinic
Space group	P 2_1	P 2_1/c	P 2_1
a (Å)	11.379(1)	11.745(1)	11.368(1)
b (Å)	8.382(1)	27.328(3)	8.365(1)
c (Å)	15.974(3)	11.337(1)	15.974(2)
α (°)	90.00	90.00	90.00
β (°)	102.26(1)	115.41(1)	102.24(1)
γ (°)	90.00	90.00	90.00
V ($Å^3$)	1487.5(4)	3286.8(5)	1484.5(3)
Z	2	4	2
D_{calc} (gcm^{-3})	1.178	1.832	1.178
$\mu_{CuK\alpha}$ (mm^{-1})	0.250	1.248	0.251
Abs. correction	multi-scan	multi-scan	multi-scan
F(000)	564	1328	564
Meas. reflections	11,920	30,600	12,353
Unique reflections	5223	7139	5205
R_{int}	0.0244	0.0303	0.0360
Obs. refl. ($I_0>2\sigma(I_0)$)	4735	4663	3637
Parameters refined	316	361	316
Goof on F^2	1.057	1.003	0.906
R_1	0.0415	0.0438	0.0437
wR_2 (I0 > 2σ(I0))	0.1023	0.1041	0.0825
wR_2(all data)	0.1040	0.1124	0.0874
Flack parameter	0.00(5)	-	-0.01(6)
Fraction of Friedle pairs	0.853	-	0.849

Bond lengths and valence angles are similar (within experimental errors) in all three compounds and in agreement with geometries observed in similar structures reported in the literature (e.g. structure of alkaloid (±) carnegine, 1,2-Dimethyl-6,7-dimethoxy-1,2,3,4-tetrahydroisoquinoline hydrochloride, CSD refcode KORWOD (Fig. 4.3.2)) [44].

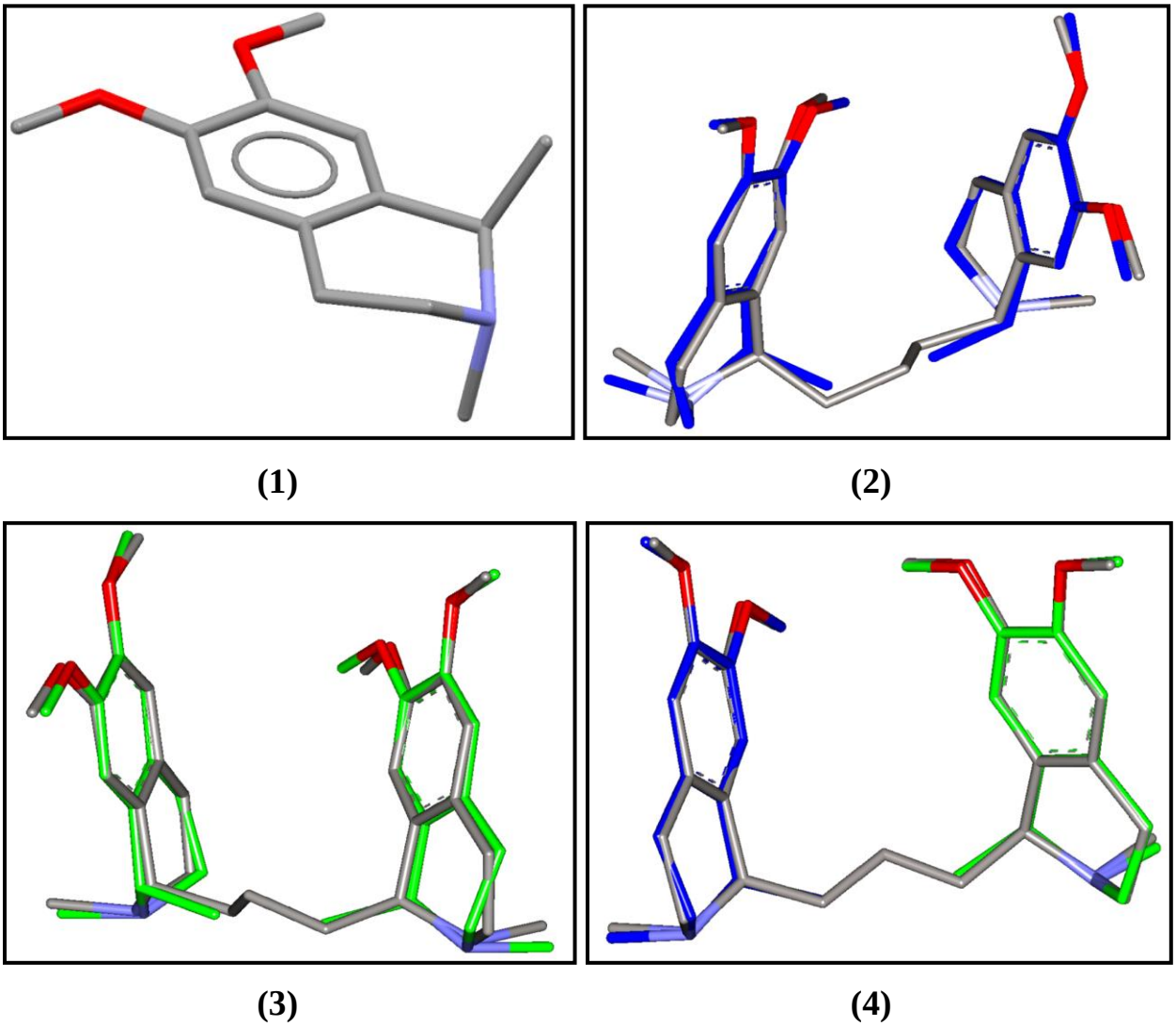

Fig. 4.3.2 **(1)** Crystal structure (capped sticks style) of (±) carnegine, 1,2-Dimethyl-6,7-dimethoxy-1,2,3,4-tetrahydroisoquinoline hydrochloride, CSD refcode KORWOD; **(2)** Superimposition between KORWOD and E2; **(3)** Superimposition between KORWOD and E1; **(4)** Superimposition between KORWOD and meso.
Superimpositions were performed by Accelrys Discovery Studio Client v 2.5.5.9350.

In all three structures, the dimethoxy substituents are coplanar to the phenyl ring of the tetrahydroisoquinoline; the methyl groups pointing in opposite directions (see the torsion angles: C24-O1-C6-C7, C25-O2-C7-C6, C26-O3-C16-C17 and C27-O4-C17-C16) Table 4.3.2.

In all three crystal structures, the two 1,2,3,4-tetrahydropyridinium rings adopt a half-chair conformation with θ and Φ angles (see puckering parameters*, Table 4.3.2) close to 60° and k × 60° [45-46]. As expected, change of the absolute configuration transforms θ into 180 - θ and Φ into 180 + Φ.

In all three structures, atoms C21 and C23 substitute the chiral center atoms C10 and C20 on the axial position. The methyl groups also occupy the axial position on the protonated nitrogen for all three isomers. The relative position of those methyl groups with respect to the dimethoxy-tetrahydroisoquinolinium rings is however significantly different in the structures of E1 or E2 compared to the meso structure as a consequence of the conformation of the propyl linker (Fig. 4.3.2). Indeed, conformation of the propane-diyl linker is all trans (*t, t, t, t*) for the meso structure while it is *t, t, t, g* for the separated stereoisomers E1 and E2 (see torsion angles N1-C10-C21-C22, C10-C21-C22-C23, C21-C22-C23-C20, and C22-C23-C20-N2). As a consequence, the relative orientation of the two 6,7-dimethoxy-2-methyl-1,2,3,4-tetrahydroisoquinolinium rings is similar in both E1 and E2 but different from the one observed in the meso structure (Fig. 4.3.3).

*****For N-membered ring the puckering coordinates q_m and Φ_m given by the equations:

- $z_j = (2/N)^{1/2} \sum_{m=2}^{N/2-1} q_m cos[\Phi_m + 2\pi m(j-1)/N]$

(N odd and m=2, 3, . . ., (N-1)/2)

- $z_j = (2/N)^{1/2} \sum_{m=2}^{N/2-1} q_m cos[\Phi_m + 2\pi m(j-1)/N] + N^{-1/2} q_{N/2}(-1)^{j-1}$

(N even and m=2, 3, . . ., (N-2)/2

z_j is the puckering displacement of j^{th} atom from the least-squares plane.

Total puckering amplitude Q is given by the equations::

$$Q^2 = \sum_m q_m^2 = \sum_{j=1}^{N} z_j^2$$

For six-membered rings (N = 6), there are three puckering degrees of freedom. These are described by a single amplitude-phase pair (q_2, Φ2) and a single puckering coordinate q_3. Alternatively, these coordinates may be replaced by a spherical polar set (Q, θ, Φ),where Q is the total puckering amplitude and θ is an angle ($0 \le \theta \le \pi$) such that

$q_2 = Q \sin\theta$

$q_3 = Q \cos\theta$

(D. Cremer and J. A. Pople, A General Definition of Ring Puckering Coordinates, JACS, 1975, 97, 6, 1354-1358)

Table 4.3.2 Selected geometrical characteristics of the three crystal structures.

Torsion angles (°)	**E1**	**Meso**	**E2**
N1-C10-C21-C22	-173.3(2)	179.4(1)	173.7(2)
C10-C21-C22-C23	172.4(2)	-176.2(1)	-172.0(2)
C21-C22-C23-C20	63.0(2)	-176.0(1)	-63.2(3)
C22-C23-C20-N2	-173.6(2)	-155.4(1)	173.8(2)
C24-O1-C6-C7	174.4(3)	-176.7(2)	-175.1(2)
C27-O4-C17-C16	169.7(3)	-174.7(2)	-169.9(3)
C26-O3-C16-C17	175.1(3)	174.8(2)	-175.2(3)
C25-O2-C7-C6	176.4(3)	178.8(2)	-175.5(2)
Ring puckering parameters	**E1**	**Meso**	**E2**
Ring I [N1 > C10]			
Amplitude Q (Å)	0.494(2)	0.474(2)	0.494(3)
θ (°)	49.6(2)	131.8(2)	130.1(3)
Φ (°)	355.0(4)	180.3(3)	173.2(5)
Ring II [N2 > C20]			
Amplitude Q (Å)	0.507(2)	0.486(2)	0.508(3)
θ (°)	58.4(3)	46.7(2)	121.5(3)
Φ (°)	337.7(4)	8.1(4)	157.2(5)

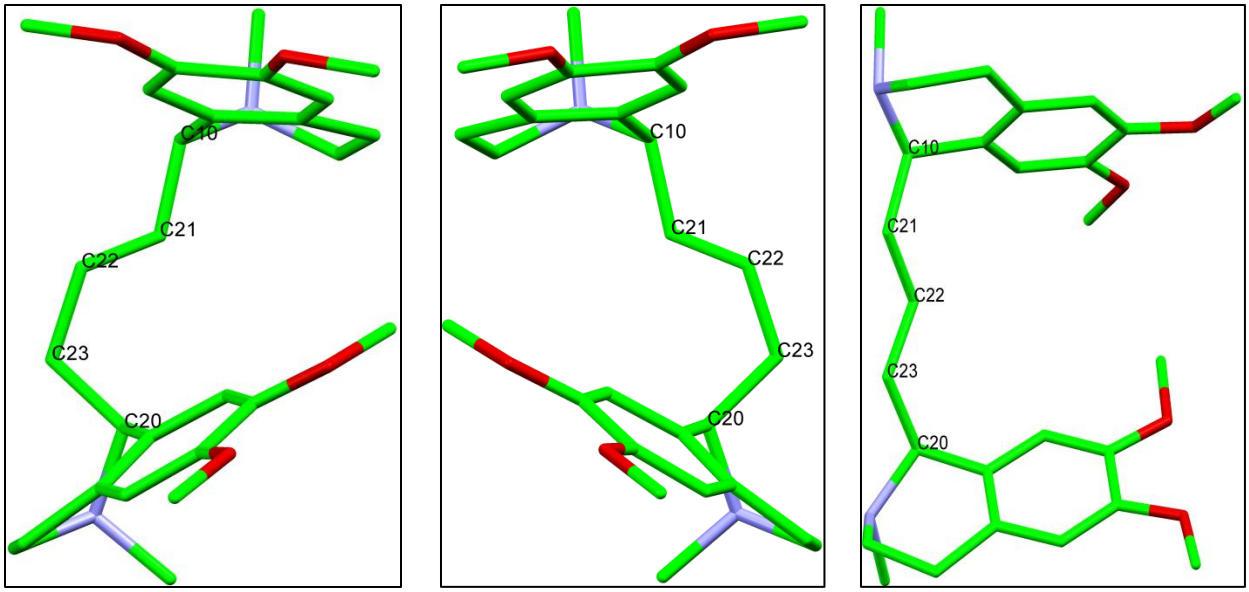

E1 ***E2*** ***Meso***

Fig. 4.3.3 Crystal structure conformation (capped sticks style) shows the propane-diyl linker in the three isomers of 1,1'-(propane-1,3-diyl)-bis-(6,7-dimethoxy-2-methyl-1,2,3,4 tetrahydroisoquinolinum). H atoms, chlorine atoms and water molecules have been omitted for clarity.

In particular, shorter inter-ring distances are observed in E1 and E2 compared to the meso structure. Indeed, centroids of the 6-membered benzene rings of the tetrahydropyridiniums are separated by 5.5 Å in the two *SS* or *RR* enantiomers (centroid distance = 5.541(2) Å and 5.535(2) Å and perpendicular distance of centroid to opposite ring =3.658 Å and 3.644 Å for E1 and E2 respectively) while the tetrahydroisoquinolinum rings are more tilted in the meso structure with a distance between centroids of the benzene rings of 5.897(1) Å (perpendicular distance of centroid to opposite ring = 5.221 Å).

Crystal packing is also distinct in the meso crystal structure when compared to the E1 and E2 structures. In addition to the two chloride counter-ions, the meso structure also co-crystallized with five well defined water molecules that largely contribute to crystal packing through H-bonding (Table 4.3.3). However, in all

three structures, molecule/ions are arranged in layers of polar groups (protonated N cations, chloride ions and water molecules for the meso structure) alternating with stacked aromatic moieties (Fig. 4.3.4). The relative orientation of the different pharmacophoric elements (tetrahydroisoquinolinium rings, methyl substituent, and protonated nitrogen) is distinct between E1 or E2 and the meso structure and could, in part, explain the differences in biological affinities observed for the three isomers. Whether the close inter-ring contacts between the dimethoxy tetrahydroisoquinolinium rings is preserved upon binding to the receptor could be studied by molecular modeling starting from the crystal structure conformations.

Table 4.3.3.Selected hydrogen bond geometries stabilizing crystal packing in the three crystal structures. For clarity, hydrogen bond network involving the water molecules has been simplified and only a selection of hydrogen bonds is presented.

	E1	Meso	E2
N1–H1N···Cl1$_{i}$			
H···A (Å)	2.12	2.17	2.13
D···A (Å)	3.020(2)	3.077(5)	3.025(5)
D–H···A (°)	169	170	169
	i: x, y, -z	***i***: x, 1/2 - y, 1/2 +z	***i***: x, y, z
N2–H2N···Cl2$_{ii}$			
H···A (Å)	2.13	2.20	2.14
D···A (Å)	3.034(2)	3.102(4)	3.038(3)
D–H···A (°)	169	171	169
	ii: x,y,z	***ii***: x, y, z	***ii***: x, y, z
Ow1···Cl2$_{iii}$			
D–H (Å)		2.36	
D···A (Å)		3.174(5)	
D–H ···A (°)		161	
		iii: -1 + x, 1/2 - y, -1/2 + z	
Ow2···Cl1$_{iv}$			
D–H (Å)		2.38	
D···A (Å)		3.212(5)	
D–H···A (°)		165	
		iv: x, y, z	
Ow2···Cl2$_{v}$			
D···H (Å)		2.41	
D···A (Å)		3.206(6)	
D–H···A (°)		157	
		v: -1 + x, 1/2 - y, -1/2 + z	

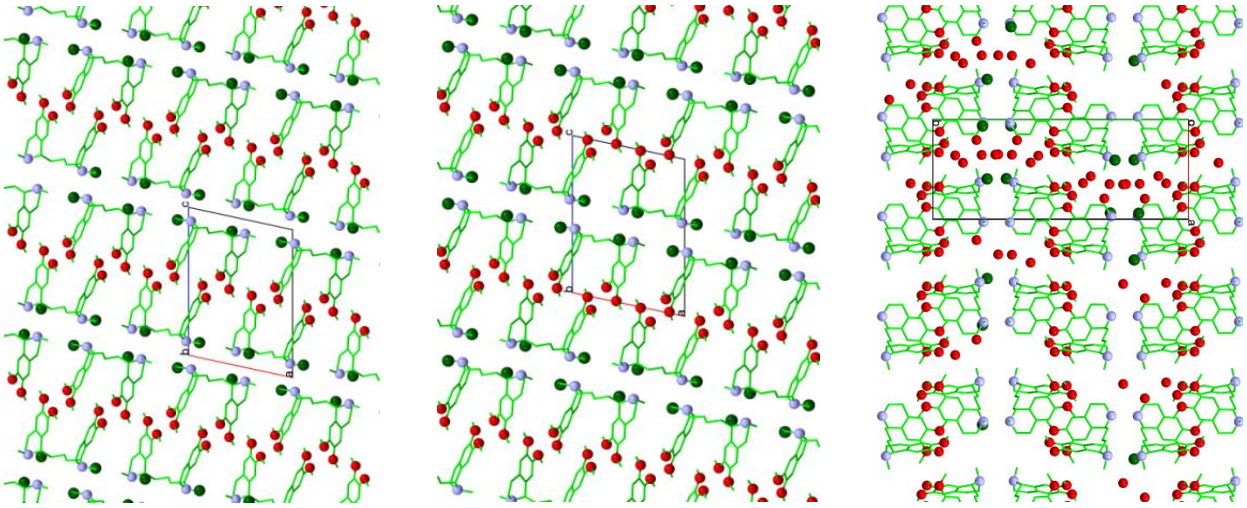

E1 E2 Meso

Fig. 4.3.4 View of the packing of crystal structure E1 and E2 in ***b***-direction and Meso in ***c***-direction showing the alternating layers of polar (protonated nitrogen atoms and chloride ions and water molecules for the Meso structure) and stacked aromatic dimethoxy tetrahydroisoquinoline rings.

4.3.2 Crystal structure of Aegelinol

Crystals of aegelinol (**1**) were obtained at room temperature by slow evaporation from a solution in ethanol. The structure belongs to the orthorhombic $P2_12_12_1$ space group with cell parameters a = 6.8921(3) Å, b = 11.4302(9) Å, c = 44.964(3) Å. The structure was solved by direct methods and refined to a final $R1$ = 4.44%. Main statistics on data quality and refinement are given in Table 4.3.4. The coumarin moiety is planar with RMSDs of fitted atoms from the least-squares plane are 0.0247, 0.0396 and 0.0181 Å for the three molecules A, B and C, respectively. The dihedral angles between these planes in crystal packing are AˆA=2.65(3)°, AˆB = 13.39(3)°, BˆC = 2.99(4)° and AˆC =10.76(2)°. The bond lengths and bond angles observed in this structure are comparable with those reported for other coumarin derivatives in CSD (e.g., GEHWEW [47] and MOFJIA [48]). [Table 4.3.5]

Table 4.3.4. Main statistics on data quality and refinement for the crystal structures of aegelinol (**1**) and its inclusion complex in β-cyclodextrin (**1-BCD**).

Crystallographic data	Aegelinol	β-CD-aegelinol
Chemical formula of asymmetric unit	$3C_{14}H_{14}O_4$	$2C_{42}H_{70}O_{35}.$ $2C_{14}H_{14}O_4.23.5H_2O$
Temperature (K)	150	150
Wavelength (Å)	Mo Kα (0.71073)	Cu Kα (1.54179)
Crystal system	Orthorhombic	Triclinic
Space group	$P2_12_12_1$	P1
a (Å)	6.8921(3)	15.404(1)
b (Å)	11.4302(9)	15.281(1)
c (Å)	44.964(3)	17.890(1)
α (°)	90.00	99.662(1)
β (°)	90.00	113.423(1)
γ (°)	90.00	102.481(1)
Volume ($Å^3$)	3542.2(4)	3618.4(5)
Z	4	1
Calculated density ($g.cm^{-3}$)	1.385	1.466
F(0 0 0)	1560	1704
Absorption coefficient (mm^{-1})	0.102	1.148
Crystal description	Long Rod	Plate
Crystal size (mm)	0.2 × 0.2 × 0.4	0.13 × 0.32 × 0.37
Theta range for data collection (°)	3.25- 25.02	2.81-69.59
Limiting indices	$-8 \leq h \leq 6$ $-11 \leq k \leq 13$ $-46 \leq l \leq 53$	$-18 \leq h \leq 14$ $-18 \leq k \leq 18$ $-21 \leq l \leq 21$
Reflections collected/unique	10327/5883	36967/15938
R (int)	0.0246	0.0355
Data / restraints / parameters	5883 / 0 / 491	15938/88/2082
Goodness-of-fit (S) on F^2	1.097	1.060
Refinement method	Full-matrix least-squares on F^2	Full-matrix least-squares on F^2
Final R indices [I>2sigma(I)]	4.44 %	6.71 %
Final R indices (all data)	5.22 %	7.1 %
Largest difference peak and hole ($e/Å^3$)	0.218 and -0.229	1.249* and -0.419
Flack x parameter	0.4(9)	0.5(2)

* The peak correspond to the density 1.249 is close to the methylene group at the primary side of cyclodextrin and it could be involved in disorder.

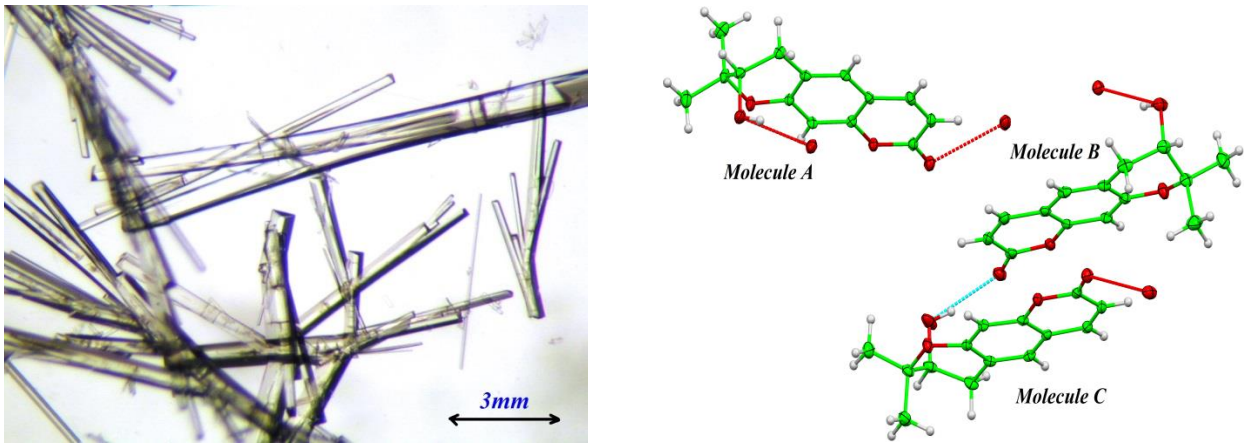

a **b**

Figure 4.3.5 (**a**) Morphology of crystals of aegelinol (**1**) obtained by slow evaporation from a solution in ethanol; (**b**) Conformation of the three independent molecules in the asymmetric unit showing thermal motion (ORTEP, 30% probability).

The packing of molecules in the unit cell gives some indication of the types of interaction that such a molecule would show in biological systems. Two types of interaction are found. First, the molecules are partially flat and pack in planes, where molecules A and its symmetrical equivalences are stacked one above the other in the opposite direction. B and C molecules have exactly the same arrangement as A molecules. The distances between these planes and the centroids of aromatic rings in the next layer are A-A = 3.481Å and B-C = 3.391Å. This arrangement allows optimal π-π interaction (Figure 4.3.6). Second, the carbonyl group interacts with hydroxyl groups in the next layer's molecule with OH…O distances ranging from 2.816(2) to 2.903(3) Å, as shown in Figure 4.3.5, Table 4.3.6.

Statistics of the Flack parameters (x = 0.4(9)) confirm that the absence of suitable heavy atoms (anomalous scatterers) in the molecule is a limitation for reliable absolute configuration of such molecules by X-ray diffraction [5].

Crystal structure of the inclusion complex of aegelinol in β-cyclodextrin (**1-BCD**) was also determined (a = 15.404(1) Å, b = 15.281(1) Å, c = 17.890(1) Å, α = 99.662(1)°, β = 113.423(1)°, γ = 102.481(1)°, P1; $R1$ = 6.71%) and allowed

Table 4.3.5. Selected structural features (bond lengths (Å), valence and torsion angles (°)) of the crystal structures of aegelinol (**1**, three molecules in asymmetric unit **(A, B, C)**) and its inclusion complex in β-cyclodextrin (**1-BCD** two molecules in asymmetric unit **(A, B)**).

Geometrical aspects	**1** A	**1** B	**1** C	**1-BCD** A	**1-BCD** B
C6-C1`	1.503(3)	1.501(3)	1.501(3)	1.488(15)	1.52(2)
C1`- C2`	1.518(4)	1.523(4)	1.520(4)	1.451(19)	1.49(3)
C2`- O2`	1.431(3)	1.422(3)	1.429(3)	1.425(15)	1.43(2)
C2`- C3`	1.522(4)	1.527(4)	1.521(4)	1.52(2)	1.45(3)
C3`- O3`	1.463(3)	1.470(3)	1.467(3)	1.461(15)	1.50(2)
C7- O3`	1.363(3)	1.361(3)	1.34(2)	1.350(14)	1.36(2)
C7-C6- C1`	120.0(2)	120.0(2)	120.1(2)	120.8(11)	120.4(15)
C6- C1`- C2`	110.4(2)	111.6(2)	110.2(2)	110.4(10)	113.4(17)
O2`- C2`- C1`	111.4(2)	111.8(2)	111.3(2)	109.8(10)	114.3(17)
C1`- C2`- C3`	110.3(2)	110.7(2)	110.6(2)	113.6(12)	111.7(17)
O3`- C3`- C2`	109.7 (2)	109.7(2)	110.6(2)	106.2(11)	113.6(14)
O3`-C7-C6	122.9(2)	123.0(2)	123.2(2)	122.4(11)	124.5(13)
C7- O3`- C3`	118.6 (2)	118.4 (2)	119.0(2)	117.6(11)	114.3(13)
C5-C6- C1`- C2`	-156.9(2)	-159.3(2)	-154.0(2)	-164.5(9)	170.3(15)
C7-C6- C1`- C2`	21.4(3)	20.5(3)	24.7(3)	13.9(13)	-10(3)
C6- C1`- C2`- O2`	70.3(3)	79.0(3)	71.9(3)	-172.1(10)	-78(3)
C6- C1`- C2`- C3`	-50.4(3)	-47.1(3)	-50.8(3)	-45.7(14)	37(3)
O2`- C2`- C3`- O3`	-62.3(3)	-67.7(3)	-65.7(3)	-172.7(10)	67.6(17)
C1`- C2`- C3`- O3`	60.0(3)	58.2(3)	57.7(3)	62.1(13)	-55(2)
O2`- C2`- C3`- C4`	177.6(2)	172.2(2)	173.7(2)	-59.8(14), 69.3(15)	-175.5(13), -52.8(19)
C1`- C2`- C3`- C4`	-60.0(3)	-62.0(3)	-62.9(3)	175.0(11), -55.9(15)	62(2), -175.1(19)
C1`-C6-C7- O3`	-0.4(4)	-4.0(4)	-4.3(4)	0.5(14)	0(2)
C8-C7- O3`- C3`	-172.5(2)	-166.6(2)	-172.4(2)	-162.8(9)	162.0(13)
C6-C7- O3`- C3`	10.1(3)	15.8(3)	11.0(4)	18.0(15)	-16(2)
C2`- C3`- O3`-C7	-39.6(3)	-42.6(3)	-37.6(3)	-46.6(14)	44(2)
C4`- C3`- O3`-C7	82.3(3)	79.1(3)	84.9(3)	-164.9(11), 74.9(14)	-77.0(19), 171.8(19)

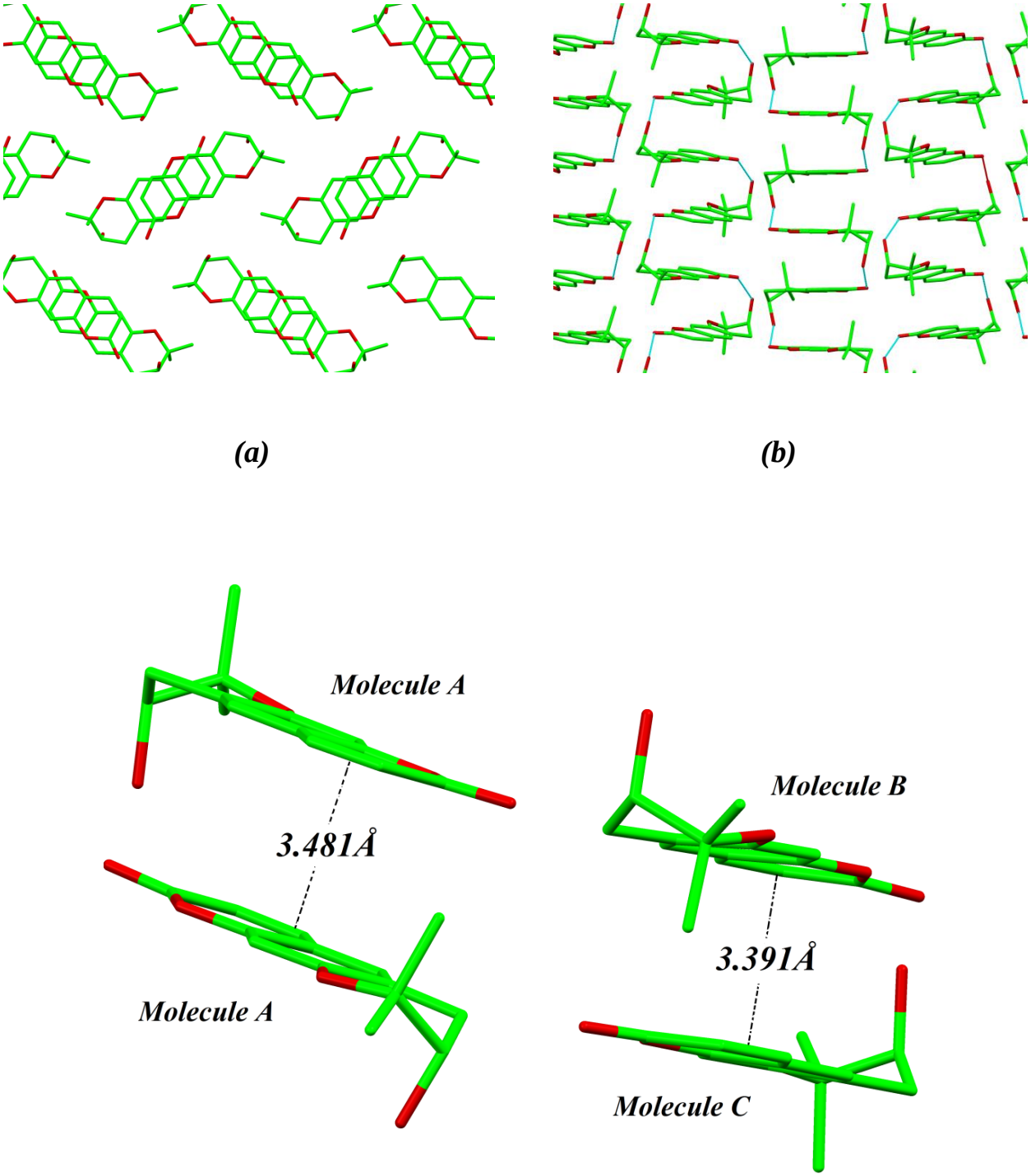

Figure 4.3.6. Crystal packing of aegelinol. ***(a)*** Stacking along the ***a*** axis; ***(b)*** Stacking along the ***b*** axis; ***(c)*** π-π stacking distances (Å) in aegelinol alone.

Table 4.3.6. Selected hydrogen bonds in aegelinol alone and in the complex with β-cyclodextrin.

D	A	d (D-H) (Å)	d (H...A) (Å)	d (D...A) (Å)	<(DHA) (°)
Aegelinol (1)					
O(2`A)	O(2A)$_{i}$	0.840	2.080	2.902	164.5
O(2`B)	O(2C)$_{ii}$	0.840	2.010	2.816	159.4
O(2`C)	O(2B)	0.840	2.030	2.851	165.8
BCD-1 complex (1-BCD)					
O2´A1	O13W	0.840	2.122	129.16	2.731
O2´B1	O61A	0.840	2.524	150.01	3.278
O2´A2	O17'W	0.840	1.824	134.51	2.487
O2´B2	O63B$_{iii}$	0.840	2.065	151.37	2.831
O65A	O2´A2$_{vii}$	0.840	2.424	98.20	2.729
O31A	O31B	0.840	1.969	173.10	2.804
O22A	O37B	0.840	2.289	148.87	3.039
O22A	O18'W$_{ii}$	0.840	2.607	143.00	3.316
O32A	O37B	0.840	1.863	166.02	2.686
O62A	O17W$_{iii}$	0.863	1.935	147.92	2.705
O62A	O17'W$_{iii}$	0.863	2.012	175.31	2.873
O23A	O36B	0.840	2.404	150.53	3.162
O24A	O35B	0.840	2.281	142.75	2.993
O64A	O67A$_{iv}$	0.840	2.261	126.43	2.841
O25A	O7W$_{v}$	0.840	2.408	125.26	2.973
O35A	O34B	0.840	1.970	171.85	2.804
O36A	O18'W	0.840	1.974	138.08	2.659
O66A	O62A$_{vi}$	0.840	2.117	133.75	2.765
O27A	O46A	0.840	2.388	111.57	2.807
O67A1	O24W	0.840	2.499	154.48	3.277
O67A2	O20W$_{vii}$	0.840	2.627	161.97	3.436
O32B	O37A	0.840	1.934	164.80	2.753
O62B	O65B$_{viii}$	0.840	2.140	132.42	2.777
O23B	O42B	0.840	2.279	114.51	2.736
O33B	O36A	0.840	1.938	162.04	2.749
O63B	O3W$_{vi}$	0.840	1.865	176.56	2.704
O24B	O35A	0.840	2.508	135.02	3.159
O24B	O26A	0.840	2.630	110.55	3.029
O64B	O51A$_{ix}$	0.840	2.196	169.12	3.025
O64B	O61A$_{ix}$	0.840	2.220	116.96	2.707
O35B	O34A	0.840	1.924	154.65	2.707
O26B	O33A	0.840	2.434	148.31	3.180
O36B	O33A	0.840	1.923	168.68	2.751
O66B	O24W$_{x}$	0.840	2.576	124.04	3.124
O27B	O32A	0.840	2.373	133.66	3.015
O67B	O63B$_{ii}$	0.840	1.957	162.82	2.770
O21B	O18W$_{ii}$	0.840	2.349	154.82	3.129
O65A	O19W	0.840	2.405	127.62	2.993
O13W	O21W$_{xi}$	0.848	1.948	149.22	2.712
O13W	O19W$_{xii}$	0.842	1.905	156.68	2.700

Symmetry: ***i*** *[x-1/2, -y+3/2, -z+2]*; ***ii*** *[x+1, y, z]*; ***iii*** *[x+1, y, z+1]*; ***iv*** *[x, y-1, z]*; ***v*** *[x-1, y-1, z]*; ***vi*** *[x-1, y, z]*; ***vii*** *[x, y, z+1]*; ***viii****[x, y+1, z]*; ***ix*** *[x-1, y-1, z-1]*; ***x*** *[x, y-1, z-1]*; ***xi****[x-1, y, z-1]*; ***xii*** *[x, y, z-1]*.

unambiguous determination of the absolute configuration of the stereogenic center of aegelinol. Crystals were grown from a solution in water/ethanol (50:50). Two morphologies of crystals are observed: the long and yellow crystals (analyzing the cell parameters on the diffractometer showed that it correspond to the aegelinol alone), and parallelepiped and colorless ones are related to the inclusion complex with β-cyclodextrin. Primary statistics on data quality and refinement are given in Table 4.3.4.

Figure 4.3.7 presents the structure of the inclusion complex. From this structure, the absolute configuration of C2' of aegelinol can unambiguously be assigned and corresponds to the (*R*) enantiomer.

Interestingly, disorder of the included aegelinol molecule within the cyclodextrin cavity was modeled in two sites, nearly similar, with 60:40 occupancy. The coumarin moieties are planar with RMSDs of fitted atoms from the least-squares plane are 0.0034 and 0.0038 Å for the two molecules A and B, respectively. The dihedral angles between these planes, inside the cavity, is 22.2(4)° in the first site and 3.0(3)° in the second site.

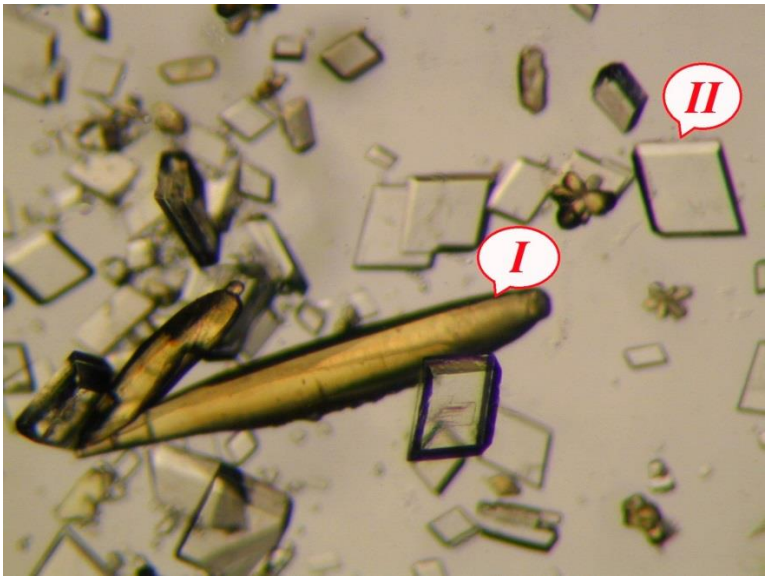

(a)

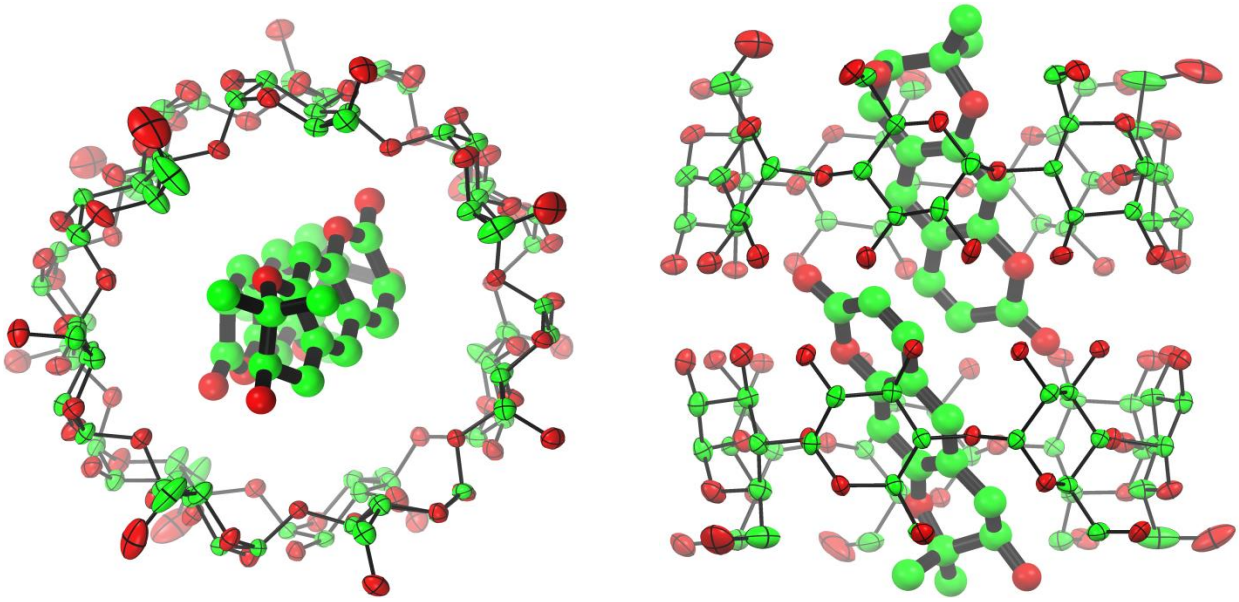

(b)

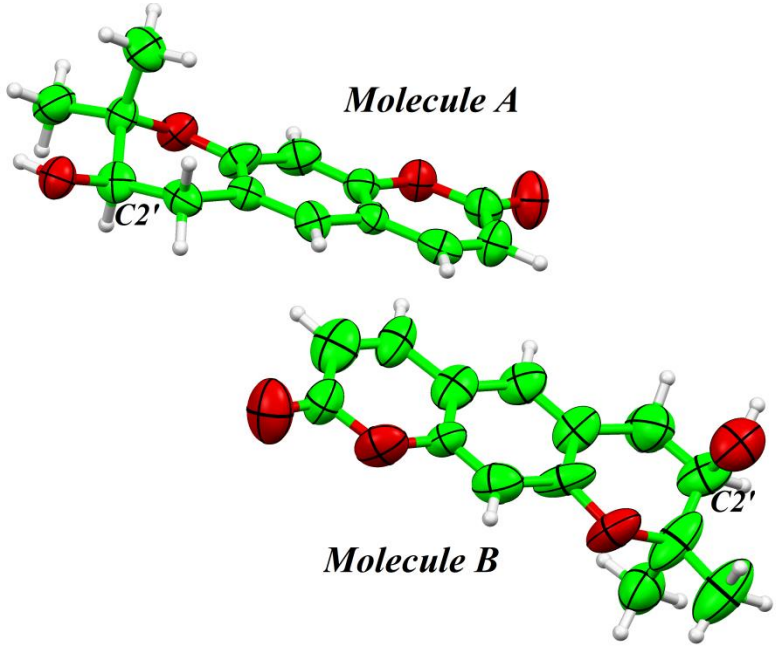

(c)

Figure 4.3.7. **(a)** Morphology of crystals of aegelinol - β-cyclodextrin inclusion complex (**1-BCD**). Two forms of crystals are observed: (***I***) corresponds to cell parameters of aegelinol alone and (***II***) corresponds to cell parameters of the inclusion complex. **(b)** Two perpendicular views showing the conformation of the **1-BCD** inclusion complex (ORTEP, 30% probability) and confirming the R configuration at C2'. Only one component of the disorder of the guest molecule inside the cyclodextrin cavity is presented and hydrogen atoms and water molecules are removed for clarity. **(c)** View of the two aegelinol molecules after removing all the rest of the structure to show their configuration.

The solution of the crystal structure revealed a 2:2 stoichiometry. The pyranocoumarin guest is included within the cylindrical cavity formed by dimeric β-cyclodextrin molecules with a head-to-head arrangement. Crystalline complexes of hydrogen-bonded β-cyclodextrin dimers complexed with organic guest molecules have been found previously to adopt one of four crystal packing motifs: a channel motif (***Ch***), a checker board motif (***CB***), an intermediate motif (***Im***), and, most recently, a tetrad motif (***Tt***). Packing diagrams are available in different reports on β-cyclodextrin complexes; the reader is referred to these works for both diagrams and discussion of the different structural properties for these packing arrangements [49–51].

The CD host molecules are associated through hydrogen bonding between secondary hydroxyl groups as dimers, packing in the previously observed (***Im***) packing arrangement [49–51]. The fact that this arrangement is common to these complexes of β-CD is important for two reasons:

(1) It implies that crystal packing does not severely limit conformational and translational freedom of guest molecules.

(2) It provides an environment for the guest molecules that resembles a macromolecular binding pocket by providing a hydrophobic pocket rimmed with a scaffolding of hydrophilic binding sites that can interact directly with guest molecules or via bridging water molecules.

As a consequence, guest molecules experience considerable variation in their specific interactions with the host molecules and waters of hydration, often resulting in the observation of crystallographic disorder. This semichannel-type packing orients along the c-axis direction (Figure 4.3.8.).

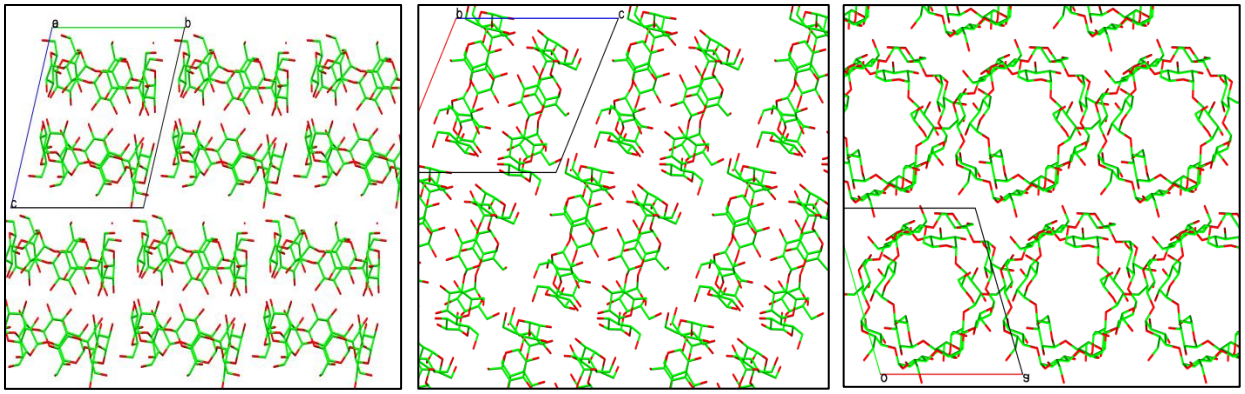

a ***c*** ***b***

Figure 4.3.8. Crystal packing of β-cyclodextrins in the **1-BCD** crystal structure shown along the ***a***, ***b*** and ***c*** directions. Guest molecules (aegelinol) and waters are omitted for clarity.

One hydrogen bond is observed between the cyclodextrin and the first site and two in the second site of the disordered guest (Table 4.3.7 and Figure 4.3.9). These hydrogen bonds are between the hydroxyl groups on the guest and on the primary side of cyclodextrin. The two molecules of aegelinol stack together (mainly involving the coumarin moieties) and are stabilized by hydrophobic effect within the cavity formed by two cyclodextrins (Figure 4.3.7). The distances between the planar coumarin and the centroid of the other coumarin are 3.233Å in the first site and 3.215 Å in the second site. Moreover, this arrangement serves a strong π-π interaction (Figure 4.3.10). Notable differences are observed at the level of the pyroano ring of the two aegelinol molecules (RMSD = 0.871 Å and Table 2) most likely resulting from less constraints in **1**-BCD compared to the structure of **1** alone. Twenty-four ordered water molecules are also observed in the structure. They are situated outside the cavity at the borders of the toroid rims and in interstices between β-CD molecules. Five water molecules are disordered over two sites.

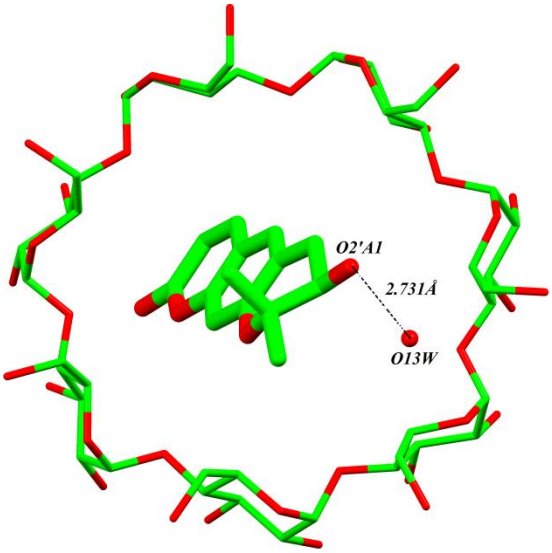

Molecule A first disorder

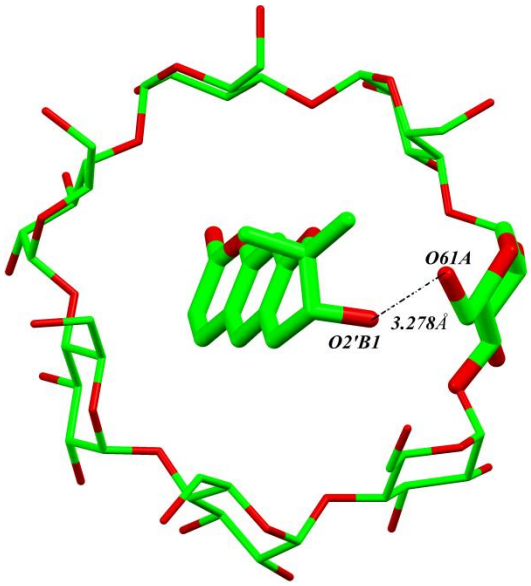

Molecule B first disorder

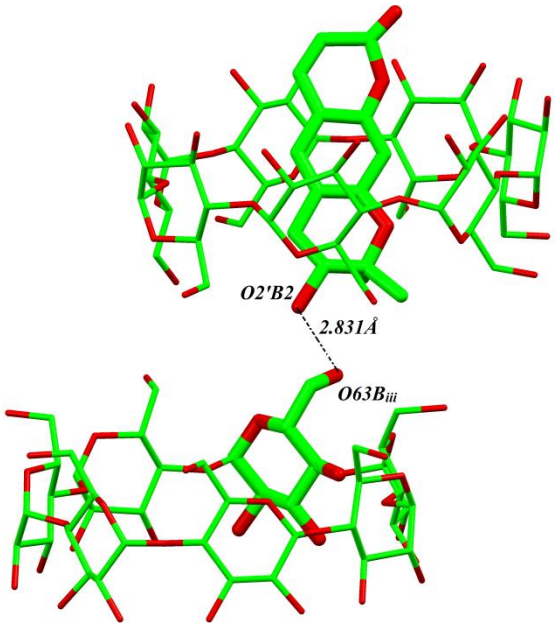

Molecule A second disorder

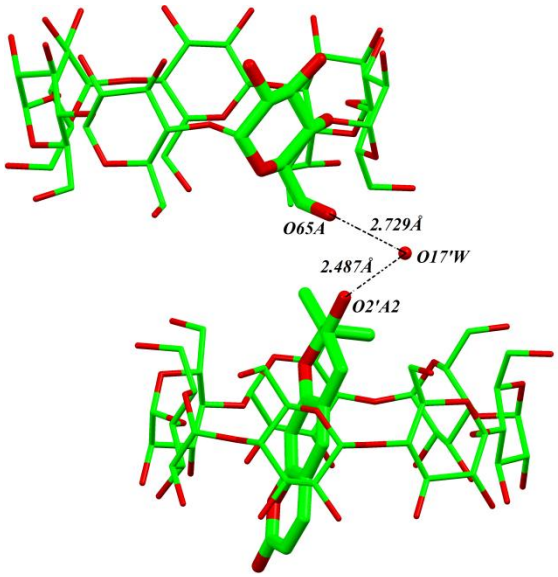

Molecule B second disorder

Figure 4.3.9. The involved hydrogen bonds in aegelinol in both disorder sites Symmetry transformations used to generate equivalent atoms: *iii* [x+1, y, z+1]; *iv* [x, y, z+1].

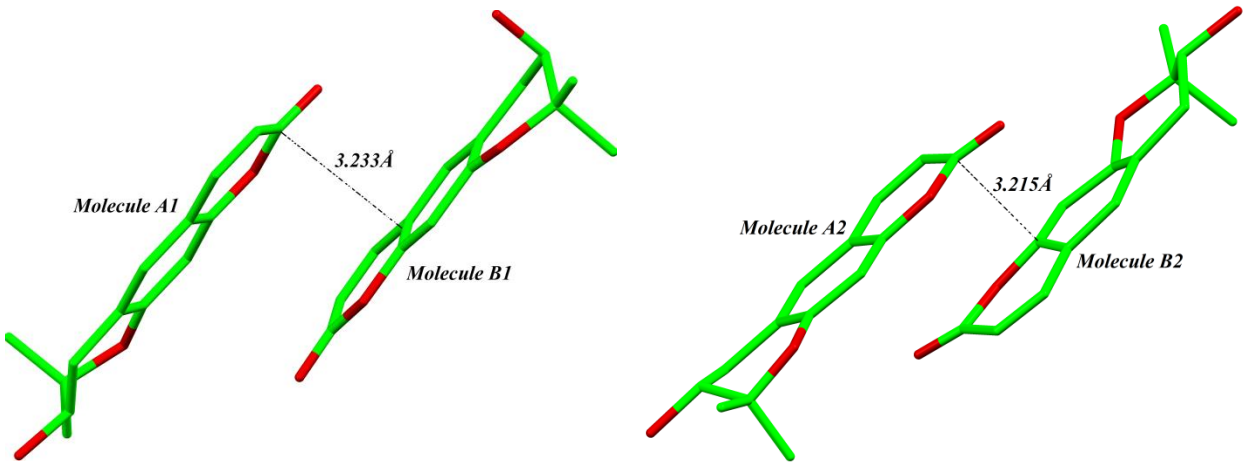

a **b**

Figure 4.3.10**.** π-π stacking distances (Å) in aegelinol-β-CD complex. (**a**) In first site; (**b**) In second site.

4.4 Experimental Section

4.4.1 Chemistry

Synthesis and purification of 1,1'-(propane-1,3-diyl)-bis-(6,7-dimethoxy-2-methyl-1,2,3,4-tetrahydroisoquinolinum) hydrochloride salt were performed by the group of Prof. J.-F. Liégeois at the University of Liège (ULg). The Compounds were obtained following the procedure detailed in reference [52]. Briefly, under inert atmosphere, $NaBH_4$ (1.76 g; 46.5 mmol) was added to a solution of the 1,3-bis[1-(6,7-dimethoxy-2-methylisoquinolylium)]-propane diiodide [10] (1.85 g; 3.1 mmol) in MeOH (100 mL) at room temperature. After 15 min, MeOH was removed under reduced pressure and the crude residue was dissolved in a 1 N aqueous HCl (100 mL). The acidic layer was washed with Et_2O (3 × 20 ml) and then basified with NH_4OH. The suspension was extracted with CH_2Cl_2 (3 × 30 mL). The organic layers were collected, dried over anhydrous $MgSO_4$ and evaporated under reduced pressure to afford colorless oil which was purified by flash chromatography on Kieselgel with a mixture of Me_2CO/MeOH (9/1, v/v) as mobile phase. The purified oily derivative was isolated as hydrochloride salt.

Separation of the three enantiomers as base was performed by semi-preparative chiral HPLC using a Chiralcel® OD-H column and a mixture of 2-propanol (80)/hexane (20) containing 0.05% diethylamine at a flow rate of 1 mL/min [52].

Isolation and purification of aegelinol (**1**) has been performed by the group of Prof. Thierry Hennebelle at Université Lille Nord de France Lille2 [11]. Briefly, roots of *F. asparagifolia* (500 g) were dried, powdered and extracted successively with light petroleum, EtOAc and MeOH at room temperature. Extracts were then evaporated and lyophilized. The EtOAc extract (4.0 g) was chromatographed over silica gel columns. Six compounds were isolated from the EtOAc extract, one of which corresponding to aegelinol.

4.4.2 X-ray studies

All the crystallization, the data collection and the crystallographic analyzing procedures have been done in our laboratory (CBS) at the University of Namur (UNamur).

Crystals of the three stereoisomers E1, E2 and Meso of the 1,1'-(propane-1,3-diyl)-bis-(6,7-dimethoxy-2-methyl-1,2,3,4-tetrahydroisoquinolinum) hydrochloride salts were obtained by slow evaporation from an acetonitrile solution. X-ray measurements were performed on a Gemini Ultra R system (4-circle kappa platform, Ruby CCD detector) using Mo Kα radiation (λ=0.71073 Å) for all three compounds (E1, E2 and Meso-1,10-(propane-1,3-diyl)-bis-(6,7-dimethoxy-2-methyl-1,2,3,4-tetrahydroisoquinoline) hydrochloride. After mounting and centering of the single crystals on the diffractometer, cell parameters were estimated from a pre-experiment run and full datasets collected at room temperature. Software for data reduction was CrysAlisPro [53]. Structures were solved by direct methods from SHELXS-97 program and then refined on F^2 using SHELXL-97 software [54]. Datasets for E1 and E2 were filtered in order to retain

reflections above theta=25° (resolution > 0.84 Å). Non-hydrogen atoms were anisotropically refined and the hydrogen atoms in the riding mode with isotropic temperature factors fixed at 1.2 times U (eq) of the parent atoms (1.5 times for methyl groups). Structures contain residual solvent accessible void of about 35 $Å^3$ that could accommodate a water molecule that was not explicitly included in the refinements. Thermal agitation is higher for atoms C3 and C13 than for neighboring atoms.

Crystals of aegelinol were prepared by dissolving a 1–2 mg amount of aegelinol in a minimal amount of ethanol. The mixture was then stored at room temperature. Colorless long crystals suitable for X-ray data collection were obtained by slow evaporation after one week.

Crystals of the β-CD in complex with aegelinol were prepared by dissolving a few milligrams of β-CD in water (2 mL) at 65 °C and aegelinol in ethanol (2 mL) at 65 °C, in stoichiometric (2:1) ratio with respect to β-CD. Both solutions were mixed and stirred at 65 °C for 6 hours. Then the mixture was stored at room temperature. Two forms of crystals (colorless plates and pale yellow needle) suitable for X-ray data collection were obtained by slow evaporation after one week.

Single crystals of aegelinol and of the β-CD-aegelinol complex were mounted on the head of a 4-circle kappa goniometer. X-ray diffraction experiment was carried out at low temperature (150 K) on an Oxford Gemini R Ultra using Mo Kα (λ=0.71073 Å) (aegelinol) or Cu Kα (λ=1.54179 Å) radiation (inclusion complex). Data reduction was carried out with the CrysAlisPro program [53]. Crystal data collection and refinement details are listed in Table 4.3.4.

The structure of aegelinol was determined by direct methods and refined using full-matrix least-squares based on F^2 with the program SHELX [54], based on 491

parameters and 0 restraints. The refinement converged to R_1 = 4.44% for I > 2σ(I) and 5.22% for all data. Hydrogen atoms were calculated at ideal positions and refined using a riding model.

The structure of the β-CD-aegelinol complex was solved by atomic coordination replacement methods using a β-CD complex structure from CSD [BOSZOZ] [55] with the same cell parameters after making suitable transformation and deleting the guest from the structure. Extra electronic density in the cavity corresponded to aegelinol. This structure was refined using full-matrix least-squares on F^2 with the program SHELX [54], based on 2083 parameters and 89 restraints. The refinement converged to R_1 = 6.71% for I > 2σ(I) data and 7.10% for all data. Most hydrogen atoms were calculated at ideal positions and refined using a riding model and the rest of the hydrogen atoms were located on a different Fourier map. Ordered water molecules were located in a difference Fourier map. All non-hydrogen atoms were anisotropically refined. Secondary hydroxyl groups were refined with two alternate conformations. Disorder of the included aegelinol molecules within the cyclodextrin cavity, five disordered water molecules and two primary hydroxyl groups in β-CD were modeled in two sites. The second sites were located from difference Fourier maps.

Coordinates have been deposited at the Cambridge Structure DataBank (CCDC 754726, 754727 and 754728 contain the supplementary crystallographic data of E1, E2 and Meso, CCDC 884098 and 884099 contain the supplementary crystallographic data of aegelinol and aegelinol-β-cyclodextrin complex), and can be obtained free of charge via *www.ccdc.cam.ac.uk/conts/retrieving.html* (or from the Cambridge Crystallographic Data Centre,12, Union Road, Cambridge CB2 1EZ, UK; fax: +44 1223 336033; or deposit@ccdc.cam.ac.uk).

4.5 Conclusions

Crystal structures of the stereoisomers of 1,10-(propane-1,3-diyl)-bis-(6,7-dimethoxy-2-methyl-1,2,3,4-tetrahydroisoquinoline) hydrochloride obtained after resolution by semi-preparative chiral HPLC (Chiralcel® OD-H column) establishes the absolute configuration of the separated compounds. The first peak (7 min) corresponds to a first enantiomer (E1) with absolute configuration *S,S* for C10, C20. $[\boldsymbol{\alpha}]_{\boldsymbol{D}}^{\boldsymbol{20}}$ of the first eluted enantiomer is +34.8°. The second eluted peak (10 min) corresponds to the meso form (formally an *R,S* and *S,R*). The third eluted peak (23 min), corresponding to the E2 enantiomer, is the mirror image of the first enantiomer, with an *R,R* configuration for C10, C20 and $[\boldsymbol{\alpha}]_{\boldsymbol{D}}^{\boldsymbol{20}}$ of -34.5°. The conformation and precise configuration of the molecules deduced from our crystallographic study, by mean of Flack parameters, will serve as starting point for further molecular modeling simulation planned to rationalize the differences in affinity of the series for small conductance Ca^{2+}-activated K^+ (SK) channels.

Crystals of aegelinol (**1**) alone were obtained and led to determination of its crystal structure. Statistics of the Flack parameters confirm that the absence of suitable heavy atoms (no strong anomalous scatterers) in the molecule is a limitation for reliable absolute configuration of such molecules by X-ray diffraction. Derivatization of the molecule by formation of a chiral salt was not an alternative as the molecule does not contain any basic or acidic function. As an alternative, we were able to grow crystals of the inclusion complex of aegelinol in β-cyclodextrin and refined the crystal structure of the complex, which allowed unambiguous determination of the absolute configuration of the stereogenic center of aegelinol. The (*R*) configuration of C2' obtained by this crystallographic study confirms previous conclusions based on indirect NMR data.

4.6 References

1. Pure & Appl. Chem., 1996, 68, 2193-2222.
2. Flack, H. D. Acta Cryst. 1983, A39, 876-881.
3. G. Bernardinelli and H. D. Flack. Acta Cryst. 1985, A41, 500-511.
4. Alexander J. Blake, William Clegg, Jacqueline M. Cole, John S.O. Evans, Peter Main, Simon Parsons, and David J. Watkin, Crystal Structure Analysis, Principles and Practice, Second Edition 2009.
5. H. D. Flack and G. Bernardinelli, J. Appl. Cryst. 2000, 33, 1143-1148.
6. O. Waroux, L. Masotte, L. Alleva, A. Graulich, E. Thomas, J.-F. Liégeois, J. Scuvée-Moreau, V. Seutin, SK channels control the firing pattern of midbrain dopaminergic neurons in vivo. Eur. J. Neurosci. 2005, 22, 3111-3121.
7. J.-F. Liégeois, F. Mercier, A. Graulich, F. Graulich-Lorge, J. Scuvée-Moreau, V. Seutin, Modulation of small conductance calcium-activated potassium (SK) channels: a new challenge in medicinal chemistry. Curr. Med. Chem. 2003, 10, 625-647.
8. J.-F. Liégeois, F. Mercier, A. Graulich, F. Graulich-Lorge, J. Scuvée-Moreau, V. Seutin, Modulation of small conductance calcium-activated potassium (SK) channels: a new challenge in medicinal chemistry. Curr. Med. Chem. 2003, 10, 625-647.
9. J. Scuvée-Moreau, A. Boland, A. Graulich, L. Van Overmeire, D. D'hoedt, F. Graulich-Lorge, E. Thomas, A. Abras, M. Stocker, J.-F. Liégeois, V. Seutin, Electrophysiological characterization of the SK channel blockers methyl-laudanosine and methyl-noscapine in cell lines and rat brain slices. Br. J. Pharmacol. 2004, 143, 753-764.
10. A. Graulich, S. Dilly, A. Farce, J. Scuvée-Moreau, O. Waroux, C. Lamy, P. Chavatte, V. Seutin, J.-F. Liégeois, Synthesis and radioligand binding studies of

bis-isoquinolinium derivatives as small conductance Ca^{2+}-activated K^{+} channel blockers. J. Med. Chem. 2007, 50, 5070-5075.

11. Alkhatib, R.; Hennebelle, T.; Roumy, V.; Sahpaz, S.; Suzgeç, S.; Akalın, E.; Meriçli, A.H.; Bailleul, F. Coumarins, caffeoyl derivatives and a monoterpenoid glycoside from Ferulago asparagifolia. Biochemical Systematics and Ecology, 2009, 37, 230–233.
12. Chatterjee, A.; Sen, R.; Ganguly, D. Aegelinol, a minor lactonic constituent of Aegle marmelos Phytochemistry 1978, 17, 328-329.
13. Adriana Basile; Sergio Sorbo; Vivienne Spadaro; Maurizio Bruno; Antonella Maggio; Nicoletta Faraone and Sergio Rosselli Molecules 2009, 14, 939-952.
14. Abyshev, A.Z.; Gindin, V.A.; Semenov, E.V.; Agaev, E.M.; Abdulla-zade, A.A.; Guseinov, A.B. Structure and biological properties of 2H-1-benzopyran-2-one (coumarin) derivatives. Pharm. Chem. J. 2006, 40, 607-610.
15. Lemmich, J.; Nielsen, B.E. Stereochemistry of natural coumarins containing the 3-hydroxy-2,2-dimethylchroman system. Tetrahedron Lett. 1969, 10, 3-4.
16. Erdelmeier, C.A.J.; Sticher, O. Coumarins derivatives from Eryngium campestre. Planta Med. 1985, 51, 407-409.
17. Adriana Basile; Sergio Sorbo; Vivienne Spadaro; Maurizio Bruno; Antonella Maggio; Nicoletta Faraone and Sergio Rosselli Molecules 2009, 14, 939-952.
18. Zacchino, S. A.; Badano, H. J. Nat. Prod. 1988, 51, 1261-1264.
19. Zacchino, S. A.; Badano, H. J. Nat. Prod. 1991, 54, 155-175.
20. Kasahara, H.; Miyazawa, M.; Kameoka, H. Phytochemistry 1995, 40, 1515-1517.
21. Harata, K.; Uekama, K.; Otagiri, M.; Hirayama, F. Crystal structures of cyclodextrin complexes with chiral molecules. Journal of lnclusion Phenomena 1984, 2, 583-594.

22. K.Harata, K.Uekama, M.Otagiri, F.Hirayama, Bull.Chem.Soc.Jpn. 1987, 60, 497-502.
23. K.Harata, K.Uekama, T.Imai, F.Hirayama, M.Otagiri, J.Inclusion Phenom.Mol.Recog.Chem. 1988, 6, 443-460.
24. G.R.Brown, M.R.Caira, L.R.Nassimbeni, B.van Oudtshoorn, .Inclusion Phenom.Mol.Recog.Chem. 1996, 26, 281-294.
25. S.Makedonopoulou,K.Yannakopoulou, D.Mentzafos, V.Lamzin, A.Popov, I.M.Mavridis, Acta Crystallogr.,Sect.B:Struct.Sci. 2001, 57, 399-409.
26. K.Yannakopoulou, D.Mentzafos, I.M.Mavridis, K.Dandika, Angew.Chem.,Int.Ed. 1996, 35, 2480-2482.
27. D.Mentzafos, I.M.Mavridis, K.Yannakopoulou, J.Inclusion Phenom.Macrocyclic Chem. 1999, 33, 321-330.
28. J.M.Alexander, J.L.Clark, T.J.Brett, J.J.Stezowski, Proc.Nat.Acad.Sci.USA, 2002, 99, 5115-5120.
29. M.R.Caira, E.De Vries, L.R.Nassimbeni, V.W.Jacewicz, J.Inclusion Phenom.Macrocyclic Chem. 2003, 46, 37-42.
30. K.Harata, Bull.Chem.Soc.Jpn. 1982, 55, 1367-1371.
31. L.Ferron, F.Guillen, S.Coste, G.Coquerel, J.-C.Plaquevent, Chirality (2006), 18, 662-666.
32. J.L.Clark, J.J.Stezowski, J.Am.Chem.Soc. 2001, 123, 9880-9888.
33. J.L.Clark, B.R.Booth, J.J.Stezowski, J.Am.Chem.Soc. 2001, 123, 9889-9895.
34. J.L.Clark, J.Peinado, J.J.Stezowski, R.L.Vold, Yuanyuan Huang, G.L.Hoatson, J.Phys.Chem.B 2006, 110, 26375-26387.
35. A.Grandeury, S.Petit, G.Gouhier, V.Agasse, G.Coquerel, Tetrahedron:Asymm. 2003, 14, 2143-2152.
36. Y.Amharar, A.Grandeury, M.Sanselme, S.Petit, G.Coquerel, Ann.Pharm.Fr. 2010, 68, 212-217.

37. A.Grandeury, L.Renou, F.Dufour, S.Petit, G.Gouhier, G.Coquerel, J.Thermal Analysis and Calorimetry, 2004, 77, 377-390.
38. M.R.Caira, V.J.Griffith, L.R.Nassimbeni, B.Van Oudtshoorn, J.Inclusion Phenom.Mol.Recog.Chem. 1995, 20, 277-290.
39. J.A.Hamilton, Longyin Chen, J.Am.Chem.Soc. 1988, 110, 4379-4391.
40. K.Harata, J.Chem.Soc, Perkin Trans.2, 1990, 799-804.
41. L.Malpezzi, G.Fronza, C.Fuganti, A.Mele, S.Bruckner, Carbohydr.Res. 2004, 339, 2117-2125.
42. T.Steiner, W.Saenger, J.Chem.Soc, Perkin Trans.2, 1998, 371-378.
43. A.Kokkinou, F.Tsorteki, M.Karpusas, A.Papakyriakou, K.Bethanis, D.Mentzafos, Carbohydr.Res. 2010, 345, 1034-1040.
44. A.T. Khalil, A.F. Halim, K. Ogata, T. Sekine, I. Murakoshi, (-)-1-Methylcorypalline, an isoquinoline alkaloid from Arthrocnemum glaucum. Phytochemistry. 1992, 31, 1023-1025.
45. J.C.A. Boeyens, The conformation of six-membered rings. J. Cryst. Mol. Struct. 1978, 8, 317-320.
46. D. Cremer, J.A. Pople, General definition of ring puckering coordinates. J. Am.Chem. Soc. 1975, 97, 1354-1358.
47. Doriguetto, A.C.; Ellena, J.; Santos, M.H.; Moreira, M.E.C.; Nagem, T.J. Mammeigin. ActaCrystallogr. Sect. C Cryst. Struct. Commun. 2006, 62, o350–o352.
48. Gonzalez, J.C.; Lobo-Antunes, J.; Perez-Lourido, P.; Santana, L.; Uriarte, E. Synthesis of angular pyrrolocoumarins. Synthesis 2002, 4, 475–478.
49. Saenger, W.; Atwood, J.L.; Davies, J.E.D.; MacNicol, D.D. Inclusion Compounds; Academic Press: London, UK, 1984, 2, 231–259.
50. Mentzafos, D.; Mavridis, M.; LeBas, G.; Tsoucaris, G. Structure of the 4-tert-butylbenzyl alcohol-[beta]-cyclodextrin complex. Common features in the

geometry of [beta]-cyclodextrin dimeric complexes. Acta Crystallogr. Sect. B 1991, 47, 746–757.

51. Brett, T.J.; Alexander, J.M.; Stezowski, J.J. Chemical insight from crystallographic disorder-structural studies of supramolecular photochemical systems. Part 2. The β-cyclodextrin-4,7-dimethylcoumarin inclusion complex: A new β-cyclodextrin dimer packing type, unanticipated photoproduct formation, and an examination of guest influence on β-CD dimer packing. Chem. Soc. Perkin Trans. 2, 2000, 6, 1095–1103.

52. A. Graulich, C. Lamy, L. Alleva, S. Dilly, P. Chavatte, J. Wouters, V. Seutin, J.-F. Liégeois, Bis-tetrahydroisoquinoline derivatives: AG525E1, a new step in the search for non-quaternary non-peptidic small conductance Ca^{2+} activated K^{+} channel blockers. Bioorg. Med. Chem. Lett. 2008, 18, 3440-3445.

53. CrysAlisPro, version 1.171.33.55; Oxford Diffraction Ltd.: Oxfordshire, UK, 2010.

54. Sheldrich, G.M. A short history of SHELX. *Acta Cryst*. **2008**, *A64*, 112–122.

55. Zhao, Y.L.; Benitez, D.; Yoon, I.; Stoddart, J.F. Inclusion behavior of β-cyclodextrin with bipyridine molecules: Factors governing host-guest inclusion geometries. *Chem. Asian J.* **2009**, *4*, 446–456.

Chapter 5

Conclusion and perspectives

The main objective of this thesis was to design, prepare and characterize new crystal systems containing cyclodextrins in combination with:

1) Para aminobenzoic acid as a drug model to study the effect of complexation phenomena on the solubility of drugs and characterize their structure and mode of interaction by combination a theoretical and experimental approach.
2) Potassium hydroxide to prepare cyclodextrin Metal-Organic Frameworks (CD-MOFs) formed by coordinating the cyclodextrins to potassium cation. Consequently taking the advantages of this interaction between cyclodextrin and alkali metal cation to favour formation of inclusion complexes as CD-MOFs drug carrier.
3) Aegelinol, a natural product, for analytical purposes to determine the absolute configuration of this compound by formation of an inclusion complex with a host of known chirality (cyclodextrins consists of several optically active D-glucose units). This should allow direct determination of the absolute configuration of the guest (aegelinol).

5.1 pABA-α-CD inclusion complex

Our crystallography study shows that pABA forms a 1:1 complex with α-CD and is deeply included into the cavity of the cyclodextrin, with the amino group protruding from the wide site of the cavity and the (unprotonated) carboxylate at the narrow side [Figure 5.1-a]. The crystal structure corresponds to the anionic form of pABA. The pABA guest is held in the host cavity mainly by van der Waals contacts and hydrogen bonds. Spectroscopic studies of the interactions of pABA

with α-CD demonstrate the insertion of pABA into the Cyclodextrin cavity in solution, with formation of a 1:1 inclusion complex with stability constant 2319.4±241.0 M^{-1} at 25°C and pH=3.5 [Figure 5.1-b]. The phase solubility studies confirm the formation of a 1:1 pABA-α-CD inclusion complex. The solubility of pABA in water is markedly enhanced by complexation with α-CD. The calculations carried out with the PM6 method show that inclusion complexes of different pABA protonation states with α-CD lead to stable structures and this confirms experimental observations. During this theoretical study, orientation A (carboxylic group inside) was more favorable than orientation B (amino group inside), in agreement with our crystal structure.

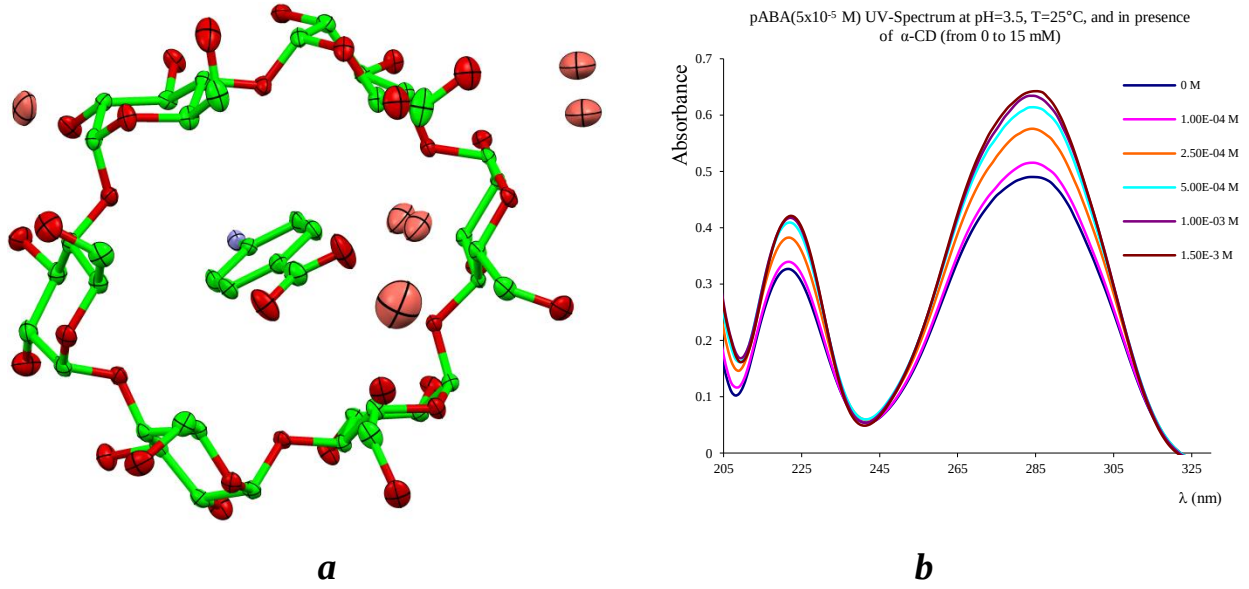

a ***b***

Figure 5.1 **a**) Axial view of the X-ray structure of the 1:1 host-guest inclusion complex of α-Cyclodextrin (α-CD) and p-Aminobenzoic acid (pABA). **b**) Absorption spectra of pABA 5×10^{-5} M at pH=3.5 in absence and presence of different concentrations of α-CD.

5.2 CD-MOFs

The interaction between potassium cations and α-CD has been established and well characterized in the crystalline state [Figure 5.2-a]. The structure shows 3D MOFs architecture and α-CD adopts a cage crystal structure packing stabilized, mainly, by coordinating the potassium cation through the –OCCO– motifs, in

addition to intermolecular and intramolecular hydrogen bondings. A new morph of α-CD belonging to the tube crystal structure packing form has also been accidentally established during the attempt to produce an inclusion complex with mABA and oABA. This new morph has a potential application in the field of gas storage and molecular absorption. Although present during crystallization, the "guest" mABA or oABA is not present in the crystal. Its presence is essential to obtain this polymorphic form and requires more investigation. A new technique was found to prepare a drug carrier based on the cyclodextrins by relying on their ability to form MOFs with alkali metals cations. These CD-MOFs possess a hydrophobic cavity able to receive the drug molecule inside. Two MOFs were prepared by this technique between α-CD and K^+mABA^- or K^+oABA^- showing 1D MOFs where K^+ cations assist in the assembly of two α-CD molecules to form a box containing a guest inside the cavity [Figure 5.2-b,c].

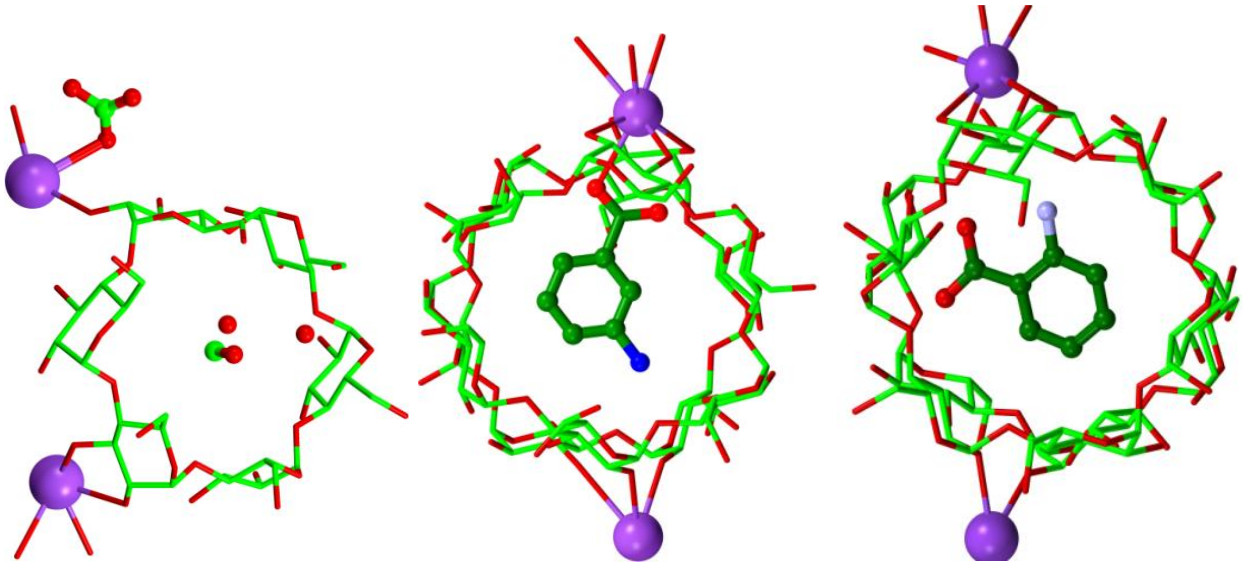

a ***b*** ***c***

Figure 5.2 **a**) 1:2 complex of α-CD with KOH. **b,c**) The structures of α-cyclodextrin MOFs with m-aminobenzoate potassium(b) and o-aminobenzoate potassium(c), respectively.

5.3 Experimental absolute configuration determination

Crystals of aegelinol (**1**) [Figure 5.3-a] alone were obtained and led to determination of its crystal structure [Figure 5.3-b]. Statistics of the Flack parameters confirm that the absence of suitable heavy atoms (no strong anomalous scatterers) in the molecule is a limitation for reliable absolute configuration of such molecules by X-ray diffraction. Derivatization of the molecule by formation of a chiral salt was not an alternative as the molecule does not contain any basic or acidic function. As an alternative, we were able to grow crystals of the inclusion complex of aegelinol in β-cyclodextrin and refined the crystal structure of the complex [Figure 5.3-c], which allowed unambiguous determination of the absolute configuration of the stereogenic center of aegelinol. The (R) configuration of C2' obtained by this crystallographic study confirms previous conclusions based on indirect NMR data.

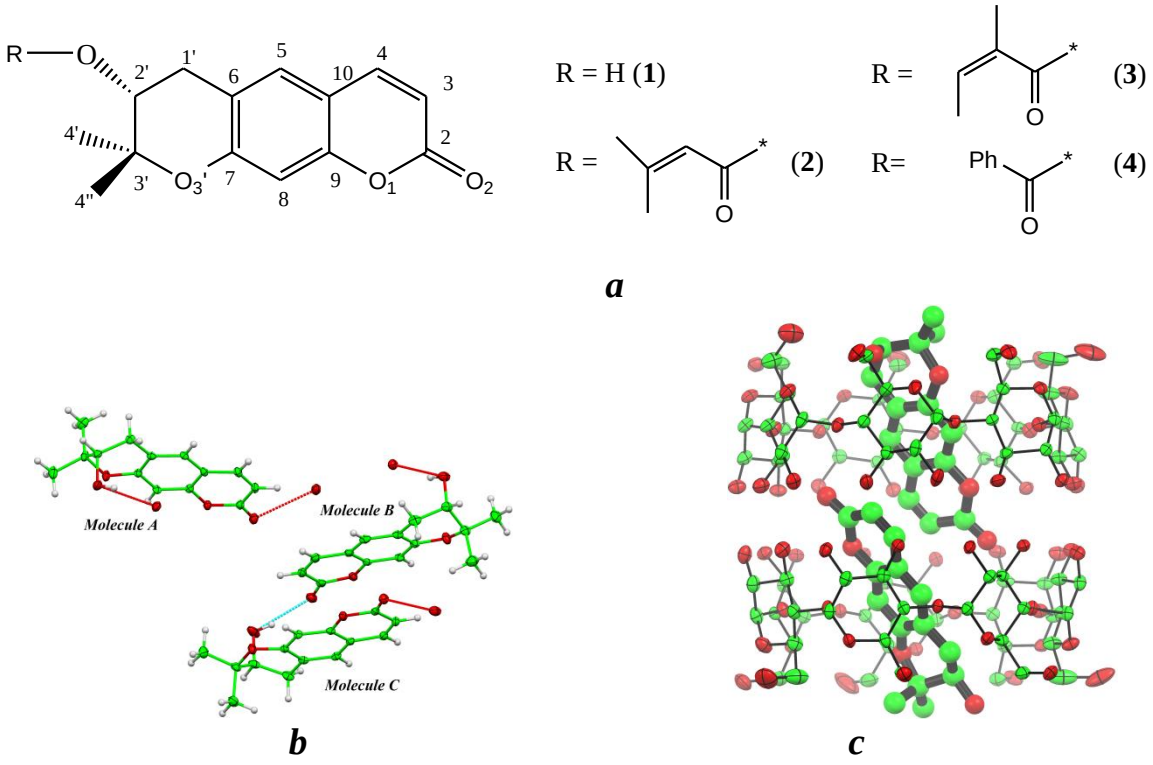

Figure 5.3 **a**) The chemical structure and numbering scheme of aegelinol. **b**) Crystal structure of aegelinol alone, three molecules in the crystal structure (A, B and C). **c**) Crystal structure of aegelinol in complex with β-CD.

5.4 Perspectives

Smaldone et al. suspected that the key to their success in assembling CD-MOFs lies in the symmetric arrangement (C_8) within the γ-CD torus of eight asymmetric (C_1) α-1,4-linked D-glucopyranosyl residues and the ready availability of γ-CD as a chiral molecular building block [1-2]. But this is not the only condition in the success in building useful porous CD-MOFs. Indeed we got a new, highly porous, structure, starting from β-CD and KOH by the same simple procedure as the one described for γ-CD-MOFs. This structure is as important as those designed by γ-CD. However, we failed to obtain a similar porous structure starting from α-CD despite the fact that α-CD has a symmetrical structure largely similar to the γ-CD symmetry while β-CD has not. We followed the same procedure as was done in preparation of γ-CD-MOFs by combining a suitable molar ratio of CD and KOH.

In case of β-CD, we got two forms of crystals with the same condition. The first form, with a parallelepiped shape and grown equally in three dimensions [Fig 5.4.1- a], forms the majority of resulting crystals. It corresponds to a structure already known in literature with stoichiometry 1(β-CD):1(K^+) [3]. This complex crystallizes in $P2_1$ monoclinic space group [*cell parameters: a = 15.223(5)Å, b = 10.578(3)Å, c = 20.204(6)Å, α = 90°, β = 108.37(7)° and γ = 90°*]. In this structure, β-CD molecules form, through the 2_1 axis, a herringbone-like pattern along the *bc* plan and the potassium cations are trapped in the lattice external to the β-CD cavity. Every β-CD molecule is connected to the adjacent β-CD molecules

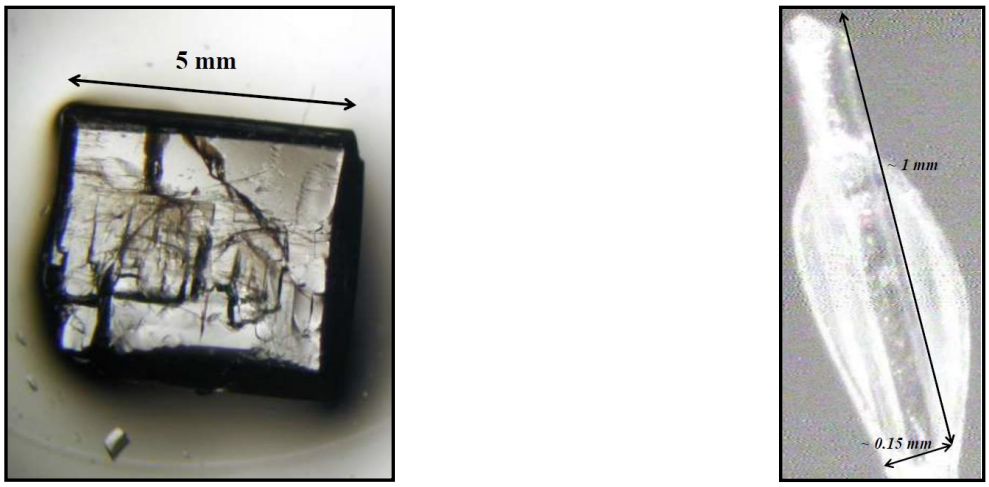

a ***b***

Figure 5.4.1 Two crystal morphs of β-CD-KOH complex: a) β-CD-KOH (1:1) complex, b) β-CD-KOH (1:2) complex.

by four K^+ cations and every K^+ cation is surrounded by four β-CD molecules and one water molecule [Fig 5.4.2-a,b]. In general, this structure is rather similar to the structure of β-CD alone [*$P2_1$ in monoclinic system: a = 21.29(2) Å, b = 10.33(1) Å, c= 15.10(2) Å, α = 90.0°, β = 112.3(5) °, γ = 90.0°*] **[4]**. The two structures have, approximately, the same cell parameters, the same distribution and stacking form within the unit cell [Fig 5.4.2-c,d,e], suggesting that some water molecules have been replaced by K^+ cations. As a result this structure might be the most favorable energetically.

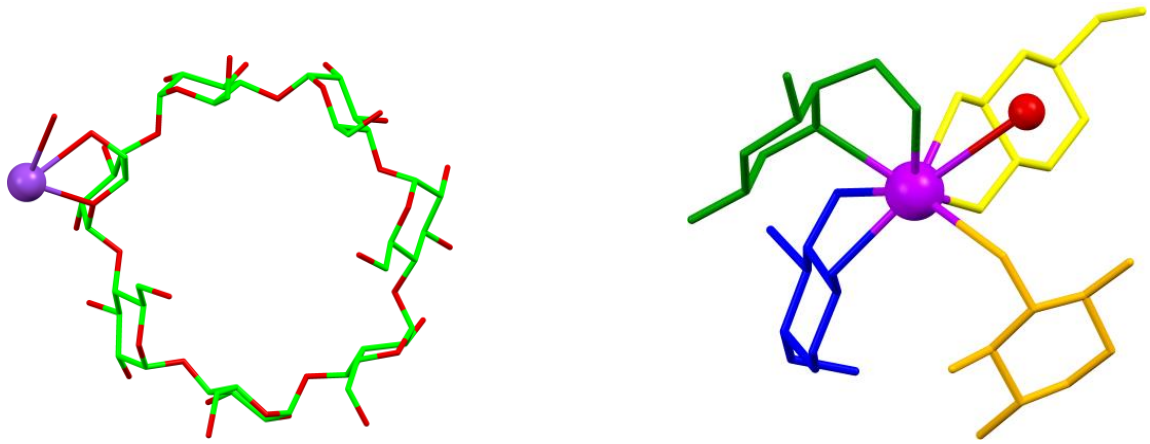

a ***b***

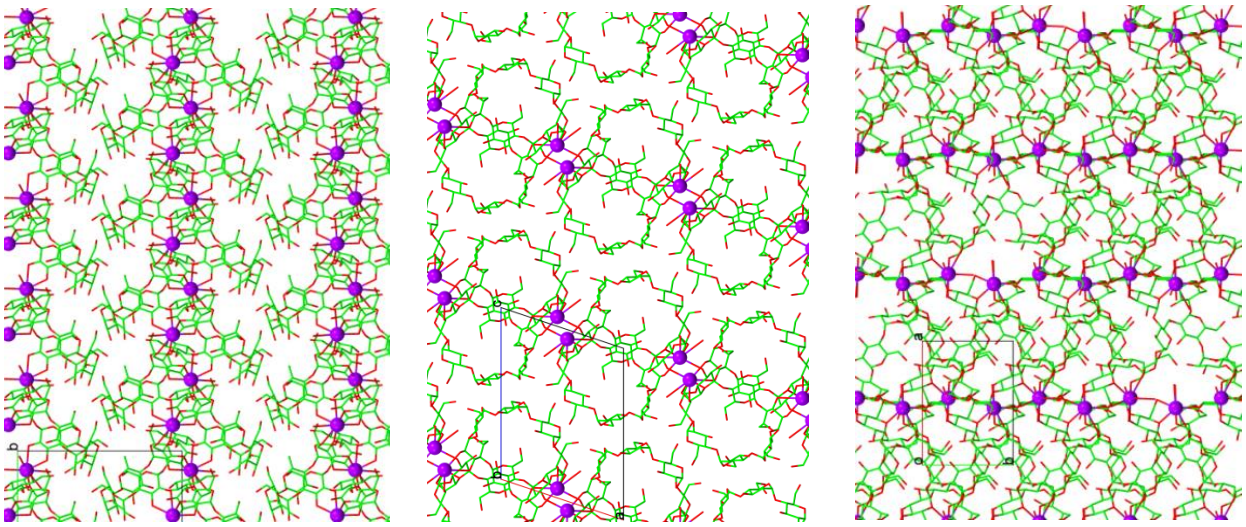

c ***d*** ***e***

Figure 5.4.2 a) 1:1 complex of β-CD with KOH , b) Potassium coordination , c) , d) and e) Crystal packing, in α-CD-KOH complex, in a, b and c direction respectively.

In parallel, we found a few number of different crystal forms with a rod-like shape [Fig 5.4.1-b]. The structure belongs to a new β-CD-KOH-MOF with stoichiometry 1(β-CD):2(K^+) [Fig 5.4.3-a,-b]. This complex crystallizes in $R3_2$ hexagonal crystal space group [*cell parameters: a = 41.525(2) Å, b = 41.525(2) Å, c = 27.1197(16) Å, α = 90°, β = 90° and γ = 120°*].

In this structure, β-CD molecules are linked together by potassium cations to form a hexagonal ring, where potassium cations occupy the corners of two parallel regular hexagons separated by a distance of 9.04 Å. The β-CD molecules form the sides with dihedral angle between their glucosidic plans and the potassium cations hexagon plan of 52.95° and 62.05°. This generates an empty space with a diameter of about 28 Å (2.8 nm) [Fig 5.4.3-c,-d]. Theoretical calculation of void volume inside the structure, using the contact surface with a 1.2 Å probe radius in ***Mercury*** software, shows an approximate value for the void volume about 19166 $Å^3$ and equal to 47.3 % of the structure. The overall stacking arrangement in the crystal structure displays winding channels in three directions and opened to each other [Fig 5.4.3-e]. This might give the new structure potential applications, in the field

of gas storage and molecular absorption. This requires to be more investigated. Also the conditions that lead to the formation of this MOF will have to be adjusted.

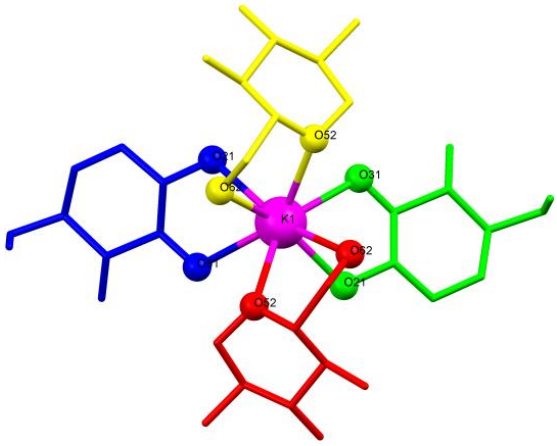

a

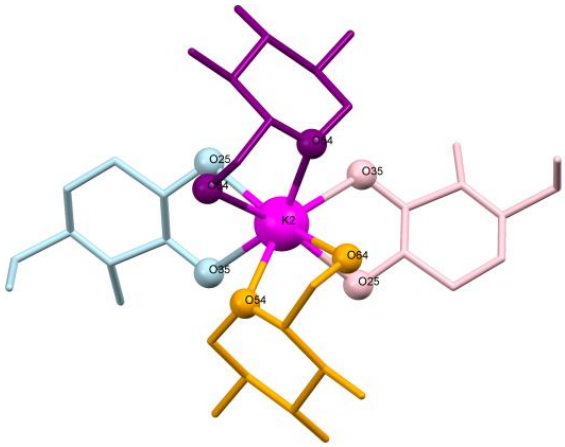

b

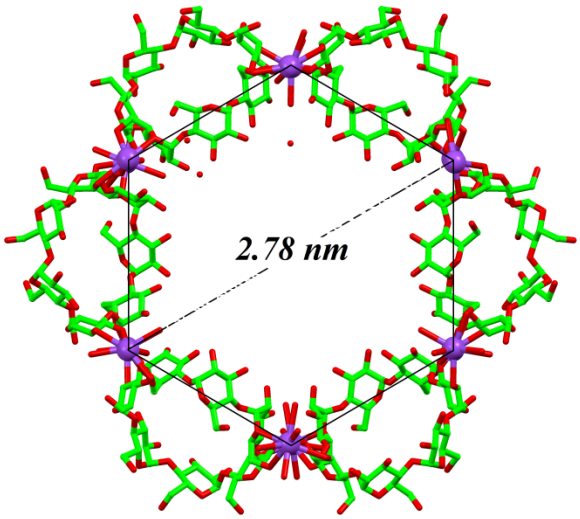

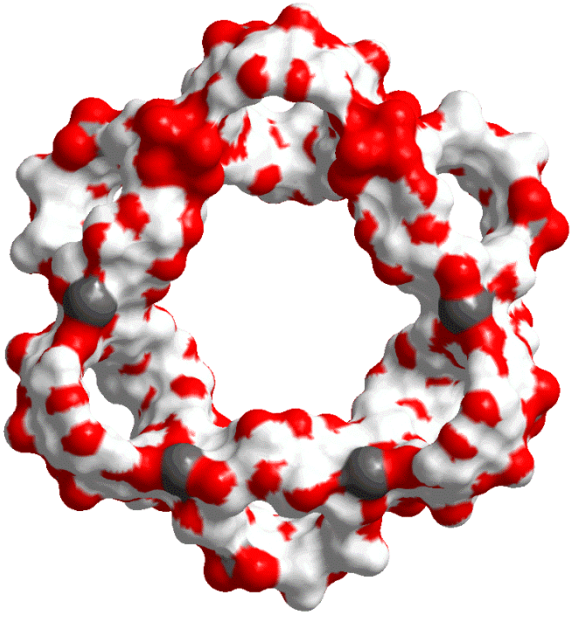

c

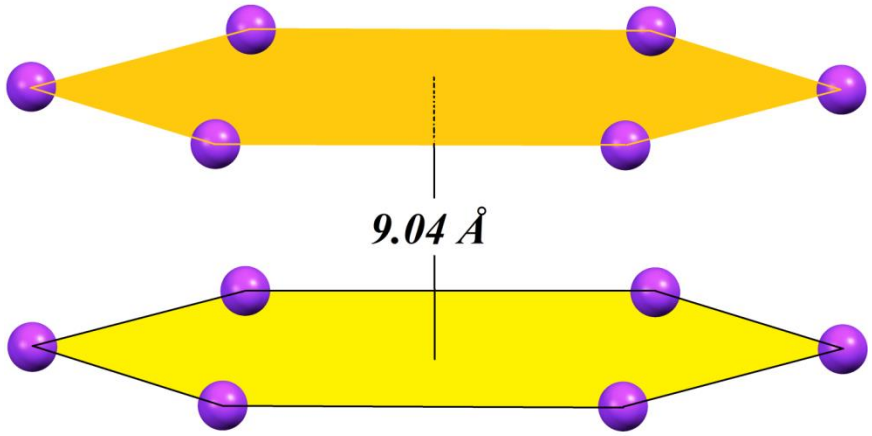

d

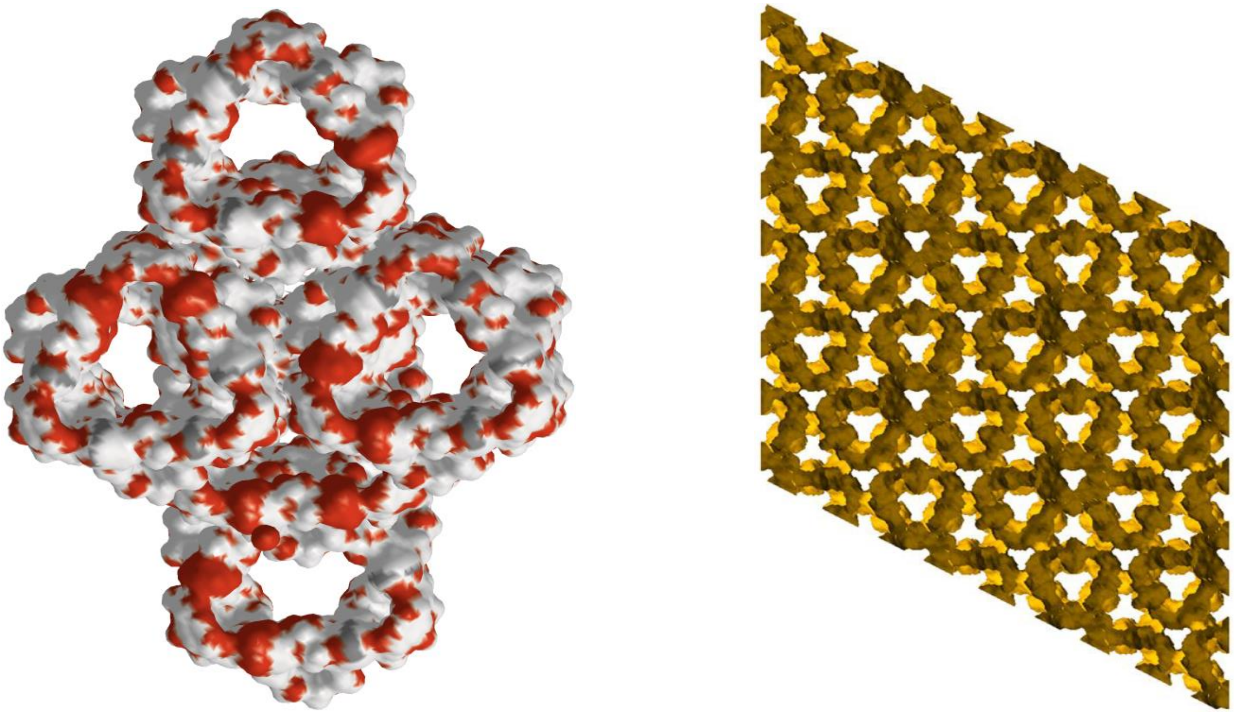

e

Fig 5.4.3 **a, b**) Potassium coordination, **c**) 1:2 complex of β-CD with KOH, **d**) Definition of the two parallel regular hexagon plans and the separated distance, **e**) crystal packing in c-direction showing the contact surface calculated by a 1.2 Å probe.

5.5 References

1. Forgan, R. S.; Smaldone, R. A.; Gassensmith, J. J.; Furukawa, H.; Cordes, D. B.; Li, Q.; Wilmer, C. E.; Botros, Y. Y.; Snurr, R. Q.; Slawin, A. M. Z.; Stoddart, J. F. J. Am. Chem. Soc. 2012, 134, 406–417.
2. Stoddart, J. F. Chem. Soc. Rev. 1979, 8, 85-142.
3. Charpin, P.; Nicolis, I.; Villain, F.; de Rango, C.; Coleman, A. W. Acta Crystallogr., Sect. C 1991, 47, 1829-1833.
4. K.Lindner, W.Saenger. Carbohydr.Res. 1982, 99, 103-115.